The contribution of brain reorganisation to recovery in patients with optic neuritis

Thomas Michael Jenkins

A thesis submitted to University College, London for the degree of Doctor of Philosophy

2010

Department of Brain Repair and Rehabilitation,

UCL Institute of Neurology,

Queen Square,

London,

WC1N 3BG,

United Kingdom

ABSTRACT

In this thesis, the mechanisms of damage and repair in clinically isolated optic neuritis (ON) were investigated *in vivo,* by combining magnetic resonance imaging (MRI), electrophysiology and optical coherence tomography (OCT). ON is a demyelinating, inflammatory condition of the optic nerve, which may be the first presentation of multiple sclerosis. The visual prognosis is generally good, despite optic nerve demyelination and axonal loss, but some patients fail to recover. The aim of this thesis was to determine the reasons underlying recovery. The hypothesis was that neuroplastic grey matter reorganisation might contribute to visual outcome.

Structural MRI, electrophysiology and OCT were used to quantify optic nerve oedema, inflammation, myelination and neuroaxonal loss, and optic radiation and visual cortical pathology, in a cohort of patients with acute ON, followed up over the following year. Visual functional MRI (fMRI) was employed to investigate neuroplasticity.

Acutely, measures of optic nerve inflammation and conduction block were associated with the severity of acute visual loss, and were used to inform an fMRI analysis, in order to dissect complex structure-function interactions. Evidence was found for neuroplasticity in dorsal higher visual areas, which may act to modulate acute visual dysfunction.

Subsequent longitudinal analyses identified associations between early fMRI activation in the lateral occipital complexes, a ventral stream higher visual area, and longer term visual outcome, which were evident on stimulation of either eye, and independent of measures of myelination and neuroaxonal loss in the visual pathways.

A quadrant-specific fMRI stimulation paradigm was used to investigate recovery from visual field defects, finding no evidence for field defect-specific neuroplastic responses.

It was concluded that cortical neuroplasticity appears more important to recovery from ON than was previously thought, and its contribution is independent of measures of tissue damage. This may provide a target for future therapeutic approaches in demyelinating disease.

DECLARATION

I, Thomas Michael Jenkins, confirm that the work presented in this thesis is my own. Where information has been derived from other sources, I confirm that this has been indicated in the thesis. I designed the fMRI paradigm, recruited the patients from clinic, consented all subjects, arranged all visits, performed the clinical examinations, was present for MRI scanning, ran the visual presentation paradigm for the fMRI experiments, gave the gadolinium injections, was responsible for data acquisition and storage, decided on the analysis approach, performed all the data analysis, wrote the thesis and papers, and fed back the results to the patients.

The MRI imaging was performed by the radiographers at the Institute of Neurology and Queen Square Imaging Centre, under the supervision of Dr. Marios Yiannakas and Mrs. Jodee Cooper, who were not aware of the patients' clinical status. The structural and functional MRI sequences were designed by Dr. Claudia Wheeler-Kingshott and Dr. Laura Mancini, respectively. Dr. Mancini also programmed the fMRI paradigm.

The visual evoked potentials were performed by the electrophysiologists at the National Hospital for Neurology and Neurosurgery, under the supervision of Dr. Steve Jones, and were not aware of the patients' clinical status.

The retinal imaging was performed by Dr. Andrew Henderson, who was not aware of the patients' clinical status.

Lesions in the optic nerves and optic radiations were identified by Dr. Katherine Miszkiel, consultant neuroradiologist, who was not aware of the patients' clinical status.

For the statistical analysis, I was advised by Dr. Daniel Altmann and Dr. Constantinos Kallis. In particular, Dr. Altmann assisted with the analysis of age interactions, and Dr. Kallis helped with the longitudinal imaging using lagged variables, both of which are reported in Chapter 5.2.

The concept for the study was derived from work by Dr. Olga Ciccarelli, Dr. Ahmed Toosy and Professor Alan Thompson. Dr. Ciccarelli and Professor Thompson wrote the grant proposal and secured funding from the MS Society for my post.

Dr. Thomas Michael Jenkins

ACKNOWLEDGEMENTS

I would like to thank the following people for their help and support. Firstly, I would like to thank the patients, who volunteered their time during an uncertain and worrying period of their lives. This research relied entirely on their generosity and reliability. I would also like to express my gratitude to the healthy control subjects.

The patients were recruited from Dr. Gordon Plant's clinic at Moorfields Eye Hospital. I would like to thank Dr. Plant for his support of my study and for introducing me to clinical neuro-ophthalmology.

I would like to thank the radiographers at the Institute of Neurology (Ros Gordon, Chris Benton, Kelly Wimpey, Karyn Chappell, Marios Yiannakis and Alaine Berry), and the Queen Square Imaging Centre (especially Robert Brehmer, Jacob Cameron, Triona Dewar and Darren Field) for all their help.

The physicists who helped me with this project were Dr. Claudia Wheeler-Kingshott and Dr. Laura Mancini. I would like to thank them both. Laura helped me a lot, especially at the start when I was trying to get to grips with fMRI, and Claudia provided valuable advice throughout with regard to diffusion tensor imaging.

I would like to thank Dr. Steve Jones for his help organising the visual evoked potentials and for his assistance explaining the technical aspects of electrophysiology, which he continued to do even after retiring.

I would like to thank Dr. Andrew Henderson for performing the retinal imaging, often at short notice, and despite not having slept.

I would like to thank my principal supervisor, Professor Alan Thompson, for giving me the opportunity to work at Queen Square, securing my funding, for his support, guidance, and insights into my work, and for teaching me the value of focus. I would also like to thank Professor David Miller for his thoughtful comments on my papers and for a discussion over Christmas dinner that led to the inclusion of retinal imaging in this study. I would like to warmly thank my secondary supervisor, Dr. Olga

Ciccarelli, for her time, patience, support and laser-like dissections of my papers and thesis chapters, and her tolerance of my occasionally eccentric use of commas. I would like to thank Dr. Ahmed Toosy for helping me understand fMRI, especially when I first started, and throughout my time at the Institute. I would like to thank the MS Society for their financial support of my research.

I would like to acknowledge the help of all the other clinical fellows at the Institute of Neurology, in particular my friends with whom I shared an office: Dr. Zhaleh Khaleeli, Dr. Benedetta Bodini, Dr. Gisele Brasil, Dr. Maria Aguirregomozcorta, Dr. Carmen Tur, Dr. Francesco Manfredonia, Dr. Nikos Gorgoraptis and Miss Olivia Goodkin. I would like to thank them for helpful intellectual discussions, their moral support and for making me laugh. I would also like to acknowledge the help of all the fellows on the 6th floor, especially Dr. Anand Trip, who taught me clinical testing.

Finally, I would like to thank my wife, family and friends. During my final year, when I was working long hours, they provided invaluable support and encouragement, as they have throughout my life. My long-suffering family, Mum, Dad, Megan, Huw and Gwen had their ears bent on many occasions. Most of all, I would like to thank my wife, Michelle. Without her love and support, I could not have completed this thesis.

PUBLICATIONS ASSOCIATED WITH THIS THESIS

Jenkins TM, Toosy AT, Ciccarelli O, Miszkiel KA, Wheeler-Kingshott CAM, Henderson APB, Kallis C, Mancini L, Plant GT, Miller DH, Thompson AJ (2010) Neuroplasticity predicts outcome of optic neuritis independent of tissue damage. Ann Neurol 67:99-113.

Jenkins TM, Ciccarelli O, Toosy AT, Miszkiel KA, Wheeler-Kingshott CAM, Altmann D, Mancini L, Jones S, Plant GT, Miller DH, Thompson AJ (2009) Dissecting structure-function interactions in acute optic neuritis to investigate neuroplasticity. Hum Brain Mapp 31:276-286.

Jenkins TM, Mancini L, Ciccarelli O, Toosy AT, Altmann D, Chappell K, Plant GT, Miller DH, Thompson AJ (2008) Using structural and functional MRI to explain visual loss at the onset of acute optic neuritis (Abstract). Multiple sclerosis 14:S1:276.

Jenkins TM, Mancini L, Toosy AT, Ciccarelli O, Plant GT, Miller DH, Thompson AJ (2008) A quadrant-specific monocular visual functional MRI paradigm designed to minimise attention and loss-of-fixation biases (Abstract) 16th Annual Meeting of the International Society for Magnetic Resonance in Medicine (ISMRM) May 3rd-9th 2008, Toronto, Canada.

Jenkins TM, Mancini L, Toosy AT, Ciccarelli O, Plant GT, Miller DH, Thompson AJ (2007) Quadrant specific visual functional MRI in acute optic neuritis (Abstract). Multiple sclerosis 13:S2:289.

Dowell NG, Jenkins TM, Ciccarelli O, Miller DH, Wheeler-Kingshott CAM (2009) Contiguous slice zonally oblique multislice diffusion tensor imaging: examples of *in vivo* spinal cord and optic nerve applications. J Magn Reson Imaging 29:454-450.

Kolappan M, Henderson APD, Jenkins TM, Wheeler-Kingshott CAM, Plant GT, Thompson AJ, Miller DH (2009) Assessing structure and function of the afferent visual pathway in multiple sclerosis and associated optic neuritis. J Neurol 256:305-319.

Jenkins TM, Thompson AJ (2009) Diagnosing and managing multiple sclerosis. Practitioner 253:25-30.

Jenkins TM, Khaleeli Z, Thompson AJ (2008) Diagnosis and management of primary progressive multiple sclerosis. Minerva Medica 99:141-155.

Jenkins TM, Thompson AJ (2007) GPs have a pivotal role in managing MS. Practitioner 251:37-46.

CONTENTS

LIST OF FIGURES

LIST OF TABLES

ABBREVIATIONS

ABN	Association of British Neurologists
AC-PC	Anterior commissure-posterior commissure
ADC	Apparent diffusion coefficient
Aff	Affected
ATP	Adenosine triphosphate
b	Diffusion weighting factor
b_0	B-zero non-diffusion-weighted image
B_0	Strength of the external magnetic field
BL	Baseline
BOLD	Blood oxygenation level dependent
cd	Candelas
CI	Confidence interval
cm	Centimetre
CNS	Central nervous system
CP	Cerebral peduncle
CRION	Chronic relapsing inflammatory optic neuropathy
CT	Computerised tomography
D	Diffusion coefficient
DT	Diffusion tensor
DTI	Diffusion tensor imaging
EAE	Experimental allergic encephalomyelitis
EDSS	Expanded Disability Status Score

EPI	Echo-planar imaging
ETDRS	Early Treatment Diabetic Retinopathy Study
F	Female
FA	Fractional anisotropy
Fell	Fellow
FLAIR	Fluid attenuated inversion recovery
fMRI	Functional MRI
FOV	Field of view
FS	Functional system
FSE	Fast spin echo
FSL	FMRIB Software Library
FSPGR	Fast spoiled gradient echo
FWHM	Full width half maximum
Fz	Mid-frontal reference electrode in 10/20 VEP system
Gad/Gadolinium	Gadolinium-diethyl-enetriaminepentacetic acid
GE	General Electric
GRE	Gradient recalled echo
HLA	Human leucocyte antigen
HMD	Humphrey mean deviation
hrf	Haemodynamic response function
Hz	Hertz
IFN-β	Interferon-beta
IFN-γ	Interferon-gamma
IFO	Inferior fronto-occipital fasciculus

kΩ	Kilo-ohm
L	Left
LCD	Liquid crystal display
LED	Light emitting diode
LGN	Lateral geniculate nucleus/nuclei
LLQ	Left lower quadrant
LOCs	Lateral occipital complexes
logMAR	Logarithm of the minimum angle of resolution visual score
LUQ	Left upper quadrant
m	Metres
M	Male
MarsBar	Marseille boite a region d'interet
MD	Mean diffusivity
MHC	Major histocompatibility complex
MHz	Megahertz
mm	Millimetres
MNI	Montreal Neurological Institute
MRI	Magnetic resonance imaging
ms	Milliseconds
MS	Multiple sclerosis
mT	MilliTesla
MTR	Magnetisation transfer ratio
n	Sample size
NEX	Number of excitations

NICE	National Institute for Clinical Excellence
NMDA	N-methyl-D-aspartic acid
NMR	Nuclear magnetic resonance
NS	Non-significant
OCT	Optical coherence tomography
ON	Optic neuritis
ONTT	Optic neuritis treatment trial
OR	Optic radiations
PD	Proton density
PE	Parameter estimate
PRISMS	Prevention of relapses and disability by interferon-beta-1a subcutaneously in multiple sclerosis
R	Right
RF	Radiofrequency
RGB	Red, green, blue
RLQ	Right lower quadrant
RNFL	Retinal nerve fibre layer
RR	Interval between consecutive electrocardiographic complexes, used in cardiac gating
RUQ	Right upper quadrant
s	Seconds
S	MR signal in the presence of a diffusion gradient

S_0	MR signal in the absence of a diffusion weighting gradient
SD	Standard deviation
SNR	Signal-to-noise ratio
SOA	Stimulus onset asynchrony
SPIR	Spectral presaturation by inversion recovery
SPM	Statistical parametric mapping
STIR	Short tau inversion recovery
T	Tesla
TE	Echo time
TI	Inversion time
TR	Time to repeat
TNF-α	Tumour necrosis factor alpha
UK	United Kingdom
USA	United States of America
VEP	Visual evoked potential
V1	Primary visual cortex, striate cortex
V2	Secondary visual cortex, prestriate cortex
V3	Third visual complex (extra-striate)
V4	An area of extra-striate cortex, located in the ventral stream of processing, anterior to V2 and posterior to posterior infero-temporal cortex, functions include perception of colour and form recognition

V5/MT	An area of extra-striate cortex, located in the middle temporal gyrus, functions include perception of motion
X	Regressor in a design matrix
Y	Observed data in a design matrix
ZOOM	Zonally magnified oblique multi-slice
β	Parameter estimate in a design matrix
Δ	Time period during which differences in diffusion are detectable (Stejskal-Tanner sequence)
ε	Eigenvector
λ	Eigenvalue
μm	Micrometres
μV	Microvolts
ω_0	Precession frequency
3D	3 dimensional
3M	3 months
6M	6 months
12M	12 months

CHAPTER 1

INTRODUCTION: DAMAGE AND REPAIR IN DEMYELINATING DISEASE

The brain is the most complex organ in the mammalian body and in humans is unique, in evolutionary terms, in developing to the extent that it can be applied to study itself. In recent years, great progress has been made in understanding how the brain works, both in health and disease. Structural changes in the brain result in diverse functional consequences, which are the product of complex interactions between pathology and physiological responses to it. Studies in non-human primates have been vital in clarifying mechanisms underlying damage and repair, but humans are unique amongst primates in many regards, and *in vivo* studies are therefore essential to understand human pathophysiology. When human subjects are studied, it is necessary to use a non-invasive approach, and therefore inferences are sometimes necessarily more indirect. However, by combining knowledge gained from animal studies, human pathological studies and human *in vivo* studies, using techniques such as magnetic resonance imaging (MRI), electrophysiology and optical coherence tomography (OCT), many new insights may be achieved. In the past, it was thought that there was little potential for repair in the central nervous system (CNS) and that the brain was particularly vulnerable to permanent damage. In recent years, it has been appreciated that, in fact, brain repair does occur, and that disease processes constitute a complex, dynamic competition between pathology and physiology to influence clinical function and outcome. *In vivo* techniques have played an important role in elucidating this. Separating the structural and functional aspects of these competing processes, in order to improve our understanding of them, is the main theme of this thesis.

This thesis aims to elucidate mechanisms of damage and repair in demyelinating disease of the CNS, using MRI, electrophysiology and OCT to study the disease model of optic neuritis (ON). Patients were studied during an acute attack of ON and followed up during recovery, over a year, with clinical, electrophysiological and multi-modal MRI assessments. OCT was introduced at 12 months to help quantify residual damage. Chapter 1 introduces the subjects of the human visual system, ON and its investigation to date. Chapter 2 focuses on the physical principles behind MRI and, in particular, quantitative techniques, such as diffusion tensor imaging (DTI) and

functional MRI (fMRI). In Chapter 3, different methods of presenting visual fMRI stimuli are considered and study design problems are discussed. The development of a novel technique used to address these difficulties is described. In Chapter 4, structural MRI and electrophysiology are used to quantify acute damage to the optic nerve, provide insights into the relative contributions of underlying pathological processes, and assess the impact ON has on the rest of the visual pathway. Structural and electrophysiological data are combined with fMRI to dissect structure-function interactions, in order to investigate neuroplasticity during the acute stage of ON, and determine whether it plays a role in modulating acute visual dysfunction. In Chapter 5, longitudinal analyses are reported, investigating mechanisms of long-term recovery in ON and predictors of visual outcome. In Chapter 6, a quadrant-specific visual fMRI technique is applied to explore the role of the fellow eye in brain reorganisation following ON, and to assess mechanisms of resolution of visual field defects. Finally, in Chapter 7, the results are summarised, and conclusions are drawn as to the contribution of this thesis to our understanding of mechanisms of damage and recovery in demyelinating disease, and how this might be applied to help patients. Future research directions are discussed.

Chapter 1 is split into four main sections. The first briefly describes relevant aspects of anatomical organisation and function of the visual system in health. The emphasis then shifts to the effects of disease. In the second section, the topic of ON is introduced and, in the third section, pathophysiological mechanisms underlying *damage* in the condition are discussed. The clinical and para-clinical methods used to investigate ON are considered, including clinical assessment tools, MRI, visual evoked potentials (VEPs) and OCT, and their role in identifying and quantifying pathology. The insights that these techniques have provided in terms of mechanisms of damage are considered. The fourth section considers mechanisms of CNS *repair* in demyelinating disease, and how the recovery process may be assessed, including a discussion of findings from fMRI studies, which have been used to investigate neuroplasticity.

SECTION 1: ANATOMY AND PHYSIOLOGY OF HUMAN VISION IN HEALTH

This section will briefly discuss the elements of normal anatomy and physiology which are directly relevant to later discussions of mechanisms of damage and repair following ON.

1.1.1 Organisation of the afferent visual system

The afferent visual system is composed of four main types of cell: retinal photoreceptors, bipolar cells, ganglion cells (with their axons forming the retinal nerve fibre layer (RNFL), optic nerves, chiasm and tracts) (Figure 1.1), and cell bodies of the lateral geniculate nucleus (LGN) (with their axons forming the optic radiations).

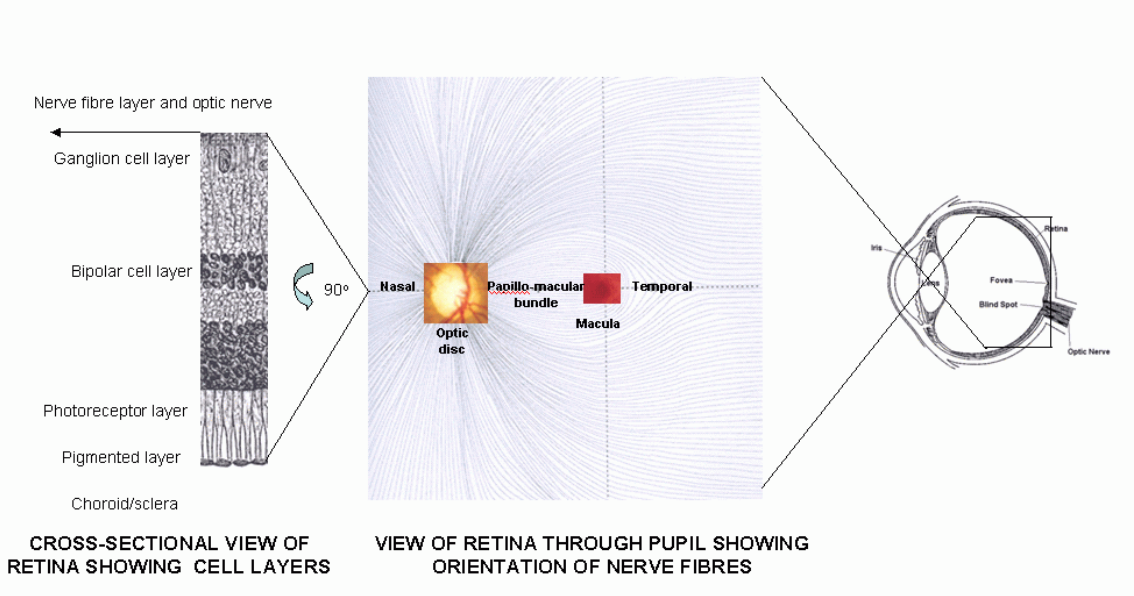

Figure 1.1 Retinal organisation. A coronal view of the retina, as seen through the pupil, is shown, in order to demonstrate the organisation and orientation of fibres in the retinal nerve fibre layer. A cross-sectional view perpendicular to the coronal plane is also shown to demonstrate the cellular layers of the retina. Modified from (Rizzo, 1998).

Photoreceptor cells are located in the retina, comprising two different types: cones and rods. Cones are concentrated around the macula and are specialised for colour vision and fine spatial discrimination in photopic (high light intensity) conditions. There are three types, which each respond to different wavelengths of light, S-cones (blue), M-

cones (green) and L-cones (red). Rods are more numerous than cones and are distributed throughout the retina, except at the macula. They are specialised for scotopic (low light intensity) conditions and motion perception, with lower spatial resolution than cones. Both types of photoreceptor cells synapse within the retina with bipolar cells. The ratio of rod-bipolar synapses is higher than cone-bipolar synapses. Bipolar cells, in turn, synapse with ganglion cells. The axonal processes of the ganglion cells form the RNFL, which then becomes the optic nerve.

The two optic nerves meet at the optic chiasm, where there is a partial decussation (crossing) of nerve fibres. Those supplying the temporal half of the visual field (located in the nasal half of the retina) cross to the opposite side. Fibres supplying the nasal visual field (from the temporal half of the retina) remain uncrossed (Figure 1.2). Posterior to the chiasm the optic nerves become the optic tracts, which synapse in the grey matter of the LGN of the thalamus.

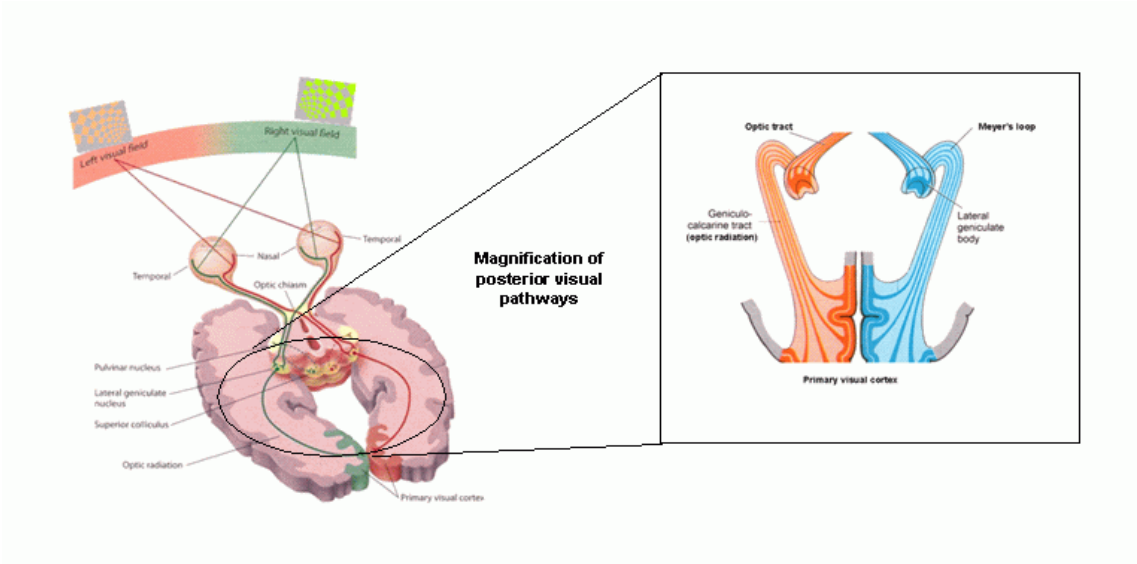

Figure 1.2 A schematic diagram demonstrating the homologous retinotopic organisation of the human visual system. Objects in the right hemi-field stimulate fibres in the right nasal hemi-retina and left temporal hemi-retina. Decussation of the nasal fibres from the right eye results in a representation from both eyes in left occipital cortex. A magnification of the posterior afferent pathway, from the lateral geniculate nuclei to primary visual cortex, is illustrated in inset. Modified from (Kahle and Frotscher, 2003).

There are six layers of the LGN, which are split according to size and function into parvocellular, magnocellular and koniocellular layers. The cells of the parvocellular

system are small and, broadly, are involved in processing colour perception and fine detail. The magnocellular cells are larger and conduct more rapidly, but at the expense of detail. They are involved in processing perception of motion and detection of coarser outlines. Koniocellular cell function is still controversial. They may be involved in integrative function, and perhaps also colour processing. Axons emerge from the cell bodies of the LGN to form the optic radiations.

The radiations sweep forwards into the temporal lobe to form Meyer's loop, before turning posteriorly and terminating in the primary visual cortex of the occipital lobe, also known as striate cortex, or V1. There are six layers of visual cortex and the parvocellular and magnocellular inputs terminate in different sub-divisions of layer 4. Koniocellular input projects to layers 2 and 3.

Visual cortex is organised in a retinotopic fashion, meaning that each point in the visual field corresponds to a given location in cortex. The macular region maps to a relatively large area of cortex in the occipital poles. The temporal hemi-field maps to the contralateral hemisphere i.e. points in the temporal hemi-field of the right eye are represented in the left occipital lobe. Conversely, the nasal hemi-field maps to the ipsilateral hemisphere. Generally, the calcarine sulcus in the occipital lobe separates the upper and lower hemi-fields. The upper hemi-field corresponds to visual cortex below the calcarine sulcus, and the lower hemi-field is represented in supra-calcarine visual cortex.

From primary visual cortex (V1), visual information is then conveyed hierarchically through secondary processing areas to higher order areas, involved in multi-modal integration of sensory input. This occurs via two distinct streams (Goodale and Milner, 1992) (Figure 1.3).

The ventral stream passes from V1 through area V2 in occipital cortex, anteriorly through area V4 and projects to the inferior temporal lobe. It includes the lateral occipital complexes (LOCs), which comprise parts of several different gyri and sulci, namely the lateral and inferior occipital gyri, fusiform gyrus and collateral sulcus. The ventral stream is concerned with recognition and identification of objects within the physical world.

Visual information in the dorsal stream is transmitted from V1 through V2 to the dorsal part of V3 in occipital cortex and then through V5/MT, a motion processing region, before projecting to posterior parietal cortex. This stream is involved in localisation of objects within the physical world and guiding actions in this space. It

was thought that the parvocellular pathway was processed by the ventral stream and the magnocellular by the dorsal stream, but this is now controversial.

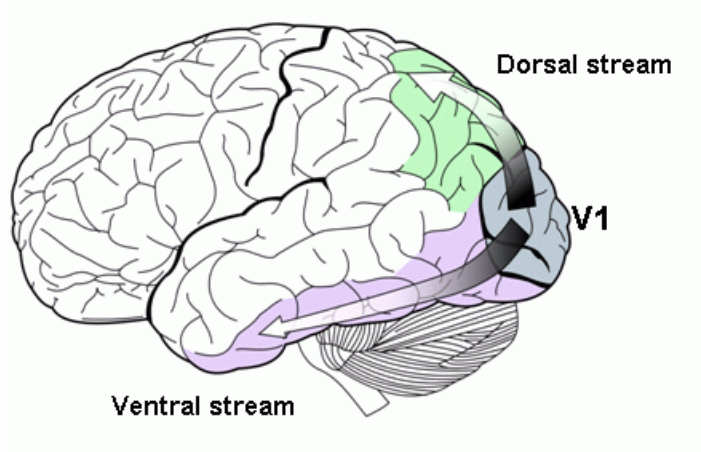

Figure 1.3 The two visual streams of higher visual processing. Modified from (Gray, 1918).

1.1.2 Generation and propagation of neural action potentials

The mechanism of transmission of neural impulses is similar throughout the CNS. A potential difference is maintained across neural cell membranes. The intra-cellular domain is relatively negatively charged, with respect to the extra-cellular domain. This potential difference is maintained by sodium/potassium exchange pumps, which export sodium ions and import potassium ions to the cell. In the resting state, the ratio of ion exchange in unequal, and leads to a net loss of positive charge from the cells.

Depolarisation occurs when the membrane potential becomes less negative. This triggers voltage-gated polypeptide sodium channels, situated in the cell membrane, to open. Once this threshold is reached, there is a rapid influx of sodium into the cell, which causes further depolarisation, and a positive feedback loop is created. The resulting ion currents cause an action potential, which constitutes the nervous impulse. After a short time delay, potassium channels open and potassium ions diffuse out of the cell. This process restores the resting potential and is referred to as repolarisation. During the repolarisation refractory period, the axon is not able to conduct further nerve impulses. Afterwards, the sodium/potassium exchange pump acts to restore the original ion concentration gradients.

Depolarisation in one region of an axon results in changes in the potential difference of adjacent regions and, therefore, the action potential is propagated along the axon.

The speed at which this occurs is dependent on axonal diameter, and the presence of a myelin sheath, produced by oligodendrocytes in the CNS. Axons less than two micrometres (μm) are usually unmyelinated, so conduction relies on the axon's cable properties and is therefore relatively slow. In larger axons, with an insulating myelin sheath, regeneration of action potentials is limited to nodes of Ranvier, areas of axon without a sheath and with a high concentration of sodium channels. This saltatory mode of conduction is much faster.

Coding for stimulus intensity in neurons is frequency modulated. The amplitude of action potentials is constant, as they are all-or-nothing phenomena, so greater intensity stimuli result in increasing frequency of axonal firing. In addition, axons differ in their threshold of depolarisation, so a higher intensity stimulus will activate more axons, a process known as recruitment.

SECTION 2: OPTIC NEURITIS

1.2.1 Optic neuritis as a model for studying demyelinating diseases

ON is defined as inflammation of the optic nerve. Whilst there are many different causes (Hickman et al., 2002b), the term is usually used to describe the most commonly encountered syndrome of acute idiopathic demyelinating optic neuropathy. This may present as an isolated event, a recurrent problem, or be followed later in life by inflammatory events elsewhere in the CNS. If subsequent events occur, which are generally restricted to the optic nerves and spinal cord, this constitutes neuromyelitis optica (NMO) (Wingerchuk et al., 2006). If subsequent events occur which are disseminated in time and space throughout the CNS, this constitutes multiple sclerosis (MS) (McDonald et al., 2001;Polman et al., 2005).

ON is a good model for studying demyelinating diseases, such as MS, because they share clinical and pathological characteristics, the visual pathways are clearly defined anatomically, and visual outcome is more easily quantified objectively than other symptoms, such as sensory or motor disturbance. Therefore, insights into damage and repair derived from the study of ON may be generalised to MS in many cases.

1.2.2 Epidemiology and aetiology

The prevalence and incidence of ON varies across the world and, like MS, becomes more common with increasing latitude. A study from the UK reported a lifetime prevalence of 0.6 per 1000 and an age and sex adjusted incidence of 1 per 100 000 per year (McDonald et al., 2000). A similar study from the USA reported an age and sex adjusted prevalence of 115 per 100 000 and an incidence rate of 5 per 100 000 per year (Rodriguez et al., 1995). A Swedish study reported rather lower age-adjusted overall incidence rates of 1.40 per 100 000 per year (2.28 per 100 000 for females and 0.53 per 100 000 for males) (Jin et al., 1998). This was somewhat surprising, given the high latitude of Scandinavia, but rates were still much higher than for people born outside of Nordic countries, for whom the rate was 0.28 per 100 000 per year. There is a seasonal pattern to the incidence, with rates highest in the spring (Jin et al., 1999).

ON most commonly affects young Caucasian women in their late 20s and early 30s. The mean age of onset is 31 to 32 years (Optic Neuritis Study Group, 1991;Sorensen

et al., 1999), although it is well recognised both in children and the elderly. The female to male ratio is approximately 3:1 (Optic Neuritis Study Group, 1991).

The cause of acute idiopathic demyelinating ON is unknown. As it is often associated with MS, it is thought that the two conditions share a common aetiology. This is probably a complex interaction between genetic predisposition and environmental triggers, which may include infectious agents, vitamin D deficiency and others (Ascherio and Munger, 2007a;Ascherio and Munger, 2007b). There are many rarer inflammatory and infectious causes of ON, which may present in an atypical manner, and have a different natural history, management, and prognosis.

1.2.3 Clinical features

Typically ON presents with subacute painful loss of vision in one eye. The pain is sometimes ill defined at first, but then usually localises in or around one eye. It is commonly worse with eye movements. The severity of the pain varies, but it is unusual for it to disturb sleep, or last longer than a few days.

This is concurrent with, or followed by, a reduction of vision in the same eye. Typical patients' reports of the early stages of visual loss, which indeed were used by patients involved in this study, are: "it is like looking through frosted glass" or "as if there is a smear of Vaseline on my eye". The severity of visual loss is very variable, ranging from minimal blurring to inability to perceive light. Flashes of light on eye movements, called phosphenes or photopsia, may be reported. Visual loss usually progresses over a few days to two weeks, remains at a nadir for a period of days up to two weeks, and then begins to improve. Sometimes, during this period of recovery, patients notice that vision temporarily worsens with a rise in body temperature, for example, after a hot shower or exercise, which is termed Uhthoff's symptom (Selhorst and Saul, 1995). This can also occasionally be the presenting symptom. Pulfrich's phenomenon may also be reported (Slagsvold, 1978). This is an anomalous perception of motion in depth. An example was given by a patient in this study, who had difficulty judging the trajectory of a tennis ball, despite significant improvement in visual acuity.

Clinical signs in the acute stage include reduced monocular visual acuity in 90% of cases (Optic Neuritis Study Group, 1991). Tests of low contrast acuity are sensitive to detecting deficits in the minority of people who have mild visual loss and are

abnormal in 98%. Colour vision is characteristically affected, sometimes more than other aspects of vision, and abnormalities on testing are detectable in 94% in the acute stage. The spectral location of colour deficits varies between patients and no consistent pattern is seen (Schneck and Haegerstrom-Portnoy, 1997).

Visual field defects are detectable in 97% of people (Keltner et al., 1999). Due to the patchy nature of the underlying pathology, a wide variety of defects is possible. The most commonly encountered is a diffuse pattern of visual loss, seen in 48% of cases (Keltner et al., 1993b). Central field abnormality is seen more commonly than peripheral deficit, and peripheral defects may improve more rapidly (Keltner et al., 1999). Isolated central and centro-caecal scotomas occur in 8% (Keltner et al., 1993b). Altitudinal defects are seen in 20% and various other types make up 23%. Chiasmal and retro-chiasmal defects are less frequent, seen in only 3% of people. Incidental abnormalities of the unaffected eye are common (Keltner et al., 1993b;Beck et al., 1993a). Recovery of visual field function is generally good and does not differ between diffuse and localised field defects (Fang et al., 1999).

Nearly all patients with unilateral ON have a relative afferent pupillary defect (Cox et al., 1981), and this was an inclusion criterion in the North American Optic Neuritis Treatment Trial (ONTT) (Optic Neuritis Study Group, 1991), the largest clinical study of ON, from which the symptom prevalences, cited above, were derived. Fundoscopy reveals a swollen disc in 35%, or may be normal, particularly if inflammation solely affects the posterior part of the nerve (retrobulbar ON). The retina is typically normal, except for perivenous sheathing (retinal periphlebitis), which is occasionally seen, and is associated with a higher risk of MS (Lightman et al., 1987). After around six weeks, the optic disc may become pale because of atrophy of the optic nerve.

There appear to be some ethnic differences in the clinical profile. Acutely, disc swelling is more common in Japanese patients than Americans, and pain was less frequent in a Japanese cohort, compared to the patients in the ONTT (Wakakura et al., 1999b).

Recovery usually begins within the first month. In the ONTT, 79% of people had started to improve by three weeks, and 93% by five weeks (Beck et al., 1994). Improvement may continue after this, especially in patients who have been severely affected, in whom recovery is slower, and significant improvements may continue for up to six months. Subtle improvement may still be detectable a year or more after the acute attack, although by this time the patients do not tend to notice changes relevant

to function. Most patients make a good functional visual recovery, improving to a Snellen acuity of 6/12 or better, but around 5%-10% of people fail to recover (Beck and Cleary, 1993). Many more complain of residual symptoms and deficits of acuity, fields, colour vision and, especially, low contrast acuity may be detectable for years afterwards (Frederiksen et al., 1997;Optic Neuritis Study Group, 1997b).

Atypical presentations occur and, whilst these may be seen in demyelinating ON, they can be a marker of a more unusual alternative aetiology. Atypical features include absence of pain, which is seen in 8% of people (Optic Neuritis Study Group, 1991), marked swelling of the nerve with retinal exudates and peripapillary haemorrhages, severe visual loss to no light perception, progression of visual loss or pain for more than two weeks and lack of recovery after three weeks (Beck et al., 2003;Hickman et al., 2002b).

Bilateral ON may occur, either simultaneously or sequentially (Pirko et al., 2004). Simultaneous disease would also be unusual for idiopathic inflammatory demyelination (Hickman et al., 2002b) and may suggest an alternative, more unusual, aetiology.

1.2.4 Diagnosis and association with multiple sclerosis

The diagnosis of ON is essentially clinical, based upon a characteristic clinical presentation, with consistent physical signs, in a patient from the most commonly affected demographic group.

If atypical features are present, further investigations are indicated to exclude differential diagnoses. The choice of investigation would depend upon the clinical features, but might include MRI of the optic nerves, especially to rule out compressive causes of optic neuropathy. Computerised tomography (CT) may help to delineate bony orbital lesions. Blood tests may be indicated if infections, such as syphilis and Lyme disease, or other inflammatory conditions, such as corticosteroid-responsive optic neuropathies due to neuromyelitis optica, sarcoidosis, systemic lupus erythematosis, Behcet's disease, or CRION (chronic relapsing inflammatory optic neuropathy), were suspected. Other differential diagnoses include ischaemic optic neuropathy, toxic neuropathies, Leber's hereditary optic neuropathy, posterior scleritis and retinal disease. Depending on the level of clinical suspicion, further more

specialised investigations, for example cerebrospinal fluid (CSF) examination, may occasionally be required to exclude these conditions (Hickman et al., 2002b).

In typical idiopathic demyelinating ON with recovery, further investigation is not mandatory. Patients are informed of the association with MS. A brain MRI helps to stratify the risk of future inflammatory events, and is generally discussed with patients. If MRI shows radiological evidence of asymptomatic demyelination in the brain, which has been reported in 59% of patients presenting with isolated ON (Beck et al., 1993b), and 70% of clinically isolated syndromes in general (Brex et al., 2002), then the risk of developing MS is higher.

1.2.5 Treatment

At present, no therapy has been shown to improve long-term visual outcome in acute idiopathic demyelinating ON. Corticosteroids shorten the duration of the attack, but do not appear to change the long-term outcome (Beck et al., 1992; Beck et al., 1993c; Kapoor et al., 1998;Wakakura et al., 1999a;Brusaferri and Candelise, 2000). In the UK, they tend to be reserved for patients with atypical features, coincident problems in the fellow eye, if pain is particularly severe, or at the patient's request.

Beta-interferon and glatiramer acetate are established disease-modifying therapies in MS, which are known to reduce the rate of relapses by around a third over two years (IFNB Multiple Sclerosis study group, 1993;Johnson et al., 1995;PRISMS study group, 1998). The indications for their use following a single neurological episode suggestive of MS, such as ON, is still debated. In the USA, disease-modifying drugs are often prescribed after clinically isolated ON if the brain MRI is abnormal, indicating a higher risk of MS (Balcer, 2006). There is evidence that this delays the onset of the disease (Jacobs et al., 2000;Comi et al., 2001;Beck et al., 2002;Kappos et al., 2006;Comi et al., 2008), which is consistent with their known efficacy in preventing a proportion of relapses in established MS. There may be an effect on short-term disability (Kappos et al., 2007), but any long-term benefits are still unclear. In addition, in a significant proportion of patients with ON, no further clinical symptoms emerge for many years, and not all patients with an abnormal brain MRI subsequently develop MS, even after 30 years follow-up (Nilsson et al., 2005).

In the UK, prescription of disease-modifying therapies is regulated by the National Institute for Clinical Excellence (NICE, 2002;NICE, 2003), following guidelines from

the Association of British Neurologists (ABN). Currently, disease-modifying therapies are not used routinely following clinically isolated ON in the UK, as two clinical relapses are required. In 2007, the ABN guidelines were revised to include the development of MS solely on MRI criteria, in the year following a clinically isolated syndrome, as an indication for treatment (ABN, 2007) but, to date, the NICE guidelines remain unchanged. The other treatments licensed in MS, mitoxantrone (LePage et al., 2006;LePage et al., 2008) and natalizumab (Polman et al., 2006;Rudick et al., 2006) are reserved for patients with severe, aggressive disease because of a risk of serious side effects, and do not have a role in the management of clinically isolated ON.

Intravenous immunoglobulin has been tried in patients with persistent visual loss, but this did not result in any clinically significant benefits in randomised trials (Noseworthy et al., 2001;Roed et al., 2005).

1.2.6 Prognosis

1.2.6.1 Visual prognosis

The majority of people with idiopathic ON make a good visual recovery, even if visual loss is initially severe (Slamovitis et al., 1991;Beck et al., 1994). Improvement usually begins in the first month. Outcome at six months is associated with the degree of initial visual loss (Beck et al., 1994), and with vision at one month (Kupersmith et al., 2007). One year later, 95% of people have improved to Snellen 6/12 or better (Beck and Cleary, 1993), equivalent to logMAR score 0.3 or Snellen USA 20/40 (see Appendix I). After five years, 28% of people in the ONTT had had a further attack, but 87% still had acuities of 6/8 or better, 94% 6/12 or better and 97% 6/60 or better (Optic Neuritis Study Group, 1997b). Ten years later, 74% had a visual acuity of 6/6 or better, and 92% and 97% still had acuities of 6/12 and 6/60 or better, respectively (Beck et al., 2004a). Recently, the 15 year final follow-up results were reported, and 72% of patients still had acuities of 6/6 or better (Optic Neuritis Study Group, 2008a). However, many patients who are able to score well on the Snellen chart still have residual deficits of low contrast acuity, colour vision and visual field defects (Fleishman et al., 1987). Most patients report that their vision is not quite as good as it was before (Cleary et al., 1997).

1.2.6.2 Neurological prognosis

The risk of developing MS depends predominantly on the length of follow-up, and whether the brain MRI at the time of presentation was normal. Five years after an attack of ON, 16% of people with a normal brain MRI had developed MS, compared with 51% of people who had three lesions or more (Optic Neuritis Study Group, 1997a). Ten years after onset, in the same cohort, the risk was reported as 22% if the initial MRI was normal, increasing to 56% if it was abnormal (Beck et al., 2003). Female gender, absence of optic disc swelling and absence of atypical features were all associated with a higher risk profile. Other studies have reported retinal vascular abnormalities (Lightman et al., 1987), HLA-DR2 genotype (Hauser et al., 2000) and the presence of oligoclonal bands in the CSF (Cole et al., 1998) as additional risk factors. Fifteen year follow up of the ONTT cohort subsequently reported conversion rates of 25% with a normal MRI, and 72% with an abnormal MRI (Optic Neuritis Study Group, 2008b). The longest reported follow-up is from a Swedish study, which found an overall 40% conversion rate after 31 years (Nilsson et al., 2005).

A different study assessed people with a variety of clinically isolated syndromes, 14 years after the acute attack (Brex et al., 2002). More than half of the patients had presented with ON, and the remainder had transverse myelitis or brainstem syndromes. The authors reported conversion rates of 19% in people who had a normal MRI at baseline, increasing to 88% if the scan was abnormal.

If MS does subsequently develop, it is said to generally follow a more benign course if ON is the presenting symptom, rather than pyramidal or cerebellar symptoms. In the ONTT, 65% of people had an Expanded Disability Status Score (EDSS, see Appendix II) of 3.0 or less ten years later (Beck et al., 2004b). However, in this study a significant number did less well. Fourteen percent had severe disability (EDSS of 6 or more), and 2/127 patients unfortunately died as a result of complications of MS.

1.2.6.3 Impact of optic neuritis

Therefore, whilst most people have a favourable visual and neurological prognosis following ON, a significant proportion of patients will follow a less benign course. Moreover, acute idiopathic demyelinating ON is common, and thus these small percentages actually represent a large number of people, in whom visual impairment

has a significant impact on their quality of life (Noble et al., 2006). At present, it is not possible to predict with certainty which patients will recover poorly, as the mechanisms of damage and recovery are incompletely understood. For those people who fail to recover, there are at present no effective treatments. Therefore, a better understanding of these mechanisms is important in enabling accurate prognostication, and to devise better treatments in the future, and that is the goal of this thesis.

SECTION 3: DAMAGE

1.3.1 Immunopathology of optic neuritis

Evidence from experimental and pathological studies of MS indicates that inflammation, demyelination and axonal damage are important disease mechanisms (Lassmann et al., 2007). However, there are relatively few studies that focus specifically on the pathology of ON. As the optic nerve is part of the CNS, it is thought that the pathology of the optic nerve lesion in MS is the same as in the brain. Therefore, much of the available data on the optic nerve lesion is extrapolated from brain studies.

In general, the demyelinating lesion develops on a background of inflammation, thought to be of autoimmune origin (Hohlfeld and Wekerle, 2004). There is breakdown of the blood-brain barrier, followed by infiltration of the tissue with lymphocytes and activated macrophages and microglia (Lassmann et al., 2007). The lymphocytes are predominantly MHC Class 1 restricted CD8+ T-cells, with relatively few CD4+ cells (Hayashi et al., 1988). MHC Class 1 antigens are expressed within MS lesions on inflammatory cells, neurons and glia (Hoftberger et al., 2004). Pro-inflammatory cytokines and chemokines are released. B-cells and plasma cells may also be seen. Demyelination occurs, accompanied by a variable degree of axonal damage. Transection of axons may occur (Trapp et al., 1998) and lead to Wallerian degeneration (Waller, 1850). This term describes the secondary effects of damage to an axonal segment, in which the initial injury results in anterograde degeneration of the remaining axon distal to the lesion, with respect to the neuron cell body. This is in contrast to retrograde degeneration, which may also occur and, in this case, secondary damage proceeds along the proximal segment of axon, towards the cell body.

Recently, four distinct patterns of demyelinating lesion have been described in the brain in MS (Lucchinetti et al., 2000). Inflammation is prominent in types 1 and 2, associated predominantly with T-cells and macrophages in type 1 lesions, and with both T and B-cells, with accumulation of immunoglobulins and complement, in type 2. Type 3 and type 4 lesions appear different, in that inflammation is not as marked. Instead, there is evidence either of a pattern of damage similar to that seen in ischaemic stroke, with hypoxic injury secondary to mitochondrial dysfunction, as a

result of production of nitric oxide and oxygen free radicals, or of primary oligodendrocyte degeneration in the white matter surrounding plaques.

Evidence from other sources, such as *in vivo* MRI studies (Youl et al., 1991), indicates that inflammation is prominent in ON, as seen in Type 1 or 2 lesions but, to date, the relative prevalence and importance of different pathological subtypes in ON is unknown.

Another relatively recent development is an increasing appreciation of the role of sodium channels in contributing to permanent axonal damage, which is thought to be especially important in accumulation of disability. For years it has been recognised that pathological effects on sodium channels are important in producing symptoms in MS (Smith, 2007). When demyelination occurs, long segments of axon are left between the nodes of Ranvier, which have a low density of sodium channels (Ritchie and Rogart, 1977) and are relatively inexcitable, resulting in conduction block (Waxman, 1977). In addition, there is evidence that factors associated with an inflammatory response may affect axonal function through direct effects on sodium channels, independent from demyelination, for example, antibody binding (Waxman, 1995) or through mediators, such as nitric oxide (Redford et al., 1997). Nitric oxide inhibits mitochondrial function (Bolanos et al., 1997), reducing production of adenosine triphosphate (ATP). ATP provides energy for sodium-calcium exchange pumps, present on axonal membranes. Axons which pass through inflammatory lesions, where nitric oxide abounds (Smith and Lassmann, 2002), may therefore become relatively ATP-deficient. This may make them vulnerable to energy demands associated with sustained impulse activity (Smith et al., 2001), and prone to failure of sodium homeostasis. The resulting rise in intra-axonal sodium concentration may eventually result in reversal of the exchange pump, culminating in a lethal influx of calcium ions which kills the axon (Stys, 1998). This mechanism of axonal damage is thought to be important in MS and, therefore, may be important in ON too.

Of the few pathological data looking specifically at the optic nerve, most are derived from post-mortem studies of patients with established MS. A study from 1950s demonstrated retinal atrophy, temporal optic atrophy, with glial cells within the optic nerve and disc, and abnormal sclerosed blood vessels at the disc (Gartner, 1953).

In the 1980s, a post-mortem study of patients with MS found that lesions of the visual pathway were common. They examined the optic nerve lesions and reported that the

lack of correlation between visual acuity and extent of demyelination in the optic nerve might be due to axonal loss (Toussaint et al., 1983).

More recently, a post-mortem study focused on the anterior visual pathways, from optic nerve to LGN, comparing patients with MS to control subjects (Evangelou et al., 2001). Patients had smaller optic nerves due to reduced axonal density, and the parvocellular cells of the LGN were particularly affected. The authors concluded that the disease process affecting the nerves was size-selective, affecting smaller diameter axons preferentially, and also that there was evidence for trans-synaptic degeneration, as the cells of the LGN were involved. Trans-synaptic degeneration differs from Wallerian and retrograde degeneration, in that it describes a mechanism of secondary damage that affects neurons and axons which were not damaged directly by the initial pathological insult. Instead, the damage occurs later, to other neurons in the tract, connected to the damaged axon through synapses. This was one of the first studies to consider the effects ON had on more distant parts of the visual pathway, an aspect of pathology which was subsequently further investigated *in vivo*, using MRI (Ciccarelli et al., 2005;Audoin et al., 2006).

In addition to human post-mortem studies, animal disease models have been used to help understand pathology. The animal model of MS is experimental allergic encephalomyelitis (EAE) (Rivers et al., 1933), and a variant exists which causes an ON (Rao et al., 1977). These models have been extremely important tools with which to study the pathology and immunology of MS, but there are some concerns that the disease process differs significantly in animals and humans, and indeed therapies that have been effective in EAE have not always proven effective in MS (Gold et al., 2006). Nonetheless, animal models continue to provide important insights into the nature of demyelinating disease, and there have been a few studies which have looked specifically at the optic nerve.

In one study, pathological features were correlated with MRI features in guinea pigs with EAE (Guy et al., 1992a). There was early electron microscopic evidence of expansion of the extracellular space and an inflammatory cell infiltrate, within three days of sensitising the animals to antigen. Inflammation started at the globe and progressed towards the orbital apex, involving longer segments of nerve around 10 to 14 days, and persisting at 30 days.

In a different study in guinea pigs, infiltration of the optic nerve with lymphocytes was seen, with multiple areas of demyelination (Rao et al., 1977). Inflammatory cell infiltrates were also observed in rhesus monkeys, together with extensive demyelination and axonal damage (Hayreh et al., 1981). A more recent study used a different technique to induce local demyelination in rat optic nerve, without first causing inflammation (Zhu et al., 1999). The authors reported cytoskeletal changes within demyelinated axons, with disassembly of neurofilaments and microtubules, and abundant macrophages. They suggested that acute demyelination might itself induce the axonal cytoskeletal changes, and that inflammation could then further damage the axons.

A recent study described conduction block in the optic nerves of rats, induced by CSF from patients with MS. This was possibly due to an effect of soluble mediators, leading to a blockade of sodium channels (Centonze et al., 2005).

1.3.2 Relation of pathology to clinical features of damage

When trying to understand demyelinating diseases, it is important to consider how pathological processes translate into clinical symptoms in people. In general, acute neurological symptoms can be classified into negative or positive symptoms. Negative symptoms relate to loss of function, whereas positive symptoms reflect excessive function.

The main positive symptom in acute ON is pain, which is probably due to the effects of inflammation within a closed space, such as the orbit and, particularly, the optic canal (Fazzone et al., 2003). Phosphenes are also reported. These visual phenomena are thought to be due to the spontaneous generation of trains of action potentials in hyperexcitable, demyelinated axons, similar to the mechanism of paraesthesia in MS (Smith and McDonald, 1980;Smith and McDonald, 1982). This hyperexcitability may be due to abnormal ion currents (Kapoor et al., 1993;Kapoor et al., 1997), generated through redistribution of sodium and potassium channels.

The main negative symptom in acute ON is loss of vision. Acutely, the mechanism underlying this can be split into two parts, reflecting different aspects of linked pathology: the effects of demyelination and the effects of inflammation. Visual deficits may be associated with neuroaxonal loss, which is also considered in the following sections.

1.3.2.1 Demyelination

Loss of vision is due to loss of conduction in the optic nerve. An important cause of this is axonal conduction block, and there is extensive evidence that demyelination can cause conduction block. The block is localised to the affected segment of axon, and conduction in unaffected segments is usually considered to be normal (McDonald and Sears, 1969). The conduction block caused by this segmental demyelination lasts for several days (McDonald and Sears, 1970). In addition, lesser degrees of demyelination can still cause block, if they occur adjacent to nodes of Ranvier and increase the inter-nodal gap (Smith, 1994;Smith and McDonald, 1999a). This widening of the gap leads to dispersion of the electrical current over a more diffuse area of axon, and increases the electrical capacitance of the node (i.e. the ability of the node to hold an electrical charge). The latter effect reduces the safety factor for conduction, by increasing the current necessary for depolarisation. The safety factor is the ratio of the current usually used to depolarise a node, compared to the minimum current necessary. In normal axons it is between three and five. In demyelinated axons the safety factor is close to zero, which results in small environmental changes having a noticeable effect on conduction.

During recovery, conduction is restored to demyelinated axons. However, frequently conduction remains abnormal and is prone to failure and block. This effect may be expressed clinically, for example, Uhthoff's symptom, when a small rise in body temperature causes temporary conduction block in demyelinated axons with critical safety factor thresholds. Remodeling of the demyelinated axon occurs over time, and involves redistribution of sodium channels (Smith, 2007).

1.3.2.2 Inflammation

In ON, there is an influx of inflammatory cells, which release cytokines. Some of these cytokines, such as interferon-gamma (IFN-γ) and tumour necrosis factor alpha (TNF-α), may play a role in causing conduction block (Moreau et al., 1996). Both IFN-γ and TNF-α stimulate the formation of inducible nitric oxide synthetase, which leads to high levels of nitric oxide, known to occur in MS lesions (Bo et al., 1994). Nitric oxide blocks axonal conduction, through effects on sodium channels (Li et al., 1998) and mitochondrial energy production (Bolanos et al., 1997). It may also impair

synaptic transmission, along with other pro-inflammatory cytokines, such as interleukins. Inflammatory cytokines may also result in activation of glial cells (Chao et al., 1995), which may also exert toxic effects, perhaps mediated through production of free radicals. It is of note that the temporal course of early visual recovery in ON is consistent with resolution of inflammation.

In summary, loss of vision in acute ON reflects conduction block, and it appears that both demyelination and inflammation contribute to this.

1.3.2.3 Neuroaxonal loss

Optic atrophy, which is thought to reflect mainly loss of axons in the optic nerve and the associated retinal ganglion cells, usually ensues in the weeks following acute ON. Neuroaxonal loss appears to be a substrate of residual visual deficit in ON. The mechanism underlying acute axonal damage is complex, and has been elucidated in the brain. Reversible conduction block may be induced by nitric oxide in normal rat axons (Redford et al., 1997). Following more prolonged exposure to inflammatory mediators (Smith et al., 2001), a more destructive sequence of events follows, with nitric oxide acting directly and indirectly on neuronal N-methyl-D-aspartic acid (NMDA) receptors (Golde et al., 2002), and involving glutamate excitotoxicity (Pitt et al., 2000). Activated microglia release factors which impair cytochrome oxidase function in mitochondria (Dutta et al., 2006), resulting in energy failure and altered ion exchange mechanisms across the axonal cell membrane. Energy failure is exacerbated by the spread of sodium channels away from the node of Ranvier, across the exposed demyelinated axonal cell membrane, with sodium influx into the cell. This is extruded by the exchange pump, resulting in a further increase in the metabolic load (Howell et al., 2006). Loss of trophic support by oligodendrocytes and myelin contributes to neuroaxonal loss, which has been shown *in vitro* to be dependent on insulin-like growth factor (Wilkins et al., 2001) and glial cell-derived nerve growth factor (Wilkins et al., 2003). These factors modulate the direct effects of nitric oxide on axons (Wilkins and Compston, 2005). The end result is axonal damage, although whether inflammation *per se* is important in causing ongoing neuroaxonal loss is still debated (Compston and Coles, 2008).

Patients with residual visual loss following acute ON often have evidence of axonal loss, but so do patients who recover well. Therefore, it appears that other factors may also be important in determining the clinical outcome.

1.3.3 Assessment of damage using clinical tests

The following sections will now consider how damage is identified and quantified in ON. Several clinical and paraclinical tools are available, for example, physical examination, electrophysiology, MRI imaging and OCT (a recently developed technique which allows visualisation and measurement of the RNFL and macula). Each of these methods provides a different perspective on an aspect of pathophysiology.

This discussion will begin with a brief description of commonly used clinical examination techniques. The aim of these tools is to enable accurate and reproducible quantification of visual function, in a standardised manner. Different tools aim to capture different aspects of clinical function, for example, central, peripheral or colour vision. The use of these tools allows generation of continuous data, which facilitate correlation with paraclinical variables in subsequent statistical analyses.

1.3.3.1 Visual acuity

Whilst the most commonly used measure of visual acuity in clinical practice has traditionally been the Snellen chart, logMAR scoring, using a retro-illuminated Early Treatment Diabetic Retinopathy Study chart (ETDRS investigators, 1991), is now often preferred in research studies. LogMAR represents the four metre logarithm of the minimum angle of resolution, and the scoring system provides a continuous statistical variable. LogMAR scores may be directly converted to Snellen scores of both UK and USA convention, and these scoring systems are used interchangeably in visual studies. A conversion table is provided in Appendix I.

The chart appears similar in style to a Snellen chart, but offers several advantages. There are an equal number of letters per row, the letters are equally spaced, and letters on each row are balanced for difficulty. The task is therefore of equal difficulty on each line, with the size of letters the only variable.

1.3.3.2 Low contrast acuity

Low contrast acuity is more sensitive than standard contrast acuity in detecting visual dysfunction in ON, especially in mild cases, or following recovery (Trobe et al., 1996). Several different measurement techniques are available. In the past, rear-illuminated sine wave gratings were commonly used, such as the Arden grating (Arden and Gucukoglu, 1978), in which the observer was required to make a choice, for example, regarding the orientation of the gratings at different contrasts. In research practice, charts are now more commonly used, such as the Pelli-Robson (Pelli et al., 1988) test or Sloan charts (Ferris, III et al., 1982). In the Pelli-Robson test, all letters are the same size, and contrast progressively decreases in each group of three letters across the chart. This was the method used to test low contrast acuity in the ONTT. Sloan charts appear similar in style to the ETDRS, but consist of several charts of progressively lower contrast, for example, 100%, 25%, 5%, and 1.25%. High measurement reproducibility has been demonstrated (Balcer et al., 2000). Low contrast charts have been used to detect visual dysfunction in MS (Baier et al., 2005), and it has been suggested that they should be included in composite disability scales (Balcer et al., 2003).

1.3.3.3 Colour vision

In clinical practice, Ishihara plates are frequently used (Ishihara, 1917). These consist of a set of chromatic plates in which it is necessary for the observer to distinguish between two different colours, in order to identify a camouflaged number.

In research practice, the more comprehensive Farnsworth-Munsell 100-hue test (Farnsworth, 1943) is often used. In this test, the subject places 85 coloured caps in order of perceived hue, and an error score is calculated. Sensitivity is increased, compared with the Ishihara plates (Optic Neuritis Study Group, 1991), dyschromatopsia may be more accurately quantified, the data is normally distributed, and the spectral location of any deficits may be determined.

1.3.3.4 Visual fields

The visual field may be measured quantitatively, using static targets with Humphrey perimetry, or qualitatively, using kinetic targets with the Goldmann method. Both techniques were applied in the ONTT.

The Humphrey perimeter is fully automated. Different programmes are available, but usually the central 30 degrees of the field are tested using a grid spaced six degrees apart. The subject is asked to respond to luminant stimuli, presented at different points in their visual field, by pressing a button. The size of the target stimulus is constant and the luminance is varied several times at each location, in order to determine the minimum luminance detectable. Randomised repeat testing is performed to estimate reliability. False positive and negative rates, and the number of fixation losses, are reported. Scores at each point in the visual field are calibrated with control data, in order to estimate the deviation from normal.

During Goldmann perimetry, a trained operator maps the field by moving a target from the periphery to the central field. The subject indicates when they can detect it. The luminance of the stimulus remains constant and targets of different sizes are used. The output is a qualitative map of the visual field to stimuli of different sizes.

In both techniques, standardisation and optimisation of the test procedure is important to ensure reproducibility (Keltner et al., 1993a).

1.3.3.5 Conclusions

There is a wide choice of clinical assessment tools available for research studies, with different advantages and disadvantages. The choice of which to use is often a balance between obtaining maximum information in the minimum time, so that testing is acceptable to patients. For this study, logMAR acuity, Sloan charts, the Farnsworth-Munsell 100-hue test and Humphrey perimetry were chosen.

1.3.4 Assessment of damage using structural MRI

The following sections will now consider paraclinical methods of assessing and quantifying damage in ON, beginning with MRI.

The development of MRI in the 1970s and 1980s (Lauterbur, 1973) allowed detailed *in vivo* imaging of CNS pathology in humans. This section will summarise the insights that structural MRI techniques have provided in understanding damage mechanisms in ON to date. A more detailed description of the principles underlying the various MRI techniques will follow in Chapter 2.

1.3.4.1 Identification of the optic nerve lesion

The optic nerves are difficult to image with MRI as they are small, mobile and surrounded by fat, CSF and air filled sinuses. The first study to overcome these challenges, and identify the optic nerve lesion, was performed in 1988 (Miller et al., 1988a). A technique to suppress intra-orbital fat was used (short tau inversion recovery, STIR), and the lesion was identified as a region of high signal within the nerve on T2-weighted images. Thirty seven people with a recent or past history of ON were imaged, and high signal was seen in 84% of symptomatic, and 20% of unaffected, nerves. The average length of lesion was around 1cm, and slow or poor visual recovery was associated both with longer lesions, and lesions occurring within the bony optic canal.

Two new techniques for suppressing fat were subsequently developed: SPIR (spectral presaturation by inversion recovery) and fat-suppressed fast spin-echo (Tien, 1992;Gass et al., 1996), which had the advantages of shorter acquisition time and higher resolution. However, the presence of CSF continued to cause difficulties, until a fluid-attenuated inversion recovery (FLAIR) technique was developed to suppress this signal too (Jackson et al., 1998). The new technique improved sensitivity further and demonstrated that lesions were more longitudinally extensive than previously recognised. Recent research studies have used these fat suppressed fast spin-echo techniques to quantify optic nerve lesion length in ON (Hickman et al., 2004c).

The observed changes in T2 signal in all of these sequences are due to changes in tissue water content and are thought to be non-specific, reflecting a mixture of oedema, inflammation, demyelination, axonal damage and gliosis (Barkhof and Van Walderveen, 1999). MRI correlates with pathology have been inferred from post-mortem imaging studies and animal models of MS (Stewart et al., 1984;Stewart et al., 1985). One animal study, focusing on the optic nerve, demonstrated a correlation between T2 signal characteristics and the extent of demyelination (Guy et al., 1992a),

and a human *in vivo* study found that optic nerve lesion length on MRI correlated with latency of VEPs (Davies et al., 1998).

In humans, high signal present during the acute phase persists following recovery. In fact, the length of the T2 lesion *in vivo* in humans may increase following an acute episode of ON, which may be due to extension of the primary demyelinating lesion, or to Wallerian degeneration (Hickman et al., 2004c). The lesion length may correlate with visual acuity (Miller et al., 1988a;Thorpe et al., 1995). With conventional T2-weighted imaging, it is not possible to distinguish the different aspects of pathology as they evolve.

1.3.4.2 Gadolinium enhancement and breakdown of the blood-brain barrier

In the early stages of inflammation of the CNS, cells gain access to the brain from the peripheral circulation. In health, this is prevented by interactions between the endothelial lining of blood vessels and astrocytes within the brain. At the start of a neuroinflammatory response, this blood-brain barrier becomes leakier, and immune cells enter the brain. An important development in MRI was the discovery that this process could be imaged *in vivo* using contrast agents, such as gadolinium-diethyl-enetriaminepentacetic acid (Grossman et al., 1986;Miller et al., 1988b;Hawkins et al., 1990;Katz et al., 1993). Gadolinium enhancement has been shown to correlate with the extent of inflammation in animal models, and it precedes T2 abnormalities (Guy et al., 1992a). As the optic nerves are part of the CNS, breakdown of the blood-brain barrier, indicating active inflammation, can be imaged in ON.

In the first study to demonstrate this, gadolinium enhancement was seen in 13/13 acutely symptomatic optic nerves, and was associated with worse vision, and reduced amplitude and increased latency of VEPs (Youl et al., 1991). After a mean period of 34 days, enhancement ceased in 9/11 lesions and, at the same time, vision and VEP amplitude improved. The authors concluded that contrast-enhanced MRI reflected inflammation, which must play an important role in the production of acute clinical deficit and electrical conduction block because, as it resolved, vision and electrophysiological parameters improved.

These findings were confirmed in other small studies (Guy et al., 1992b;Tien et al., 1991). A larger study of 107 patients reported 94% sensitivity for lesion detection in acute ON, with no unaffected nerve enhancing, and visual function was found to

correlate with enhancing lesion length (Kupersmith et al., 2002). Lesions longer than 17mm were associated with worse acute visual loss.

The use of triple-dose gadolinium increased sensitivity further to 96% (Hickman et al., 2004c). In this study, the median duration of enhancement was 63 days, and was related to the initial lesion length. The length of the optic nerve lesion was again associated with the degree of acute visual loss.

Together, the length of the gadolinium-enhancing segment and T2 lesion length provide a useful measure of the severity of structural damage caused by ON, and both were applied to the patients studied in this thesis.

1.3.4.3 Optic nerve swelling and atrophy

Inflammation is associated with oedema and, during the acute stage of ON, swelling of the optic nerve has been detected. A longitudinal study, using a fat-saturated FLAIR sequence (Hickman et al., 2001), demonstrated that the mean area of the intra-orbital segment was 16.1mm^2, compared with 13.4mm^2 for unaffected nerves, and 13.6mm^2 for control optic nerves (Hickman et al., 2004a). The measurements were made after a median delay of 13 days from onset of visual symptoms. Over time, swelling evolved to atrophy, with a mean area of 11.3mm^2 at 12 months. More swollen nerves were associated with worse acute visual loss, but not with the eventual degree of atrophy or visual function one year later. In addition, in this study, there was no correlation between optic nerve atrophy and visual outcome at 12 months.

Other studies have found correlations between atrophy and visual outcome, but generally these have been modest (Hickman et al., 2002a;Inglese et al., 2002). This is of interest, as atrophy is thought to predominantly reflect axonal loss, with a smaller contribution from myelin (Miller et al., 2002). Axonal loss in other regions of the brain in MS correlates with disability. Several hypotheses have been postulated to explain this discrepancy between tissue loss in the optic nerve and clinical function. These include confounding associations, such as a detrimental effect of pathology in the posterior visual pathways on acuity, or a contribution from gliotic tissue to increase the area of the optic nerve. Neuroaxonal redundancy in the optic nerve has also been suggested, in which it is hypothesised that the axons of the optic nerve are able to maintain clinical function, despite loss of nerve fibres, up to a critical threshold, as a result of tissue reserve. Lastly, an alternative hypothesis is that

compensatory changes in grey matter processing of visual input may contribute to clinical recovery. This will be discussed in more detail later. To date, the relative importance of each of these mechanisms is still unclear, and this is one of the key questions that this thesis aims to answer.

1.3.4.4 Magnetisation transfer imaging and myelination of the optic nerve

Magnetisation transfer ratio imaging (MTR) is an MRI technique that can quantify constituents of the optic nerves, by measuring magnetisation exchange between free water protons and those bound to macromolecules. These include myelin and axonal membranes. MTR is higher in white matter than grey matter, and is usually interpreted as reflecting myelin content, although it is probably not entirely specific (Wolff and Balaban, 1989). Whilst MTR was not applied to the patient cohort described in this thesis, previous studies using this modality have provided relevant insights into demyelination and remyelination following ON, and these will be briefly summarised.

Most studies have found reduced MTR in affected optic nerves, both during the acute stage (Boorstein et al., 1997) and later (Thorpe et al., 1995), suggesting demyelination. However, clinico-electrophysiological correlations have not always been consistent between studies. For example, in this latter study, MTR correlated with prolonged VEP latency, another marker indicating demyelination, but no correlation with visual acuity was found. However, another group compared optic nerve MTR in patients classified according to good or poor recovery (Inglese et al., 2002). They found lower MTR values in those with poor recovery, but no correlation with VEP latency.

One small study actually found increased MTR in the very early stages after the acute attack, before a subsequent fall (Melzi et al., 2007). The authors suggested that this could be due to inflammatory cell infiltrates present during the acute stage.

Another cross-sectional study selected patients with poor visual recovery, and found correlations between MTR and a thinner RNFL, measured using OCT (Trip et al., 2007). There was also an association with VEP latency in this study, suggesting that a relationship exists between MTR and both axonal loss and demyelination. The investigators also reported reduced MTR in unaffected nerves, compared with controls, suggesting that subclinical demyelination may occur in the fellow eye.

A longitudinal study traced MTR over time in a group of patients following acute ON (Hickman et al., 2004b). At baseline, there was no difference between patients and controls, but MTR fell over eight months to reach a nadir, before starting to increase again at 12 months (although the increase was not statistically significant). Time-averaged MTR was lower in patients than controls. This study found complex interactions between MTR, visual function and time, with no clear linear relationships, either at baseline or one year. However, eventual visual recovery was better in patients with higher time-averaged ratios of diseased to healthy MTR. In addition, patients with lower time-averaged MTR had more prolonged VEP latencies. Therefore, it appeared that demyelination progressed over months after the initial insult, before beginning to recover, but there was not a clear relationship between the myelin status of the optic nerve and visual function at any given time-point. This is another example of the dissociation between markers of tissue damage and clinical function, which is investigated in this thesis.

1.3.4.5 Diffusion tensor imaging, optic nerve integrity and axonal loss

Diffusion tensor imaging (DTI) is a quantitative MRI technique, which is sensitive to tissue microstructure as a result of the diffusion behaviour of water molecules. It allows assessment of the integrity of white matter tracts, including the optic nerve. Parameters such as apparent diffusion coefficient (ADC), mean diffusivity (MD) and fractional anisotropy (FA) may be derived, which reflect fibre coherence. DTI was applied to the optic radiations of the cohort investigated for this thesis, but has also been applied to the optic nerve in recent studies, although this is technically challenging, and requires a long scan time. Optic nerve DTI is relevant to this thesis, in terms of future directions, so a brief discussion of current progress follows.

An early study found increased ADC, suggesting reduced tissue integrity, in chronic, but not acute, ON (Iwasawa et al., 1997). In acute ON, the ADC was actually less than in controls, which may have been secondary to infiltration of inflammatory cells and oedema, resulting in restricted diffusion.

A new technique, named ZOOM-EPI, was subsequently developed, which improved resolution (Wheeler-Kingshott et al., 2002). ADC was again found to be higher in patients with previous ON than in unaffected nerves and controls (Hickman et al.,

2005). This study also found that ADC correlated with clinical measures, and modestly with lesion length, but not with optic nerve area.

Following further optimisation of the sequences to allow rotationally invariant measures to be obtained, such as MD and FA (Wheeler-Kingshott et al., 2006), DTI was applied to an ON cohort selected for poor recovery (Trip et al., 2006b). MD was increased and FA reduced in affected nerves, consistent with reduced fibre coherence. This correlated with smaller VEP amplitudes, and probably reflected axonal loss, although demyelination and gliosis could also have contributed. There was no association between DTI parameters and clinical scores in this study.

A more recent study confirmed that optic nerve FA four years after acute ON correlated with VEP amplitude, but found no association with atrophy of the nerve on MRI (Kolbe et al., 2009).

1.3.4.6 Impact of optic neuritis on the optic radiations

In clinically isolated ON, there are frequently incidental lesions of the optic radiations (Hornabrook et al., 1992). These may sometimes affect vision, especially if they are large (Plant et al., 1992). In patients with MS, visual psychophysical deficits have been correlated with lesion load in the post-chiasmal pathways (Caruana et al., 2000). In addition, lesions in the optic nerve could potentially have effects on other parts of the visual pathway, either through retrograde, Wallerian, or trans-synaptic degeneration (Evangelou et al., 2001).

To date, there has been only one study focused on the effects of an attack of ON on the optic radiations. The authors used DTI-based tractography to reconstruct the white matter tracts *in vivo*, in a group of patients one year after the acute episode (Ciccarelli et al., 2005). It was found that connectivity scores were reduced in the optic radiations. They showed that the reduced connectivity could not be fully explained by incidental lesions, and hypothesised that it could be due to trans-synaptic degeneration.

1.3.4.7 Impact of optic neuritis on occipital cortex

Brain MTR scans were obtained six months after an acute episode of ON in a group of 80 patients, in order to identify any regions of abnormality in grey matter (Audoin

et al., 2006). Reduced MTR was seen in the visual cortex bilaterally, which may reflect trans-synaptic degeneration, or cortical synaptic changes.

An Italian cross-sectional study found regional cortical thinning in the occipital pole and calcarine sulcus, in a subgroup of 42 patients who presented with clinically isolated ON, studied at an average of eight months from symptom onset (Calabrese et al., 2007). Many of the patients fulfilled the MRI criteria for dissemination in space (Barkhof et al., 1997;Tintore et al., 2000), and could thus be considered at high risk of later developing MS. Although patients with MS may develop generalised grey matter atrophy, the localised and clinically relevant nature of the volume loss led the authors to conclude that these changes might reflect a contribution from tract-specific trans-synaptic degeneration.

These studies both represent further evidence that damage affecting the optic nerve may have consequences for the rest of the visual pathway, and it is important to consider these remote effects when investigating the balance between damage and repair mechanisms.

Functional MRI has also been applied to patients with ON, in order to study occipital cortical physiological responses to visual stimuli in the presence of damage, and will be discussed in Section 4 of this chapter, when recovery mechanisms are considered.

1.3.4.8 Conclusions

MRI has contributed greatly to our understanding of the mechanisms underlying optic nerve damage in ON. Whilst not entirely pathologically specific, it allows *in vivo* estimation of the relative contributions of inflammation, oedema, demyelination and axonal loss. Optic nerve swelling and enhancing lesion length have been shown to correlate with the degree of acute visual loss, suggesting that the intensity of initial inflammation is an important determinant of acute visual symptoms. In addition, evidence is emerging from quantitative MRI studies that there may be secondary consequences on the rest of the visual pathway. For this reason, a comprehensive structural assessment of the visual pathway covering the optic nerves, optic radiations and occipital cortex was included in the work reported in this thesis, in order to take into account the effects of any secondary damage, or incidental lesions, when considering mechanisms of damage and repair.

1.3.5 Assessment of damage using electrophysiology

In the previous section, the contribution of inflammation and demyelination to acute visual loss in ON was described. The effect of these processes on electrical conduction within the optic nerve and visual pathway will now be considered. This may be studied in patients *in vivo* using visual evoked potentials (VEPs), a technique developed in the 1950s (Berry and Harman, 1956), and optimised in the 1970s, with a series of experiments establishing an important role in the diagnosis of demyelinating diseases, and clarifying the nature of demyelination (Halliday et al., 1972;Halliday et al., 1973;Halliday and McDonald, 1977).

1.3.5.1 The normal visual evoked potential

To acquire VEP data, the subject observes a visual stimulus, usually through each eye in turn, with the other eye patched. The stimulus is commonly reversing black and white checkerboards presented on a computer screen. Electroencephalographic responses are recorded over the occipital lobe. Viewing distance, check size and averaging techniques are standardised within laboratories. The VEP is a measure of conduction of the whole afferent visual pathway, from retina to visual cortex. Therefore, any observed abnormalities are not anatomically specific. However, due to the organisation of the visual system, with decussation of fibres in the optic chiasm, the VEP is most useful and sensitive in assessing the anterior visual pathway, in particular the optic nerve.

The normal VEP is triphasic. An initial negative peak occurs after approximately 75ms, and is referred to as N75, or sometimes N1. A positive peak follows after around 100ms, which is called the P100, or P1. Lastly, a second negative peak occurs, called N135 or N2 (Figure 1.4).

Usually, it is the P100 waveform which is of clinical interest, and its amplitude and latency are reported. Amplitude normally shows considerable between-subject variability, in the range 4-30μV. Latency shows less variation in healthy subjects, and a normal value is around 100ms.

Several factors can influence normal VEP values including age (Mitchell et al., 1987), pupil size (Martins et al., 2003), blood glucose levels (Sannita et al., 1995) and medications such as anticonvulsants (Geller et al., 2005), as well as stimulus factors,

such as the size of the checkerboard squares (Chan et al., 1986). Women, on average, have slightly shorter VEP latencies than men (Gregori et al., 2006).

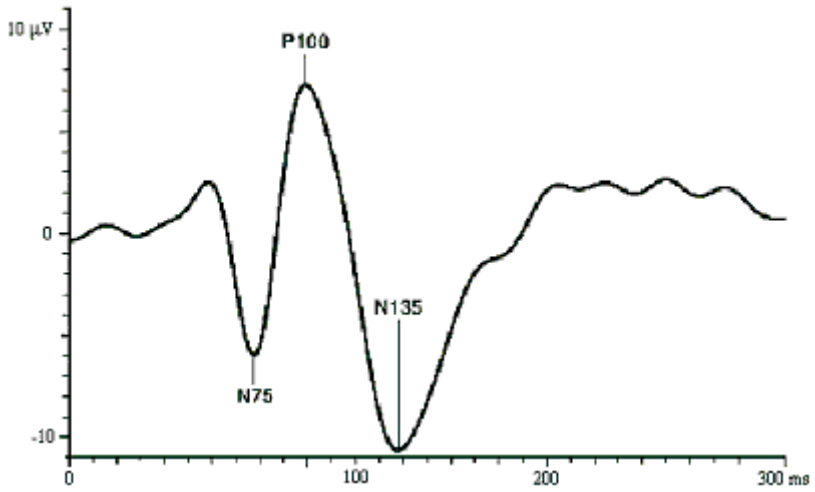

Figure 1.4 The normal visual evoked potential (Odom et al., 2004)

1.3.5.2 The visual evoked potential in optic neuritis

Acutely, the amplitude of the VEP is associated with visual acuity, and is thought to reflect the number of optic nerve fibres in functional continuity (Frederiksen and Petrera, 1999;Jones and Brusa, 2003). It is usually reduced in acute ON, when inflammation and demyelination lead to conduction block. In severe cases, with complete block, it may be impossible to elicit a potential. Most of the subsequent recovery in VEP amplitude occurs over the following two to three months, as conduction block resolves, and occurs in parallel with improvements in vision (Jones, 1993), and cessation of contrast enhancement on MRI (Youl et al., 1991).

This is in contrast to the VEP latency. In the 1970s, it was first recognised that VEP latencies were delayed in patients with ON (Halliday et al., 1972), and delay in conduction was experimentally linked to demyelination (Koles and Rasminsky, 1972;Rasminsky and Sears, 1972). In acute ON, if it is possible to elicit a potential, then delay is usually evident with a mean of approximately 30ms, as reported in one large study (Jones, 1993). Subsequently, in this group, the delay gradually reduced to a mean of 16ms after two years. Therefore, the time taken for optic nerve conduction velocity to improve was significantly longer than the time taken for vision to recover,

which was usually only weeks to months, and indeed VEP latency and acuity were not correlated.

Delayed VEPs are thought to reflect demyelination, and gradual shortening of latency over time to be a marker of remyelination. Therefore, after an episode of acute ON, it appears that vision recovers despite persistent demyelination, and the resulting slowing of conduction in the optic nerve. Prolonged VEP latencies may persist for many years (Halliday et al., 1972), and this tends to be more marked in older patients (Jones, 1993).

Subclinical demyelination in asymptomatic optic nerves is a common finding in MS (Halliday et al., 1973), is supportive evidence for the diagnosis, and is incorporated into the diagnostic criteria (McDonald et al., 2001;Polman et al., 2005). In prospective studies following patients with acute ON, in a mixed cohort of clinically isolated disease, recurrent ON and ON associated with MS, electrophysiological deterioration was noted in unaffected optic nerves (Brusa et al., 1999;Brusa et al., 2001). This manifested as a slight reduction of VEP amplitude during the second year, and prolongation of latency during the third. Clinically, contrast sensitivity worsened over time. Therefore, it appears that insidious ongoing demyelination in the fellow optic nerve occurs after ON, which may be independent of acute inflammation and oedema, and might affect axons as well. It is unclear if this process differs depending on whether the patient has ON in the context of MS or not.

1.3.5.3 Conclusions

VEP studies have demonstrated that acute conduction block occurs early in ON. This may be secondary to demyelination, at least in part, but it improves rapidly, coincident with resolution of inflammation, whereas demyelination persists. In addition, there is evidence for ongoing, more generalised and insidious optic nerve demyelination, and axonal damage, over the following years. Electrophysiology complements the structural information provided by MRI, elucidating its impact on nerve function, and was applied to the patients studied in this thesis.

1.3.6 Assessment of damage using optical coherence tomography

OCT uses the echo time delay of low coherence light to visualise and measure the RNFL (Huang et al., 1991). This provides an opportunity to quantify axonal loss, independent from demyelination, as these fibres of the CNS are unmyelinated in more than 99% of people (Straatsma et al., 1981). Assessment of the macular volume provides an estimate of ganglion cell numbers.

OCT measurements have been correlated with retinal morphology on light microscopy in monkeys (Toth et al., 1997), and in laser-excised human specimens (Chauhan and Marshall, 1999), although both studies reported an underestimation of RNFL thickness on OCT, in comparison with histology. These two studies used older OCT machines. A more recent study, using a newer generation instrument, demonstrated improved accuracy of OCT, although discrepancies were still evident if scans were taken too close to the optic nerve (Skaf et al., 2006).

The first application of OCT to the study of demyelinating disease was in 1999, in patients with MS and an episode of ON up to a year previously (Parisi et al., 1999). Thinning of the RNFL was reported in affected eyes, compared to fellow or control eyes. This was confirmed in subsequent studies (Trip et al., 2005;Fisher et al., 2006;Costello et al., 2006;Klistorner et al., 2008a). Experimental studies in animals suggested that these effects on retinal axons, secondary to pathology in the optic nerve, were due to retrograde "dying back" axonal degeneration (Quigley et al., 1977). The primary insult affects the optic nerve, which comprises axonal processes from the retinal ganglion cells (section 1.1.1), and results in secondary damage to the axonal segment situated between the site of injury and the cell body. In squirrel monkeys, this was observed to occur simultaneously throughout the length of this segment, rather than progressively back along the optic nerve, over a period of three to six weeks.

A group of patients with unilateral ON, three or more years after the acute episode, was investigated with OCT, VEPs and MRI of the optic nerves (Trip et al., 2005). The cohort included patients with clinically isolated ON and people with MS. The authors reported that a thinner RNFL correlated with worse visual acuity, colour vision and visual field mean deviation. A 10μm decrease corresponded to a 0.1 unit decrease in logMAR acuity (equivalent to a line of five letters on the chart). There were also associations between macular volume and visual measures, which were strong for

colour vision, but prone to outlier influence for acuity and visual field mean deviation. Both OCT measures correlated with VEP amplitudes, but not latencies. There were associations between optic nerve atrophy, measured with MRI, and RNFL thickness, macular volume, VEP amplitude and visual acuity (Trip et al., 2006a). These data suggested that optic atrophy on MRI, thinning of the RNFL, macular volume loss and reduced VEP amplitude share a common underlying substrate of axonal loss.

A different group studied patients with MS and investigated differences in subgroups, with and without a prior history of ON (Fisher et al., 2006). As well as confirming a reduction in RNFL thickness in ON affected eyes, they also showed that eyes with no prior history of ON had thinner RNFLs than control subjects. This suggested that subclinical axonal loss occurred in the optic nerves of people with MS. Later work showed that this correlated with brain atrophy (Gordon-Lipkin et al., 2007), and OCT has been proposed for use in clinical trials as a surrogate marker of axonal loss (Balcer et al., 2007).

A prospective study followed up patients after an acute episode of clinically isolated ON (Costello et al., 2006). They found that RNFL thinning appeared between three and six months after the acute episode. They also found correlations with visual function below a threshold of 75μm for visual field mean deviation, and 70μm for acuity.

A recent study in progressive MS found some evidence that the temporal quadrant of the RNFL, which comprises fibres of the papillo-macular bundle, responsible for central vision, may be more sensitive to subtle degrees of axonal loss (Henderson et al., 2008).

Another recent development was the finding of an association between RNFL thickness and VEP latency, suggesting that demyelination might promote axonal loss (Klistorner et al., 2008a). The results contrasted with the earlier results of Trip *et al*., but the cohort was unselected for recovery, and the VEP methodology differed, using a multifocal approach, which may be more sensitive (Klistorner et al., 2008b).

In summary, OCT appears to be a relatively specific surrogate marker for neuroaxonal loss in ON. The stronger correlations with visual function, compared with the inconsistent and modest correlations seen between clinical function and atrophy of the optic nerve, may reflect this greater specificity. Therefore, it appears that neuroaxonal loss contributes significantly to permanent neurological deficit following ON, just as it does in MS. The finding of thresholds below which there are correlations with

worse vision may suggest some degree of neuroaxonal tissue reserve in the optic nerve, which is termed redundancy. OCT provides a method of indirectly assessing this effect, through quantification of neuroaxonal loss, and was used for this purpose in this thesis, together with MRI measures of optic nerve atrophy and VEP amplitude. OCT was applied to patients at the 12 month time-point.

1.3.7 Conclusions

The current level of understanding of the mechanisms of damage in ON has been achieved by combining the results of pathological studies in humans, EAE work in animals, and *in vivo* studies in patients, using MRI, electrophysiology and OCT.

During the acute stage, inflammation and demyelination occur. These two distinct, but linked, processes have detrimental effects on neural conduction, which may lead to acute conduction block in the optic nerve, manifested clinically as visual loss.

Subsequently, there is persistent demyelination, neuroaxonal loss and probably gliosis. There are secondary effects on the rest of the visual pathway, which are incompletely understood, but may involve retrograde, Wallerian and trans-synaptic degeneration. Atrophy is detectable in the optic nerve, and neuroaxonal loss occurs in the RNFL and macula. Despite this, most patients make a good clinical recovery, and the correlation between tissue loss and visual outcome is often relatively modest.

Therefore, several unanswered questions remain, when considering how damage occurs. It appears from MRI studies that the initial severity of inflammatory insult is important in determining the degree of acute visual loss. However, the involvement of other factors has not been studied in detail. In particular, the potential contribution to visual loss from damage to the posterior visual pathways is not known. If lesions, or secondary degeneration, in the optic radiations had a significant impact on vision, this could partly explain why visual recovery is only weakly and inconsistently correlated with tissue loss in the optic nerve. In addition, it is increasingly evident that in acute inflammatory disease, there is a complex interplay between pathology and physiological responses. Therefore, it may be that during acute ON, physiological responses act to modulate the impact of damage on clinical function. This possibility has also not been studied before in depth.

It is interesting that whilst the severity of inflammation in the optic nerve does appear to contribute to the magnitude of acute visual loss, it does not seem to be as important

in determining eventual visual outcome. This suggests that other factors, which are independent from the magnitude of post-inflammatory damage and tissue loss, may be important in recovery.

SECTION 4: REPAIR AND RECOVERY

1.4.1 Difficulty of predicting visual recovery

At the present time, it is not possible to predict which patients will recover from ON, and which will not. This causes uncertainty and anxiety for patients, and makes it difficult to select patients who might be candidates for experimental therapies, such as stem cells (Pluchino and Martino, 2005;Kolappan et al., 2008a). Several studies have looked for predictors of visual recovery, but the results have been conflicting. Early studies reported correlations between longer optic nerve lesions on fast spin-echo MRI sequences and slow or poor recovery (Miller et al., 1988a;Thorpe et al., 1995), but a more recent longitudinal study did not find any association (Hickman et al., 2004c). Instead, this latter study found that patients with a longer gadolinium enhancing segment at baseline (using triple dose gadolinium), lower VEP amplitudes during recovery, and a less steep initial gradient of recovery had worse vision at 12 months. However, a large study (using single dose gadolinium) found no association between enhancing lesion length and visual recovery at six months (Kupersmith et al., 2002).

In the ONTT, although baseline and six month visual acuity were associated (Beck et al., 1994), no single measure or combination of baseline measures was a significant predictor of a poor visual outcome (6/15 or worse), because relatively few patients had visual loss to this level at six months. Visual acuity was 6/15 or worse at six months in 79% of patients with a baseline acuity of 6/60 or worse, compared with 17% of patients with baseline vision 6/15 to 6/57, and 7% of patients with acute visual loss of 6/12 or better (Beck et al., 1994). A more recent study reported no association between baseline acuity and visual outcome a year later (Hickman et al., 2004c). However, a different study from the ONTT cohort, which investigated later cut-points, found that acuity at one month was significantly associated with a poor outcome (6/15 or worse) at six months (Kupersmith et al., 2007).

No associations have been found between age, gender, ethnicity, abnormalities on brain MRI (Beck et al., 1994), VEP parameters during the acute stage (Hickman et al., 2004c), or optic nerve MTR (Hickman et al., 2004b) and recovery. Therefore, although baseline acuity may be of some value, a clinical predictor of visual outcome, which can be used at the time of presentation, is still awaited, and there is no clear

consensus on which, if any, structural measures might be important in determining subsequent recovery.

1.4.2 Correlations between structural damage and visual recovery

Most patients with ON recover well, despite evidence of residual structural damage within the optic nerve, as outlined in the previous sections.

Several studies have reported associations between atrophy in the optic nerve and visual recovery (Hickman et al., 2002a;Inglese et al., 2002;Trip et al., 2006a), but these have generally been relatively modest, and indeed some studies have found no correlation (Hickman et al., 2004a). RNFL thickness may be a more specific marker of axonal loss, and associations between a thinner RNFL and worse vision have been reported (Trip et al., 2005), with one study suggesting a threshold effect at 70-75μm (Costello et al., 2006). Taken together, these data suggest that whilst axonal loss in the optic nerve contributes to permanent visual disability in ON, there appear to be other factors influencing the clinical picture, which confound the association.

The hypotheses as to what these factors might be were briefly outlined in section 1.3.4.3: an impact of posterior pathway damage, gliotic tissue disguising optic nerve atrophy, optic nerve neuroaxonal redundancy, or differing efficacy of mechanisms which modulate damage or contribute to repair. Repair will now be considered in more detail. This could be mediated through a mechanism of redistribution of sodium channels in the optic nerve, remyelination, or adaptive grey matter plastic changes. Currently, it is unclear which, if any, of these mechanisms are important in determining differences in clinical recovery between individuals following ON.

1.4.3 Pathophysiology of recovery

Inflammatory conditions which affect the CNS, such as MS and ON, are often characterised by relapses and remissions. Previous work has identified several mechanisms by which remission might occur. Again, much of this work was carried out in MS and its animal models, and the data extrapolated to ON.

1.4.3.1 Resolution of inflammation

As the immune response to the antigenic stimulus resolves, levels of pro-inflammatory cytokines and nitric oxide fall, and hence their inhibitory effects on axons are removed. Conduction may then resume. This occurs despite significant demyelination being present in most cases (Felts et al., 1997).

1.4.3.2 Redistribution of sodium channels

It is perhaps surprising that demyelinated axons retain the ability to conduct nerve impulses. This may be facilitated through redistribution of sodium channels, even in the absence of remyelination (Bostock and Sears, 1976). These appear within two to three weeks of the acute episode, over the axonal segment which is denuded of myelin (Felts et al., 1997). This helps conduction to be restored, although it may now be of a continuous, rather than saltatory, morphology. The sodium channels in new locations were initially thought to be existing ones, which had been redistributed from the nodes, but subsequently it was shown that some develop *de novo*. Work in EAE first demonstrated that a proportion of the new channels differed from the usual subtype. Some were of the type seen during neural development prior to myelination (Nav-1.2), rather than the usual type seen in adult myelinated nerves (Nav-1.6) (Craner et al., 2003). This was also observed in MS lesions (Craner et al., 2004). It has been suggested that this process might explain why demyelinating lesions can sometimes remain clinically silent, even if they are large and in eloquent locations such as the optic nerves (Smith, 2007). However, even after this redistribution of sodium channels, the velocity of conduction that is restored is slower than before. Refractory periods are prolonged from 0.5-1.4ms to 1.0-6.0ms, and times as long as 27ms have been recorded (Felts et al., 1997). Conduction is therefore less secure, and periods of successful conduction can be interspersed with intermittent complete conduction block (Felts et al., 1995).

1.4.3.3 Remyelination

Another important mechanism of repair is remyelination, which may occur extensively in some people with MS (Patrikios et al., 2006). It has been demonstrated

experimentally that central remyelination can restore conduction (Smith et al., 1979), although this experimental study was not focused specifically on MS. Remyelination may improve both the velocity and security of conduction, even with high frequencies of depolarising stimuli. There is evidence that this improves clinical function from experimental models of demyelination in rats (Jeffery and Blakemore, 1997). However, it occurs slowly, months to years after the initial insult in ON (Jones and Brusa, 2003), by which time most of the clinical improvement has already occurred. Recently, evidence has emerged that remyelination may also prevent subsequent degeneration of the axon (Lappe-Siefke et al., 2003), which has led to interest in remyelination as a therapeutic strategy to prevent neurodegeneration. Although remyelination is usually dependent on oligodendrocyte function in the CNS, it is also possible using a variety other different cell types, such as exogenous Schwann cells (Honmou et al., 1996), olfactory ensheathing cells (Imaizumi et al., 2000) and neural stem cells, derived from bone marrow (Pluchino and Martino, 2005).

In both health and disease, maintenance of the myelin sheath in the CNS is a dynamic process. Following demyelination, remyelination may occur spontaneously (Woodruff and Franklin, 1999), through the action of oligodendrocytes recruited from precursor cells, expressing platelet-derived growth factor (Woodruff et al., 2004). The recruitment and differentiation of oligodendrocytes from these precursors appears to be critical for successful remyelination to occur. Sometimes remyelination fails, and this is either because oligodendrocytes are not present or, if present, are inactive. The reasons for this remain incompletely understood. Work in animals has suggested that differentiation, rather than recruitment, of oligodendrocytes from precursors is the main problem in MS (Arnett et al., 2004). The migration of precursors to the demyelinated lesion appears to be impaired, perhaps through dysregulation in cellular signalling molecules, such as semaphorins (Williams et al., 2007). A role has also been suggested for macrophages, as the presence of residual myelin debris appears to influence the effectiveness of remyelination (Kotter et al., 2006).

It remains unclear how important remyelination of the optic nerve is to recovery from ON. Although the evidence from VEP studies suggests a minimal contribution to the rapid initial recovery of vision following acute ON, as significant VEP delays persist for months and years (Brusa et al., 1999;Brusa et al., 2001), it may be important later in the recovery process, to prevent subsequent axonal degeneration.

1.4.3.4 Neuroaxonal redundancy

Following acute ON, a good visual recovery may occur despite residual axonal loss in the optic nerve, which is frequently associated with residual clinical dysfunction in demyelinating diseases (Miller et al., 2002), including ON (section 1.3.2.3). This restricted clinical impact despite neuroaxonal loss may be determined, in part, by the large number of axons in the optic nerve, in excess of the critical threshold necessary to maintain function.

This hypothesis is supported by studies which correlated optic nerve fibre counts with visual acuity, in 14 patients with a variety of conditions resulting in optic atrophy (Frisen and Quigley, 1984). They found that a normal acuity of 6/6 could be maintained despite loss of 40% of the axons. As more axons were lost, visual dysfunction worsened (to 6/15 and 6/60 with axonal loss of 90% and 99%, respectively).

Animal studies of optic nerve crush injury reported that vision improved in rats after two weeks, despite only 10% of retinal ganglion cells remaining viable and cortically connected (Sabel, 1999). They reported that cell survival in the retina did not correlate well with recovery of vision (although this is difficult to quantify in animals), and concluded that other factors must play a role.

1.4.3.5 Grey matter plastic changes

Lastly, plasticity of the CNS merits consideration. It is possible that reorganisation of central grey matter processing, in response to an altered afferent input, may compensate for tissue damage, and preserve clinical function. Neuroplasticity is a subject of increasing research interest. It used to be thought that cortical maps representing different neurological functions were permanent in the adult, and that damage to them was irreversible. However, this belief was challenged by experimental work, initially investigating sensory maps in animals (Merzenich et al., 1984;Pons et al., 1991), which found that reorganisation occurred on a macroscopic scale of several centimetres of neural tissue (Pons et al., 1991). Subsequently, this was also recognised in the visual system, and the mechanism was observed to be through axonal sprouting at cortical level (Darian-Smith and Gilbert, 1994), rather than any change in projections from the thalamus (Darian-Smith and Gilbert, 1995). In these

animal studies, homologous lesions in the retina resulted in the primary visual cortical representation of that region shrinking, whilst the representation of adjacent areas increased in size. In humans, evidence for neuroplasticity has been derived predominantly from fMRI studies.

Neuroplasticity is formally defined as reorganisation of distributed patterns of normal task-associated brain activity that accompany action, perception and cognition, and that compensate impaired function resulting from disease or brain injury (Frackowiak, 1997). Plasticity may be maladaptive, which describes a "stress response" with no discernable benefit on function (or even occasionally a detrimental effect, for example, phantom pain following limb amputation), or adaptive, which implies a contribution to clinical recovery.

Adaptive plasticity may result from several different mechanisms. There may be changes at neuronal or axonal level, such as altered sodium channel expression (Smith, 2007), dendritic arborisation (Jones and Schallert, 1992), or axonal sprouting (Darian-Smith and Gilbert, 1994). Remodulation of synapses may occur through changes in distribution, density or strength of connection (Jacobs and Donoghue, 1991). Neural circuits transform visual inputs into complex spatio-temporal patterns of electrical activity, and correlated cortical neuronal firing may influence cortical processing, through a mechanism of synaptic plasticity (Karmarkar and Dan, 2006). These effects at a cellular level may then be translated into differing patterns of reorganisation at systemic level. Four types have been suggested (Baker et al., 2005). In *homologous area adaptation*, functions localising to the damaged area of brain are transferred to undamaged homologous regions of the opposite hemisphere. When considering sensory processing, *cross-modal reassignment* describes the transfer of processing from a damaged region to an undamaged region, which is usually devoted to a different sensory modality. *Map expansion* describes an increase in the cortical representation of a function, either in response to repeated stimuli (a "learning effect"), or in order to compensate for damage to an adjacent area, as observed in the early animal work. Lastly, *compensatory masquerade* describes a change in cognitive strategy in order to achieve a task, which shifts processing from a damaged network to an alternative working one. Each of these mechanisms results in a change in location of cortical neural activity, which can be detected using fMRI.

1.4.4 Imaging plasticity using functional MRI

Reorganisation of the CNS can be imaged *in vivo* in humans using fMRI. This technique exploits the magnetic properties of haemoglobin, which differ depending on whether it is oxygenated or not. Areas of increased neural activity have greater oxygen requirements, so areas of reorganisation in response to simple tasks can be identified.

There is strong evidence for visual cortical reorganisation in human disease from studies of macular degeneration, a condition which results in progressive permanent central visual loss (Baker et al., 2005). It was demonstrated that peripheral field stimuli resulted in activation in regions usually reserved for the central field.

In inflammatory disease of the CNS, such as ON, the insult is often more transitory, and so evidence for plasticity may be more subtle and indirect. Nonetheless, there have been several studies which have investigated plasticity in ON, as well as other neurological syndromes which occur in MS (Comi et al., 2004).

The first fMRI studies in ON were carried out in the late 1990s (Rombouts et al., 1998). In general, patients with ON have smaller fMRI responses in primary visual areas when the affected eye is stimulated. The magnitude of the response has been correlated with VEP latency (Gareau et al., 1999), VEP amplitude (Russ et al., 2002) and visual acuity (Langkilde et al., 2002). It is thought that this smaller response reflects a reduced afferent neuronal input, which is most marked during the acute stage, when there is active inflammation and conduction block in the optic nerve.

The first evidence that fMRI responses were redistributed in areas outside primary visual cortex following ON was reported in 2000 (Werring et al., 2000). The authors studied seven patients, between six months and 14 years after acute ON, and seven controls. All of the patients had made a good visual recovery, but some still had delayed VEPs. The fMRI response maps to a simple visual checkerboard stimulus differed in patients and controls. Controls activated only visual cortex. In the patient group, visual cortical activation was seen but, in addition, there was activation in a large number of extra-striate areas, which included the insula-claustrum, corpus striatum, lateral temporal and posterior parietal cortices, orbitofrontal regions and the thalamus, on stimulation of the affected eye. In addition, when patients' unaffected eyes were stimulated, insular activity was seen. Differences were also observed when patient and control activations were directly compared. Patients demonstrated greater

responses in the insula-claustrum, orbitofrontal and lateral temporal cortex, corpus striatum, cingulate and right inferior frontal gyri, as well as some areas of visual cortex. Controls activated more than patients in several areas of visual cortex and also, on stimulation of the left eye only, the right superior and middle temporal gyri. The authors concluded that the redistribution of fMRI responses seen in patients reflected functional reorganisation, in response to a persistently abnormal input. They noted that some of the areas identified had strong visual connections, and were involved in multi-modal sensory processing. Surprisingly, the extra-striate neural activity actually occurred during the rest condition of darkness, rather than during checkerboard stimulation. This was subsequently confirmed in a study which used longer duration blocks of stimuli to conclude that this was a phase-specific phenomenon, and truly reflected relative deactivation during checkerboard stimulation, rather than a delayed haemodynamic response (Toosy et al., 2002). Since these studies were performed, advances have been made in understanding and interpreting deactivations in fMRI. They are thought to reflect activity of the brain's default mode networks. This term describes ongoing neural processing that occurs during rest, rather than being directed towards a specific task, and is a somewhat controversial area (Harrison et al., 2008). However, it is still not clear why neural reorganisation activity following ON was related to default mode processing, rather than to the task, in these studies.

The nature of plasticity in ON was clarified further by a longitudinal study in 20 patients with clinically isolated disease (Toosy et al., 2005). They were investigated with both structural and functional MRI imaging of the optic nerves. The authors used a novel methodology in order to identify areas of plasticity which contributed to clinical function, and could therefore be considered adaptive. They correlated fMRI activity indirectly with vision, after accounting for any variance in visual function which could be explained by structural MRI measures of optic nerve lesion length and swelling. An association was reported in the lateral occipital complexes (LOCs), which are higher visual processing areas, at the baseline time-point only, at a mean of 15 days from symptom onset. The authors hypothesised that these data represented evidence for genuine adaptive plasticity, occurring within the ventral processing stream.

A subsequent cross-sectional study used retinotopic mapping to identify hierarchical lower visual areas, and a specific localiser task to identify the LOCs, in patients with ON (Levin et al., 2006). Eight patients were studied between ten days and 69 months

after the acute episode. All the patients had good visual function (better than 6/9), but delayed VEP latencies. The aim was to investigate whether ON had differential effects in lower and higher visual areas. The authors reported that fMRI response profiles in the LOCs were similar on stimulation of the affected and fellow eyes and, in the inferior and lateral occipital gyri, the affected eye response was actually greater. This was in contrast to lower visual areas V1 and V2, where greater activation was seen, as expected, in the fellow eye. The authors offered two different hypotheses. Either LOC responses might be robust to disruption of visual input, or compensatory plastic responses could be occurring within them, on stimulation of the affected eye.

A later longitudinal study reported evidence for plasticity in the LGN (Korsholm et al., 2007). These were defined using anatomical landmarks on structural MRI, and the fMRI data were then extracted. The authors also defined regions-of-interest in the LOCs and primary and secondary visual cortex, using atlas-based coordinates. In contrast to Levin *et al.*, they reported that the fMRI response profiles were similar in lower and higher visual areas, and both were diminished on stimulation of the affected eye, compared with the fellow eye. As vision improved over time, the differences in LGN activation between the two eyes decreased. Most of this change was due to an increase in signal from the affected eye, as vision recovered, but a reduction in fMRI signal from the fellow eye also contributed. The authors hypothesised that this change represented plasticity, occurring at an early stage in the processing hierarchy, and it appeared that the fellow eye was involved. However, the study did not include a control group, which complicated interpretation of this longitudinal fMRI data.

It is unclear whether structural plasticity occurs following ON, and how fMRI responses representing plasticity relate to the anatomy of the visual pathways. One study reported that the optic radiations were located more postero-laterally in patients a year after ON than in controls, using reconstruction with DTI-based tractography (Ciccarelli et al., 2005). The authors hypothesised that this might represent structural reorganisation. It is interesting, in this regard, that a study in healthy controls found correlations between FA of the optic radiations and occipital fMRI responses, suggesting that cortical activity was constrained by external connections to the subserving white matter tracts (Toosy et al., 2004).

1.4.5 Brain repair: conclusions and unanswered questions

Therefore, to date, evidence for adaptive plasticity in ON has been identified in both lower and higher visual processing areas, in several different regions. With regard to the timing of these changes, there is still no clear consensus, but it appears, from longitudinal studies, that the acute phase may be important. There is some evidence that processing in the fellow eye is abnormal, but its exact role requires further clarification. The pattern of response profiles to visual stimuli in lower and higher visual areas and how they relate to one another is still controversial. In addition, the relative importance of plasticity in explaining recovery despite tissue damage, compared with remyelination, neuroaxonal redundancy in the optic nerve and posterior pathway pathology, remains to be elucidated.

No previous MRI studies have combined structural measures of the whole visual pathway with fMRI in ON. In addition, OCT has never been used in conjunction with fMRI in this condition. By combining these different *in vivo* techniques, each of which offers a different perspective, it may be possible to dissect the complex interactions between structure and function, pathology and physiology, damage and repair, in the anterior and posterior pathways. This approach has been used in this thesis, with the aim of answering the questions mentioned above.

Therefore, the primary underlying hypothesis is that an inflammatory insult to the optic nerve results in damage to myelin and axons, which is still detectable a year later. This insult to the optic nerve may have secondary consequences on the rest of the visual pathway, and there might also be incidental lesions of the optic radiations, which could be clinically significant. Despite this, a good visual recovery occurs in the majority of people. The reasons for this may include optic nerve remyelination, neuroaxonal redundancy, or adaptive neuroplasticity, either at subcortical or cortical level. If neuroaxonal loss is severe, or if remyelination or neuroplastic compensatory mechanisms fail, then patients may fail to recover.

The importance of investigating this hypothesis is, firstly, to develop better predictors of visual recovery, based on either markers of tissue damage, or the efficacy of responses to it. This would have important implications for clinical trials of experimental therapies, as patients with a poor prognosis could be identified. At present, no effective treatments exist for these patients, and future clinical trials may entail more invasive therapies, such as stem cells (Kolappan et al., 2008a), which may

necessitate careful patient selection. Secondly, elucidating the location and timing of any plastic responses, and the role of the fellow eye, is important when considering how to intervene to improve outcome, either with drugs, stem cell approaches, or even visual rehabilitation strategies (Kasten et al., 1998). Thirdly, a better understanding of mechanisms of damage and recovery in ON may also translate into MS, and form a basis for new therapeutic approaches.

In order to investigate the hypothesis outlined above, it is necessary to answer several more specific questions, in stages, which reflect the order of the results chapters of this thesis.

The first stage is to consider the acute phase of ON, to identify which structural and electrophysiological measures are associated with the severity of acute damage in ON, in this cohort, and what can be inferred regarding mechanisms of damage. Next, the effect of optic nerve damage on the rest of the visual pathway is studied, and the prevalence of incidental lesions of the optic radiations at this time. The role of neuroplasticity during the acute episode is investigated and, in particular, whether it has any role in modulating the impact of damage on clinical function. This may be complicated by complex interactions between visual acuity, structural damage and fMRI responses, which will require dissection. After this, the longer term consequences of ON are investigated. Residual structural damage is quantified, and evidence sought for secondary degeneration in the rest of the visual pathway, either of retrograde, Wallerian or trans-synaptic type. Recovery is considered, in particular, whether any paraclinical tests are able to predict the group of patients who fail to recover in the longer term. Important factors in recovery are investigated, focusing on the severity of acute inflammatory insult, magnitude of neuroaxonal injury in the optic nerve, damage to the posterior pathways and influence of reparative processes, such as remyelination and grey matter plastic responses. Plasticity is then investigated in more depth, and the location, timing, role of the fellow eye, and nature of interactions between lower and higher visual areas are elucidated. Recovery of visual field defects is used as a model to study homologous area adaptation, and the role of the fellow eye, by investigating neural processing in cortical regions mapping to field defects, and comparing affected and fellow eye stimulation.

These questions have not been addressed previously, and the process of attempting to answer them required that the different *in vivo* techniques, discussed in this chapter, be combined, in order to account for the many complicating factors. It was also

necessary to develop several novel technical innovations. A new method of presentation of visual stimuli for fMRI is designed, in order to address sources of attention and loss-of-fixation bias. For the DTI-based tractography analysis, a strategy of combining structural and functional data is used, that has not been applied previously to the study of disease of the human visual system, with the aim of reducing operator-dependent bias in seed placement. The use of quadrant-specific fMRI stimulation to investigate recovery from visual field defects, and compare affected and fellow eye responses, exploiting the principle of homologous retinotopic cortical representation, is also novel work.

CHAPTER 2

PRINCIPLES OF MAGNETIC RESONANCE IMAGING

In this chapter, the physical principles underpinning MRI will be described. General principles will be discussed first, which are relevant to all MRI imaging techniques. The focus will then shift to the newer techniques of diffusion tensor imaging (DTI) and functional MRI (fMRI), which will be described in more detail. These two techniques enable detailed *in vivo* investigation of the structural integrity of white matter tracts, and physiology of cortical activity, and are central to the work described in this thesis.

SECTION 1: PRINCIPLES OF MRI

2.1.1 Electromagnetic properties of biological tissues

MRI exploits the electromagnetic properties of protons. The biological tissues of the human body consist of organic molecules, which are abundant in hydrogen nuclei. Each hydrogen nucleus consists of one proton, and when subjected to a magnetic field, these protons precess. Precession describes a spinning motion about a central axis (Figure 2.1). Protons have a positive electrical charge, so this creates an electrical current, which induces a local magnetic field.

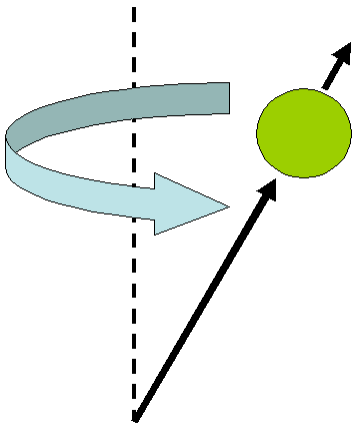

Figure 2.1 A diagrammatic representation of proton precession

The frequency of precession of the protons is dependent on the strength of the external magnetic field and the gyromagnetic ratio, which is specific to each element. This relationship is described by the Larmor equation:

$$\omega_0 = \gamma B_0$$

ω_0 is the precession frequency in megahertz (MHz), B_0 is the strength of the external magnetic field in Tesla (T) and γ is the gyromagnetic ratio. The gyromagnetic ratio of hydrogen protons is 42.5MHz/T.

When an external magnetic field is applied to a group of mobile protons, they align themselves with it, because of this magnetic property of precession. This can occur in two different ways: the protons may align parallel, or anti-parallel, to the principal direction of the external field. The direction of alignment is dependent on the energy state of the protons.

2.1.2 Longitudinal and transverse magnetisation and relaxation

Therefore, when a patient is placed in the external magnetic field of the MRI scanner, protons in the biological tissues align with the external field. As parallel alignment requires less energy than anti-parallel alignment, there is a net magnetic moment in the direction of the external magnetic field. This directional magnetisation is called longitudinal magnetisation.

If a radiofrequency (RF) pulse is then applied at the same frequency that the protons precess, energy is transferred to the protons, which results in resonance. This means that some protons change their alignment from parallel (lower energy state) to anti-parallel (higher energy state). The result is a net decrease in longitudinal magnetisation, in the direction of the external field. In addition, the RF pulse causes the precessing protons to synchronise, so that they precess in phase. This creates a new magnetisation moment, perpendicular to the external magnetic field. This is called transverse magnetisation.

After the RF pulse is switched off, the system gradually returns to the *status quo*. The protons return from the high energy anti-parallel alignment to their previous lower energy parallel alignment, with emission of thermal energy to the surrounding

environment, or lattice. The magnitude of the longitudinal magnetisation vector therefore increases in the direction of the external field. This change is termed longitudinal relaxation, or spin-lattice relaxation. When plotted against time, it follows an exponential curve. The shape of this curve is described by a constant, termed the T1 constant (Figure 2.2).

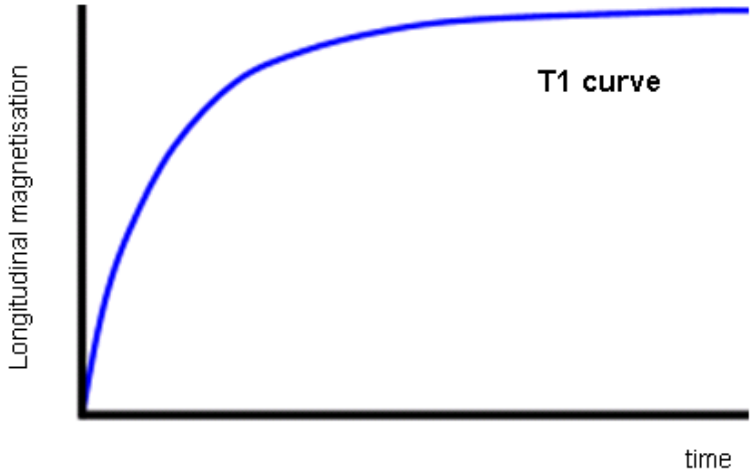

Figure 2.2 A T1-curve, showing relaxation of longitudinal magnetisation over time

In addition to longitudinal relaxation, the transverse magnetisation also gradually returns to its previous state, before the RF pulse was applied. The protons desynchronise their precession frequencies, or dephase. This occurs because they are subject to small local variations in the magnetic field which, according to the Larmor equation, determine precession frequency. Some local inhomogeneity is inherent to any external magnetic field, but additional inhomogeneities also result from local effects of neighbouring protons, which have small magnetic fields of their own. This gradual dephasing of protons results in a net loss of transverse magnetisation, which is referred to as transverse relaxation. When plotted against time, it is also described by a constant, termed the T2 constant (Figure 2.3).

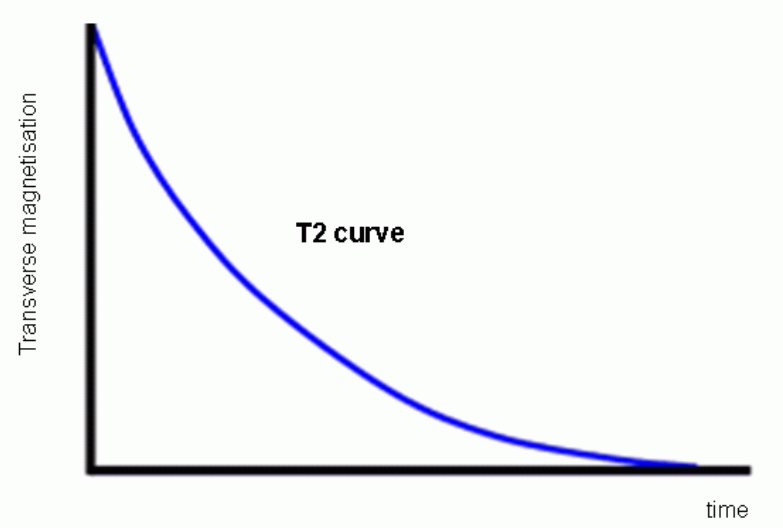

Figure 2.3 A T2-curve, showing relaxation of transverse magnetisation over time

2.1.3 T1 and T2 characteristics of biological tissues

There are differences in T1 and T2 relaxation characteristics between biological tissues. In human tissue, T1 generally varies between 300-2000ms, and T2 from 30-150ms. This can help to differentiate tissues, for example, T1 and T2 times are longer in liquids than in fats. These differences are partly due to tissue composition. However, T1 is also affected by the structure of the surrounding lattice, and the strength of the external magnetic field. Longitudinal relaxation times are longer in a given tissue, if the surrounding lattice contains protons with precession frequencies that differ greatly from it. Most biological tissues have a much lower precession frequency than water, so energy exchange from water to a biological tissue lattice is slow. Therefore, in human tissue, liquids have a long T1. Fat precession frequencies are closer to those of biological tissues, so T1 is relatively shorter.

In addition, as the strength of the external magnetic field increases, so does the precession frequency of protons in tissues. This will also affect the rate of transfer of energy to the lattice, which becomes slower. For this reason, stronger fields also result in longer T1.

The rate of T2 relaxation is predominantly influenced by the degree of magnetic field inhomogeneity. In liquids, unrestricted diffusion of protons results in rapidly fluctuating fields, with no net magnetic moment. In this environment, there are fewer local field inhomogeneities, and T2 relaxation is therefore slower. In contrast,

biological tissues contain macromolecules which impede free diffusion, resulting in greater local field inhomogeneities, more rapid dephasing of protons, and shorter T2.

2.1.4 Radiofrequency pulses and free induction decay signal

The RF pulse may be varied in terms of its effect on the net magnetic moment vectors. If sufficient energy is applied to cancel all of the net longitudinal magnetisation, and only transverse magnetisation remains, due to phase coherence of protons, this corresponds to a magnetic vector 90° to the perpendicular. This is called a 90° RF pulse (Figure 2.4). If even more energy is applied, such that longitudinal magnetisation is reversed, this corresponds to an 180° pulse. The net magnetic moment can also be tilted by smaller increments, or flip angles, which will be discussed later in this chapter.

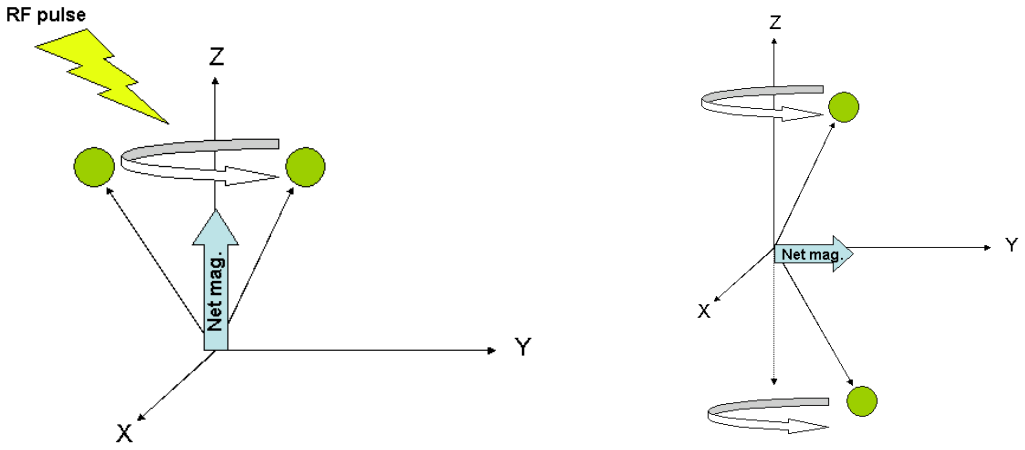

Figure 2.4 The effect of a 90° pulse on longitudinal and transverse magnetisation. Energy from the RF pulse results in an equal number of protons in parallel and anti-parallel alignment, and phase coherence. Therefore, there is no net longitudinal magnetisation, and only transverse magnetisation remains. Modified from (Schild, 1990).

After the RF pulse is switched off, both longitudinal and transverse magnetisation subsequently relax, or decay, to baseline. Longitudinal and transverse relaxations occur simultaneously and independently. Therefore, at any given time after the RF pulse, the net magnetisation can be represented by a sum vector, which spirals in the direction of precession. This moving magnetic field induces an electrical current, which is detected by a receiver coil, providing a nuclear magnetic resonance (NMR)

signal (Bloch et al., 1946). The signal magnitude is greatest straight after the RF pulse is switched off, when transverse magnetisation is maximal and longitudinal magnetisation minimal. Subsequently the signal decays over time. This is the basis of the free induction decay signal (Figure 2.5).

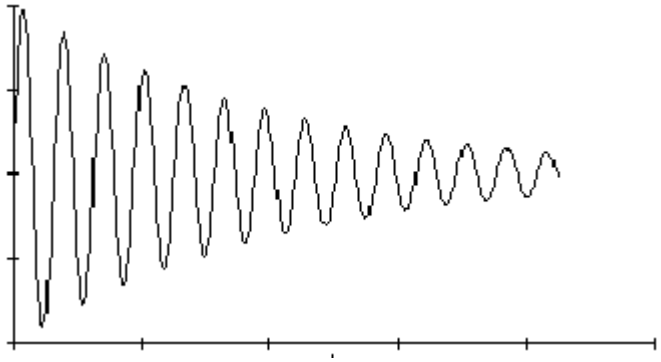

Figure 2.5 Free induction decay signal

2.1.5 Tissue contrast and pulse sequences

Tissue contrast in MRI is based on differences in T1 and T2 relaxation times. In order to exploit this, more than one RF excitation is usually required. If a second RF pulse is applied before longitudinal relaxation is complete, then differences in relaxation times between tissues may be accentuated. Combining pulses in this way results in a pulse sequence. Sequences can be optimised to exploit differences in magnetic relaxation characteristics between tissues, to maximise contrast. The time between successive repetitions of the same pulse sequence is called the time to repeat (TR). The use of TR intervals which maximise tissue contrast, based on differences in longitudinal magnetisation, is referred to as T1-weighting.

If a long TR is used, and longitudinal magnetisation returns to the resting state, then contrast is only dependent on differences in tissue composition itself, and not relaxation times. This results in a proton-density, or spin-density, image. TR is generally considered long if it is greater than 1500ms and short if it is less than 500ms.

Transverse relaxation occurs more rapidly than longitudinal relaxation. The application of successive 180^{o} RF pulses slows this process. Each pulse has the effect of reversing the direction of precession of the dephasing protons. Prior to the

application of the 180° pulse, the most rapidly precessing protons will be most dephased from the resting state. After the pulse, these protons will then be least dephased. The converse will be true for the slowest precessing protons. After a time interval, the rapidly precessing protons will once again be in phase with the slower precessing protons. At this point of phase coherence, the net transverse magnetisation, and hence the MR signal, will be greater. The 180° pulse can be repeated several times, each of which will sustain this signal echo. This sequence of 90° pulse, followed by repeated 180° pulses, is the basis of the spin echo technique (Figure 2.6). The time between successive echoes is called the TE. Again, this can be manipulated in order to exploit differences in characteristics of different tissues and achieve tissue contrast. If a long TE is used, so that differences in proton phase are maximised, the resulting image is said to be T2-weighted. A TE of greater than 80ms is usually considered long, and less than 30ms short.

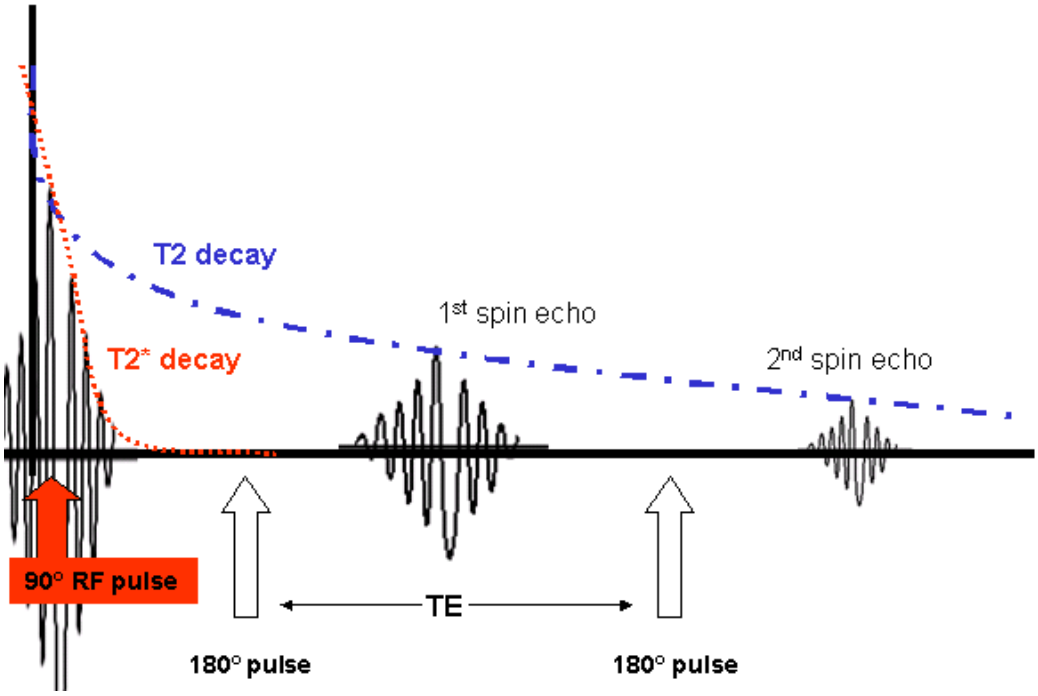

Figure 2.6 The spin echo sequence. After an initial 90° pulse, successive 180° pulses refocus the transverse magnetisation, resulting in the spin echo effect. T2* effects are not influenced by the 180° pulse, therefore T2* decay is more rapid than T2 decay.

2.1.6 T2* effects

The resulting signal echos become progressively weaker over time. This is because the 180^{o} pulse is only able to influence constant sources of inhomogeneity in the external magnetic field. There is no influence on inconstant local field inhomogeneities, and these T2* effects are responsible for the progressive diminuition of signal. If 180^{o} pulses are not applied, transverse magnetisation decays much more quickly, and this steeper decay curve is called the T2* curve (Figure 2.6). Exploitation of T2*-effects is an important principle of fMRI, which will be discussed later in this chapter.

2.1.7 T1 and T2-weighting

Combining the T1 and T2 curves can determine the signal intensity of a tissue, using a spin-echo sequence. The longitudinal magnetisation can be calculated from the T1 curve, at time TR, and this serves as the starting point for subsequent T2 relaxation. The transverse magnetisation can then be calculated from the T2 curve, at time TE.
Differences in T1 between tissues tend to be more marked with shorter TRs, as differences in longitudinal magnetisation are greatest at this point, and resolve over time. Conversely, differences in T2 between tissues are more marked with longer TEs, as phase differences become more pronounced over time.
Combining a short TR with a short TE will therefore result in a T1-weighted image, and combining a long TR with a long TE will result in a T2-weighted image.
If TR is very long and TE very short, then tissue contrast will be predominantly determined by tissue composition, and a proton-density (PD) weighted image will be obtained.
If TR is short and TE long, then there will be minimal longitudinal and transverse magnetisation, and the signal will be difficult to distinguish from background noise. For this reason, such pulse sequences are generally not useful. This illustrates an important issue in MRI that is the signal-to-noise ratio (SNR). For example, in T2-weighted pulse sequences the improvement in tissue contrast that is achieved using longer TEs has to be balanced against the reduced SNR that is seen with increasing time.

PD, T1 and T2-weighting thus provide different tissue contrast, and are differentially sensitive to pathology. In healthy brain tissue, CSF is generally bright on T2-weighted images and dark on both T1-weighted and PD-weighted scans. With T1-weighting, grey matter is darker than white matter, whereas on PD the reverse is the case. The changes in signal intensity that occur in pathology such as ON are diverse, and will be discussed in later chapters.

2.1.8 Spatial encoding

The problem of anatomical localisation remains to be considered. The MR signal must be spatially localised, in order to reconstruct an interpretable image. This is achieved with additional magnetic fields (Lauterbur, 1973), superimposed on the main external field, using gradient coils. These additional gradient fields gradually increase in strength in a given direction.

Firstly, a *slice-selecting gradient* is applied during the RF pulse, which localises the cross-sectional plane to be examined. This results in slight differences in precession frequency of protons, in a gradually increasing manner along the z-axis, for example, from the subjects' feet to their head. A slight variation in frequency of the RF pulse will then selectively excite a fairly narrow band of protons, thus selecting the slice. Slice thickness can be determined either by changing the bandwidth of radiofrequencies of the RF pulse, or the gradient of the field.

In order to localise protons within each slice, it is necessary to define their position in two planes. A second gradient field is applied shortly after the slice-select gradient is switched off, that enables localisation in one of these planes, for example, in the direction of the y-axis (anterior/posterior). This *frequency-encoding gradient* again results in slightly different precession frequencies, depending on location, which establishes the row of origin of the protons.

A third gradient field is then applied in the remaining plane, for example, along the x-axis (left/right), which results in dephasing of the protons. This *phase-encoding gradient* results in protons within the same row, which were precessing previously with the same frequency, each having a slightly different phase, allowing localisation of protons within that row.

A mathematical operation, the Fourier transform, allows conversion of this frequency and phase information into a spatial location, which can then be assigned a signal intensity to reconstruct an image.

2.1.9 K-space

Prior to the application of the Fourier transform, the MRI data exists in non-Euclidean theoretical space, called k-space. The data forms a matrix, and each data-point in the matrix corresponds to a point in k-space, which has experienced different combinations of dephasing along the x and y-axes. Sampling the whole of k-space results in one complete volume of interest, for example the brain. Most of the information is concentrated in the centre of k-space, and extra detail is then obtained by sampling points further away from the centre. Advances in the techniques used to sample k-space allowed development of the modern fast imaging sequences, used in DTI and fMRI, and are described in more detail later in this chapter.

2.1.10 Tissue suppression

Pulse sequences can be adapted based on the number and angle of RF pulses that are applied. The spin-echo sequence consisting of a 90^{o} pulse, followed by 180^{o} pulses, has already been discussed.

Inversion recovery sequences differ from spin-echo, in that the 180^{o} pulse precedes the 90^{o} pulse. This has the effect of producing a strongly T1-weighted image, and can be used for tissue suppression, for example, orbital fat or CSF surrounding the optic nerve. This was applied to patients with ON in this thesis. The magnitude of T1-weighting in this sequence is dependent on the time between the initial 180^{o} pulse and the subsequent 90^{o} pulse, which is termed the inversion time (TI).

2.1.11 Towards faster imaging sequences

It is important to minimise MRI acquisition time for patient comfort, to reduce motion artefacts and to make advanced techniques, such as DTI and fMRI, feasible. Imaging time is mostly dependent on the length of TR, so in order to develop faster imaging sequences, it was necessary to reduce TR. However, this was difficult for two reasons.

Firstly, in a spin-echo sequence, the rate-limiting step is the 180^{o} pulse and, as this is delivered during the TR, it is difficult to shorten it, unless an alternative method of rephasing protons is used. Secondly, with shorter TRs, longitudinal magnetisation recovers less completely, and there is therefore less magnetisation tilted transversely with subsequent RF pulses, resulting in a weaker signal. The first problem was overcome by using gradient fields to rephase the protons, instead of an 180^{o} pulse. The second problem was solved by using smaller flip angles, typically 10-35 degrees, to tilt magnetisation into the transverse plane. In general, smaller flip angles result in less T1-weighting.

Faster acquisition may also be achieved using multi-slice imaging, by acquiring data from multiple slices during each TR.

In addition to TR, imaging time is dependent on the number of excitations (NEX), and the size of the matrix. Several excitations are usually averaged, in order to increase SNR. Matrix size refers to the number of pixels which make up the final image, and results in a trade-off between resolution and acquisition time.

2.1.12 Echo-planar imaging

In conventional MRI, one phase-encoded line of k-space is collected every TR. Therefore, a large number of excitations are required to sample the whole k-space. Echo-planar imaging (EPI) was developed to speed up this sampling process. In single-shot EPI, an entire volume is acquired during each TR, by repeatedly refocusing the phase and frequency encoding gradients (Figure 2.7). This samples the data in k-space more efficiently. The EPI acquisition of the whole brain in a TR can be preceded either by a spin echo (spin echo EPI, resulting in T2 contrast), or by a gradient echo, in which the echo is refocused using gradient fields instead of an 180^{o} RF pulse (gradient recalled echo (GRE) EPI, resulting in T2* contrast).

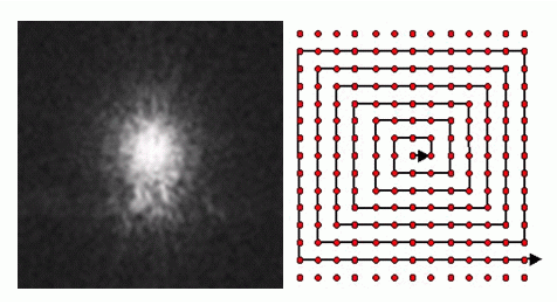

Figure 2.7 Sampling k-space (left) using a spiral EPI technique (right). Modified from (Sykora, 2005, www.ebyte.it, and Miquel, 2008, www.scopeonline.co.uk).

A limitation of this technique is that rapid switching of magnetic gradients creates eddy currents, which can distort the data, and may result in stimulation of the subject's peripheral nerves. Data distortions include Nyquist ghost artefact, which is a result of cumulative phase errors, from repeated passes in opposite directions through k-space. These can be corrected by collecting a reference non-phase encoded dataset (Bruder et al., 1992).

Another problem with EPI is susceptibility artefact at interfaces between different tissues, which may result in signal dropout, or distortion, through sensitivity to marked T2* effects in these regions. Air-bone interfaces are especially problematic, such as the paranasal sinuses and ear canals, and may result in artefact in the orbito-frontal and temporal regions.

2.1.13 Contrast enhancement

MR signal may be manipulated using contrast agents, such as gadolinium, which is paramagnetic. This increases local magnetic inhomogeneity, and T2 relaxation times are therefore shortened. T1 relaxation time is also reduced, via magnetic dipole-dipole interactions between the paramagnetic contrast agent and the protons. Together these effects can be used to improve tissue contrast, by exploiting the differential perfusion of tissues with blood, for example, demonstrating inflammatory disruption of the blood-nerve barrier in ON (Figure 2.8).

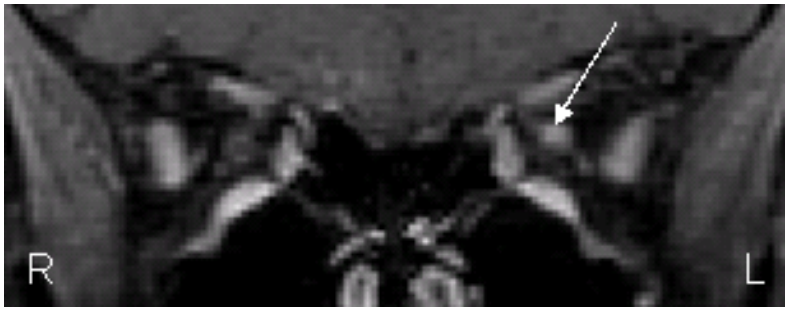

Figure 2.8 Post-triple dose gadolinium T1-weighted MRI demonstrating left optic nerve enhancement (arrow).

SECTION 2: DIFFUSION TENSOR IMAGING

2.2.1 Diffusion in biological tissues

DTI exploits the principles of Brownian motion (Brown, 1828). This term describes random motion of molecules, such as water, and was first described in the 19th century. Biological tissues are abundant in water, and the extent of random motion may be constrained by physical barriers, such as cell membranes. This differs according to tissue, for example, there is greater random diffusion in CSF than in brain tissue. In addition, diffusion is directionally sensitive to tissue microstructure. White matter consists of tightly packed tubular structures, such as axons, which facilitate diffusion along their long axis, but impede it in the perpendicular direction. In contrast, whilst grey matter contains cell membranes that impede random diffusion, these are less directionally coherent than white matter, and the two tissues may therefore be differentiated.

The degree of directional selectivity imposed on diffusion is referred to as the degree of isotropy. Diffusion in CSF is highly isotropic, or non-directionally selective, which may be visually represented as a sphere at the scale of an imaging voxel. In contrast, diffusion within white matter is highly anisotropic, or directionally selective, and may be represented with a cigar-shaped diffusion ellipsoid (Figure 2.9). The overall diffusion behaviour within the ellipsoid may be summarised by three vectors, known as eigenvectors, describing diffusion along the x, y and z axes, with the principal eigenvector along the main axis of diffusion.

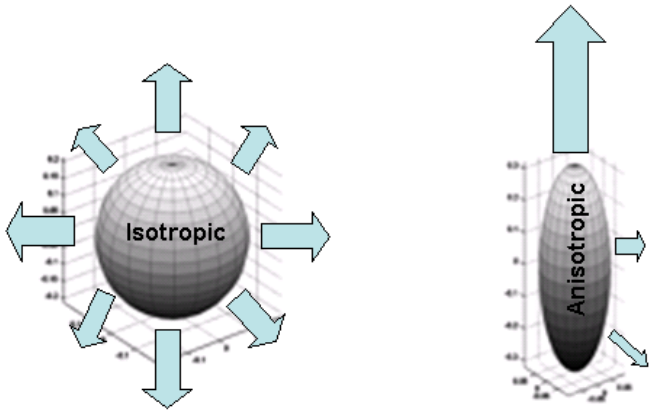

Figure 2.9 An illustration of different types of diffusion at voxel level. On the left, isotropic diffusion and, on the right, anisotropic diffusion, represented with a diffusion ellipsoid. Diffusion along the main axis is described by the principal eigenvector.

2.2.2 Diffusion weighted MRI imaging

The MRI signal is sensitive to diffusion of water. During a spin echo sequence, the precessing protons are first dephased then rephased. If random diffusion occurs in the intervening time interval, then rephasing will be incomplete, transverse magnetisation will be relatively less, and the MRI signal will be attenuated. The magnitude of this attenuation will depend upon factors related to both the tissue structure and the magnetic field. Specific pulse sequences have been developed, which are sensitive to diffusion. This was first achieved using a pulsed field gradient method (Stejskal and Tanner, 1965). This technique is based on a spin echo sequence, but two gradient fields are applied either side of the 180^{o} pulse (Figure 2.10).

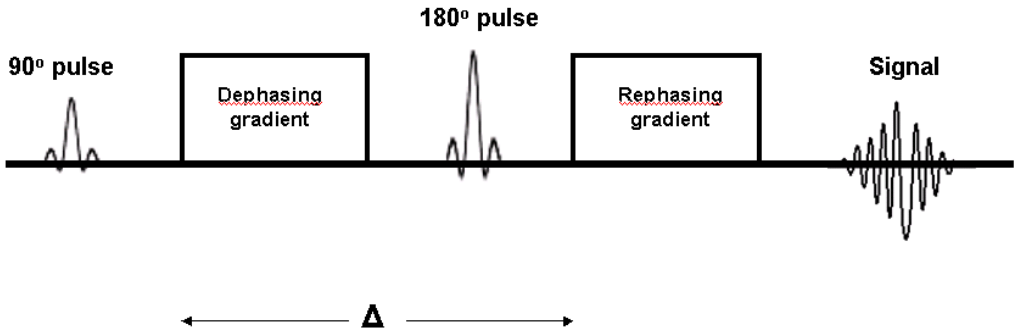

Figure 2.10 Pulsed field gradient sequence. Δ represents the time period in which differences in diffusion are detectable.

The additional two gradients induce a phase shift, and then reverse it. Less rephasing occurs following the second gradient, as diffusion increases. Comparing this acquisition to a non-diffusion-weighted acquisition, or b_0 image, allows calculation of the magnitude of diffusion, using the Stejskal-Tanner equation.

$$S = S_0 e^{-bD}$$

S and S_0 represent the MRI signal in the presence and absence of diffusion gradients, respectively. b refers to the diffusion weighting factor (Le Bihan et al., 1986), which may be experimentally manipulated. D is the diffusion coefficient, which can then be calculated at each voxel.

From this equation, it may be seen that the greatest reduction in signal occurs when D is maximised. This means that in regions in which diffusion is anisotropic, such as white matter, signal will be attenuated when a diffusion gradient is applied parallel to the main axis of the ellipsoid (that is parallel to the axons). Therefore, regions of anisotropy parallel to the main direction of diffusion appear dark on a diffusion-weighted image. From these measurements the apparent diffusion coefficient (ADC) is derived for each voxel. The word "apparent" indicates that the underlying diffusion process is constant; it is the interaction between water and macromolecular structures which results in changing values (Cercignani and Horsfield, 2001).

2.2.3 The diffusion tensor

A major problem with diffusion-weighted imaging is that, as a result of the principles of directionality on which it is based, it is extremely sensitive to artefacts from head motion. This is inevitable during an MRI scan, even in cooperative subjects. In addition, ADC values only provide one-dimensional information, along a single diffusion direction. These limitations were overcome by the development of the diffusion tensor (Basser et al., 1994). A diffusion tensor (DT) is derived from a b_0 image and diffusion weighted images, acquired in six or more non-collinear directions, along the x, y and z axes, and their combinations, xy xz, yz. A 3x3 matrix is then created, which parameterises diffusion in three dimensions, along the x, y and z axes. The matrix is diagonalised, meaning that the off diagonal elements are mathematically reduced to zero.

$$DT= \begin{Bmatrix} \lambda_1 & 0 & 0 \\ 0 & \lambda_2 & 0 \\ 0 & 0 & \lambda_3 \end{Bmatrix} \begin{Bmatrix} \varepsilon_1 \\ \varepsilon_2 \\ \varepsilon_3 \end{Bmatrix}$$

In this manner, diffusion direction can be fully characterised. ε_1 ε_2 and ε_3 are referred to as eigenvectors, and they represent the magnitude of diffusion of water along the x, y and z axes, previously illustrated with the diffusion ellipsoid in Figure 2.9. They are ordered such that ε_1 always represents the principle diffusion direction. λ_1 λ_2 and λ_3 are the eigenvalues, which correspond to the ADC values for each eigenvector.

2.2.4 Mean diffusivity and fractional anisotropy

Scalar invariant values may be derived from the diffusion tensor, summarising aspects of diffusion.

Mean diffusivity (MD) is simply the mean of the three eigenvalues. Higher values indicate more isotropic diffusion.

Fractional anisotropy (FA) is an estimate of directionality of diffusion. Higher values indicate more anisotropic diffusion. It is calculated from the MD and eigenvalues, as follows.

$$FA = \frac{\sqrt{(\lambda_1 - MD)^2 + (\lambda_2 - MD)^2 + (\lambda_3 - MD)^2}}{\sqrt{\lambda_1^2 + \lambda_2^2 + \lambda_3^2}}$$

In FA maps, areas of high anisotropy, such as white matter tracts, appear bright and areas of low anisotropy appear dark (Figure 2.11). This is the reverse of the diffusion-weighted maps, from which they were originally derived.

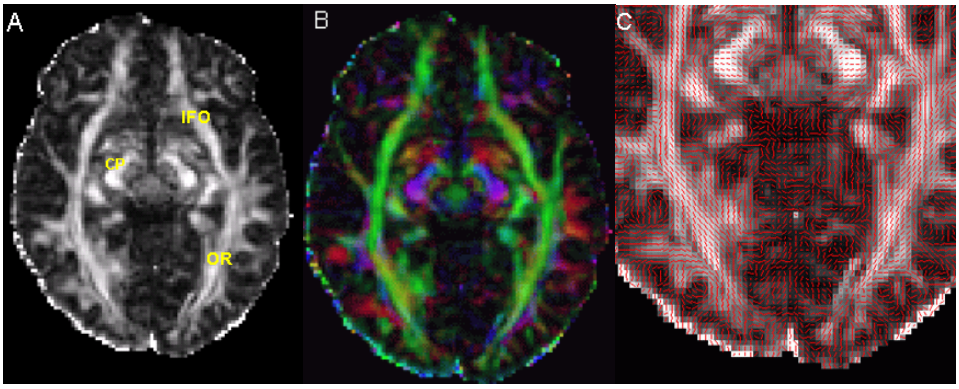

Figure 2.11 An FA map of a control subject. (A) Areas of high anisotropy appear bright, and represent white matter tracts. The optic radiations (OR), inferior fronto-occipital fasciculi (IFO) and cerebral peduncles are seen. In (B), the same map is colour coded to show the principal direction of diffusion. The ORs and IFOs are green, which represents a principal eigenvector in the anterior-posterior direction. In contrast, the CPs are blue/purple which represents superior-inferior diffusion. Voxels within tracts in red have principal eigenvectors orientated in the left-right direction. (C) A magnification of the optic radiations from the same FA map overlaid with the principal eigenvector map. The red line in each voxel demonstrates the principal direction of diffusion.

2.2.5 Technical problems in DTI

Minimisation of motion artefacts remains a technical challenge in DTI. The problem is compounded by the relatively long scan times necessary to acquire data in several different directions. Moreover, in order to improve SNR, either signal averaging or acquisition in more than the minimum six directions (plus b_0) is usually required.

Motion effects may be reduced by using fast imaging sequences, such as EPI. However, cardiac pulsation and respiratory motion may still cause problems. In order to minimise pulsation artefact, sequences may be cardiac-gated, when data is only acquired during diastole. However, this further increases the scan time.

Another problem is that the selection of principal diffusion axes, used to derive the tensor, introduces a directional bias. This is because voxel SNR characteristics vary, depending upon whether they are aligned with one of the principal diffusion axes. Therefore, a voxel's directionality may subsequently influence the complex noise calculations, and introduce bias into the estimates. This problem may be reduced by sampling more diffusion directions.

2.2.6 Diffusion-based tractography

DTI provides directional information about the diffusion behaviour of water within each voxel. However, it does not provide information about connections between voxels. These relationships are of central interest when investigating white matter tracts of the brain, and further techniques have been developed to study them, such as diffusion-based tractography.

An algorithm is applied to the diffusion tensor data, to assess the likelihood of connection of neighbouring voxels, based on the collinearity of the vectors in each voxel. If the angle between principal vectors in adjacent voxels is less than a predetermined threshold, it is inferred that the voxels are connected, and a pathway, or streamline, is propagated. If the angle is greater than threshold, then the pathway is terminated. Several different algorithms have been developed, with probabilistic tractography currently most commonly used. Probabilistic methods use uncertainty principles to estimate confidence of connections, between each voxel and a given seed-point (Parker et al., 2003).

Tractography provides an important tool to investigate the structure of white matter tracts *in vivo*, and has been applied extensively to the study of neurological disease (Ciccarelli et al., 2008). However, there are some limitations. The diffusion tensor data contains noise, which may bias the estimates of the reconstructed tracts. Using a probabilistic method, estimation errors tend to accumulate as the distance from the seed-point grows, and can be influenced by the shape of the trajectory, anisotropy of the underlying tissues, and parameters related to the imaging technique used, such as

image resolution (Mori and van Zijl, 2002). In addition, it is not possible to determine if an identified pathway is functional, whether conduction occurs in an anterograde or retrograde direction, and where pathways break to synapse (Johansen-Berg and Behrens, 2006). Challenges also remain in tracking crossing, or kissing, fibre tracts and it is still difficult to fully eliminate operator-dependent bias in selecting seed-points. Techniques have been developed to address some of these limitations, for example, smoothing may be applied to reduce noise in the tensor data. High angular resolution DTI (Frank, 2002), and processing algorithms which allow for multiple fibre orientations (Behrens et al., 2007), have been used to help accommodate crossing fibres, and fMRI has been combined with DTI to help define seed-points in an unbiased manner (Conturo et al., 1999;Guye et al., 2003;Powell et al., 2007).

SECTION 3: FUNCTIONAL MRI

2.3.1 The BOLD effect

The development of fMRI provided a powerful new tool to study the physiology of the CNS, in health and disease. The principle was first demonstrated in rats (Ogawa et al., 1990), and shortly afterwards human cortical activation was demonstrated (Ogawa et al., 1992;Bandettini et al., 1992;Kwong et al., 1992), with many of the early studies focusing on the visual system. The technique is based upon the principle of blood oxygenation level dependent (BOLD) responses, in which the MRI signal of blood differs, depending on whether it is oxygenated or not. In the brain, increased neural activity results in a greater metabolic demand, which results in increased local concentrations of oxygenated haemoglobin and less deoxyhaemoglobin (neurovascular coupling), and therefore regions of brain activity can be visualised using MRI.

Typically, patients perform a task in the scanner, selected specifically to investigate a certain aspect of cortical processing. The task is presented intermittently with a control condition, and differences in BOLD response are observed. The sequence of physiological events that occurs during task performance has been clarified in recent years, although some aspects are still debated. The following hypothesis is generally agreed. An increase in neuronal activity increases metabolic demand, and initially the deoxyhaemoglobin concentration increases in the local draining capillaries and veins (Vanzetta and Grinvald, 1999). Deoxyhaemoglobin is paramagnetic, whilst oxyhaemoglobin is diamagnetic (Pauling and Coryell, 1936). An increase in local deoxyhaemoglobin concentration therefore results in increased local magnetic field inhomogeneity, and MRI signal is attenuated (Thulborn et al., 1982). A rapid physiological response follows, with a marked increase in local blood flow and oxyhaemoglobin concentrations. This response greatly exceeds metabolic demand (Fox and Raichle, 1986), and the resulting change in oxyhaemoglobin concentration leads to an increase in MRI signal, as local magnetic inhomogeneities decrease. The increase in blood flow results in a greater volume of blood in the local veins, which have balloon-like elastic qualities (Buxton et al., 1998). These properties lead to a persistent increase in local blood volume, which lags behind local normalisation of flow to the resting state. Therefore, there is a late, transient local increase in

deoxyhaemoglobin concentration, after neural activity has ceased, which is thought to explain the observed post-stimulus undershoot of MRI signal. These haemodynamic changes occur over a longer time scale than the neural events which trigger them, over approximately ten seconds (Figure 2.12), although the exact temporal characteristics of the haemodynamic response differ slightly, depending upon the brain region and type of stimulus (Bandettini et al., 1997). In most fMRI studies, it is the main increase in BOLD signal which is of interest and is detected. Following visual stimulation, this corresponds to a change of around 1-3% intensity at 1.5T, and is a result of BOLD signal contributions from both the intravascular and extravascular compartments (Boxerman et al., 1995).

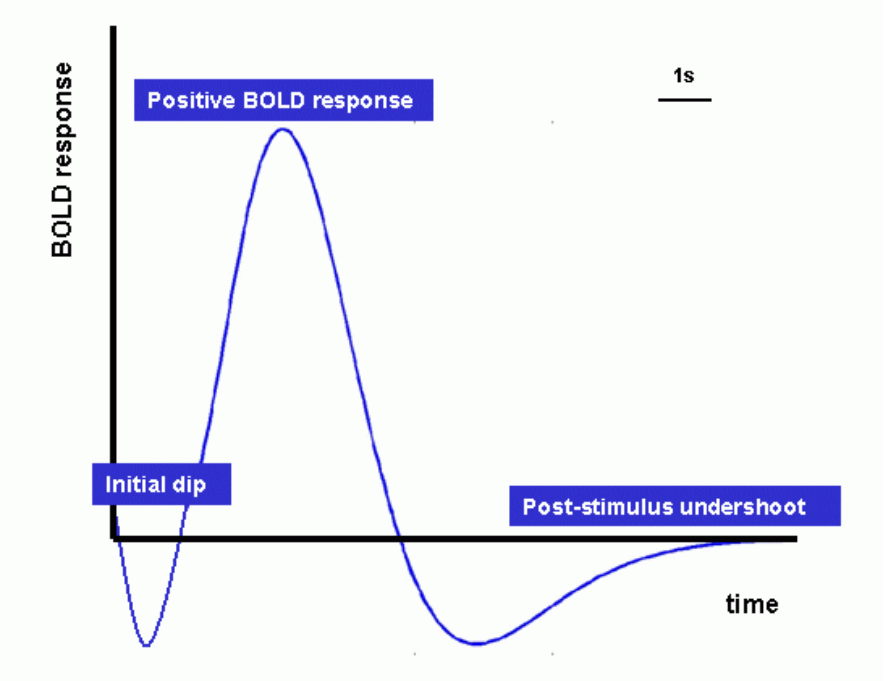

Figure 2.12 The haemodynamic response function, which describes the temporal characteristics of the BOLD response. In this diagram, the amplitude of the dip and undershoot are exaggerated for display purposes.

2.3.2 Neurophysiological correlates of the BOLD signal

Studies in monkeys showed that BOLD signal increases reflect a greater contribution from neural local field potentials, compared to spiking activity (Logothetis et al., 2001), although both were correlated with the BOLD signal. Local field potentials are believed to be predominantly due to sustained synchronised synaptic activity in

dendrites, from an area of a few millimetres of brain. On the other hand, spiking, or multi-unit activity, is thought to represent transitory neuronal firing near the recording electrode tip. In this important study, in which simultaneous data from fMRI and direct intracortical electrodes were collected, the authors concluded that BOLD signal change is influenced mainly by neural input and intracortical processing, rather than neural output. Other authors have since pointed out that local field potentials only accounted for 7.6% more variance in the BOLD response than multi-unit activity, and that the contribution of each may vary with the level of brain activation, so the association between BOLD response and local field potentials does not appear to be absolute (Bandettini and Ungerleider, 2001).

2.3.3 Detecting changes in BOLD signal

The BOLD signal is best detected using T2*-weighted MRI sequences, which are most sensitive to small changes in the homogeneity of the local magnetic field. Gradient echo sequences are used more frequently than spin echo, because using sequential RF pulses to rephase protons reduces sensitivity to T2* effects. Fast image acquisition techniques, such as EPI, are important to minimise motion artefacts, including cardio-respiratory effects. In order to maximise the difference between activation and resting T2* decay curves, short TEs are usually selected. The choice of TR depends on the number of slices required, and is usually longer than a second, in order to avoid flow velocity artefacts. Using higher field strength magnets improves SNR, but susceptibility artefacts may also be magnified.

2.3.4 Experimental design

This subject will be discussed in more detail in Chapter 3, in which the visual stimulation paradigm used for this study is described. In this section, a few basic principles will be outlined.

Designs may be categorical or parametric. In categorical designs, two conditions are contrasted, one of which may be a control condition, and any differences in BOLD activation are interpreted as condition-specific cortical processing (Turner et al., 1991). In parametric designs, stimuli are continuously varied (for example, visual stimulation at different flicker frequencies), and cortical responses are modeled to

observe which areas respond in a corresponding manner. More recently, interest has developed in brain default networks which are active during resting conditions. To investigate these, no specific task is required, and the method of data processing and interpretation is different, incorporating principal or independent components analysis.

Design presentation may be epoch-based or event-related. During an epoch-based design, conditions are presented in blocks lasting many seconds, whereas in an event-related design, stimuli are much more transitory and random. The choice of method depends upon experimental considerations, which include efficiency of effect detection, neuropsychological validity, the relative importance of avoiding adaptation and habituation effects, necessity of *post-hoc* categorisation (for example, correct or incorrect response), and whether the temporal characteristics of the BOLD response are of interest.

Stimuli are repeated and averaged to increase SNR. A single attendance for scanning at a given time-point is referred to as a session. Within a session, there are usually several periods of stimulus presentation, and each of these time intervals is called a run. Within processing software packages, these two terms are sometimes used interchangeably.

2.3.5 Data processing: statistical parametric mapping

Functional MRI scans comprise a complex dataset, representing a four dimensional time series reflecting dynamic changes. For ease of interpretation, it is usually necessary to convert this into a three dimensional map, that summarises which anatomical regions of the brain are activated. This temporal dimension causes several problems, including an increased likelihood of motion artefacts, the different time scales over which neural and vascular responses occur, and the impossibility of acquiring each slice in a volume simultaneously. It usually takes a few seconds to acquire an entire brain volume, corresponding to the TR, which results in a slight time delay between slices in the phase of the haemodynamic response that is sampled. In addition, in order to generalise inferences regarding brain activity to population level, it is necessary to investigate group effects. This raises difficulties due to inter-individual differences in anatomy. Finally, there are problems related to statistical testing. In particular, if a mass univariate approach is used, in which tests are carried

out simultaneously across all voxels, then the problem of correcting for multiple comparisons must be considered.

Many of these difficulties may be addressed by pre-processing fMRI data. Several different software packages are available, which have the same core processes in common: data are spatially and temporally preprocessed, a statistical model is specified and estimated, and inferences are made. One of the most widely used is Statistical Parametric Mapping (SPM, Wellcome Department of Neuroimaging London, UK), which was used for all of the fMRI analysis described in this thesis. In SPM, preprocessing incorporates slice timing adjustment, realignment, normalisation and smoothing, a general linear model is used to model the data, and statistical inferences are made by specifying contrasts of interest (Figure 2.13). The statistics are calculated based on how closely the observed data fits the experimentally defined model, and multiple corrections are accounted for, using random field theory.

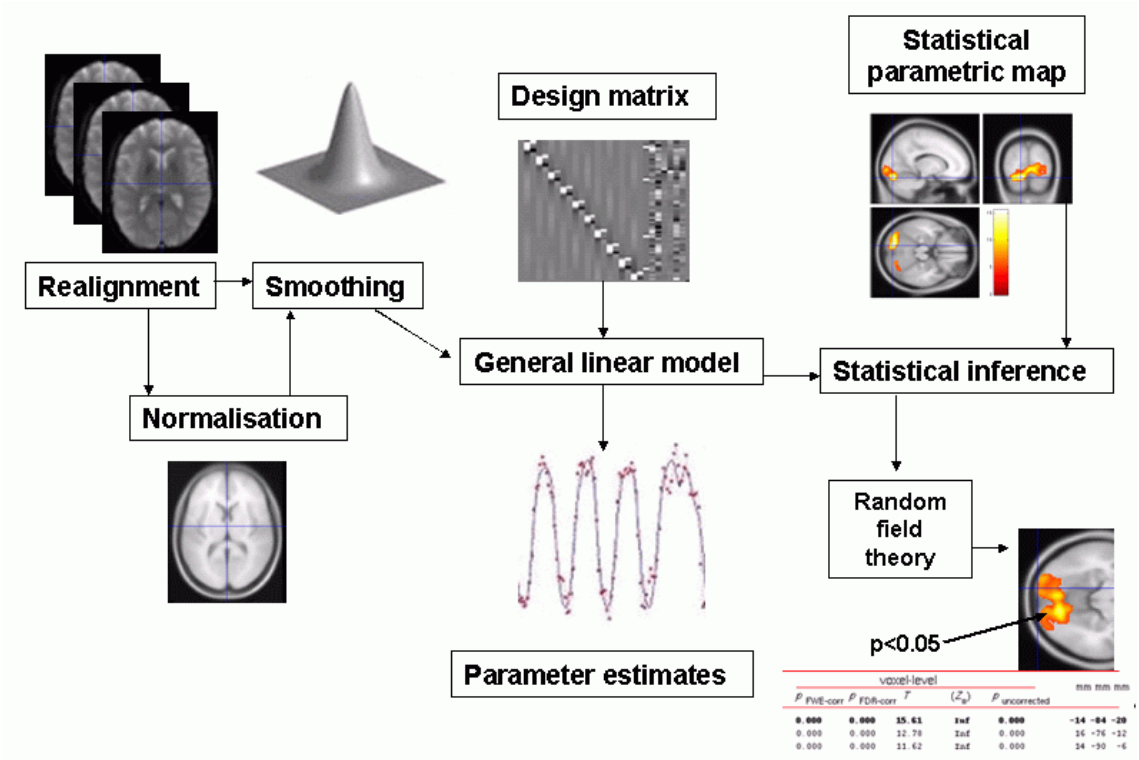

Figure 2.13 A summary of the stages of processing an fMRI time series in SPM. Modified from (Friston, 2003).

2.3.5.1 Slice timing

Differences in slice acquisition time within a volume, resulting from non-simultaneous sampling, may be accounted for in two different ways. If the TR is relatively short, the data may be adjusted with respect to a reference slice. However, if the TR is longer than approximately two seconds this approach is less accurate, and instead a time derivative of the haemodynamic response function is incorporated into the model. This is convolved with the data, in addition to the haemodynamic response function, in order to capture variance in the data associated with differences in time of slice acquisition. The term convolution describes a mathematical operation, performed on two functions, to create a new function, and is used in fMRI pre-processing to reconcile the different time scales over which neural and haemodynamic events occur. This is discussed further in Chapter 3. This method was used to adjust for differences in slice acquisition time in the studies described in this thesis, as the TR was approximately four seconds.

2.3.5.2 Realignment

Over the course of a time series, patient motion may result in misallocation of data from a given voxel to one of its neighbours. In order to prevent this, the time series is realigned in a two stage procedure. Each brain volume is realigned to the first scan of each run (Friston et al., 1995a). These volumes are then all realigned to the first scan of the first run. This is achieved using a six parameter, rigid-body transformation. The six parameters refer to the directions of correction, and comprise translation in the x, y and z directions, and rotation in the pitch, roll and yaw planes. The sum of squared differences between each scan and the reference scan, in each of these directions, is estimated and applied to the data. This process results in an output of the corrections required in each of the six directions, which can be entered later as covariates into the general linear model. Realignment is generally effective, but persistent errors may remain if patients move during volume acquisition, rather than between runs (Grootoonk et al., 2000), and secondary to interactions between patient motion and local field inhomogeneities (Andersson et al., 2001). In addition, motion during previous volumes may influence later ones, through a mechanism of “spin history” effects (Friston et al., 1996b).

2.3.5.3 Spatial normalisation

In order to draw group inferences about areas of brain activation, it is important that all subjects are in the same reference space. This is achieved using normalisation, in which each subject's realigned brain volumes are registered to a standard template. In SPM5, the Montreal Neurological Institute (MNI) template, derived from 305 brains is used (Evans et al., 1993). This is broadly similar to the other commonly used template (Talairach and Tournoux, 1988). Firstly, a linear 12-parameter affine transformation is applied, which incorporates the six parameters used in a rigid body transformation and, in addition, six zoom and shear parameters. During linear registration, transformations are applied to the brain in a uniform manner. In the second stage, non-linear registration is applied. During non-linear registration, transformations are allowed that differentially affect different regions of the brain, a procedure known as warping. Constraints are placed on unlikely warps, which is called regularisation (Ashburner and Friston, 1999).

2.3.5.4 Spatial smoothing

During smoothing, data in a given voxel is averaged with that of its neighbours. This is performed using a smoothing kernel, which is of Gaussian shape, a three dimensional representation of a normal distribution (as shown in Figure 2.13). The purpose is to increase SNR, facilitate group averaging, and render the data more amenable to later statistical analysis, by making errors more normally distributed. The size of the smoothing kernel is decided by the operator, is described by its full width at half maximum (FWHM), and is typically two to three times the voxel size.

2.3.5.5 Model specification

At this stage, details of the experimental procedure are provided by the operator. The times of onset of stimulation are specified (stimulus onset asynchrony, SOA) for each condition of interest (regressor), and the duration of the stimulus. These data are convolved with a haemodynamic response function (illustrated in Figure 2.12), in order to adjust for the different temporal scales over which neural and haemodynamic events occur. The motion parameters from realignment may be entered as covariates

of no interest at this stage, to account for any associated signal variance. In this manner, it is ensured that any observed activations are not a result of patient motion. This is one of the strengths of the general linear modeling (Worsley and Friston, 1995) approach, which is described further in the next section. Other covariates of no interest can also be entered at this point.

2.3.5.6 Model estimation

In SPM, a mass univariate approach is used, in which the experimental model is fitted to the data simultaneously at every voxel (Friston et al., 1995b). A general linear model is used, and the fit of this model to the observed data is then estimated and expressed as a beta value, or parameter estimate, for each regressor, leaving a residual error term. The following equation summarises the general linear model.

$$Y = X\beta+\varepsilon$$

Y is the observed data. There may be multiple X terms, which each correspond to an explanatory variable, known as regressors, and may represent both effects of interest and covariates of no interest. In SPM, these are expressed as a design matrix, in which each column represents one regressor, and the rows correspond to observations over time, from the MRI scans. Beta is the parameter estimate, which describes how well each regressor fits the experimental model, and ε is the error term, which summarises any residual variance in the data that is not explained by any of the regressors in the model.

2.3.5.7 Statistical inference

To test effects of interest, weighted linear combinations of regressors are specified, known as contrasts. Examples of common contrasts include activation versus baseline (1 0), or patient activation versus control activation (1 -1). For each contrast, at each voxel, a t or F statistic is reported. These are derived by comparing the effect of interest (in terms of the change in signal intensity over time, which can be attributed to the regressor), and dividing it by its standard error (in terms of the overall variance

in signal intensity over the course of the experiment). At each voxel, the null hypothesis is that there is no change in signal intensity attributable to that regressor.
The statistics are calculated based on the fit of the model, and corrected for multiple comparisons using random field theory (Worsley et al., 1996). At standard voxel sizes, an average brain volume may comprise more than 200 000 voxels. Accepting a conventional type I error rate of 5% will therefore result in 10 000 false positives. Using a Bonferroni correction would require application of a significance threshold of $p<0.00000025$. However, this is overly conservative, as the test assumes independent observations. This is not the case in the brain, in which groups of voxels represent integrated regional neural networks. Gaussian random field theory is applied to help define an appropriate statistical threshold. In this approach, the brain is considered in terms of resolution elements (resels), rather than voxels. A resel represents an independent observation, and is determined from an estimation of the smoothness of the data. The correction for multiple comparisons is then based on the number of resels, rather than voxels. Subsequent inferences may be made either at voxel or cluster level.

2.3.5.8 Fixed and random effects analyses

The process described up to this point is usually applied to a single subject, and results in a statistical parametric map that summarises regions of activation within that individual. This is known as a fixed effects, or first level, analysis, and the error variance is estimated between scans. In order to make group inferences, which may be generalisable to a population, a second level, random effects analysis is necessary, in which the error variance is estimated between subjects. In a random effects analysis, each individual contributes a first level contrast image, and these may then be interrogated using a variety of statistical models, such as one and two-sample t-tests, analysis of variance, and multiple regression models. More complex factorial designs allow interactions between different conditions to be assessed. Taking individual contrast images from the first level into group analyses at the second level is a summary statistic approach.

2.3.6 Conclusions

The development of the techniques described in this chapter has allowed *in vivo* investigation of mechanisms of pathophysiology of neurological disease, such as ON. Conventional MRI enables visualisation of brain and optic nerve anatomy with superior resolution, DTI facilitates detailed investigation of the integrity of white matter tracts, and fMRI allows assessment of brain physiology. Together, these techniques provide a powerful tool with which to probe disease mechanisms. In this thesis, they are combined to study patients with ON, and the results are reported in chapters 4 to 6. First, in chapter 3, the development and testing of a novel visual stimulation paradigm is described, that was used during subsequent fMRI experiments.

CHAPTER 3

AN FMRI VISUAL STIMULATION PARADIGM DESIGNED TO MINIMISE ATTENTION, ADAPTATION AND LOSS-OF-FIXATION BIASES

In order to overcome some of the current limitations of visual stimulation fMRI paradigms, a novel methodology to facilitate visual stimulation was developed, which is described in this chapter. The paradigm was then applied to the subjects in this study in subsequent experiments. This chapter is divided into three sections. The first two sections deal with the main issues related to fMRI study design. An important general consideration is design efficiency, and issues related to this are discussed first. In the second section, problems specific to visual stimulation paradigms and the study of ON are outlined. Methodologies used in previous studies are summarised, and remaining difficulties are identified, which relate to attention, adaptation and loss-of-fixation biases, in the context of monocular stimulation. These issues are then addressed in the third section of this chapter, which presents the description and validation of the experimental design in a pilot group of healthy subjects. Proof-of-concept is tested in a patient with severe visual loss.

SECTION 1: DESIGN EFFICIENCY

In general terms, efficiency in the context of fMRI may be defined as a quantification of how well a design is able to answer the experimental question, through detecting effects of interest. When considering this further, the concept of efficiency may be approached from either a signal processing perspective, or in terms of the general linear model.

3.1.1 Design efficiency in terms of the general linear model

During fMRI processing, experimental conditions are convolved with the haemodynamic response function (Figure 2.12), which allows for the differing time scales over which haemodynamic and neural events occur (see section 2.3.5.1). The haemodynamic response function is convolved with a box-car function representing

the time scale of experimental events. This results in a new function, which is a prediction of fMRI responses and forms the basis for the experimental model. The model may be expressed in general linear terms, as discussed in Chapter 2:

$$Y=X\beta + \varepsilon$$

The observed data (Y) is then fitted to this model and parameter estimates (β) for each effect of interest (X) are calculated, leaving a residual error term (ε), which summarises unexplained variance in the data. The experimental aim is to minimise the variance in β. This will then be reflected in a higher sensitivity to detect statistical significance. As the variance in β is reduced, design efficiency is increased. Variance in β may be minimised either by the data itself, or by the experimental design. Factors in the design which affect efficiency include design type (epoch or event-related), noise filtering, sequencing and spacing of trials, and the temporal relationship between stimulus presentation and scan acquisition. These factors will be discussed in turn.

3.1.2 Design efficiency in terms of signal processing

Design efficiency is related to stimulus presentation, through signal processing considerations. Efficiency calculations for six commonly used fMRI designs are shown in Figure 3.1 (Friston et al., 1999). A fixed deterministic design refers to an event related design in which stimuli are presented at equal intervals, and is relatively inefficient. In a stochastic event-related design, the probability of stimulus presentation may be constant or varied, and the rate of variation may be slow or fast. All of these factors affect efficiency. A variable deterministic design is synonymous to a blocked design, and it may be seen from Figure 3.1 that this type of design is highly efficient.

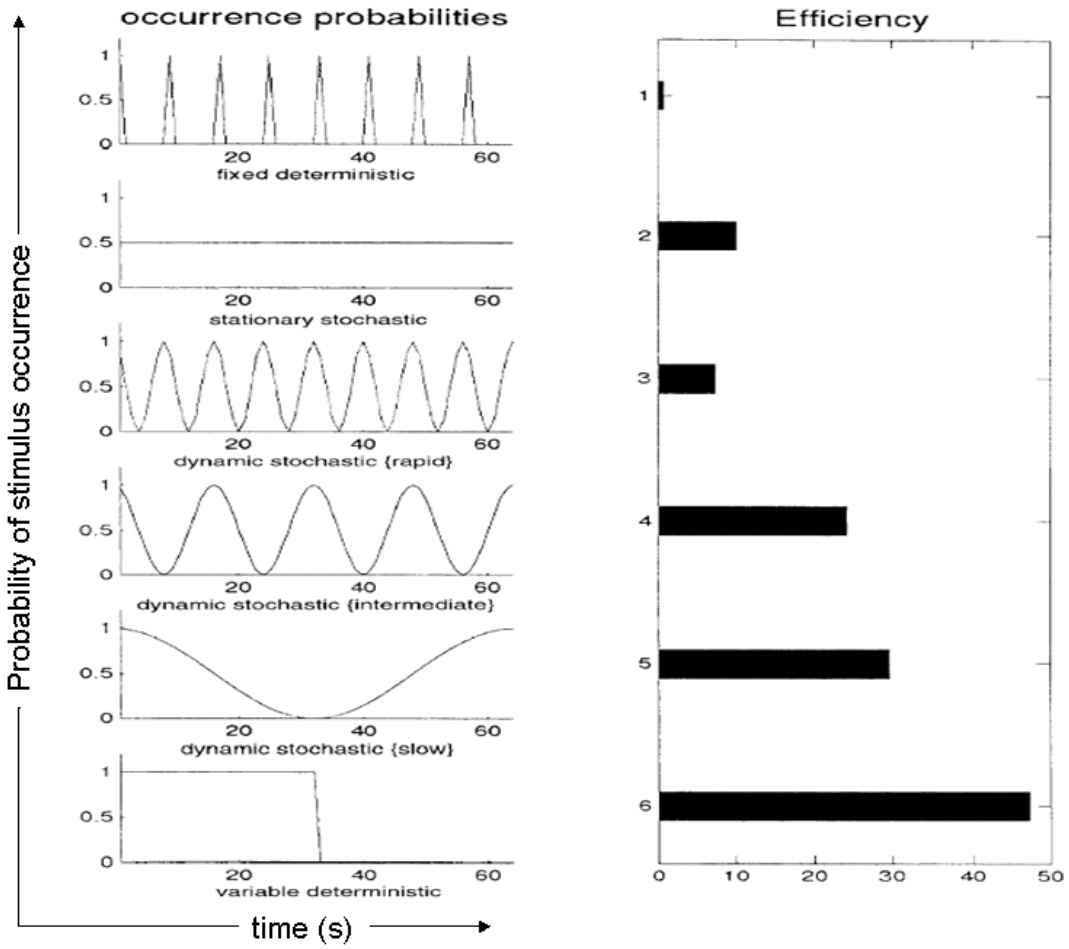

Figure 3.1 Design efficiency calculations for different types of design. Modified from (Friston et al., 1999).

The reasons for these differences in efficiency are related to the temporal characteristics of the haemodynamic response function (hrf). From an MRI signal processing perspective, design efficiency may be considered as the ability to detect signal related to effects of interest from surrounding noise. Efficiency may be optimised by using a design which maximises the predicted variability in signal between contrasting conditions, as illustrated in Figure 3.2.

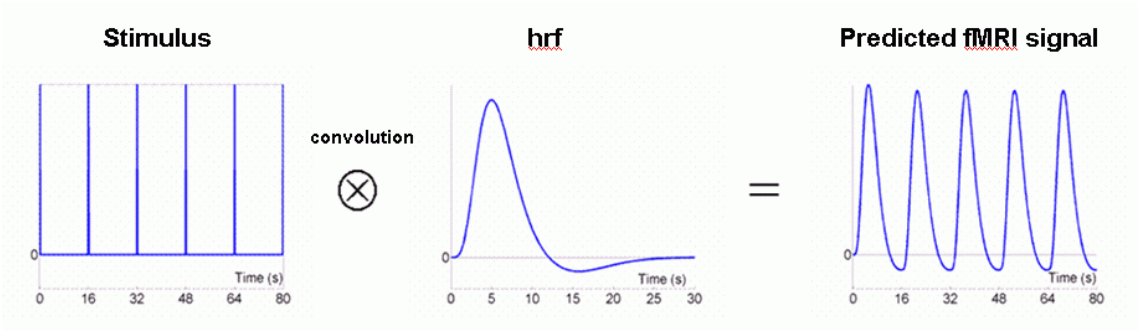

Figure 3.2 Convolution of a neural stimulus with the haemodynamic response function. This results in a prediction of the fMRI signal, which varies widely in this experimental model. Modified from (Henson, 2005, http://imaging.mrc-cbu.cam.ac.uk).

Therefore, the timing of delivery and duration of stimuli affects efficiency because, after convolution with the hrf, the variability of predicted signal is affected. This can be illustrated using an inefficient design, such as a fixed deterministic event-related design with short inter-stimulus intervals. The result is minimal variation of predicted signal, which merely oscillates around a raised baseline (Figure 3.3).

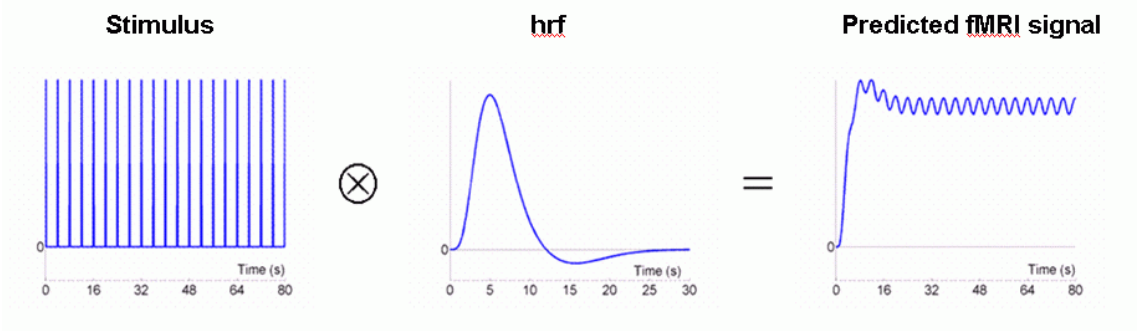

Figure 3.3 An example of an inefficient design. Rapid, regular presentation of stimuli without spacing results, after convolution, in minimal variation of predicted MRI signal. Modified from (Henson, 2005, http://imaging.mrc-cbu.cam.ac.uk).

The efficiency of the blocked design can then be explained in terms of wide variations in predicted signal, as shown in Figure 3.4. The optimal length of block has been shown to be 16 seconds (Friston, 2003). Shorter duration blocks result in less variability, because of the temporal characteristics of the hrf, and longer block durations encounter problems related to noise filtering.

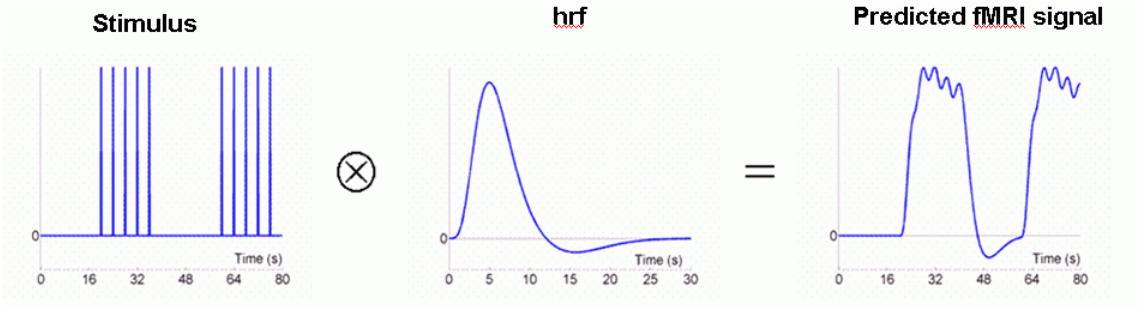

Figure 3.4 An example of an efficient design. This epoch-based design has block lengths of 16s, resulting in wide variability in the predicted signal. Modified from (Henson, 2005, http://imaging.mrc-cbu.cam.ac.uk).

3.1.3 Noise filtering

There are several different sources of noise in fMRI data. Head motion, cardiac pulsation and respiratory oscillation effects were discussed in Chapter 2. In addition, "white noise", related to scanner hardware, is constant and randomly distributed throughout the image. There is also low frequency noise, which is thought to be related to slow periodic haemodynamic changes, involved in maintenance of tone in the cerebrovascular vessels. This is referred to as 1/f noise (Figure 3.5), and is removed using a high pass filter during processing.

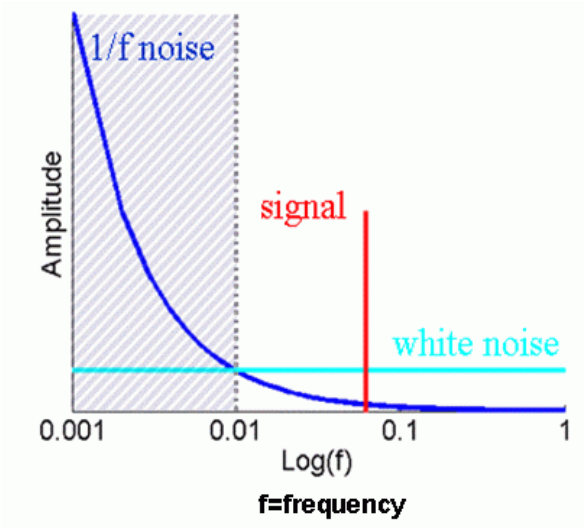

Figure 3.5 Sources of noise in fMRI data, plotted by frequency.

In order to explain how this relates to the decrease in efficiency of longer duration epochs, it is necessary to consider the Fourier transform, which converts MRI data from the time domain to the frequency domain (Figure 3.6).

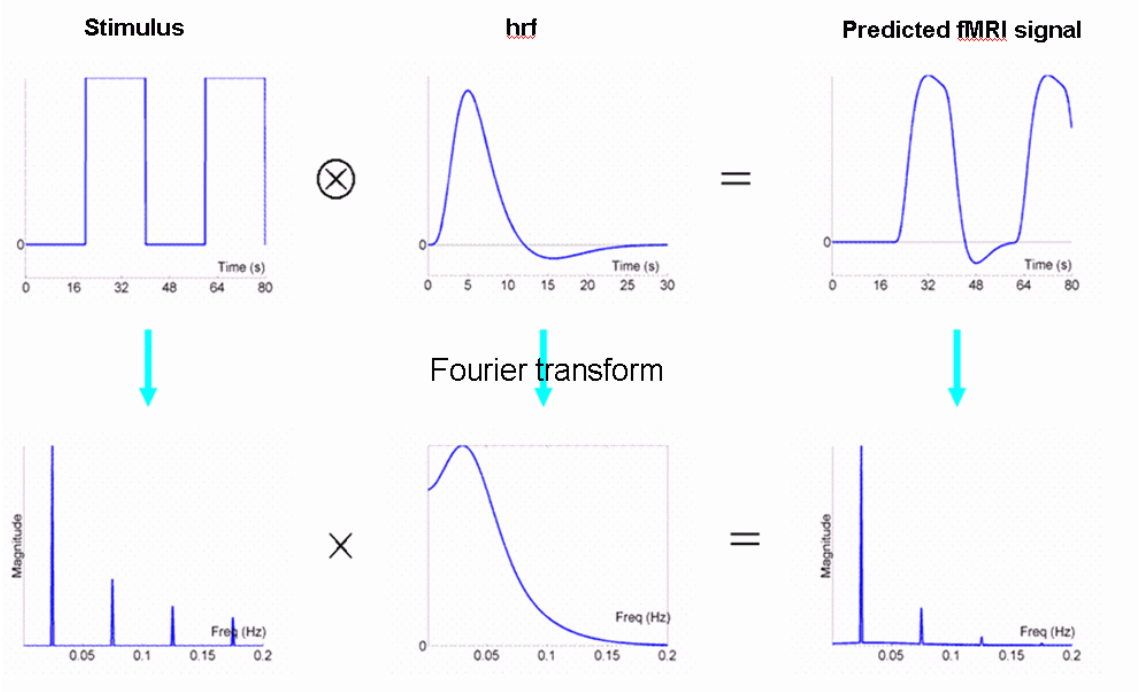

Figure 3.6 Fourier transform of design stimuli, hrf and predicted MRI signal from the time domain into the frequency domain. Modified from (Henson, 2005, http://imaging.mrc-cbu.cam.ac.uk).

It may be observed from Figure 3.6 that in this design, following the Fourier transform, the majority of the predicted data is of low frequency. The frequency is determined by the length of stimulus blocks, with longer blocks resulting in lower frequencies. It is also clear that the shape of the hrf is transformed, so that low frequency data is removed and, indeed, the hrf may be considered as a high pass filter. Whilst this usefully removes 1/f noise, it also means that data of interest may be filtered, if stimulation blocks are long (Figure 3.7).

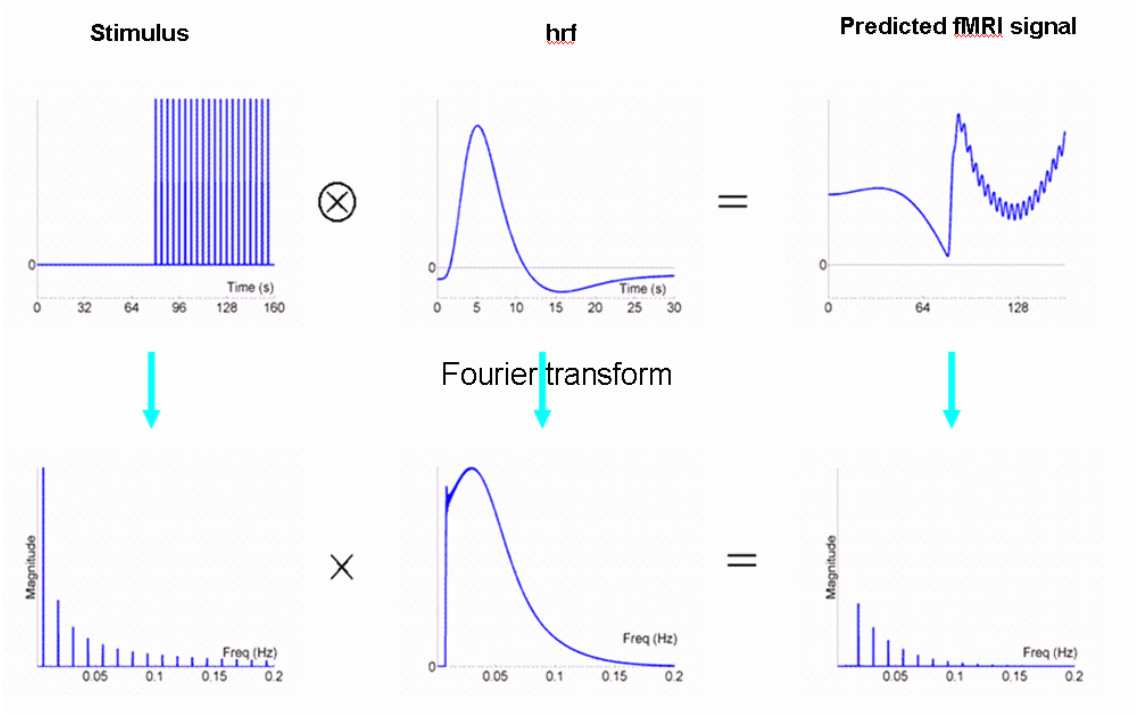

Figure 3.7 The effect of long duration blocks on predicted signal, after a Fourier transform. The hrf acts as a high pass filter, and removes the data along with low frequency noise. Modified from (Henson, 2005, http://imaging.mrc-cbu.cam.ac.uk).

3.1.4 Sequencing and spacing of stimuli

An epoch-based design with block lengths of 16 seconds was selected for this study, in order to optimise efficiency. Sequencing and spacing are more pertinent to event-related designs, and so will not be discussed in depth. Spacing describes the time between events of the same type, and sequencing the presentation order of different trial types, and both these factors affect design efficiency. Optimal spacing depends upon whether the experimental effect of interest is the mean of two or more conditions, or the difference between them. This is also a consideration when considering the most efficient sequence, for example, alternating (e.g. ABABAB) or permutational (e.g. ABBABA). The decision to include null events, a "baseline" condition, also affects contrast efficiency.

3.1.5 Stimulus presentation and scan acquisition

Bias may be introduced if the duration of stimulus blocks is an exact multiple of the volume acquisition time, for example, a block length of 16s and a TR of 4s. This may

result in each slice of brain being sampled at the same point of the hrf, in each successive TR. This can cause a problem, as regions sampled near the peak of the hrf may show greater changes in BOLD signal. Therefore, it may be avoided either by choosing a block length which is not an exact multiple of TR, or introducing a jitter between stimulus onset and scan acquisition (Figure 3.8).

For this study, as block durations of 16s were used, the TR was chosen to be 3.95s to avoid this effect.

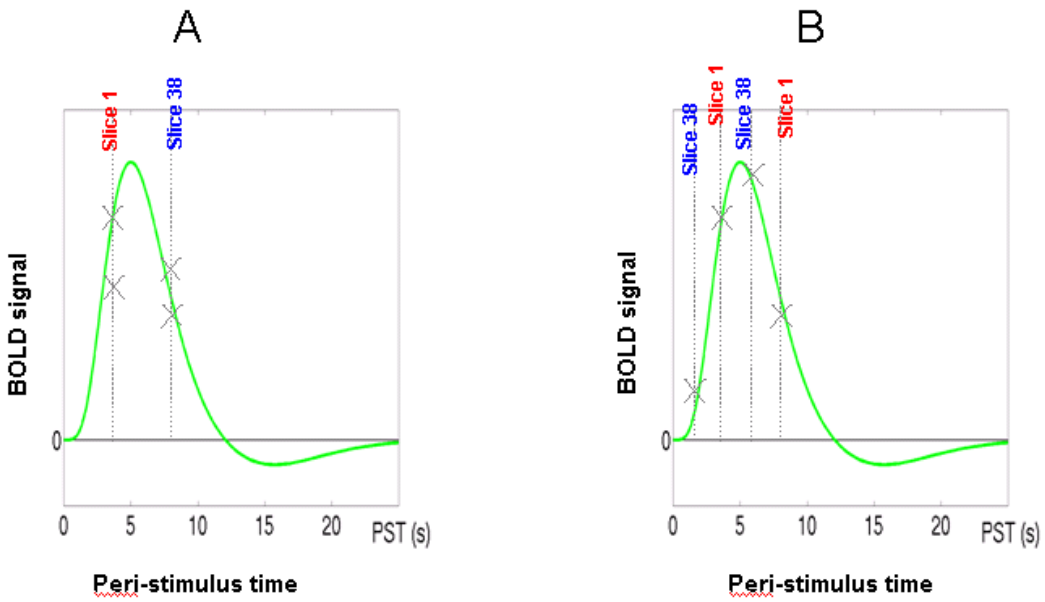

Figure 3.8 The relationship between block length and scan acquisition time. In the left graph (A), sampling of the hrf is illustrated when block length is an exact multiple of TR. In the right graph (B), sampling is shown when block length is not a multiple of TR, or jitter is introduced. Modified from (Jones, 2004, http://www.fil.ion.ucl.ac.uk/spm/).

SECTION 2: PROBLEMS IN VISUAL PARADIGM DESIGN

3.2.1 Methodology of visual activation

A variety of different methods of stimulus presentation have been used in previous visual fMRI studies, depending on the experimental aims. In particular, the selection depends upon whether a specific aspect of visual processing is of interest (for example, motion or colour), or if the goal is to deliver a stimulus which results in robust, generalised activation of visual areas. In the latter case, flashing or reversing checkerboards are most commonly used, and were applied in the earliest fMRI experiments (Ogawa et al., 1990;Ogawa et al., 1992), as well as in recent studies.

Stimulation may be monocular or binocular. In studies of diseases which result in monocular blindness, such as ON, comparisons between affected and fellow eye responses are often of interest. Most previous fMRI studies in ON have therefore used paradigms which stimulate the monocular whole field* using flashing lights (Rombouts et al., 1998), or reversing checkerboards (Gareau et al., 1999;Werring et al., 2000;Russ et al., 2002;Toosy et al., 2002;Langkilde et al., 2002;Toosy et al., 2005;Levin et al., 2006; Korsholm et al., 2007;Korsholm et al., 2008), although some early studies also applied binocular stimulation (Rombouts et al., 1998;Gareau et al., 1999). Whole field paradigms produce activation in the entire primary visual cortex, which encompasses the calcarine fissure, and also in higher hierarchical visual processing areas. Hemi-field stimulation has also been applied, which selectively activates the contralateral hemisphere (Langkilde et al., 2002). The development of retinotopic mapping (Sereno et al., 1995) allowed more accurate localisation of activation, including identification of hierarchical visual areas (V1, V2, V3, V4, V5/MT, etc) in individual subjects, but this approach necessitates more extensive post-processing.

*The term whole field is used to refer to a stimulus covering the whole projection screen or goggle, rather than just part of it, such a single hemi-field. It is not synonymous with the term Ganzfeldt stimulation, which describes stimulation of the entire extent of perceived visual field.

3.2.2 Stimulus presentation, attention, adaptation and loss of fixation

With regard to the method of stimulus presentation, there is no universally agreed "gold standard". Previous studies have used projection screens, with patching of the fellow eye (Russ et al., 2002;Langkilde et al., 2002;Korsholm et al., 2007;Korsholm et al., 2008), or voluntary eye closure (Russ et al., 2002), light proof light emitting diode (LED) goggles (Gareau et al., 1999;Werring et al., 2000;Toosy et al., 2002;Toosy et al., 2005), and liquid crystal display (LCD) shutter glasses (Barnes et al., 2001). The alternative strategies of using glasses/goggles, or a projection screen, have different advantages and disadvantages.

Maintaining fixation and monitoring attention are particular problems when using LED goggles, or LCD shutter glasses, to deliver monocular stimuli if visual acuity is reduced in one eye. During periods of affected eye stimulation, the patient may not be able to see the fixation cross, or respond to visual cues ensuring attention. This makes it very difficult to determine if the patient is fixating and attending to the stimulus, which can introduce errors, and confound subsequent data interpretation. Loss of fixation may be especially problematic, if the experimental aim is to alternately stimulate different regions of the visual field, for example, during retinotopic mapping.

On the other hand, using goggles or glasses facilitates the alternation of a monocular stimulus between the two eyes, within the same scanning run. This is a practical problem when using projection screens, but it is important to do it, as attention and adaptation effects may vary across the course of a run, and influence the fMRI response to visual stimuli (Posner and Petersen, 1990;Watanabe et al., 1998;Chawla et al., 1999;Rees and Lavie, 2001;Haynes et al., 2005a). Adaptation refers to a decrement in fMRI response, seen with repeated stimulus presentation. A recent study showed that short-term adaptation effects were evident in controls, and preserved in patients with MS, over a series of four runs of a simple motor task, presented over a 25 minute period (Mancini et al., 2009).

3.2.3 Colour

Different stimuli have been used in previous studies, for example, black and white checkerboards (Russ et al., 2002), chromatic stimuli, such as blue and yellow

checkerboards (Gareau et al., 1999), and red LED checkerboard displays (Werring et al., 2000;Toosy et al., 2002;Toosy et al., 2005). This may be a relevant consideration when studying patients with optic nerve diseases, as deficits of colour and contrast sensitivity may persist after recovery of acuity (Mullen and Plant, 1986;Plant and Hess, 1987). Therefore, the choice of whether to use a black and white or chromatic stimulus may have advantages and disadvantages. Black and white stimuli provide a strong luminance contrast. This is relatively reduced using chromatic stimuli, which could potentially result in less activation. However, it is possible that detection of differences between groups of patients with good and poor recovery might be enhanced, through an increased sensitivity to patients with incomplete recovery of colour vision. Achromatic stimuli are detected via the magnocellular pathway, whereas chromatic stimuli are detected via the parvocellular pathway. It is debated whether magnocellular (Regan et al., 1991;Phillips et al., 1994) or parvocellular fibres (Wall, 1990;Porciatti and Sartucci, 1996; Caruana et al., 2000; Evangelou et al., 2001) may be preferentially affected in ON, or whether they are equally susceptible to damage (Russell et al., 1991). Therefore, it is possible that selective stimulation of the parvocellular and magnocellular pathway could influence sensitivity to detect disease effects with fMRI, and this type of psychophysical manipulation has been performed in previous studies (Phillips et al., 1994; Caruana et al. 2000).

SECTION 3: EXPERIMENTAL DESIGN

3.3.1 Introduction: aims and objectives

The aim was to devise a practical strategy to overcome the difficulties outlined in the previous two sections, which could then be applied to subjects with monocular visual loss. In this section, the results of a pilot study are reported, involving a group of healthy control subjects. In addition, a patient with severe visual loss is included, to demonstrate proof-of-concept in a subject who represents an extreme example of the problems of fixation and confirmation of attention inherent in the main study group.
The experimental objectives were as follows: (1) To achieve alternating monocular stimulation of each eye within the same scanning run (2) To ensure and confirm maintenance of attention in control subjects, and in conditions of monocular visual loss (3) To facilitate central fixation in controls, and in conditions of monocular visual loss.

3.3.2 Methods

3.3.2.1 Participants

Seven healthy controls with normal vision (mean age 30, 6 females) were recruited, together with a patient (age 30, female) with severe acute unilateral ON. The patient had complete monocular visual loss (to no light perception), with normal vision in the fellow eye. All subjects gave informed written consent. The study was approved by the local Ethics Committee.

3.3.2.2 MRI scanning

Scans were performed on a 1.5T Signa Excite whole-body MRI System (GE, Milwaukee, USA), with an 8-channel head coil. FMRI data were acquired in 8-10 runs using a T2*-weighted echo-planar imaging sequence. Thirty eight slices were acquired, each 2mm thick, with a 1mm inter-slice gap, parallel to the AC-PC line,

covering the whole brain, with TE 50ms, TR 3950ms, field of view 20cm, matrix size 64x64 and an acquisition time of approximately 5 minutes per run.

3.3.2.3 Paradigm design

The idea of combining plano chromatic filter goggles with monochromatic checkerboards, presented on a projection screen, was devised to allow alternating monocular stimulation of both eyes within the same scanning run. The methodology has subsequently been implemented in another fMRI study (Levin et al., 2006). A rectangular projection screen was used, which covered 28 degrees of visual angle vertically and 30 degrees horizontally, at a viewing distance of 57cm. The goggles had one green filter, and one red filter (Haag-Streit, UK) (Figure 3.9).

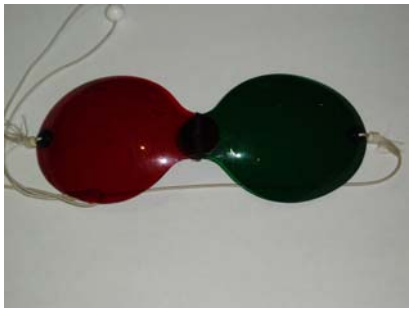

Figure 3.9 Transparent plano chromatic filter goggles used in visual fMRI experiments.

Green checkerboards of a particular spectral density distribution, presented on the projection screen, were invisible through the red filter, and likewise for red checkerboards viewed through the green filter. Monocular stimulation could then be achieved, by alternately presenting green and red checkerboards, whilst subjects were instructed to fixate a blue central cross, visible to both eyes. During periods of affected eye stimulation in patients, the fellow eye could still see the fixation cross, and it was therefore possible to confirm that the patient was continuing to pay attention, by responding to visual cues. It was also possible to infer that the affected eye was aligned with the stimulus, through a mechanism of conjugate fixation.

The experiment began with four runs of quadrant-specific activation, through chromatic goggles, to assess the feasibility of the technique using localised stimuli. This was followed by two runs of stimulation through the goggles, covering the whole

projection screen, and then two runs of whole screen black and white stimulation, without chromatic goggles, using an alternated eye patch. This was in order to compare the performance of the new technique with a more traditional method, using similar stimuli. The subjects remained in the head-coil between sessions.

The experimental paradigm is summarised graphically in Figure 3.10.

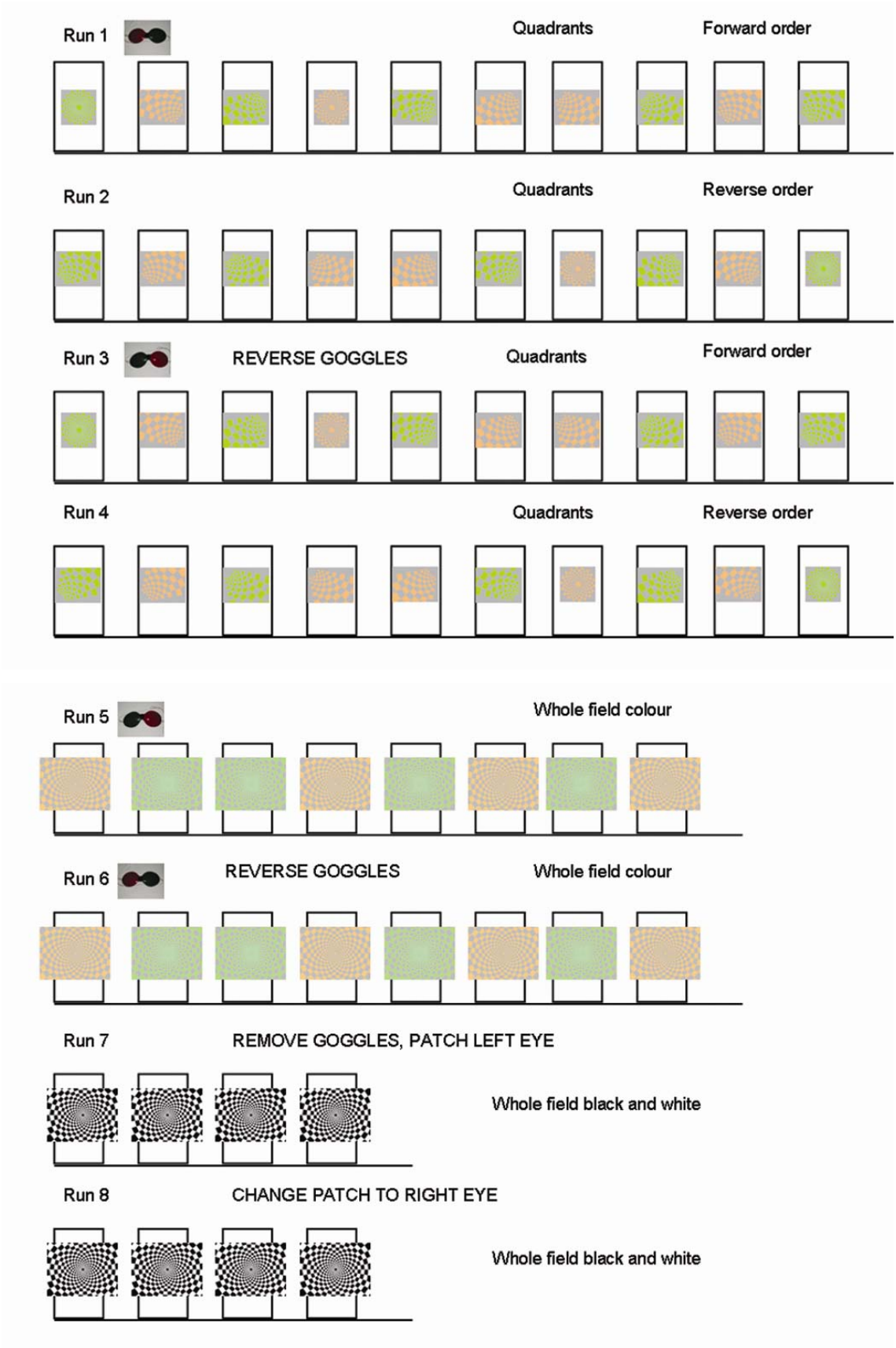

Figure 3.10 Graphic summary of the main visual fMRI protocol, comprising eight runs.

In four of the controls, an additional experiment was performed for a further two runs, during which the degree of "crosstalk" between the goggles was assessed. In this experiment, the subjects wore a patch on one eye underneath the chromatic goggles, and the condition of interest was the epochs in which the subject was looking at the opposite colour checkerboard, which was supposed to be invisible (Figure 3.11).

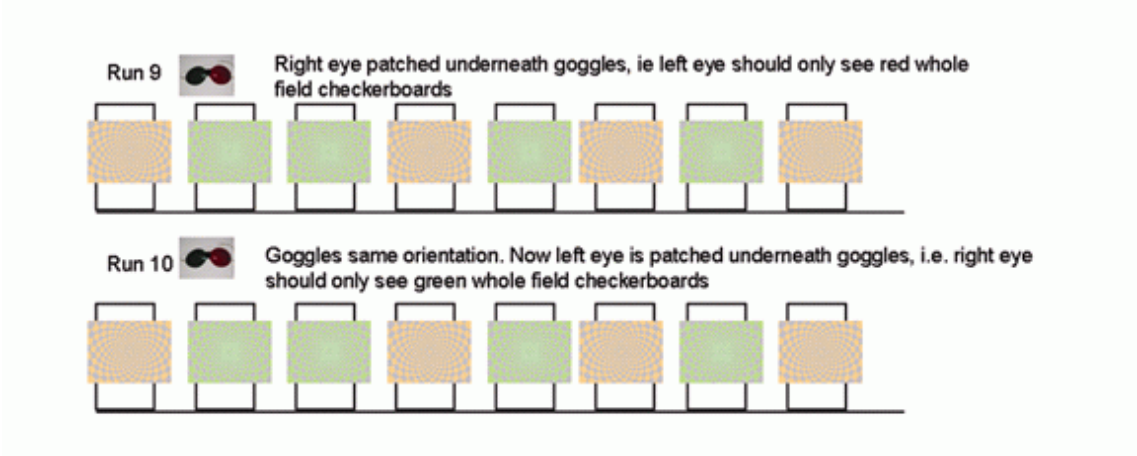

Figure 3.11 Graphic summary of the crosstalk experiment.

3.3.2.3.1 Lateralisation and localisation of quadrant-specific activation

Quadrant-specific checkerboards were used to demonstrate the feasibility of the approach using localised stimuli, and with later investigation of visual field defects in mind (Chapter 6). The hypothesis was that lateralised occipital activation, located appropriately above or below the calcarine sulcus, would be expected if attention and central fixation were generally well maintained, and each eye adequately isolated.

Subjects were instructed to fixate a central blue cross, which appeared black to each eye through the goggles. They viewed 8Hz flickering checkerboard stimuli, which were either a peripheral quadrant or a central circle. The quadrants extended from 5 to 15^{o} eccentricity horizontally, and 5 to 14^{o} vertically, in sectors of 70^{o}, centred on the 45^{o}, 135^{o}, 225^{o} and 315^{o} radii. The central checkerboard extended from 0 to 5^{o} eccentricity, in a complete circle. The borders of the checkerboard squares were radii 10^{o} apart. The size of the squares increased with distance from the centre in a linear manner, consistent with the cortical magnification factor (Slotnick et al., 2001) (Figure 3.12).

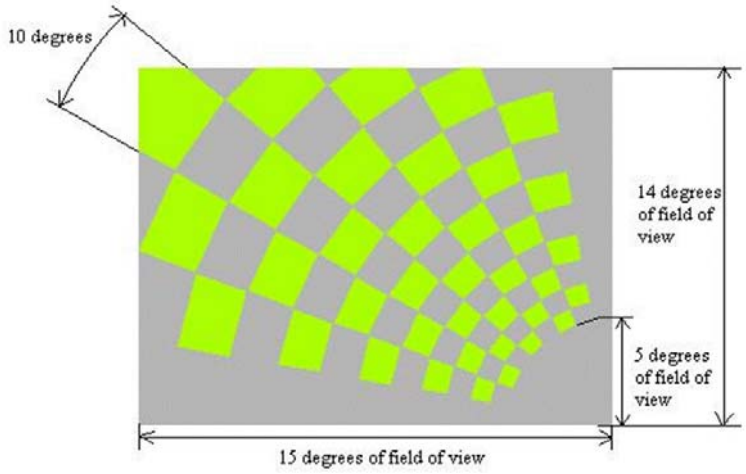

Figure 3.12 Dimensions of a quadrant.

The luminances of the checkerboards were approximately equal (green 1.32cd/m^2; red 1.23cd/m^2). The chromaticities (RGB gun intensities) of the checkerboard stimuli were as follows: 0.31 red and 0.46 green comprising the green checkerboard, and 0.44 red and 0.34 green comprising the red checkerboard. These parameters resulted in red checkerboards that were judged to be of zero contrast when viewed through the green filter, and likewise for the green checkerboards through the red filter.

This part of the experiment comprised four runs. The initial orientation of the goggles (i.e. red filter on right or left eye) was randomised. After two runs, the orientation of the goggles was reversed. Each of these runs consisted of ten epochs of stimulation and ten of rest. The duration of each epoch was 16 seconds. For sessions 1 and 3, the ten stimulation epochs were applied in pseudo-randomised sequence, to the central field and all four quadrants of each eye. In runs 2 and 4, this sequence was repeated in reverse. During rest, the subjects continued to fixate on the blue cross, presented on a grey background screen without checkerboards.

3.3.2.3.2 Adequacy of isolation: assessment of crosstalk

In addition to assessment of lateralisation, an additional experiment was performed in a subset of controls to quantify how well the goggles isolated each eye. A patch was applied to each eye, in turn, underneath the filter goggles. Activation was assessed during the epochs when the unpatched eye was looking at the opposite colour

checkerboard, which covered the whole screen. This was supposed to be invisible to the subjects, who were stimulated in this manner for four epochs, each of 16 seconds duration, interspersed with four epochs of visible checkerboards, in a pseudo-randomised order.

3.3.2.3.3 Goggles versus patches: assessment of attention

The performance of the new technique, using chromatic goggles, was compared to a more traditional technique of alternated eye patching. The outcome measure was the number of correct responses to changes in the central fixation cross.

For this part of the experiment, each subject underwent two runs of stimulation through the chromatic goggles, with checkerboards covering the whole screen, for a total of eight epochs, four for each eye, in pseudo-randomised order. Each epoch was of 16 seconds duration. The orientation of the goggles was reversed between runs.

The chromatic goggles were then removed, and two runs of black and white checkerboard stimulation followed. An eye patch was applied, first to one eye, and then switched to the other, between runs. The black and white checkerboards covered the whole screen, and were presented for four epochs, followed by four of rest. Each epoch was again of 16 seconds duration.

The subjects' performance was assessed at a task, designed to ensure maintenance of attention, and assist fixation. The subjects were asked to press a button, with their right index finger, when the central fixation-cross changed to a hash symbol (#). This occurred at a random frequency several times during each of the sessions, during rest epochs. Responses were recorded, and entered as covariates into the design matrix, in order to account for any variance associated with activation of motor areas.

3.3.2.4 Post-processing

Post-processing was performed, using SPM5 (www.fil.ion.ucl.ac.uk/spm). Each fMRI series was realigned, normalised to MNI stereotactic space and smoothed, using an 8mm isotropic Gaussian kernel. Realignment parameters and time derivatives were entered as covariates into the general linear model, together with the time-points at which the subjects pressed the button during the task to maintain attention.

3.3.2.4.1 Lateralisation and localisation of quadrant-specific activation

For each subject, first-level fixed effect contrasts were specified for each eye individually (1 0 and 0 1 respectively), combining epochs of stimulation through the red and green filters. The effectiveness of the stimuli, and accuracy of lateralisation of quadrant-specific activation, was assessed using a first-level +1 contrast in SPM5, for each condition, in each subject. For each quadrant condition, successful activation was defined as a significant, lateralised maximal cluster ($p<0.05$ corrected), centred appropriately above, or below, the calcarine sulcus. For the central circle, successful activation was defined as significant bilateral occipital clusters. The number of successful stimulation conditions was divided by the total number of presented conditions, and expressed as a percentage, for the control group and the patient's fellow eye.

3.3.2.4.2 Adequacy of isolation: assessment of crosstalk

The amount of crosstalk between the two eyes was quantified, in order to assess how effective the goggles were at isolating each eye, to ensure that stimulation was truly monocular. Data was extracted from a region-of-interest, placed in primary visual cortex, using a generic Brodmann area 17 brain atlas template (Rorden and Brett, 2000). Mean activation was compared during the condition in which the controls were looking at a checkerboard designed to be invisible, and the condition when the checkerboard was visible, from the same run, by entering the contrast images from the first-level analysis into a second-level paired t-test. The hypothesis was that no significant fMRI activity would be evident in the visual cortex during observation of the invisible checkerboard, and that this would differ significantly from observation of the visible checkerboard. The results reported are parameter estimate units, which reflect the magnitude of BOLD signal change.

3.3.2.4.3 Goggles versus patches: assessment of attention

The number of correct responses to fixation cross changes was compared between the chromatic goggle and eye patch techniques in controls, using a paired t-test in Stata-9.2 (StataCorp, Texas, USA). Two-tailed values of $p<0.05$ were considered significant. In addition, the percentage of correct responses was reported for the patient.

3.3.2.5 Visual phenomena

The control subjects were asked to report any visual phenomena noted whilst in the scanner, by filling in a questionnaire.

3.3.3 Results

3.3.3.1 Lateralisation and localisation of quadrant-specific activation

Following quadrant stimulation in the control subjects, and the patient's unaffected eye, activation was seen localising, as anticipated, to the contralateral hemisphere of the occipital lobe, with the lower quadrants represented above, and the upper quadrants below, the calcarine fissure. Stimulation of the central circle resulted in bilateral occipital activation. Successful activation was seen 80% of the time. Examples of statistical parametric maps from a control subject (Figure 3.13), and the patient's fellow eye (Figure 3.14), are shown. No activation was seen on stimulating the patient's affected eye.

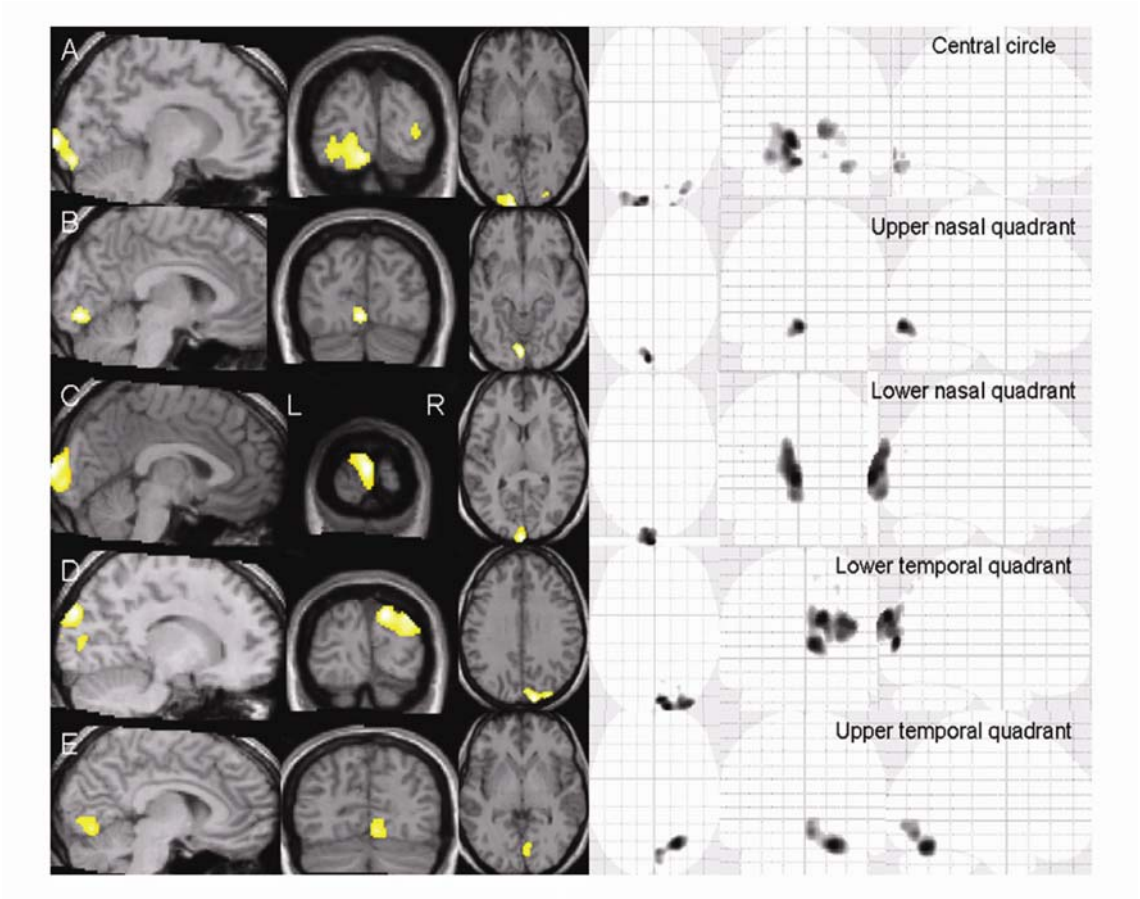

Figure 3.13 A statistical parametric map demonstrating fMRI responses to stimulation of a control subject's left eye, using region-specific stimuli and the chromatic filter goggles. Activation clusters are thresholded at a voxel-level family-weighted-error rate of $p<0.05$, and overlaid on to the patient's structural image, and the SPM5 glass brain. (A) Bilateral occipital activation is demonstrated following stimulation with the central circle. (B) Following stimulation of the upper nasal quadrant, left sided activation below the calcarine sulcus is seen. (C) Lower nasal quadrant stimulation resulted in left sided supra-calcarine activation. (D) Lower temporal stimulation resulted in right sided supra-calcarine activation. (E) Upper temporal stimulation resulted in right sided infra-calcarine activation.

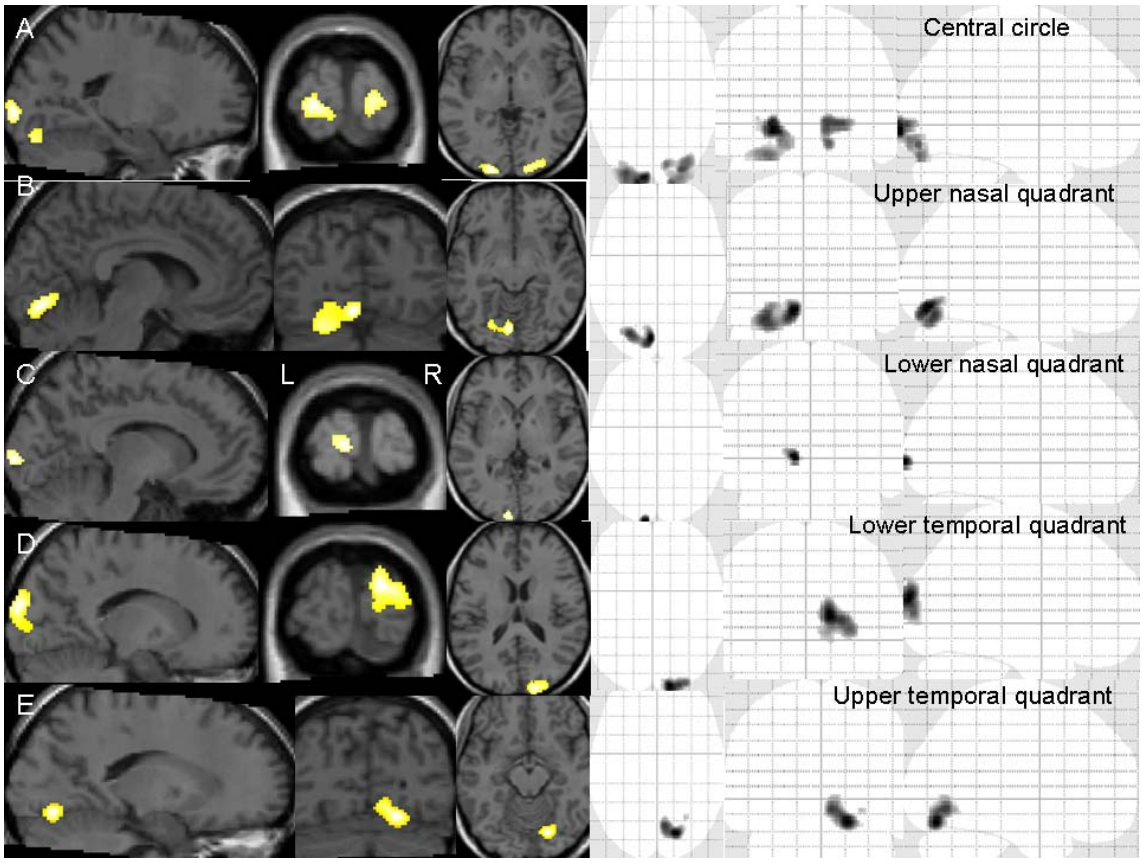

Figure 3.14 A statistical parametric map demonstrating fMRI responses to stimulation of the patient's fellow left eye, using region-specific stimuli and the chromatic filter goggles. Activation clusters are thresholded at a voxel-level family-weighted-error rate of $p<0.05$, and overlaid on to the individual's structural image, and the SPM5 glass brain. (A) Bilateral occipital activation is demonstrated following stimulation with the central circle. (B) Following stimulation of the upper nasal quadrant, left sided activation below the calcarine sulcus is seen. (C) Lower nasal quadrant stimulation resulted in left sided supra-calcarine activation. (D) Lower temporal stimulation resulted in right sided supra-calcarine activation. (E) Upper temporal stimulation resulted in right sided infra-calcarine activation.

3.3.3.2 Adequacy of isolation: assessment of crosstalk

There was no evidence of any significant crosstalk. Results are plotted in Figure 3.15. Mean activation during the epochs observing the invisible checkerboard was 0.028 units (95%CI -0.22, 0.28), with the confidence interval including zero. This was compared to a mean parameter estimate of 0.880 units for the stimulation condition

(95%CI 0.64, 1.11, t=8.55, p<0.001).

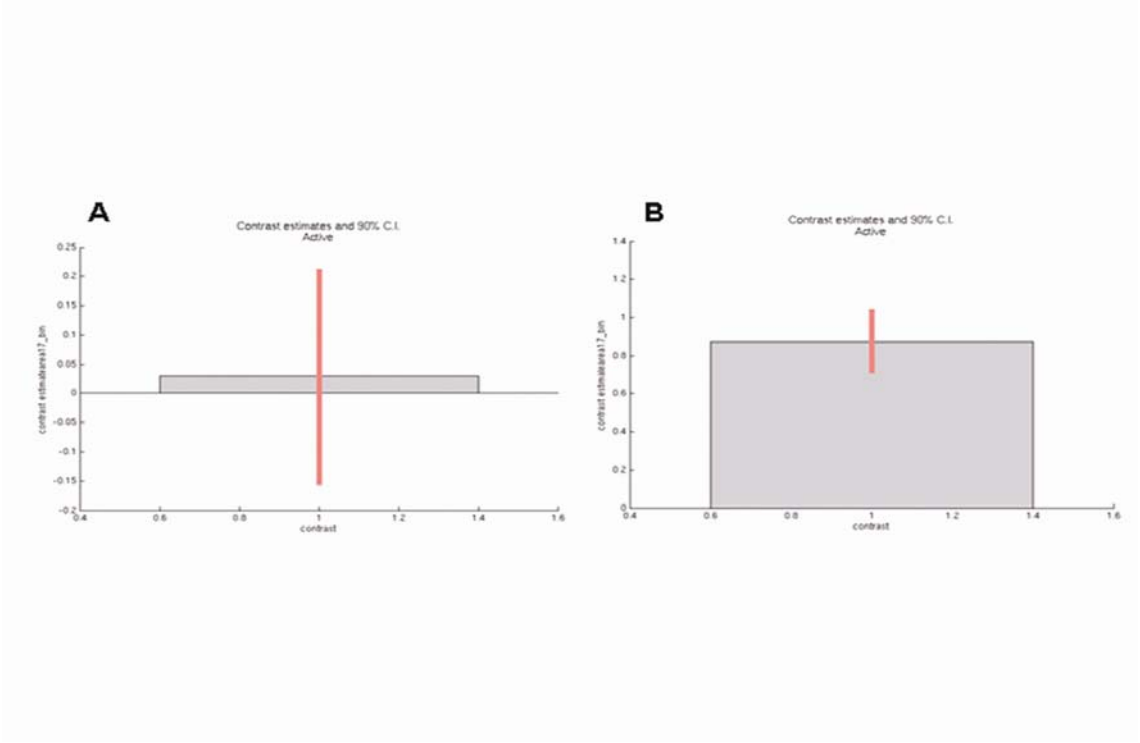

Figure 3.15 Graphs demonstrating the magnitude of activation in primary visual cortex in controls, during (A) the crosstalk test condition, and (B) following checkerboard stimulation through chromatic goggles, during the same run. The scale on the y-axis is in parameter estimate units, representing blood-oxygenation level dependent (BOLD) signal change.

3.3.3.3 Goggles versus patches: assessment of attention

The patient was unable to perceive light in the affected eye at the time of the scan, but successfully detected 93% of fixation cross changes, using the chromatic goggles, compared with 0% with patches.

In controls, there were no significant differences between the two techniques (chromatic goggles mean 94%, patches 81%, t=1.75. p=0.14).

3.3.3.4 Visual phenomena

The control subjects reported some transient instability of the visual percept, when using the chromatic goggles: six of the seven reported seeing the fixation cross move, four said that the cross disappeared intermittently, two said that parts of the checkerboard disappeared intermittently, and one reported double crosses.

3.3.4 Discussion

The results of this study demonstrated that using the chromatic goggles: (1) Alternating monocular stimulation of each eye was achievable, allowing both to be tested within the same scanning run, minimising problems with varying attention and adaptation effects across the session. (2) Attention was generally well maintained and could be confirmed in control subjects, and in a patient with severe monocular visual loss. (3) Central fixation was maintained sufficiently to allow accurate detection of cross changes, and lateralised and localised fMRI activation to be demonstrated. Therefore, several sources of bias were addressed which could be problematic using patches, which have been commonly used to isolate each eye in previous fMRI studies. In addition, there are potential advantages over techniques such as LED goggles, with regard to facilitating fixation and confirming attention, in eyes with severe visual loss.

3.3.4.1 Lateralisation and localisation of quadrant-specific activation

Lateralisation and localisation of fMRI responses to region-specific stimuli was observed, consistent with the retinotopic organisation of the visual system. This was important for later studies of visual field defects in patients, and also suggested that central fixation was generally well maintained. If large fixation losses had occurred, then fMRI activity might be expected to be poorly lateralised. In addition, the feasibility of stimulation using goggles together with localised stimuli was demonstrated.

It should be noted that although homonymous quadrantopias may help clinically localise lesions to V2/V3, rather than V1 (Horton and Hoyt, 1991), quadrant-specific visual stimulation is not designed to accurately distinguish the borders of hierarchical visual areas within an individual, which may vary considerably between subjects, and requires formal retinotopic mapping. However, it does improve anatomical resolution, compared with whole field stimulation, and may provide a balance between spatial localisation and maximising effect size. For this reason, this approach was chosen to investigate visual field defects, as described in Chapter 6.

3.3.4.2 Adequacy of isolation: assessment of crosstalk

The results of the crosstalk experiment demonstrated that the goggles effectively isolated each eye. The confidence interval of the parameter estimate included zero, indicating that no significant positive or negative fMRI activity occurred in primary visual cortex.

3.3.4.3 Goggles versus patches: assessment of attention

The new technique also helped enable confirmation of attention during stimulation of an eye with complete visual loss, as the fellow eye was still able to respond to visual cues. This difficulty was not addressed using the traditional eye patch technique. Using patches, both attention and gross fixation losses could occur, during stimulation of the affected eye, and the investigator would be unaware. The new methodology therefore may facilitate data interpretation, by detecting and quantifying these potential confounds.

Using chromatic goggles may also facilitate patient adherence to the stimulation protocol, by providing a fixation point for the fellow eye, which is not available using eye patches. This might indirectly assist fixation of the affected eye, through a mechanism of conjugate fixation, provided the subject does not have a latent phoria (tendency of the eyes to deviate when fusion is suspended). However, this was difficult to confirm, as a direct measure of eye movements was not included, which is a limitation of the study. In addition, some subjects reported perceiving small fixation cross movements. These movements were likely to be due to brief disturbances in maintenance of conjugate gaze, due to the limited points of reference in the scanner environment, and may indicate that the strategy used to maintain fixation was imperfectly achieved. However, any such errors are likely to be transient and small, in comparison with eye patching. There is some support for this from the observations of well lateralised quadrant-specific activation in controls, and the high accuracy of responses to fixation cross changes. This suggests that conjugate fixation is reasonably well maintained, at least for the practical purposes of most fMRI experiments.

3.3.4.4 Visual phenomena

The goggles effectively isolated each eye, and this may have led to some of the visual phenomena reported by control subjects in the scanner. Some people reported transitory instability of the visual percept, when using the chromatic goggles. Part of the checkerboard stimulus disappearing could be due to binocular rivalry, and subconscious alternation of the fixating eye (Lumer et al., 1998;Haynes et al., 2005b;Tong et al., 2006). Disappearance of the fixation cross itself may be due to the "filling-in" phenomenon that can occur, in the context of competing visual stimuli (in this case, cross and checkerboard), resulting in an artificial scotoma, which is filled in by the background (Ramachandran and Gregory, 1991;Weil et al., 2007). This could potentially affect the ability of the subjects to detect the cross changing to a hash symbol, but the accuracy of detecting changes actually remained high. The perception of double crosses is probably due to instability of vergence at small viewing distances (<1 metre), resulting in failure of fusion. These effects do not appear to significantly inhibit activation, perhaps because they are so fleeting, often disappearing when subjects blinked. In addition, although the luminance contrast associated with the use of colour filters may be lower than black and white stimulation, activation was still reliably detected in the majority of cases.

3.3.5 Conclusions

In conclusion, a new visual stimulation technique was devised, in order to facilitate monocular visual stimulation in patients with monocular visual loss. This technique was tested in a control group, and in a single patient with a severe unilateral visual deficit. It was demonstrated that the new technique allowed both eyes to be tested within the same scanning run, effectively isolated each eye in controls, and was superior to a traditional eye patching method, in terms of confirming maintenance of attention. It is also likely that fixation was facilitated, and there was no evidence of gross fixation losses. The technique was therefore applied to the subjects involved in this thesis, and may also be useful for other investigators interested in studying patients with monocular visual loss, using fMRI.

In the next chapters, the fMRI protocol described here is applied to a cohort of patients with acute ON. The same patients also performed structural imaging, to investigate mechanisms of damage and responses to it.

CHAPTER 4

COMBINING MULTI-MODAL MRI AND ELECTROPHYSIOLOGY TO PROBE PATHOPHYSIOLOGICAL MECHANISMS IN ACUTE OPTIC NEURITIS

In this chapter, fMRI is combined with structural MRI and electrophysiology in a group of patients with acute ON. The objective of this study was to elucidate the pathophysiological mechanisms occurring during the acute phase of ON, with a particular focus on neuroplastic responses to damage. The aim was to determine why there is such a wide variation in the severity of acute visual loss in ON. In order to answer this question, it was necessary to dissect complex structure-function interactions between inflammation, demyelination and conduction block in the optic nerve, pathology in the optic radiations and pericalcarine cortex, and cortical responses to visual stimuli in the presence of damage. In particular, the interpretation of fMRI measures is complicated by a two-way interaction with visual function. On one hand, poor vision is associated with a reduction in afferent input, resulting in a smaller BOLD response, and better vision is associated with a higher BOLD response to visual stimuli. On the other hand, greater fMRI activity can reflect plasticity, which may contribute to better vision. Therefore, the different and complementary perspectives that each MRI and electrophysiological test provides into structural pathology, the consequences for neural conduction, and cortical responses were exploited in order to separate these interactions. To this end, a comprehensive structural MRI assessment of both the anterior and posterior visual pathways was necessary, in order to identify important mechanisms of damage and their impact on acute vision. Structural and electrophysiological predictors of visual loss were then used to inform the fMRI analysis, to explore the role of neuroplasticity, after separating out the effects of damage on vision.

The hypothesis was that grey matter plastic responses to visual stimuli might play a role in reducing the impact of damage on the acute clinical deficit.

A novelty of this study is that the impact of damage on both the anterior and posterior visual pathways on vision in acute ON was assessed. Therefore, it was important to assess the structural integrity of the optic radiations, which were reconstructed using diffusion-based tractography. The development of a methodology designed to address

sources of bias in this technique, related to placement of the seed, is described in section 1. This methodology used the approach of combining structural and functional data. In section 2, this methodology was then applied to the patient cohort, together with the other structural, electrophysiological and functional measures, to test the hypothesis outlined earlier.

SECTION 1 DIFFUSION-BASED TRACTOGRAPHY OF THE OPTIC RADIATIONS

4.1.1 Development of a methodology for tracking the optic radiations, using diffusion and functional MRI data

Diffusion-based tractography (Basser and Pierpaoli, 1996;Mori et al., 1999;Ciccarelli et al., 2008) is a sensitive method of assessing the integrity of white matter tracts, and represents an important tool in the assessment of tissue damage in the optic radiations *in vivo*. Tractography has provided many insights into white matter tract pathology in demyelinating disease (Ciccarelli et al., 2008), and several different techniques are available. One of the most commonly used algorithms is probabilistic tractography, and this approach was used in this study to reconstruct the optic radiations, using FMRIB Software Library (FSL) tools (http://www.fmrib.ox.ac.uk /fsl/fdt/fdt_probtrackx.html (Behrens et al., 2003a;Behrens et al., 2003b)).

A general limitation of all tractography techniques is that extracted tract parameters, such as FA, may be significantly influenced by the choice of seed-point, which is usually an operator-dependent step. An example of this effect is shown in Figure 4.1. Reconstruction of the right optic radiation was performed, using a seed voxel placed in the apex of the right Meyer's loop. The estimates of the tracts, and the extracted mean tract FA, differed significantly (>5%) if the seed voxel was shifted laterally by just one voxel, from 0.359 for the illustrated red/yellow tract, to 0.380 for the tract shown in blue.

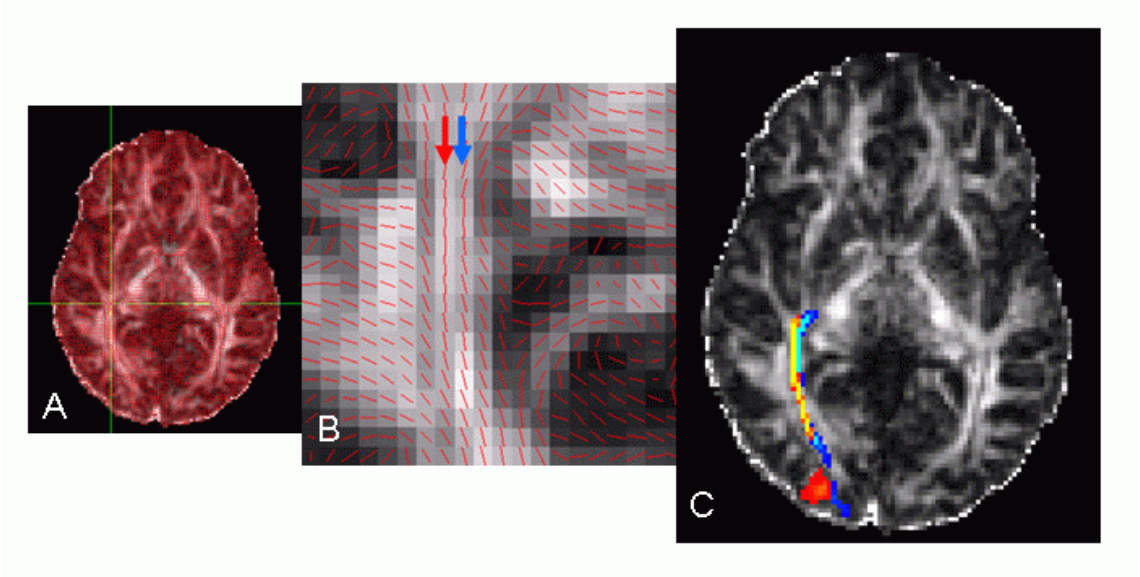

Figure 4.1 The effect of variability in seed-point placement on the mean FA of the reconstructed tract. (A) Seed voxels in the apex of the right Meyer's loop are shown, on an axial slice of the FA map, overlaid with the principal eigenvector map, and (B) a magnification of Meyer's loop is shown. The red arrow indicates a seed voxel, placed at MNI coordinate 42 51 12, and the blue arrow indicates a second seed, placed in the immediately adjacent voxel 43 51 12. (C) The reconstructed tract estimates are displayed overlaid on to an axial slice of the FA map. The blue tract corresponds to the seed voxel indicated by the blue arrow, and the red/yellow tract to the seed voxel indicated by the red arrow. In each case, identical coronal and sagittal exclusion masks were applied, and the maps were thresholded at a voxel-scale connectivity value of 75. The extracted mean FA values were 0.359 for the red/yellow tract, and 0.380 for the blue tract.

Previous studies have used various methods to attempt to minimise this variability, for example, following strict operator rules for voxel selection (Ciccarelli et al., 2005), or normalising the seed coordinates, using a group-specific template (Toosy et al., 2004). A different approach is to use fMRI data to define seed-points. An early study used fMRI to identify the LGN and visual cortex, and applied tractography to demonstrate proof-of-concept in individual healthy subjects (Conturo et al., 1999). This approach was later applied to patients to study the motor system, in order to investigate individual differences in corticospinal tract anatomy, related to brain tumours (Holodny et al., 2001;Krings et al., 2001). A more recent study combined fMRI definition of seed-points with diffusion-based group mapping (Guye et al., 2003). FMRI seeds were identified in the motor cortex in native space, coregistered to the individual's DTI data, the tractography algorithm was run, and the resulting connectivity maps were normalised. This technique permitted comparisons between a group of controls and a single patient with a frontal tumour. The reduction of operator

bias in seed placement, that is the advantage of using the functional data, could be exploited to investigate group-level differences, by normalising the fMRI data to define cohort-specific seed-points, and then reverse normalising them back into native space for tractography. This approach has been used to investigate temporal lobe epilepsy, applying an fMRI language paradigm to define the cortical seeds (Powell et al., 2007), but has not been previously applied in the visual system.

The operator is required to make other decisions when performing tractography, such as whether to include a target mask and exclusion masks, and, if so, in which location. In addition, the levels of curvature thresholding used to terminate the algorithm, and noise thresholding, must be decided. These variables may be optimised for a given cohort, using pilot data, and then should be kept constant for all subjects, when they are applied to the study group. For this thesis, experiments were first performed using the control data from the baseline time-point, with the aim of choosing the parameters for the tractography algorithm, in order to achieve the most reliable and accurate reconstructions of the optic radiations in this cohort. Examples of the problems addressed by these pilot experiments are described in the following sections.

4.1.2 Target mask

In order to test whether a target mask was required, the right optic radiation was reconstructed by choosing a seed-point in the apex of Meyer's loop on the right side. The tractography algorithm provided by FSL was run without, and with, a target mask, leaving all other parameters as default. The target mask chosen was the primary visual cortex, which was outlined in each subject using a previously described methodology (Ciccarelli et al., 2006). It consisted of manually drawing the visual cortex on the standardised T1 image, that is the individual T1-weighted image coregistered into a standardised space defined by the Montreal Neurological Institute (MNI152), using affine transformation, as employed by FSL (Jenkinson and Smith, 2001). This was done by using, as a guide, a region-of-interest derived from area 17 in the Brodmann atlas. The visual cortical areas were then transferred back to the individual T1 images, and their correct location was confirmed by visual inspection in all cases. Probabilistic tissue-type segmentation and partial volume estimation were then performed on the individual T1-weighted images (Zhang et al., 2001). The output images were thresholded to include only voxels estimated at >30% grey matter and

the results were used to mask the visual cortical areas to obtain the final target masks. The T1 target mask was then transformed into native diffusion space before running tractography (an example is given in Figure 4.2).

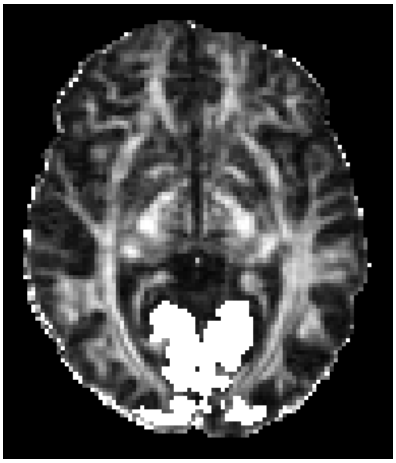

Figure 4.2 Target mask, in native space, overlaid on to an axial section of the FA map.

The results of tractography without, and with, a target mask are shown in Figure 4.3.

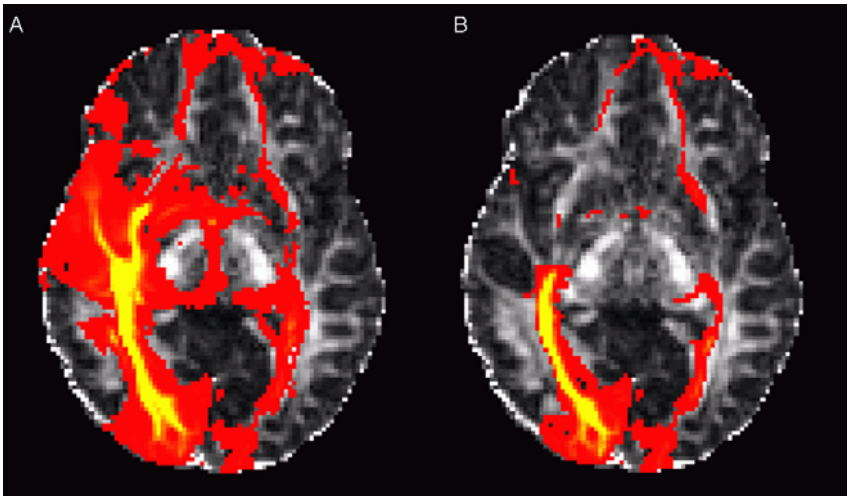

Figure 4.3 The effect of using a target mask. Results of tractography are shown for a control subject (A) without, and (B) using, a target mask. The reconstructed, unthresholded optic radiations are illustrated in red/yellow, with yellow indicating a higher probability of connection, overlaid on to an axial slice of the FA map, in native space, without exclusion masks.

The inclusion of a target mask substantially reduced the number of false positive streamlines, although some were still seen in the contralateral optic radiation, as a result of crossing via the corpus callosum, and in the inferior fronto-occipital

associative tracts. Therefore, a primary visual cortical target mask was included in the tractography algorithm used in the work described in this thesis.

4.1.3 Exclusion mask

In order to test whether an exclusion mask was required, the left optic radiation was reconstructed using a seed-point in the apex of Meyer's loop on the left side. The FSL tractography algorithm was run without, and with, an exclusion mask, leaving all other parameters as default. Separate experiments were performed, using a mid-sagittal mask, a coronal mask placed immediately anterior to the apices of Meyer's loops, and both together. A primary visual cortical target mask was added (section 4.1.2). The results showed that, if an exclusion mask was not used to constrain the tractography algorithm, white matter tracts outside the optic radiations were also tracked from the seed-point, such as the inferior longitudinal fasciculus, inferior fronto-occipital fasciculus and corpus callosum (examples shown in Figure 4.4A and B). These tracts were not of interest to this study, and the problem occurred despite the use of a target mask. When exclusion masks were used, only the tracts belonging to the optic radiations were displayed. The best results were obtained using a combined mid-sagittal and coronal exclusion mask (illustrated in Figure 4.4C), which was selected for the experiments described in this thesis.

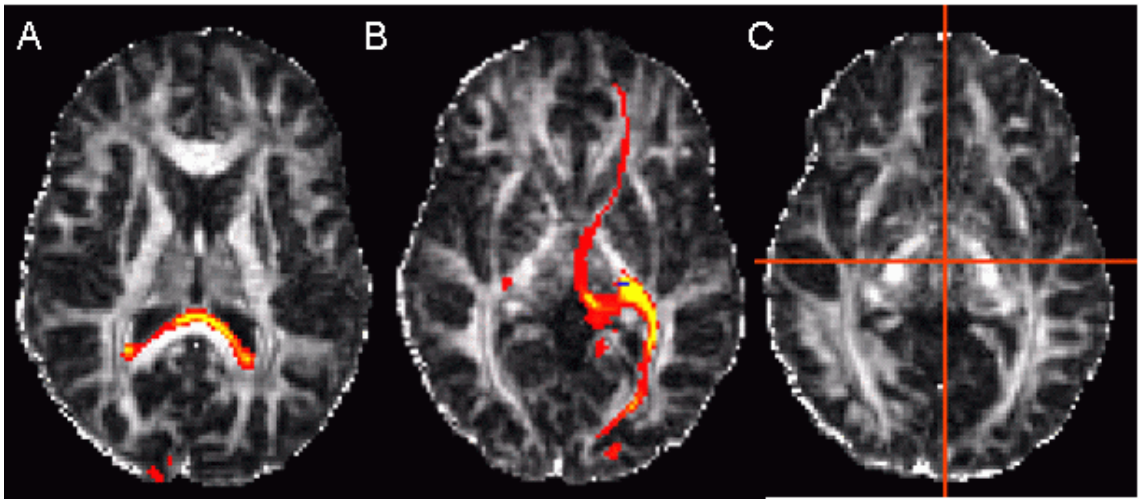

Figure 4.4 Results of tractography without using an exclusion mask, showing erroneous tracking across (A) the corpus callosum and (B) inferior fronto-occipital fasciculus. These problems may be solved using (C) coronal and sagittal exclusion masks.

4.1.4 Defining seed-points using fMRI data

4.1.4.1 Defining the LGN using fMRI

The effect of small differences in the placement of seed-points was illustrated in Figure 4.1. In order to reduce the bias associated with operator-dependent placement, an approach was chosen in which seed-points were derived from the fMRI data. The lateral geniculate nuclei (LGN) were selected, as they represented grey matter structures, adjacent to the anterior optic radiations, near Meyer's loops. In order to test this approach, both optic radiations were reconstructed using fMRI-derived seed-points in the LGN. At 1.5T, it was not always possible to visualise the LGN with fMRI. Therefore, it was necessary to define them using a second-level group fMRI contrast, derived from the main study cohort, and then transform the group LGN estimates from normalised fMRI space into native diffusion space.

For each subject in the study, the visual fMRI data were realigned, normalised and smoothed in SPM5, as described in Chapter 3. First-level +1 contrasts were specified for each of the whole field conditions, separately, for the chromatic and black and white checkerboard conditions, for each eye. The resulting contrast images from all subjects were combined in a second-level analysis. A one-sample t-test model was specified, entering all of the contrast images together combining both conditions (i.e. both chromatic and black and white checkerboard stimulation of the whole field), and both groups (i.e. both patients and controls). This was repeated at each time-point. Consideration was given to combining data across all time-points, but there was concern that subject dropout might introduce bias into the estimates, and it was important to include all available subjects' data, to optimise statistical power. Therefore, at the second level, time-point specific contrast images were estimated. The resulting statistical parametric maps were thresholded at a family-weighted error level $p<0.05$ and the baseline time-point result is shown in Figure 4.5.

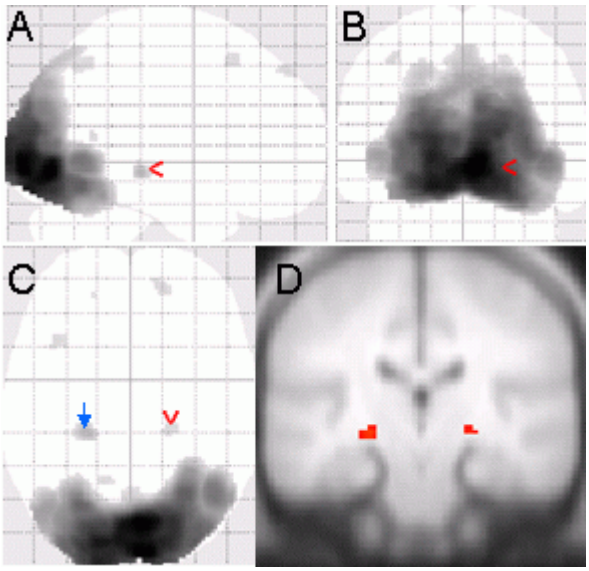

Figure 4.5 Statistical parametric group map, demonstrating the results of visual stimulation, at the baseline time-point, combined for all the patients and controls involved in the main study, and combined for black and white and chromatic whole field stimulation. Activation is seen in the bilateral occipital cortex and left (blue arrow) and right (red arrowhead) LGN. The results are overlaid on to the SPM5 glass brain, shown in (A) sagittal, (B) coronal and (C) axial projections, and (D) a coronal section of the MNI305 template. The maps are thresholded at a voxel-level family-weighted error rate of $p<0.05$.

The results demonstrated that it was possible to identify the LGN using fMRI, at group level, in this cohort. However, there was slight left/right asymmetry in the size of the fMRI estimates, which might bias the subsequent tract estimates if these clusters were used as seed-points for tractography. This was addressed in the next stage.

4.1.4.2 Construction of LGN-based seed-points

In order not to introduce a laterality bias, symmetrical seed-points were constructed, based on the LGN estimates. This was performed using the MarsBar region-of-interest SPM5 toolbox (Brett et al., 2002). Spherical regions were defined, centred on the global maximal coordinates of each LGN. These were at MNI coordinates 22 -24 -4 on the right, and -22 -26 -4 on the left. The reconstructed spheres centred on these points were each of 3.5mm radius, resulting in volumes of $180mm^2$. These dimensions were chosen to approximate the published volumes of the LGN (i.e. 5x6x9mm), which are of spatulate shape (Horton et al., 1990). The spheres were then reverse

normalised into each subject's native space, using the SPM5 algorithm, and coregistered to each individual's brain diffusion data. The coregistration was a two stage procedure, in which the whole brain fMRI data was first registered to a whole brain b_0 image. This whole brain b_0 image was then registered to the main DTI dataset, which comprised a partial brain acquisition (details in section 4.2.2.5.2). The spheres were resliced in native diffusion space, binarised and used as seed-points for tractography. In order to reconstruct both optic radiations, seed-points were placed in the region of the right and left LGN, in turn, and the FSL tractography algorithm was run, using a primary visual cortical target mask (section 4.1.2) and an exclusion mask (section 4.1.3), leaving all other parameters as default, including the curvature thresholding (0.2 radians). The results from two different control subjects are shown in Figure 4.6.

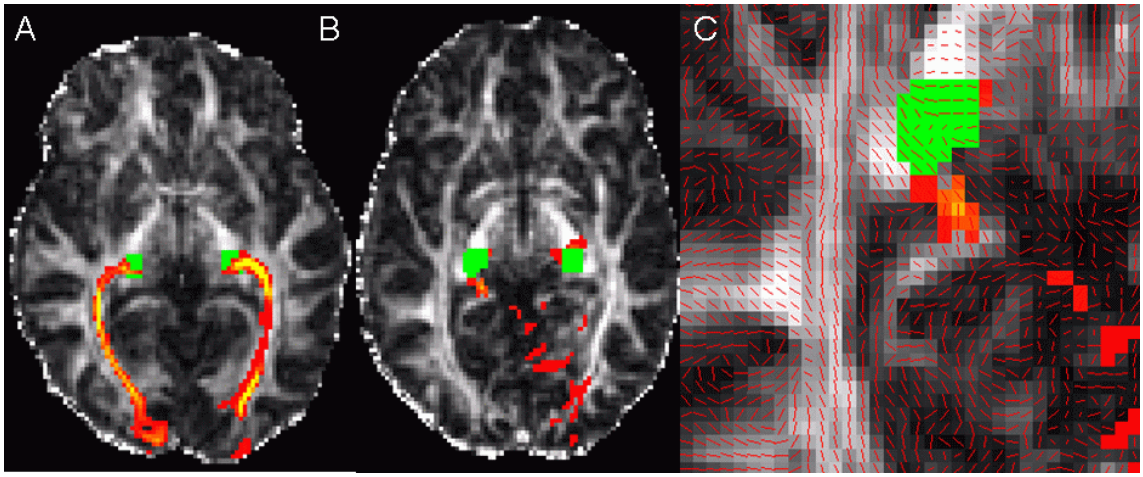

Figure 4.6 Results of tractography in two different control subjects, unthresholded and overlaid on to axial slices of the FA maps. The default curvature threshold of 0.2 radians was applied. The images demonstrate tracking round the angle of Meyer's loop (A) successfully and (B) unsuccessfully. Seed masks are shown in green, probabilistic streamlines in red/yellow. (C) Magnification of the right Meyer's loop, overlaid with a principal eigenvector map from the unsuccessful tractography, demonstrates difficulties related to tracking round the sharp angle, and from beginning tracking within the grey matter.

The approach was only partially successful. In some control subjects accurate reconstruction of the optic radiations was achieved (Figure 4.6A) but, in others, the algorithm failed to track round Meyer's loops (Figure 4.6B). This was probably due to inter-individual differences in the anatomy of the loop of Meyer and the estimated location of the LGN, resulting in difficulties tracking round a sharp angle in some

subjects, and difficulties tracking from within isotropic grey matter to white matter in others (see also Figure 4.7). Therefore, the next stage was to attempt to address the problem of tracking round the sharp angle.

4.1.4.3 Curvature thresholding

Tractography algorithms incorporate a curvature threshold, which constrains the angle between eigenvectors in adjacent voxels, and connectivity is inferred at a given threshold. If the angle between eigenvectors is more acute than this threshold, the streamline is terminated. The FSL tractography algorithm applies default settings of 5000 samples and a curvature threshold of 0.2 radians (11.5 degrees) (http://www.fmrib.ox.ac.uk/fsl/fdt/fdt _probtrackx.html). In order to facilitate tracking round Meyer's loop, the curvature threshold was reduced. A seed-point was placed in the right LGN, and the algorithm re-run, with all of the parameters left identical to the previous experiment (section 4.1.4.2), except that now the curvature threshold was reduced to 0.1 radians. The experiment was then repeated again with a threshold of 0 radians, and these results are shown in Figure 4.7.

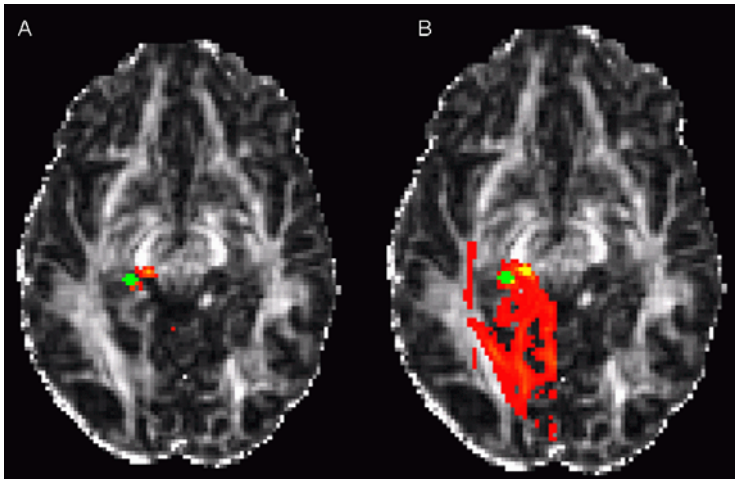

Figure 4.7 The effect of changing the curvature threshold. Results of tractography are demonstrated, using (A) a standard curvature threshold of 0.2 radians, and (B) a threshold of zero. Results are overlaid on to FA maps, with seed masks shown in green.

This approach was unsuccessful, as reducing the threshold resulted in unacceptable noise, with many erroneous streamlines passing through the grey matter.

4.1.4.4 Tracking from Meyer's loop

In order to overcome these difficulties, the methodology was modified, as follows. The LGN-derived seed points were shifted laterally into the apex of Meyer's loops, within coherently oriented, anisotropic white matter. This was performed manually, in each subject's native space, using FSL, following a standardised guideline. Each seed-point was shifted 8-10 voxels laterally, and the maximum number of voxels was always used for this shift. This shift allowed the seed voxels to be placed within the apex of the loop, as confirmed visually in all cases. In order to assess the reproducibility of this approach, the seed-point shift was repeated in eight datasets, more than a month later, by the same operator, blinded to image identity, and the intra-observer coefficient of variation was calculated.

The results demonstrated that this approach was fully reproducible, with a coefficient of variation of 0%. Therefore, despite this modification, the methodology continued to minimise operator dependence. The optic radiations were reconstructed successfully in all cases. This methodology was used for the experiments described in this thesis, and is summarised in Figure 4.8.

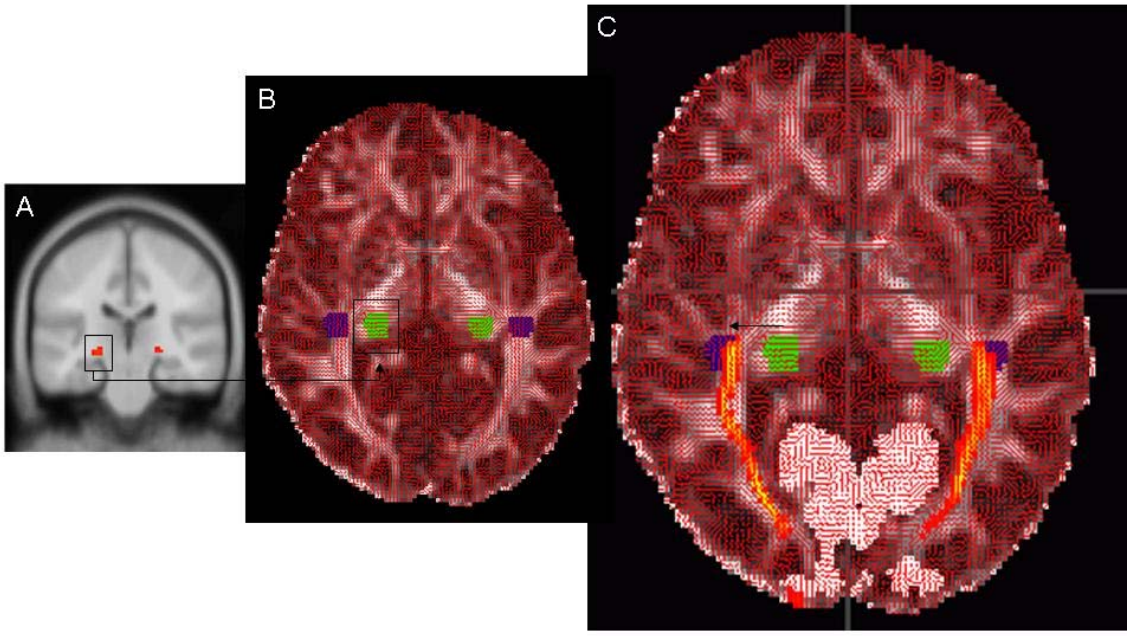

Figure 4.8 Using fMRI to define seed-points for probabilistic tractography. (A) The LGN group activation clusters are shown, overlaid on to a coronal section of the MNI152, T1-weighted average brain map in SPM5, thresholded at voxel-level $p<0.05$ corrected. (B) The reconstructed LGN seed masks are shown at their original locations in native diffusion space in green, and following a 10 voxel lateral shift in blue, within the apex of Meyer's loop, in one of the control subjects. The seed masks are overlaid on to an axial section of the FA map, with the principal eigenvector map superimposed in red. (C) The results of tractography for the same control subject are shown. The exclusion mask is shown in grey, the target region in white, and the reconstructed optic radiations in red/yellow, where yellow is the highest probability of connection.

4.1.5 Connectivity map thresholding

Thresholding of the connectivity map, which results from tractography, is generally used to limit the effect of image noise, and reconstruct only the tracts under investigation (Guye et al., 2003;Ciccarelli et al., 2006;Thottakara et al., 2006;Ciccarelli et al., 2007). There is no general consensus on the optimum threshold to use, which may vary depending on the dataset and tract of interest, and the choice essentially represents a trade-off between sensitivity and specificity. In this pilot group of controls, experiments were performed to compare the effect of applying different voxel-scale connectivity thresholds. Seed-points were placed in each

Meyer's loop, in turn, in order to reconstruct both optic radiations, using the methodology summarised in figure 4.8. The FSL algorithm was run, using a primary visual cortical target mask (section 4.1.2), an exclusion mask (4.1.3), and leaving all other parameters as default. Connectivity thresholds of 0, 50, 75, 100 and 200 were applied. The results are shown in Figure 4.9.

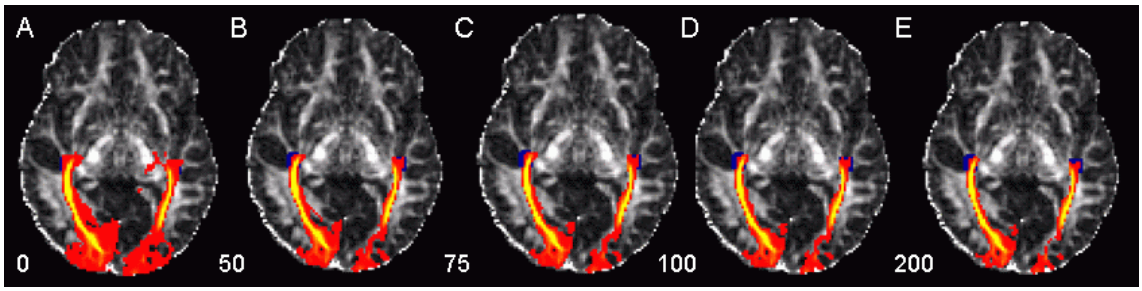

Figure 4.9 Noise thresholding. Results of tractography in a single control subject, overlaid on to an axial slice of the FA map, illustrating the effect of thresholding, at voxel-scale connectivity levels of (A) 0, (B) 50, (C) 75, (D) 100 and (E) 200.

In this pilot study, a threshold of 75 was judged to maximise specificity, compared with the lower thresholds, whilst higher thresholds did not significantly improve sensitivity, and true positive voxels were sometimes discarded, especially in subjects with relatively low overall tract connectivity. Therefore, a noise threshold of 75 was used in this thesis.

The final thresholded connectivity maps were transformed into binary images, which were used to mask the anisotropy maps, to delineate the optic radiations, in both the patient and control groups. The mean voxel values of fractional anisotropy (FA) within this tract were obtained, for each subject, which is a well established measure of the integrity of the posterior visual pathways (Schmierer et al., 2007).

4.1.6 Summary

In summary, the results of these pilot experiments, in the cohort of control subjects, were used to decide on the parameters for the tractography algorithm to apply in subsequent experiments, described in this thesis. The methodology included a primary visual cortical target mask and mid-sagittal and coronal exclusion masks. The seed-points were defined, by reconstructing spheres centred on the fMRI estimates of the LGN, which were then shifted into the apices of Meyer's loops. A voxel-level

connectivity noise threshold of 75 was applied to the resulting maps. These modifications of a previously published technique, combining fMRI and diffusion data, resulted in reproducible estimates of the optic radiations, which appeared reliable and anatomically accurate. However, some limitations of this technique must be borne in mind, with regard to tractography in general, and specifically combining multi-modal data.

In general, the results reflect a probability of connection to the optic radiations for each voxel, and false positives and negatives may occur. It is not possible to distinguish afferent from efferent fibres, and pathological modifications may lead to partial volume effects between the eigenvectors in neighbouring voxels. Using group fMRI data to define the seed-points may introduce registration errors, as a result of different susceptibilities and other artefacts between functional and diffusion MRI (Powell et al., 2007). The normalisation step could also potentially result in errors, due to inter-individual anatomical variability. For the same reason, the sensitivity to detect subtle effects between individuals is also likely to be reduced. Despite these limitations, the method of defining seed-points using fMRI group activation peaks reduced operator bias, and permitted the assessment of group-level differences, which is discussed in the next section.

SECTION 2: DISSECTING STRUCTURE-FUNCTION INTERACTIONS IN ACUTE OPTIC NEURITIS TO INVESTIGATE NEUROPLASTICITY

4.2.1 Introduction

A striking clinical characteristic of ON is the wide variability in severity of acute visual loss. Some people experience only mild blurring, whilst others are unable to perceive light. It is unclear whether this depends solely on the degree of structural damage within the optic nerve itself, or if it is influenced by other factors, such as pathology elsewhere in the visual pathways, or compensatory brain responses. In this study, structural MRI, electrophysiology and fMRI techniques were combined *in vivo* in a group of patients with acute ON, in order to attempt to define the structural and functional contributions underlying this variability in acute clinical deficit.

4.2.1.1 Damage to the optic nerve

Paraclinical *in vivo* techniques have previously been applied individually to clarify aspects of pathology in the optic nerve in ON. Previous MRI studies have identified measures of optic nerve damage that correlate with acute visual dysfunction in ON. For example, swelling of the optic nerves has been shown to correlate with the severity of acute visual loss (Hickman et al., 2004a). Visual loss has been associated with gadolinium enhancement, and its recovery with cessation of enhancement, this evolution suggesting that inflammation *per se* contributes to the acute reversible visual deficit (Youl et al., 1991). Correlations have been demonstrated between acute visual dysfunction and the length of the enhancing segment (Kupersmith et al., 2002;Hickman et al., 2004c). Lesions on non-contrast-enhanced T2 weighted sequences reflect non-specific changes in intra and extra-cellular water, which may be due to oedema, inflammation, demyelination, gliosis or axonal loss (Barkhof and VanWalderveen, 1999). These are seen in the acute phase, persist, and may correlate with lower acuity (Miller et al., 1988a;Dunker and Wiegand, 1996). Electrophysiological studies have demonstrated acute prolongation of VEP latencies, which remained evident even after vision had recovered (Halliday et al., 1972;Brusa et al., 2001). Overall, the data from previous MRI and electrophysiological studies

suggest that the important pathological processes in acute ON are oedema, inflammation, and demyelination within the optic nerve, and that these factors may be associated with the severity of acute visual loss.

More recently, the possibility of combining newer quantitative MRI techniques, such as diffusion-based tractography and fMRI, has provided an opportunity to investigate pathological mechanisms and physiological responses in greater detail.

4.2.1.2 Damage to the posterior pathways

The impact of changes in the rest of the visual system which result from acute ON is less clear, and has not been investigated in depth. Posterior visual pathway involvement and occipital cortical responses may contribute to the clinical picture, either by sustaining damage, or modulating its effects on visual function. For example, patients with clinically isolated ON commonly have inflammatory lesions on brain MRI and, as these are often periventricular in location, they may involve the optic radiations (Hornabrook et al., 1992). These lesions may affect vision, especially if they are large (Plant et al., 1992). In addition, inflammation in the optic nerve may have secondary consequences for the posterior pathways. The occurrence of trans-synaptic degeneration in the LGN following an optic nerve insult is recognised (Goldby, 1957;Madigan et al., 1996). This term describes a phenomenon in which damage to one part of a neural pathway results in secondary degenerative consequences for other neurons connected through synaptic junctions. Evidence for trans-synaptic degeneration in the LGN following ON has been demonstrated by a histological study (Evangelou et al., 2001), and supported by the results from *in vivo* MRI studies. A diffusion-based tractography study demonstrated reduced connectivity in the optic radiations a year after acute ON (Ciccarelli et al., 2005), and another study reported reduced MTR in occipital cortex, six months after ON (Audoin et al., 2006). At present, it remains unclear when these changes first appear.

In the work reported in this chapter, the impact of incidental lesions in the posterior visual pathways on acute visual loss was studied, and whether any secondary changes in the integrity of the optic radiations were detectable at this early stage. The morphology of the occipital cortex was also investigated to detect any abnormalities of pericalcarine cortical surface area, volume or thickness.

4.2.1.3 Functional responses to visual stimuli in optic neuritis

The brain functional response to visual stimuli in ON appears to be complex. Previous studies have shown that during the acute episode there is a widespread reduction in the fMRI activation throughout the grey matter of the afferent visual pathway, which correlates with visual acuity (Rombouts et al., 1998;Langkilde et al., 2002;Toosy et al., 2005;Korsholm et al., 2007). This can be explained by a reduced afferent input, secondary to active inflammation and conduction block in the anterior pathway. However, it appears that fMRI activation reflects more than the magnitude of visual input to primary visual cortex. Activation has been demonstrated in extra-striate areas, thought to represent neuroplastic reorganisation, which may contribute to visual recovery (Werring et al., 2000;Toosy et al., 2005;Levin et al., 2006;Korsholm et al., 2007). The timing of these changes remains somewhat uncertain, but at least some of them appear to occur soon after the initial insult.

It is not known whether cortical responses to visual stimuli can modulate visual acuity during the acute stage, or whether they are just consequent to it. For example, an observed region of fMRI activation which correlates with visual acuity could be interpreted in two ways. It may be that patients with better vision have a greater afferent input to occipital cortex, and hence greater fMRI activity. Alternatively, increased fMRI activity may reflect a compensatory grey matter plastic response to pathology, which is actively contributing to preservation of vision. These two possibilities are difficult to disentangle, but elucidating this is important when considering how the brain responds to injury, and if it contributes to recovery.

In order to dissect out cause and effect, structural MRI, electrophysiology and fMRI were combined in a cohort of patients with acute ON. The objectives of the study were twofold: firstly, to identify which structural and electrophysiological measures in the afferent pathways were associated with acute visual loss. Secondly, to use these important structural and electrophysiological measures to inform a further analysis, in which fMRI data were also entered. This strategy aimed to separate the effects of a reduced afferent input from any cortical influence on vision. It was hypothesised that any fMRI activity correlating with vision, independent from measures of the structural and electrophysiological integrity of the optic nerve, might represent a neuroplastic modulatory effect.

In a model such as this, it was important that the structural assessment was comprehensive, to include any potential influences on vision from the posterior, as well as the anterior, pathways. To this end, the combination of optic nerve, optic radiation and visual cortical structural imaging, together with visual fMRI, represented the most detailed MRI assessment of the visual system in ON to date.

4.2.2 Methods

4.2.2.1 Participants

Patients with a typical, acute, unilateral, clinically isolated ON were recruited from Moorfields Eye Hospital. This was defined as a painful unilateral loss of vision, which progressed over a few days to two weeks, without any additional neurological symptoms (Hickman et al., 2002). Healthy age and sex matched controls were also studied. Patients with a diagnosis of MS, bilateral ON, or other chronic neurological conditions were excluded. The presence of brain inflammatory lesions was not considered an exclusion criterion. Treatment with steroids was noted. Patients were invited for clinical assessment, VEPs, structural and functional MRI, on the same day, within a month from symptom onset. All subjects gave informed written consent. The study was approved by the local Ethics Committee.

4.2.2.2 Clinical assessment

On the day of scanning, the patients' best corrected visual acuity, using glasses and pinhole correction if necessary, was measured using a retro-illuminated Early Treatment Diabetic Retinopathy Study Chart. Scores were recorded as 4m logMAR visual acuity (Ferris, III et al., 1982). When no letters could be correctly identified, a score of 1.7 was assigned (Optic Neuritis Study Group, 1991).

4.2.2.3 Electrophysiological assessment

Each patient was invited to have a whole field, pattern-reversal visual evoked potential (VEP) study on the day of scanning. The screen subtended 28^{o} of visual angle horizontally and 22^{o} vertically, and check size was 40'. Luminance was $4cd/m^2$

and 60cd/m^2 for the black and white checks, respectively. An occipital electrode 5cm above the inion was used to reference Fz. The amplitude of the response and the latency of the P100 waveform were calculated.

4.2.2.4 MRI acquisition and analysis

Two 1.5T GE Medical Systems scanners (Milwaukee, WI, USA) were used to acquire MRI data, using an 8-channel receive-only head-coil. The scanners were chosen based on their dedicated setup. Structural imaging of the optic nerves and brain was performed in all subjects with a 1.5T Signa Echospeed MRI system, with a maximum gradient strength of 33mTm^{-1}, whilst functional imaging was performed, on the same day, on a 1.5T Signa Excite whole-body MRI system, with a lower gradient strength of 22mTm^{-1}, but with the equipment for paradigm presentation for visual stimulation (described in Chapter 3).

4.2.2.5 Structural MRI imaging

4.2.2.5.1 Optic nerves

(1) A coronal-oblique fast spin echo sequence (TR 2300ms, TE 68ms, 2 excitations, echo train length 8, matrix size 512x384, field of view (FOV) 24x18cm, 16 contiguous 3mm slices) was acquired to calculate lesion length, which was determined by an experienced neuroradiologist (Dr. Katherine Miszkiel), blinded to image identity and side affected, by multiplying the number of consecutive slices of optic nerve returning abnormal signal by the slice thickness. The intra-observer coefficient of variation, which is equal to the ratio of the standard deviation to the mean, multipled by 100%, and was calculated on eight patients, was 2.8%.

(2) Post triple-dose gadolinium-enhanced coronal-oblique fat-saturated T1-weighted spin echo was acquired in patients only (TR 600ms, TE 20ms, 1 excitation, matrix size 256x192, FOV 24x18cm, 16 contiguous 3mm slices).

(3) Coronal-oblique FLAIR imaging (TR 2500ms, TE 12.7ms, TI 995ms, 6 excitations, echo train length 6, matrix size 512x384, FOV 24x18cm, 16 contiguous 3mm slices) was performed to obtain the optic nerve cross-sectional area, which I calculated, blinded to image identity, from five contiguous slices anterior from the orbital apex (Hickman et al., 2001), using a semi-automated contouring technique

(Plummer, 1992). The intra-observer reproducibility coefficient of variation was 4.6%. In order to account for normal inter-individual variability, the ratio of affected to fellow nerve area was calculated.

4.2.2.5.2 Optic radiations

(1) Axial-oblique dual-echo fast spin echo of the whole brain (TR 2000ms, TE 17ms/102ms, echo train length 8, matrix size 256x256, FOV 24x18cm, 28 contiguous 5mm slices) were used to calculate the optic radiation lesion load, after lesions were identified by Dr. Miszkiel, using standard anatomical landmarks. The intra-observer coefficient of variation was 2.6%.

(2) DTI of the optic radiations and occipital lobe was obtained using an optimised single-shot, cardiac-gated, diffusion-weighted echo-planar imaging sequence (TR 10 RR~11-13s, TE 82ms, 1 excitation, matrix size 96x96 (reconstructed to 128x128), FOV 22x22cm^2, in-plane resolution 2.3x2.3mm^2 (reconstructed to 1.7x1.7mm^2), 30 contiguous 2.3mm slices, parallel to the AC-PC line, diffusion gradients applied along 61 directions (Cook et al., 2007), b=1200s/mm^2, optimised for white matter), and seven interleaved non-diffusion-weighted b_0 scans, acquisition time 10-15 minutes, depending on cardiac cycle). One additional b_0 volume was acquired, covering the whole brain (60 slices, extended from the original 30), to assist coregistration of partial brain diffusion data to whole brain fMRI data, which was necessary for tractography. Head motion and eddy-current induced distortions were corrected and the diffusion tensor was then calculated on a pixel-by-pixel basis, using FSL tools (http://www.fmrib.ox.ac.uk/fsl/).

The optic radiations were reconstructed, using the probabilistic tractography algorithm provided by FSL (http://www.fmrib.ox.ac.uk/fsl/fdt/fdt_probtrackx.html, (Behrens et al., 2003a;Behrens et al., 2003b). The seed-points were defined in each Meyer's loop using fMRI data, as described in the first section of this chapter, and summarised in Figure 4.8. The mean FA within the tractography-derived tract was obtained for each side, in each subject.

4.2.2.5.3 Visual cortex

Three dimensional fast prepared spoiled gradient recall (3D-FSPGR) of the whole brain was acquired (TR 14.3ms, TE 5.1ms, 1 excitation, matrix size 256x128, FOV 31x31cm, 156 contiguous 1.2mm slices).

The images were analysed with FreeSurfer software (http://surfer .nmr.mgh.harvard.edu), in which they were reconstructed as 1x1x1mm axial images, and the brain extracted. The skull-strip was assessed visually in all cases, and I performed manual correction if necessary, blinded to image identity. Fully automated cortical parcellation was then performed, and pericalcarine cortical surface area, volume and thickness estimates were obtained (Dale et al., 1999;Fischl et al., 1999;Fischl and Dale, 2000;Fischl et al., 2004). This surface-based methodology assigns labels to each cortical region, based on the gyral and sulcal anatomy of the individual patient data, prior probability information, and after taking into account the labels of neighbouring regions. The prior probabilities are derived from a manually segmented cortical atlas model, which includes geometric information and elements of neuroanatomical convention. The surface area and volume of each cortical region may then be calculated, and representations of cortical thickness extracted, calculated from the minimum distances from the grey-white matter boundary to the grey matter-CSF boundary. The maps produced are therefore not simply reliant on absolute signal intensity, and are not restricted to the voxel resolution of the original data, which allows detection of sub-millimetre differences in thickness between groups. These methods have been shown to be reliable (Han et al., 2006), and have been validated against manual segmentation (Desikan et al., 2006) and histology (Rosas et al., 2002;Hinds et al., 2008).

An SPM5 segmentation-based methodology was used to extract whole brain grey matter fractional volume (Chard et al., 2002), which was quantified using in-house software (http://www.nmrgroup.ion.ucl.ac.uk/atrophy/). The grey matter fraction was calculated by dividing the grey matter volume by the total intracranial volume (the sum of the grey matter, white matter and CSF), for each patient, as in previous studies (Dalton et al., 2004;Fisher et al., 2008).

4.2.2.6 Functional MRI imaging

The fMRI imaging acquisition protocol and experimental design were described in Chapter 3. Only the data from the whole field stimulation conditions were used for the analyses described in this chapter. The data from the conditions of whole field stimuli using the chromatic goggles were used for the main analyses. The data using black and white checkerboards and patches were only used to help define the LGN-derived

seed-points used for tractography. Post-processing was performed using SPM5. Each fMRI series was realigned, normalised to MNI stereotactic space and smoothed, using an 8mm isotropic Gaussian kernel. Realignment parameters and time derivatives were entered as covariates into the general linear model, together with the time-points at which the subjects pressed the button during the task to maintain attention. The patients responded correctly to the cross changing 74% of the time, and controls 97% of the time, indicating generally good attention and fixation, despite visual loss which was severe in some cases.

For each subject, first-level fixed effect contrasts were specified for affected and fellow eyes individually (1 0 and 0 1 respectively), combining epochs of stimulation through the red and green filters. Controls right and left eyes were pseudo-randomised arbitrarily to "affected" or "fellow", in order to maintain exactly the same methodology as the patients. The subsequent contrast images, representing the main effect of stimulation for each eye were entered into the second-level regression models, described in the next section.

4.2.2.7 Statistical analysis

Statistical analysis was performed using Stata-9.2 (StataCorp, Texas, USA), and variables were considered significant and reported at $p<0.05$, unless otherwise stated.

4.2.2.7.1 Structural and functional differences between patients and controls

Two-tailed unpaired t-tests were used to compare the following parameters between patients and controls (which were normally distributed): optic nerve area, optic radiation FA, pericalcarine cortical surface area, volume and thickness, whole brain cortical volume and grey matter fraction, VEP amplitude and latency. For the controls, optic nerve area, VEP amplitude, and VEP latency were averaged for the two eyes, to maximise use of the available data. Paired t-tests were used to compare affected and fellow eye parameters in patients. The group means, standard deviation (SD) and p value were reported for each t-test.

As there were no differences between the right and left optic radiations (using the Wilcoxon test) in either the patient or control groups, mean FA values of the right and left optic radiation were calculated, and compared between patients and controls.

For pericalcarine cortical surface area and volume, measurements were combined for the two hemispheres, as each hemisphere receives input from both eyes. The pericalcarine cortical thickness was averaged across both hemispheres. A multivariable regression approach was used, and adjusted for age and gender, with patient or control status always the binary dependent variable (0-control, 1-patient). Each cortical variable was entered, in turn, together with age and gender as dependent variables. Pericalcarine volumetric comparisons were also adjusted for whole brain grey matter volume. Group differences were quantified by dividing the patient group parameter by the control parameter, and multiplying by 100%.

A further *post-hoc* analysis was performed, in the case of finding significant differences in brain volumetric parameters between patients and controls, to determine whether there were any relationships between brain volumes and the presence of T2 lesions in the brain, T2 lesions in the optic radiations, and optic radiation FA.

Voxel-wise differences in fMRI activity between patients and controls were compared for affected and fellow eyes, using SPM5. A second-level two-sample t-test model was used to identify any regions where patients activated more than controls (contrast 1 -1), or vice versa (-1 1). The resulting statistical parametric maps were thresholded at cluster-level $p<0.05$ (corrected). Regions of significant activation were localised using the SPM5 Anatomy toolbox (Eickhoff et al., 2005).

4.2.2.7.2 Associations between structural and electrophysiological measures and vision

Separate linear regression models were estimated to identify any imaging, electrophysiological or demographic variables which were associated with logMAR visual acuity. LogMAR visual acuity scores were always the dependent variable, and the following variables were entered individually as predictors: fast spin echo and gadolinium-enhanced optic nerve lesion length, optic nerve area, optic radiation lesion load and mean FA, pericalcarine cortical surface area, volume and thickness, VEP amplitude and latency, age, gender, side affected and the number of days from presentation to assessment. Acuity in the fellow eye was always entered into the model, to correct for any normal inter-subject variability.

4.2.2.7.3 Associations between fMRI activation and vision

In order to identify areas of brain functional activity associated with visual acuity, after adjusting for structural damage in the visual system, conduction defects and demographic characteristics, any significant variables from the previous analysis were entered into a whole brain voxel-based multiple regression analysis in SPM5, together with the fMRI data, affected eye visual acuity scores, age, gender, and side of ON. Positive and inverse associations between visual acuity in the affected eye and fMRI activity were assessed, by specifying +1 and -1 contrasts, respectively, with zeros for all other variables. Separate models were specified, in turn, for the affected and fellow eye fMRI data.

A further *post-hoc* analysis was performed, in order to separate the individual influence of structural and electrophysiological variables in these models.

4.2.3 Results

4.2.3.1 Patient characteristics

Twenty eight consecutive patients were recruited. Their mean age was 32 years (SD 7) and 23 were female. The ten controls were age and sex matched, with a mean age of 30 years (SD 3) and eight females.

In the patient group, the median duration of symptoms was 22 days (range 7-34) and the median number of days from presentation to assessment was 19 days (range 3-33). Patients' mean logMAR score was 0.72 for the affected eye (SD 0.69, range -0.06, 1.7, for conversion to Snellen see Appendix I) and -0.05 (SD 0.10) for the fellow eye. The ON affected the left eye in 14 patients and the right eye in the other 14. Seven patients (25%) were treated with steroids, three prior to MRI assessment, and four after the initial scans.

With regard to the timing of assessments, all were performed on the same day in 19/28 patients, and within two days of each other in 25/28. In two patients, the structural scans (and, in addition, the VEP in one of these two) were performed five days after the clinical and fMRI assessment. In one patient, the fMRI scan could not be performed until 21 days after the other assessments.

Gadolinium-enhanced scans were obtained for 26 of the 28 patients, with the remaining two patients declining an intravenous injection.
In one patient, DTI data was unavailable and, in another, the connectivity of one of the reconstructed optic radiations was too low to survive thresholding. These data were omitted from further analysis.

4.2.3.2 Structural and functional differences between patients and controls

Differences in structural and electrophysiological measures between patients and controls are summarised in Table 4.1.

ANTERIOR PATHWAY STRUCTURE	**Patients**	**Controls**	**p value**
T2-weighted optic nerve lesion length (mm)	**21.6 ± 10.4**		
Gad-enhanced segment lesion length (mm)	**23.5 ± 13.3**		
Affected optic nerve area (mm^2)	14.6 ± 3.2	12.8 ± 1.4	NS
Fellow optic nerve area (mm^2)	12.3 ± 1.3		NS
POSTERIOR PATHWAY STRUCTURE	**Patients**	**Controls**	**p value**
Optic radiation lesion load (mm^2)	**63 ± 117**		
Mean FA optic radiations	0.35 ± 0.03	0.36 ± 0.03	NS
Pericalcarine surface area (mm^2)	2440 ± 483	2780 ± 532	NS
Pericalcarine cortical volume (mm^3)	**3630 ± 981**	**4232 ±722**	**0.047**
Pericalcarine cortical thickness (mm)	1.61 ± 0.13	1.63 ± 0.10	NS
Whole brain grey matter volume (cm^3)	715 ± 54	740 ± 53	NS
Grey matter fraction	0.44 ± 0.04	0.45 ± 0.02	NS
ELECTROPHYSIOLOGY	**Patients**	**Controls**	**p value**
Affected VEP amplitude (µV)	**5.30 ± 3.90**	**9.70 ± 3.34**	**0.003**
Fellow VEP amplitude (µV)	12.00 ± 4.4		NS
Affected VEP latency (ms)	**120 ± 18**	**95 ± 6**	**<0.001**
Fellow VEP latency (ms)	95 ± 7		NS

Table 4.1 MRI and VEP parameters from the anterior and posterior visual pathways in patients and controls. Means ± standard deviations are reported. Significant between-group differences are highlighted in bold font. Gad-gadolinium, FA- fractional anisotropy, NS- non-significant, VEP-visual evoked potential.

4.2.3.2.1 Optic nerves

T2 lesions were visible in the patients' affected optic nerve in 96% of cases and, in one case, a segment of high T2 signal was seen in the fellow nerve.

Contrast enhancement was detected in 92% of affected optic nerves and no fellow nerve enhanced.

The patients' affected optic nerves were swollen during the acute phase, compared with the fellow eye (19% greater area, $p<0.001$), and the difference from controls was of borderline significance (patients 14% greater area, $p=0.088$). There were no differences in the area of patients' fellow nerves, compared with controls.

4.2.3.2.2 Optic radiations

Seventy five percent of patients had asymptomatic brain lesions, and in 50% the optic radiations were involved. The brain lesions fulfilled the MRI criteria for diagnosis of dissemination in space (McDonald et al., 2001;Polman et al., 2005) in four cases (14%). There were no significant differences in FA of the optic radiations between the patient and control groups.

No optic nerve abnormalities or brain lesions were found in controls.

4.2.3.2.3 Visual cortex

The volume of the pericalcarine cortex was 14% smaller in patients than controls ($p=0.047$). The mean whole brain grey matter volume was 3% less in patients, which was not statistically significant, and there were no differences in the grey matter fraction between patients and controls. The difference in pericalcarine cortical volumes retained significance after correction for age and gender ($p=0.049$), and retained borderline significance after adjustment for whole brain grey matter volume ($p=0.080$) and grey matter fraction ($p=0.051$). Pericalcarine cortical surface area was 12% smaller in patients, which was of borderline significance before ($p=0.071$), and after ($p=0.067$), adjustment for age and gender. There were no differences in pericalcarine cortical thickness between patients and controls.

Significant associations were found between smaller volumes and the presence of lesions, both in the brain ($p=0.020$) and optic radiations ($p=0.030$). These associations were independent of age, gender, whole brain grey matter indices and the number of days from symptom onset to MRI. There was no association between pericalcarine volume and FA of the optic radiations. There were no associations between whole

brain grey matter indices and the presence of brain lesions, optic radiation lesions or FA.

4.2.3.2.4 Cerebral cortical function

Differences in fMRI activity between patients and controls are summarised in Table 4.2. For the affected eye, ON patients exhibited lower fMRI activation than controls within the bilateral visual cortex. There were no areas where ON patients' affected eyes activated more than controls.

For the fellow eye, ON patients activated more than controls in a region centred on the right pre-central gyrus, extending into the right post-central gyrus. There were no areas where controls activated more than patients, with respect to the fellow eye.

FMRI RESPONSE	**Patients>Controls**	**Controls>Patients**
Eye tested	Fellow	Affected
Region (MNI coordinates)	Right pre-central gyrus (48 -16 56)	Bilateral visual cortex (-24 -82 -14)
Spatial extent (voxels)	576	3208
Voxel-level t-score	3.70	5.64
Cluster-level p value	0.041	<0.001

Table 4.2 Regions of differential fMRI activation between patients and controls. The location, Montreal Neurological Institute (MNI) coordinates, spatial extent, global maximal t-score and cluster-level p value are reported.

4.2.3.3. Associations between structural and electrophysiological measures and vision

Among all the parameters tested, fast spin echo lesion length, enhancing lesion length and VEP amplitude were found to be significantly associated with visual acuity (Table 4.3).

PREDICTOR	Partial correlation coefficient (r)	p value
Fast spin-echo optic nerve lesion length	**0.55**	**0.001**
Gad-enhanced optic nerve lesion length (n=26)	**0.47**	**0.010**
Optic nerve cross-sectional area	0.35	NS
Optic radiation lesion load	-0.01	NS
Optic radiation FA (n=27)	0.21	NS
Pericalcarine surface area	-0.15	NS
Pericalcarine volume	-0.07	NS
Pericalcarine thickness	0.18	NS
VEP amplitude	**-0.84**	**<0.001**
VEP latency (n=23, 5 flat responses)	-0.08	NS
Age	-0.09	NS
Gender	-0.06	NS
Side affected	0.00	NS
Number of days from presentation	-0.08	NS

Table 4.3 Structural, electrophysiological and demographic associations with visual acuity. Partial correlation coefficients are reported, with the associated p value. Only significant p values are reported. The sample size was 28, unless otherwise stated. Significant variables are highlighted in bold font. FA-fractional anisotropy, Gad-gadolinum, NS-non-significant, VEP- visual evoked potential.

A more positive logMAR score, indicating worse vision, was associated with longer lesions and smaller VEP amplitudes. None of the optic radiation or occipital cortical parameters was associated with visual acuity. Therefore, fast spin echo and gadolinium-enhancing measures of lesion length, and VEP amplitude, were entered into the next step of the analysis (i.e. the whole brain voxel-based SPM5 multivariable regression model).

4.2.3.4 Associations between fMRI activation and vision

There was a significant association between greater fMRI activation, in response to stimulation of the affected eye, and better vision (i.e. lower logMAR) in the bilateral visual association cortex of the cuneus, when adjusting for lesion length, VEP amplitude, age, gender and side of ON (Figure 4.10).

No associations were identified between vision in the patients' affected eye and fellow eye fMRI activity.

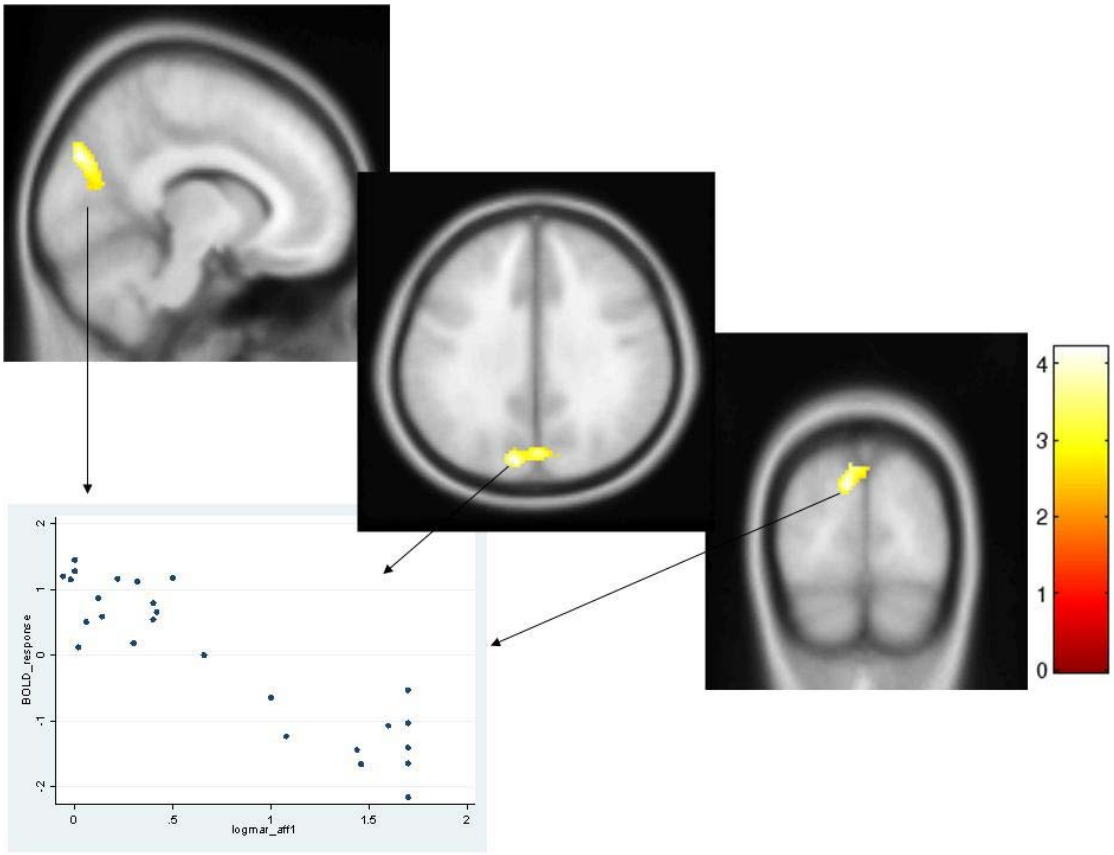

Figure 4.10 Statistical parametric map, showing group correlations between fMRI response and visual acuity, after correcting for fast spin echo lesion length, gadolinium-enhanced lesion length, VEP amplitude, age, gender and side affected. A correlation was seen in the region of the cuneus bilaterally, where better visual acuity was associated with a greater fMRI response. The graph plots logMAR visual acuity against the mean corrected fMRI response (approximate percentage blood oxygenation level dependent (BOLD) signal change), at the peak voxel. The statistical parametric map is thresholded at cluster level $p<0.05$ (corrected), and overlaid on to the MNI-305 template. The scale bar indicates the voxel-level t-scores.

The model was re-estimated with VEP amplitude taken out, in order to separately assess any fMRI associations with vision, after accounting only for markers of inflammation in the optic nerve, and demographics. More extensive correlations were seen in similar areas to the full model, but also extending into the precuneus of the parietal lobe, and involving primary visual cortex (Figure 4.11).

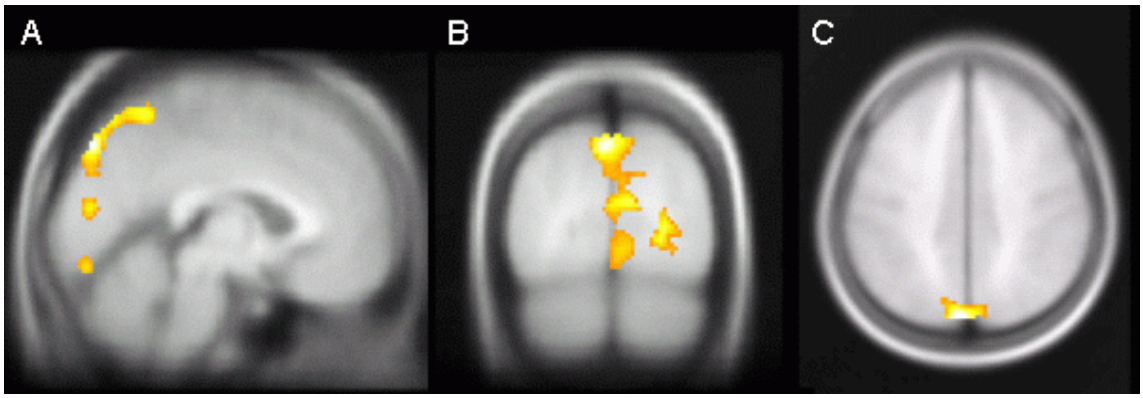

Figure 4.11 Statistical parametric map, showing group correlations between fMRI response and visual acuity, after correcting for fast spin echo lesion length, gadolinium-enhanced lesion length, age, gender and side affected. VEP amplitude has been removed from the model. The correlation in the region of the bilateral cuneus remains, and extends into the precuneus. Activation is also seen in primary visual cortex. The direction of the correlations again indicates that better visual acuity is associated with a greater fMRI response. The map is thresholded at cluster level $p<0.05$ (corrected), overlaid on to the MNI-305 template, and (A) sagittal, (B) coronal and (C) axial sections are shown, centred on the global maximum.

4.2.4 Discussion

The most important finding of this study is the association between visual acuity at presentation, and extra-striate cortical activation, located in the cuneus, part of the dorsal stream of visual processing. This was identified following a voxel-based whole brain multivariable regression analysis, after taking into account structural and electrophysiological measures of the effects of pathology on both the anterior and posterior visual pathway. It can be argued that this may represent an influence of neuroplasticity on acute visual function.

In this section, first the differences between patients and controls will be discussed, and then the associations between vision, structure, and function in patients, followed by a discussion of neuroplasticity in ON.

4.2.4.1 Structural and functional differences between patients and controls

Structural and electrophysiological measures were abnormal during the acute stage of ON, which confirm the presence of optic nerve inflammation and oedema, and consequent conduction delay and block. Half the patients had incidental lesions in the optic radiations, but optic radiation FA did not differ between patients and controls, suggesting that tract integrity is preserved. However, there was a suggestion of volume loss in the patients' pericalcarine cortex. This novel finding appeared to be partly independent of whole brain grey matter volume loss, which has been reported in clinically isolated syndromes (Anderson et al., 2007;Fisher et al., 2008). The smaller calcarine cortex could be due to trans-synaptic degeneration (Evangelou et al., 2001;Calabrese et al., 2007), but this explanation is not in agreement with a normal integrity of the subserving optic radiations. An alternative hypothesis is that this may reflect a generalised susceptibility of the visual system to damage from demyelinating disease. It is known that the optic nerve is particularly vulnerable (McDonald and Barnes, 1992), as ON is the presenting symptom of MS in approximately 20% of patients (Sorensen et al., 1999), optic radiations lesions are common (Hornabrook et al., 1992), and it is conceivable that occipital grey matter may also be susceptible to damage.

This could be either through a mechanism of discrete cortical lesions, which are more difficult to visualise at 1.5T than white matter lesions, or through primary grey matter neurodegenerative change. There was a correlation between pericalcarine atrophy and the presence of white matter lesions in the brain, suggesting that these subclinical grey matter changes are associated with the subsequent development of MS, although longitudinal studies are required to confirm this, and will follow in Chapter 5. The question of whether grey or white matter damage appears first in MS has been debated in the literature (Geurts and Barkhof, 2008). It is not possible to provide an answer from this study, but the observation of grey matter atrophy which is, to some degree, region-specific in patients presenting with clinically isolated syndromes is of interest.

In the direct voxel-wise comparison of fMRI responses, controls' eyes activated more in visual cortex than patients' affected eyes. This can be explained by a reduced afferent input in patients, and is consistent with the findings of previous studies. There was no evidence of differential activation in the cuneus between patients and controls,

which might be anticipated if adaptive plastic changes were genuinely occurring in this region. However, the sensitivity of the voxel-based whole brain analysis approach to detect neuroplasticity in this region may be limited in patients with ON; these patients have structural damage in the optic nerve which reduces the afferent input, resulting in a generally small BOLD signal in all visual areas.

It is interesting that there was, to some degree, a structure-function dissociation. Patients had smaller pericalcarine volumes and less activation in V1 than controls on stimulating the affected eye, but no there were no differences in V1 activation on stimulating the fellow eye. Patients with better vision had more activation in the cuneus than patients with poor vision (after correcting for structural damage in the optic nerve and demographics), but there were no differences in V1. In this study, cortical thickness in the cuneus was not measured, and investigation of structure-function associations in this region could be of potential interest. However, direct comparisons could prove practically problematic, as the Freesurfer cortical parcellation of the cuneus may not map precisely to the identified area of fMRI activation.

The finding of differential activation in the right precentral gyrus was somewhat surprising, and could represent a noise spike artefact. Alternatively, it could relate to the motor task, in which the subjects pressed a button when the fixation-cross changed, although the times of motor responses were entered as covariates into the analysis. It could reflect an abnormal spatial and temporal profile of motor processing in the patient group. Abnormal motor processing is known to occur in MS (Rocca et al., 2005), although whether it occurs in clinically isolated ON is unknown. In the future, studies could correct for possible motor task related activation by introducing a "control" condition during the fMRI experiment, such as pressing a button while watching the grey background.

4.2.4.2 Associations between structural and electrophysiological measures and vision

It was found that the severity of acute visual loss in ON was associated with measures of the extent of optic nerve inflammation (lesion length) and conduction block (VEP amplitude). This is in line with previous experimental and clinical imaging, electrophysiological and pathological studies, which have demonstrated that inflammation and demyelination in CNS lesions each contribute to conduction block

and clinical deficit (Smith and McDonald, 1999). These results confirm that acute visual loss is related to the magnitude of the insult locally within the optic nerve, rather than in the posterior visual pathways.

4.2.4.3 Associations between fMRI activation and vision

An association was detected between greater fMRI activity in the cuneus and better vision, when correcting for optic nerve inflammation and conduction block. This suggests a possible adaptive neuroplasticity in this extra-striate cortex during the acute stage of the disease. The cuneus is an area of visual association cortex, outside primary visual cortex, which is part of the dorsal processing stream, involved in spatial localisation of objects in the physical world. Whilst this study did not include a retinotopic mapping sequence to identify the borders between hierarchical visual areas within individual subjects, the cuneus generally corresponds to Brodmann areas 18 and 19, with the region adjacent to the parieto-occipital sulcus encompassing dorsal area V3. This area is sensitive to coherent motion stimuli (Braddick et al., 2001), and receives major, excitatory feed-forward projections from lower areas such as V2 (Anderson and Martin, 2005).

Extra-striate activation has been reported before in several areas: the insula, claustrum, thalami, corpus striatum, orbitofrontal and lateral temporal cortices, and the posterior parietal cortex, which is also part of the dorsal stream (Werring et al., 2000). More recent longitudinal MRI studies have suggested that adaptive neuroplasticity might occur during the acute stage of ON. Both lower visual areas, such as the LGN (Korsholm et al., 2007) and higher visual areas, such as the lateral occipital complexes (LOCs) (Toosy et al., 2005), located in the ventral processing stream (Goodale and Milner, 1992), have been implicated. At present, it remains unclear whether the location of extra-striate neuroplastic reorganisation is important, in terms of the relative ability of neurons in different regions to adapt their normal function in response to pathological insult (a process known as *cross-modal reassignment*, see section 1.4.3.5). Location might be important if neuroplastic processes, such as dendritic arborisation or synaptic plasticity (Johansen-Berg, 2007), were facilitated in certain regions, through a mechanism of reorganisation of existing, but previously inactive, neural networks. The location of such networks could be patient-specific, or common across groups of patients. Alternatively, location may not

be important, and reorganisation may represent a non-specific *map expansion* from adjacent primary visual areas, in response to a reduced afferent input. With regard to the remaining mechanisms of brain reorganisation, this does not appear to be a case of *homologous area adaptation*, as the primary clinically affected region is in the optic nerve, and the resulting neural input is normally processed by bilateral visual cortex. *Compensatory masquerade* also does not appear relevant as alternative visual strategies are limited. The finding of novel regions, such as the cuneus, and previous reports implicating several different areas, may suggest that either non-specific map expansion, or subject-specific cross-modal reassignment, is more likely than a population-level common "emergency" anatomical network. Interestingly, a subsequent longitudinal study on the same patient cohort which used a region-of-interest analysis, has found that the baseline activation in the cuneus in patients was not associated with visual acuity at one year (see Chapter 5). Further longitudinal studies in larger cohorts are needed to confirm the role of the extra-striate, associative cortices in modulating clinical function in response to pathology in both the acute stage and long-term phase. It is possible that different regions play a role in adaptive plasticity during different stages of the injury.

It is interesting to consider whether the triggers for neuroplastic reorganisation originate at optic nerve, optic tract, optic radiation or visual cortical level. Triggers local to the pathological insult in the optic nerve could include trophic factors, such as cytokines related to inflammation, or stimulation of damaged optic nerve axons. More remote triggers might include a reduction in afferent input to central grey matter, either in the LGN or primary visual cortex, or a combination of both.

Smaller scale mechanisms of reorganisation also merit some consideration, such as changes at cellular level. The time scale of days to weeks in which changes were evident in this and other studies (Toosy et al., 2005), may provide some guidance as to which of the various proposed mechanisms are more likely. It is unclear whether axonal sprouting or dendritic arborisation could occur over this short temporal scale. A change in the expression and distribution of sodium channels appears more feasible, or perhaps synaptic changes, with an alteration in the strength, density, and distribution of connections, or in neurotransmitter function. Over a time period of days to weeks, it might be considered that processing would be more likely to be redistributed along previously existing, but quiescent, pathways, rather than involving the development of entirely new neural circuits. These observations are speculative,

and cannot be answered by the data from this study, requiring further work in animal models. Nevertheless, the results of this study contribute to an assessment of the balance of probabilities, with regard to these mechanisms, by clarifying the temporal course over which neuroplastic changes appear to occur.

There is an alternative explanation for the findings of this study, which is that the observed association reflects a smaller afferent input as vision worsens, independent of the structural and electrophysiological measures included in the model. Correlations were also observed in primary visual cortex when VEP amplitude was removed from the model, suggesting that this part of the variance in fMRI activity did indeed relate to a reduced afferent input, secondary to conduction block. Therefore, it is possible that there is a particular aspect of visual processing occurring in the cuneus, in which the variance in fMRI signal was not captured by the measures included in our model, for example, sensitivity to motion of the checkerboard stimulus. However, if this was the case, correlations might be expected in other motion-sensitive visual areas, such as V5/MT. Moreover, as the structural and electrophysiological measures included in the model reflect disruption to neural transmission through inflammation and conduction block within the optic nerve, it might be expected that all aspects of visual information would be affected together at such an early stage in the afferent pathway.

4.2.4.4 Study limitations

The patient cohort included a small proportion of people in whom structural and functional scans were separated by more than two days, and acute ON is a time of dynamic pathophysiological change. In particular, in one patient the scans were separated by a much longer period. In addition, there was some heterogeneity within the cohort in the time from symptom onset to assessment. To investigate the influence of these factors, the SPM5 multivariable regression model was respecified, firstly, omitting the subject with a delay and, secondly, including an additional regressor, representing the number of days from symptom onset. In both cases, the associations between vision and fMRI activity in the cuneus remained significant (results not shown).

In addition, the influence of steroids on the fMRI response remains unknown, but an influence on the electrophysiological parameters has been reported (Trauzettel-Klosinski et al., 1995). However, in this study, only three patients had steroids before their imaging and electrophysiological assessment. There were no differences in the fMRI response and VEP amplitude and latency between patients treated with steroids and those untreated (results not shown).

Whilst this study incorporated the most comprehensive structural MRI assessment of the visual pathways to date in ON, it is possible that an influence of optic tract pathology was missed, as it was not assessed. Diffusion-based tractography of the optic tract may be possible, but would necessitate longer scan-times. For this reason, it was unfeasible to include either optic nerve or optic tract DTI in the present study. Prohibitive scan-times remain a limiting factor when aiming for a comprehensive MRI assessment of the visual system. In the future, this may be addressed with advances in technology, such as higher strength magnetic fields (Chapter 7).

Finally, a two stage analysis strategy was applied in order to dissect structure-function relationships. This helped to limit the number of variables in the final analysis. Future studies may incorporate a larger sample size, which would allow a more complete assessment of all structural and electrophysiological variables in a single regression model with brain fMRI response. The relatively large number of variables investigated also raises the issue of multiple comparisons. The p values reported in this chapter are uncorrected. This issue is discussed in detail in section 5.1.4.5.

4.2.4.5 Conclusions

In summary, MRI and electrophysiological techniques were combined to assess structural damage, and its effects on neural conduction, within the anterior and posterior visual pathways in acute ON, and the results used to inform an analysis of cortical responses, measured using fMRI. Whilst structural abnormalities were detectable throughout the afferent pathway, the severity of acute visual loss was determined predominantly by direct damage to the optic nerve. Cortical activity was identified within the dorsal stream of visual processing, which was associated with better vision, after adjusting for the influence of structural damage in the optic nerve,

and its electrophysiological consequences. This suggested some degree of adaptive neuroplasticity within the dorsal stream of higher visual processing, occurring during the acute episode of ON, which may act to modulate acute clinical deficit.

The next goal of this thesis is to elucidate the nature of neuroplasticity in ON further, to investigate how fMRI responses change over time in different regions of the brain, how this relates to dynamic clinical and structural changes and, in particular, long-term visual recovery. A longitudinal methodology is required to clarify these aspects, and follows in the next chapters.

CHAPTER 5

A LONGITUDINAL STUDY OF MECHANISMS OF DAMAGE AND RECOVERY IN ACUTE OPTIC NEURITIS

In this chapter, structural and functional data are combined in a longitudinal study, in order to assess the evolution of damage following ON, and to investigate mechanisms of recovery. The chapter is divided into three sections. In the first, visual recovery is considered. The aim was to identify the factors associated with visual outcome, a year after the acute episode. This is important from a clinical perspective, and also to determine why some patients recover well despite significant tissue loss. In particular, the relative importance of myelination, axonal loss and neuroplasticity are considered, as evidenced by VEP, OCT and MRI measures.

In the second section, variables resulting from the first analysis are explored in more detail, with a particular focus on relationships between fMRI activity, structure and clinical function. More complex analysis techniques are employed to explore changing temporal relationships.

In the final section, neurological outcome is considered, by investigating the development of MS following ON, with a particular focus on associations with measures of cortical tissue loss.

SECTION 1 MECHANISMS OF DAMAGE AND RECOVERY IN OPTIC NEURITIS

5.1.1 Introduction

Most patients with acute, idiopathic, demyelinating ON make a good visual recovery. However, 5-10% recover poorly (Beck et al., 2004a), and many more notice residual qualitative deficits (Cleary et al., 1997). For these people, there are no effective treatments to improve vision. It is not clear why some people fail to recover whereas others recover well, even following severe visual loss and despite evidence of residual tissue damage. The focus of this section is to investigate the mechanisms underlying

damage and recovery, and to identify any predictors of visual outcome during the acute episode which could be of potential clinical utility.

5.1.1.1 Acute inflammation

During the acute episode, there is inflammation, oedema, demyelination and conduction block in the optic nerve (Smith and McDonald, 1999). In Chapter 4, it was demonstrated that inflammation and conduction block were associated with the severity of acute visual loss, and this must be taken into account when considering visual outcome. Intuitively, it might be expected that patients with a more severe acute inflammatory insult would have a worse outcome and, indeed, there was a statistical association between baseline visual loss and visual outcome in the ONTT (Beck et al., 1994). However, studies in the same cohort found that this association did not usefully predict recovery at six months at the level of the individual, as most patients with severe baseline visual loss still had potential for a good recovery. In a clinical setting, worse visual function at one month was found to be more useful at predicting poor eventual recovery (Kupersmith et al., 2007). A study in a different cohort found no association at all between baseline visual loss and recovery at 12 months (Hickman et al., 2004c). With regard to paraclinical measures of the severity of acute inflammation, the data are also inconsistent. A longer gadolinium-enhancing lesion in the optic nerve during the acute episode was associated with worse visual outcome in one study (Hickman et al., 2004c), but not in another (Kupersmith et al., 2002).

5.1.1.2 Myelination and axonal loss

In the weeks following acute ON, inflammation resolves and electrical conduction, and consequently vision, begins to improve. However, there is frequently evidence of persistent optic nerve demyelination, such as a prolonged VEP latency (Jones, 1993) and reduced optic nerve MTR (Hickman et al., 2004b). Neuroaxonal loss occurs and optic atrophy generally ensues, becoming clinically evident as disc pallor on fundoscopy at around six weeks, and detectable later using optic nerve MRI (Inglese et al., 2002;Hickman et al., 2004a), and OCT of the RNFL (Trip et al., 2005;Costello et al., 2006). Evidence for remyelination, such as shortening VEP latency, may be

seen later but generally not until clinical recovery is almost complete (Jones, 1993). Therefore, it is of interest that most patients make good visual recoveries, considering the frequency of residual tissue damage, including axonal loss, a phenomenon usually associated with permanent disability in demyelinating diseases (Miller et al., 2002).

5.1.1.3 Visual recovery despite tissue damage

The key factors determining visual recovery following acute ON remain unclear. Early initial improvement appears to be temporally related to resolution of acute oedema and inflammation in the optic nerve (Youl et al., 1991), and occurs despite residual tissue damage. Hypotheses to explain the relative dissociation between optic nerve tissue damage and degree of visual recovery include an influence of pathology in the posterior pathways. Alternatively, the restricted clinical impact despite optic nerve axonal loss may be partially explained by the large number of axons in the optic nerve, in excess of the critical threshold necessary to maintain function, a concept known as *neuroaxonal redundancy*. *Remyelination* of the visual pathways may occur. An independent hypothesis implicates compensatory reorganisation of cortical processing, which is known as *adaptive neuroplasticity*, and was introduced in earlier chapters of this thesis.

5.1.1.4 Predicting prognosis during the acute episode

Currently, it is not possible to predict reliably which patients will fail to recover from an attack of ON. Worse visual acuity at one month (Kupersmith et al., 2007), a less steep initial gradient of improvement of acuity and smaller amplitude VEPs during the recovery phase (Hickman et al., 2004c) have been associated with a worse visual prognosis, but are not helpful at the time of diagnosis. Similarly, whilst measures of tissue loss such as thinning of the RNFL (Trip et al., 2005;Costello et al., 2006), optic nerve atrophy (Hickman et al., 2002a;Inglese et al., 2002) and reduced optic nerve MTR (Inglese et al., 2002) have been associated with a worse outcome, they are not evident until months or years after the event. Therefore, prognostication in patients with ON currently follows an expectant approach. This is a problem when counselling patients at the time of diagnosis, and also causes difficulties when selecting patients

for trials of experimental therapies, for example, neural stem cells (Kolappan et al., 2008a).

5.1.1.5 Aims

The aims of this serial ON study were in part hypothesis-driven, based on previous reports implicating the lateral occipital complexes (LOCs), a ventral stream higher visual processing area, in neuroplasticity (Toosy et al., 2005). The primary hypothesis was that early LOC activation would be significantly associated with visual outcome, after accounting for markers of anterior and posterior visual pathway damage. The relative contributions of acute inflammation, myelination, and neuroaxonal loss in determining the visual outcome from ON were also investigated. It was possible to address these questions through a comprehensive structural and functional imaging protocol over time. Structural and diffusion MRI techniques assessed optic nerve and radiation involvement. VEP latency and amplitude reflected myelination and surviving axonal populations, respectively. OCT (Huang et al., 1991;Fercher et al., 1993) assessed macular volume and RNFL thickness, reflecting loss of retinal ganglion cells and their axons, secondary to retrograde degeneration from pathology within the optic nerve (Quigley et al., 1977). Visual fMRI investigated neuroplasticity.

5.1.2 Methods

Many of the methodological details have been described previously in Chapter 4, and are not replicated here. Aspects of the methodology specific to the longitudinal studies described in this chapter are reported in depth in the following sections.

5.1.2.1 Participants

The longitudinal cohort of patients with acute, clinically isolated ON was the same as for the cross-sectional study, described in Chapter 4. Patients were invited for clinical assessment, VEPs, structural and functional MRI, on the same day, within a month from onset and three, six and 12 months later. In addition, at one year follow-up,

patients were invited for OCT imaging. A summary of the different techniques used, and the different perspectives they provided, is shown in Figure 5.1.

Healthy age and sex matched controls were recruited at baseline, and were invited for follow-up MRI at each time-point, and one VEP and OCT assessment. All subjects gave written informed consent. The study was approved by the local Ethics Committee.

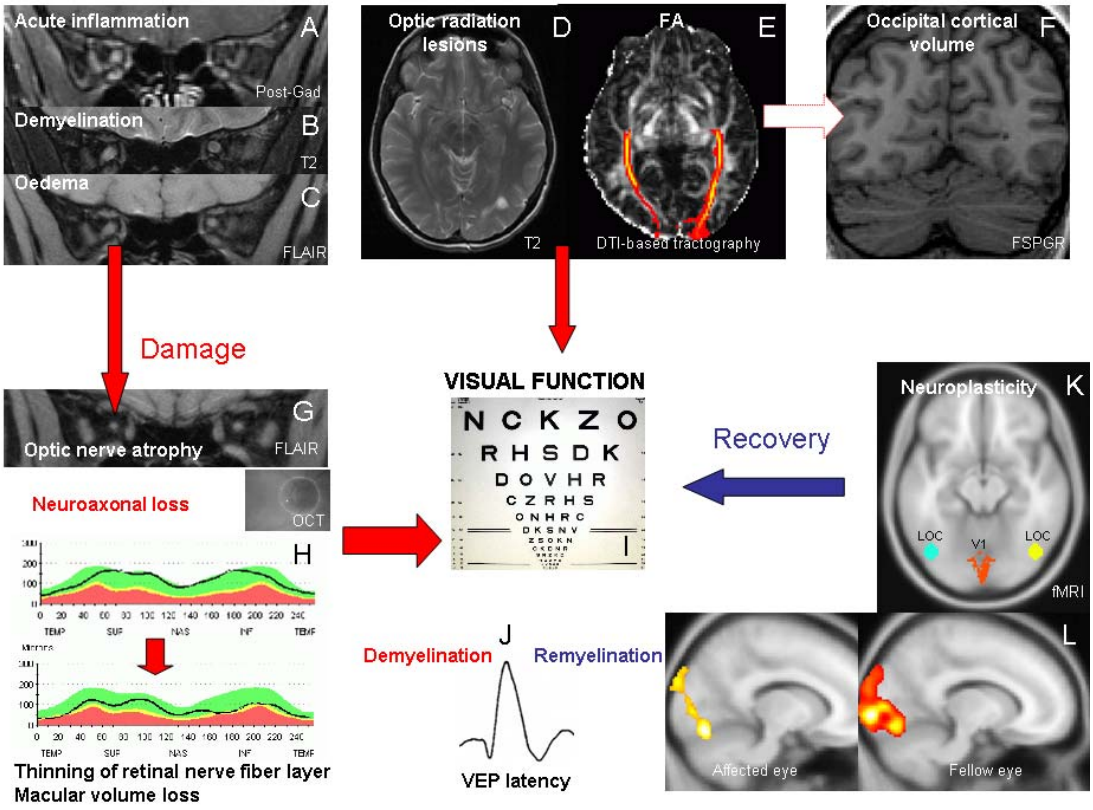

Figure 5.1 Techniques used to assess mechanisms of damage and recovery in ON in this study. (A) Coronal optic nerve MRI: post-gadolinium sequence shows right sided optic nerve enhancement. (B) T2-weighted sequence shows high signal in the right optic nerve. (C) Fluid attenuated inversion recovery (FLAIR) sequence shows right optic nerve swelling. (D) Axial T2-weighted fast spin echo (FSE) of the brain shows a lesion suggestive of demyelination in the left optic radiation. (E) DTI-based tractography allows reconstruction of the optic radiations. Parameters were extracted, such as fractional anisotropy (FA), which summarise the integrity of the tracts. (F) T1-weighted fast spoiled gradient echo (FSPGR) was used to assess pericalcarine cortical surface area, volume and thickness. This coronal slice shows the calcarine sulcus. (G) A follow-up optic nerve FLAIR from the 12 month time-point shows right optic nerve atrophy. (H) Optical coherence tomography (OCT): an example of a retinal scan and the results, demonstrating a reduction in the thickness of the right retinal nerve fibre layer. (I) LogMAR chart for assessment of visual acuity. (J) Visual evoked potentials may detect conduction delay representing demyelination in the visual pathways. (K) FMRI scans demonstrating regions-of-interest in the lateral occipital complexes (LOCs) and primary visual cortex (V1). (L) A reduced fMRI response is seen on stimulating the affected eye, compared with the fellow eye.

5.1.2.2 Clinical assessment

LogMAR scores were used to assess visual acuity. The testing methodology was identical to the description in Chapter 4.

5.1.2.3 Electrophysiology

Each patient had longitudinal VEP assessments, whilst each control had a single VEP study. Both whole field and central field VEPs were acquired. The whole field procedure was identical to that used in Chapter 4. VEPs were also recorded to interleaved (cyclic) stimulation of five different areas, comprising the central field and the four quadrants. The radius of the circular central field was 4^{o} at the eye. For the interleaved central field and each quadrant, the interval between reversals was 265ms, and three averages of 100 responses were obtained for each eye, after assessment of their consistency. The quadrant data was not used in the analyses described in this chapter, and will be reported in more detail in Chapter 6.

5.1.2.4. Optical coherence tomography

This examination was performed only at the 12 month time-point. OCT imaging was acquired with a Stratus OCT Model 3000 (Carl Zeiss MediTec, Dublin, Ca, USA). RNFL images were averaged from three 3.4mm diameter scans centred on the optic disc (Fast RNFL protocol). Macular thickness maps were calculated by taking six linear radial scans centred on the fovea (Fast macular thickness map scanning protocol). The OCT Model 3000 assesses signal strength and assigns a score. Images were only accepted if the score was >7/10, and the inter-eye difference was <2/10. This is in line with previous OCT studies (Henderson et al., 2008). All scans were performed by the same operator (Dr. Andrew Henderson).

5.1.2.5 MRI acquisition and analysis

Both the structural and functional MRI acquisition protocols were identical to those described in Chapter 4. During the fMRI protocol, the percentage of correct responses

to the fixation cross changing, averaged across time-points, was 88% for patients and 97% for controls. This indicated generally good attention and fixation.

5.1.2.6 Functional MRI analysis: regions-of-interest

The whole field fMRI data acquired with the chromatic goggles was analysed using a region-of-interest approach. The regions were selected based on previous work (Toosy et al., 2005;Korsholm et al., 2007;Jenkins et al., 2008 and Chapter 4 of this thesis). Each region chosen represented a different area of the visual processing hierarchy. This was in order to determine the relative importance of changes at different levels of processing, how the regions interacted with one another, and how each was related to structural damage and clinical recovery. Regions were as follows: 1) the primary visual cortex, 2) the LGN, 3) the LOCs, which represented the ventral stream of the higher visual processing areas, and 4) the cuneus, identified in Chapter 4, which represented the dorsal stream of the higher visual processing areas. The primary visual cortex and cuneus comprised bilateral regions. For the LGN and LOCs, there was one region for each side of the brain, and the data was combined, as each side receives neural input from both eyes. The primary visual cortex region was specified utilising a normalised Brodmann area 17 mask, as described in section 4.1.2, since it was also used as a target for tractography. The LGN region was defined using two spherical seed regions, centred on the global maximal voxels, derived from the fMRI data, as reported in section 4.1.4, since they were used as seed-points for tractography. Essentially, the LGN clusters were identified at group level in SPM5, averaging checkerboard stimulation through the goggles, and also the two sessions of black and white checkerboard stimulation, for both affected and fellow eyes, from all patients and controls, at each time-point. The LOCs were defined using two spherical regions-of-interest, each of $1cm^3$ volume, centred on the coordinates reported from previous studies (+/-43, -70, -13) (Toosy et al., 2005). This methodology was used by previous investigators (Korsholm et al., 2007), and is an alternative to the use of a localiser task to identify the LOCs. Finally, the cuneus was selected on the basis of the results reported in Chapter 4. The identified cluster within the bilateral cuneus, comprising 580 voxels, with its global maximum at MNI -10 -84 32, significant at $p<0.05$ (corrected), was used to investigate longitudinal changes in the dorsal stream of higher visual processing.

Mean parameter estimates were extracted from each region-of-interest, from each subject, at each time-point, using the MarsBar SPM toolbox (Brett et al., 2002). The results reported are parameter estimate units, which reflect the magnitude of BOLD signal change.

5.1.2.7 Statistical analysis

All statistical analysis was performed using Stata-9.2 (StataCorp, Texas, USA), unless otherwise stated. The analysis proceeded in several stages, detailed below. $P<0.05$ was chosen to represent statistical significance.

5.1.2.7.1 Longitudinal analysis

To explore longitudinal changes, mixed effects models were specified separately, for each variable, in patients and controls, and the resulting predicted means, using all available data, were reported at each time-point (Results: Table 5.4). In addition, for variables in which changes were significant, the median and inter-quartile ranges were reported for change between baseline and 12 months (section 5.1.3.3). This approach was used in preference to reporting rates of change, as some changes were non-linear.
Unpaired t-tests were used to assess differences in VEP and OCT parameters between patients and a randomly selected control eye, at the 12 month time-point. Differences in the same parameters between patients' affected and fellow eyes were assessed using paired t-tests.

5.1.2.7.2 Associations between visual outcome and baseline (or 12 month) variables

Visual outcome was defined as logMAR (affected eye) at 12 months. To identify baseline predictors of visual outcome, regression models were separately specified, entering baseline structural MRI, VEP and fMRI measures, and demographic parameters as independent variables, with logMAR acuity at 12 months as the dependent variable. The model was repeated, in turn, for each independent variable. The number of days from symptom onset to initial assessment and acuity in the fellow eye were included as covariates in the model, to allow for any inter-individual differences in the stage of evolution of pathology, and pre-morbid acuity. To identify variables measured at 12 months that were associated with visual outcome at 12

months, regression models were specified, with logMAR acuity at 12 months as the dependent variable, and the 12 month structural MRI, VEP, OCT and fMRI measures as independent variables. For the OCT data, fellow eye parameters were also added to the model, to adjust for normal inter-individual variability (Alamouti and Funk, 2003).

5.1.2.7.3 Relationship between baseline LOC responses and visual outcome

As a result of significant associations between LOC activation and visual outcome (see Results) the two variables were plotted. A threshold of affected eye LOC fMRI response was visually determined that would dichotomise visual outcome into two groups of better relative outcome, and worse relative outcome, with high sensitivity and specificity.

5.1.2.7.4 Inter-variable structure-function relationships and visual outcome

The five significant variables found in the analysis described in 5.1.2.7.2 were investigated further. Two of these were affected and fellow eye LOC fMRI responses. The others were baseline acuity, age and 12 month macular volume. Multivariable regression models were specified, with logMAR at 12 months as the dependent variable as before, except now each of the other demographic, structural and functional variables was also added, in turn, to the model to assess its influence on the relationship between the variable of interest and logMAR at 12 months. This was performed for the dependent variables separately at baseline and 12 months. These analyses involved numerous statistical tests and raised the issue of multiple comparisons. Although there is no ideal method to address this for the family wise error rate (FWER), it was felt to be prudent to report p values both uncorrected and corrected for multiple comparisons (by variable), using the relatively conservative Holm procedure (Holm, 1979;Aickin and Gensler, 1996). For analyses of LOC activation, based on the *a priori* hypothesis of their neuroplasticity-related contribution to visual outcome, greater attention should be paid to the uncorrected p values (first two columns of Tables 5.7 and 5.8).

5.1.3 Results

5.1.3.1 Patient characteristics

The patients' clinical and demographic data is presented in Table 5.1. Twenty eight patients and ten age and sex-matched controls were recruited at baseline. The median duration from symptom onset to baseline assessment was 22 days (range 7-34).

Patient	Age (years)	Sex	Side	LogMAR			
				Baseline	3 months	6 months	12 months
1	38	F	R	0.4			
2	27	F	L	-0.02	-0.02	0.08	0.1
3[a]	24	F	L	1.7	0.5	0.4	0.32
4	27	F	R	0.5	0.1	0	0.06
5	20	M	L	0.4	0.4	0.06	0.22
6	25	F	L	0.14	0.1	0	0.02
7	39	F	L	0.06	-0.1	0.02	-0.1
8	36	F	R	0	-0.06		-0.04
9	33	F	L	0.12			
10	33	M	R	0.3	0.02		
11	32	F	L	-0.06	-0.06	-0.04	-0.08
12	44	F	L	0	-0.08	-0.06	0.02
13	30	F	L	1.46	0.04	-0.04	0.02
14	43	F	R	1.62			
15	38	M	R	0.02	-0.14	-0.06	0.04
16	31	F	L	1	0.02	0	0
17[b]	33	M	L	1.7	1.26	0.34	0.28
18	41	F	R	1.7	0.04	-0.1	-0.1
19	42	F	R	0.22	0	0.02	-0.08
20	30	F	R	-0.06	-0.18	-0.06	-0.12
21	34	F	R	1.6	0.18	0.22	0.22
22	26	F	L	1.44	1	1.06	0.92
23	34	F	L	0.42	0.1	0.08	0.02
24	24	F	R	0.32	0	0.02	0.02
25	23	F	R	0.66		0.28	0.22
26	30	F	R	1.7	0.06	0	-0.06
27	35	F	R	1.08	0.22	-0.04	0.02
28	25	M	L	1.7	0.54	0.32	0.26
Patients	Mean 32	5M 23F	14R 14L	0.72 (0.69)	0.16 (0.35)	0.11 (0.25)	0.09 (0.22)
Controls	Mean 30	2M 8F					

Table 5.1 Patient characteristics. The mean visual acuities of the patients are reported in the bottom row, with the standard deviations in brackets.

[a]This patient had a recurrence of mild ON in the fellow eye at three months (worst logMAR 0.3), from which she recovered well (logMAR -0.08 by the six month time-point), and was included in the analysis.

[b]This patient had coexistent bilateral keratoconus with best corrected acuity of 0.18, and was included in analyses which included fellow eye acuity as a covariate, but excluded when looking at predictors in which recovery was classified purely on the basis of affected eye logMAR, without entering the fellow eye as a covariate.

5.1.3.2 Patient adherence

The number of patients and controls who attended each of the follow-up visits is reported in Table 5.2.

	Baseline	**3 months**	**6 months**	**12 months**
No. patients attending	28	24	23	24
No. controls attending	10	8	8	8

Table 5.2 Longitudinal dataset. The number of participants who returned for follow-up at each time-point.

The reasons for the missing visits were as follows: three patients and two controls decided they did not want to continue in the study after the first visit and a further one patient after the second visit. One patient missed the three months visit due claustrophobia in the scanner, but decided subsequently to return. One patient missed the six months time-point due to pregnancy, but returned after delivery for her 12 months assessment.

With regard to the tests performed, all of the controls had all of the MRI scans at each time-point, and one VEP examination. Nine of the ten controls had one OCT examination; one control missed this test because she had moved away from the region. The tests that were performed in each patient, at each time-point, are summarised in Table 5.3.

	Baseline	3 months	6 months	12 months
No. of optic nerve FSE acquired	28	24	22	20[a]
No. of optic nerve Gad acquired	26[b]			
No. of optic nerve FLAIR acquired	28	24	22	20
No. of brain FSPGR acquired	28	24	21[c]	20
No. of brain FSE acquired	28	24	22	20
No. of DTI OR acquired	27[c]	24	21[c]	17[c]
No. of OCT acquired				18[d]
No. of VEP acquired	28	24	23	21[c]
No. of fMRI acquired	28[e]	24	22	20[e]
No. of patients with a delay between tests of >2 days[f]	3	2	3	4

Table 5.3 Tests performed in the patient group. DTI-diffusion tensor imaging, FLAIR-fluid attenuated inversion recovery, FSE-fast spin echo, FSPGR-fast spoiled gradient echo, Gad-gadolinium-enhanced MRI scan, OCT-optical coherence tomography, OR-optic radiations.

The explanations to the superscripts in Table 5.3 are as follows:

[a] The reasons for the missing tests were the following: Five patients became pregnant during the study, three missing MRI at 12 months, one MRI at six and 12 months, and one all tests at six months. Four of these patients, who could not have MRI scans, did attend for clinical assessment, VEPs and OCT during pregnancy.

[b] Two patients declined an intravenous injection.

[c] Test unavailable, due to time constraints, technician availability, or technical failure.

[d] OCT became available on-site during the course of the study. Patients in the study who had not yet reached the 12 month time-point were eligible for the OCT examination.

[e] In one patient at baseline, and two patients at 12 months, a parameter estimate for LOC extraction was unobtainable, due to temporal signal dropout. For the analysis in which the clinical utility of baseline fMRI as a predictor of visual outcome was evaluated, data was available for 23/28 patients. This included one patient who had recovered well at three months and was then lost to follow-up. Visual outcome data was not available for the three patients who were lost to follow-up after baseline. In addition, a patient with coexistent keratoconus was excluded from this analysis (see also Table 5.1).

[f] The patients had all the tests on the same day in 81% of time-points, and within two days in 88% of cases. In the remainder, the median delay was 10.5 days. At baseline, there were three delays of 5, 5 and 21 days, with the delayed tests being structural MRI, structural MRI and VEP, and fMRI, respectively. All analysis was repeated excluding the patient with a 21 day delay, and the results were materially unaffected.

5.1.3.3 Longitudinal analysis

These data are summarised in Table 5.4 and Figure 5.2.

PATIENTS		Baseline mean (95%CI)	3 months mean (95%CI)	6 months mean (95%CI)	12months mean (95%CI)	Change from baseline to 12 months (p value)
OPTIC NERVE	**FSE lesion length (mm)[a]**	**22.07 (18.35-25.79)**	**24.82 (20.98-28.66)**	**29.82 (25.92-33.72)**	**31.26 (27.28-35.23)**	**<0.001**
	Gad lesion length (mm)	23.54				
	Area ratio (Affected: Fellow)	**1.19 (1.13-1.24)**	**1.01 (0.94-1.07)**	**1.00 (0.93-1.06)**	**0.89 (0.82-0.95)**	**<0.001**
OPTIC RADIATIONS	**Lesion load (mm^2)**	63 (3-123)	85 (25-146)	**102 (41-162)**	**118 (57-179)**	**<0.001**
	FA[b]	0.36 (0.34-0.37)	0.36 (0.34-0.37)	0.35 (0.34-0.37)	0.36 (0.34-0.38)	0.693
OCCIPITAL CORTEX	Pericalcarine surface area (mm^2)	1212 (1123-1301)	1215 (1124-1307)	1196 (1103-1289)	1218 (1124-1312)	0.836
	Pericalcarine volume (mm^3)	1808 (1666-1950)	1824 (1679-1969)	1764 (1616-1911)	1798 (1650-1946)	0.830
	Pericalcarine cortical thickness(mm)	1.61 (1.57-1.66)	1.61 (1.56-1.66)	1.60 (1.55-1.65)	1.60 (1.55-1.65)	0.441
WHOLE BRAIN	Grey matter fraction	0.44 (0.43-0.45)	0.44 (0.42-0.45)	0.44 (0.42-0.45)	0.44 (0.43-0.45)	0.461
VISUAL EVOKED POTENTIALS	**Whole field amplitude (µV)**	5.30 (3.97-6.64)	6.57 (5.17-7.98)	**6.67 (5.24-8.09)**	**7.14 (5.68-8.61)**	**0.008**
	Central latency (ms)[c]	123 (115-131)	123 (115-131)	119 (111-127)	**114 (106-122)**	**0.020**
CONTROLS						
OPTIC NERVE	Area ratio	1.03 (0.98-1.07)	1.00 (0.95-1.05)	1.01 (0.96-1.06)	0.97 (0.92-1.03)	*0.091*
OPTIC RADIATION	FA	0.36 (0.34-0.38)	0.37 (0.35-0.39)	0.37 (0.35-0.40)	0.38 (0.36-0.41)	*0.072*
OCCIPITAL CORTEX	Pericalcarine surface area (mm^2)	1390 (1241-1538)	1342 (1185-1500)	1376 (1218-1533)	1391 (1233-1548)	0.989
	Pericalcarine volume (mm^3)	2116 (1827-2405)	2066 (1771-2362)	2148 (1853-2444)	2062 (1767-2358)	0.447
	Pericalcarine cortical thickness(mm)	1.63 (1.56-1.70)	1.64 (1.56-1.72)	1.69 (1.61-1.77)	1.60 (1.52-1.68)	0.523
WHOLE BRAIN	Grey matter fraction	0.45 (0.43-0.46)	0.45 (0.43-0.46)	0.44 (0.42-0.46)	0.45 (0.44-0.47)	0.393

Table 5.4 (on the previous page). Longitudinal changes in structural and electrophysiological measures in patients and controls. Significant changes are highlighted in bold font. CI-confidence interval, FA-fractional anisotropy, FSE-fast spin echo, Gad-gadolinium-enhanced MRI, LGN-lateral geniculate nuclei, LOC-lateral occipital complex, NS-non-significant, V1-primary visual cortex. Note that the reported pericalcarine cortical surface area and volume estimates are averaged for each hemisphere.

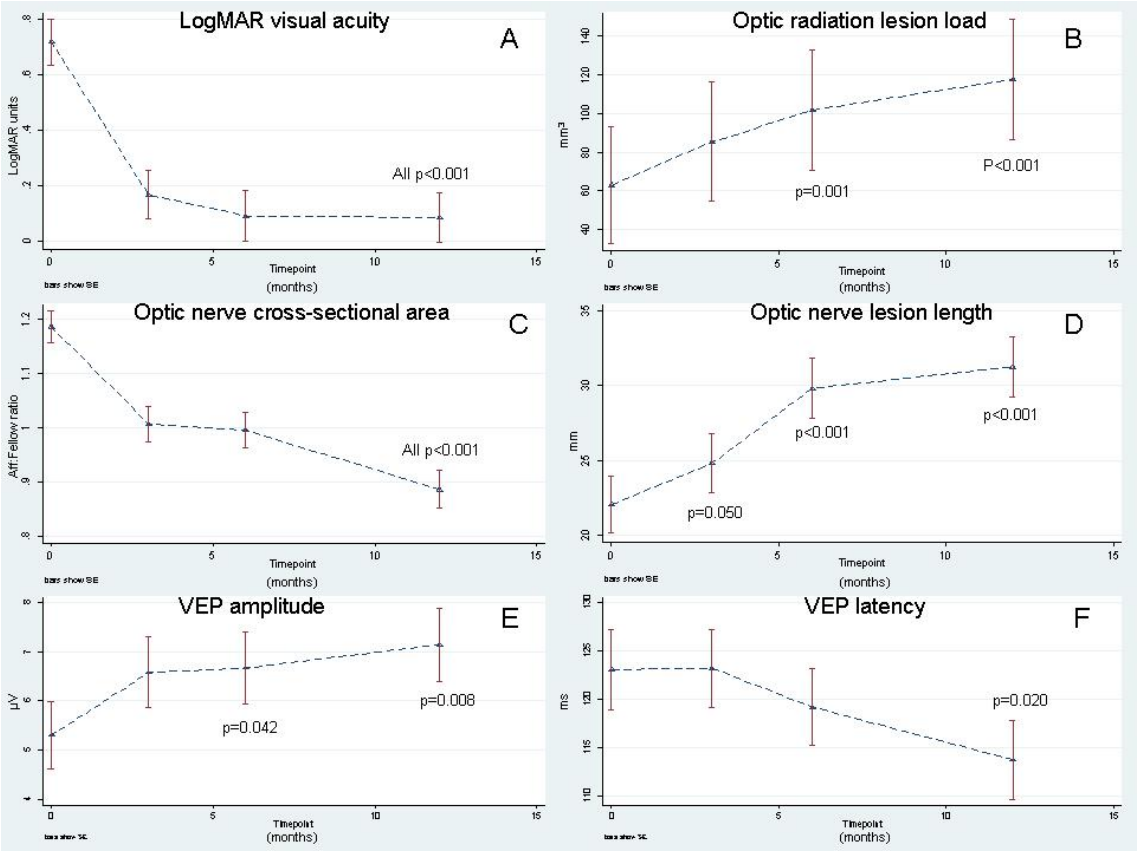

Figure 5.2 Graphs showing longitudinal changes in clinical, electrophysiological and MRI parameters: (A) visual acuity, (B) optic radiation lesion load, (C) optic nerve cross-sectional area, (D) optic nerve lesion length, (E) VEP amplitude and (F) VEP latency. Significant changes from baseline are indicated by the associated p-value. The bars show standard errors. Higher logMAR scores indicate worse acuity.

Over the year, patients' vision improved by a median of 0.42 logMAR units (inter-quartile range (IQR) 0.11, 1.38). Seventy four percent of patients recovered acuity to logMAR<0.2 (better than Snellen equivalent 6/10). Optic nerve lesion length

increased by 9mm over the year (IQR 6, 13), and optic nerve area ratio decreased by 25% (IQR 10%, 38%). The median increase in optic radiation lesion load was 15mm^2 (IQR 0, 78). VEP amplitude improved by 2.63μV (IQR -0.49, 4.44) and VEP latency reduced by 11.7ms (IQR 5.6, 20.2). For some variables, the rates of change varied over time (Table 5.4, Figure 5.2)

In controls, there were no significant changes over time in the variables examined.

Longitudinal changes in fMRI responses in patients are plotted in Figure 5.3. In lower visual areas (LGN and primary visual cortex), affected eye responses showed the greatest increase over the first three months, and the observed decreases in fellow eye responses did not reach statistical significance. In contrast, in higher visual areas (LOCs and cuneus), responses were more complex and decreases in fellow eye activation were evident over time. These included significant decreases in the fellow eye responses in the LOCs. There were no changes in controls between baseline and 12 months.

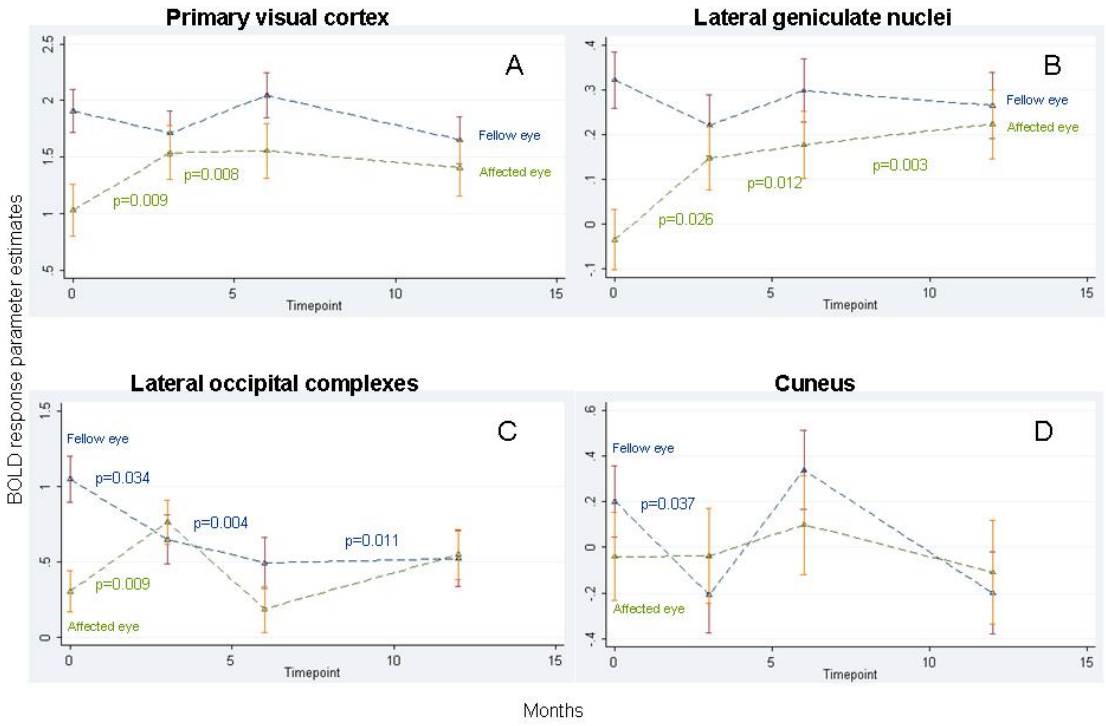

Figure 5.3 Graphs showing longitudinal changes in fMRI activity, on stimulation of the affected and fellow eyes, in the four regions-of-interest implicated in neuroplastic responses by previous studies: (A) primary visual cortex, (B) LGN, (C) LOCs and (D) cuneus. Affected eye responses are plotted in green and fellow eye responses in blue. Significant changes from baseline are indicated by the associated p-value. The bars show standard errors. BOLD-blood oxygenation level dependent.

At 12 months, macular volume and RNFL thickness were reduced and VEP latency was prolonged in the patients' affected eyes, compared to controls (Table 5.5). There were no significant differences in fellow eye parameters between patients and controls.

	Patients: affected eye	Patients: fellow eye	Controls	Patients vs controls t-tests	
				Affected eye	Fellow eye
Macular volume (mm^3)	**6.01**	6.62	**6.82**	**p=0.001**	*0.085*
RNFL (μm)	**79**	100	**106**	**p<0.001**	0.167
VEP amplitude (μV)	*7.2*	9.4	*9.5*	*p=0.054*	0.930
VEP latency (ms)	**112**	96	97	**p=0.020**	0.826

Table 5.5 Residual damage at 12 months. Results of OCT and VEP at 12 months are reported for patients' affected and fellow eyes, and controls. The p values are derived from two-sample unpaired t-tests. Significant differences between patients and controls are highlighted in bold font. NS-non-significant, RNFL-retinal nerve fibre layer.

The macular volume in the patients' affected eye was reduced by 9%, compared with the fellow eye, and 12% compared with controls

The RNFL thickness in patients' affected eye was reduced by 21%, compared with the fellow eye, and 27% compared with controls.

5.1.3.4 Associations between visual outcome and baseline (or 12 month) variables

The strongest baseline predictor was fMRI response in the LOCs, on stimulating the affected eye (Table 5.6, Figure 5.4); greater fMRI activity was associated with better logMAR acuity at 12 months (p=0.007). There was also an association in the same region between fMRI response and visual outcome, when the fellow eye was stimulated (p=0.020). No acute structural measures were significantly associated with visual outcome. There was an association with the initial severity of visual loss and a weak influence of age, with older patients tending to have better acuities at 12 months. At 12 months, the only significant result was a weak association between smaller macular volume and worse outcome (Table 5.6). An increase in macular

volume of 1mm^3 corresponded to an improvement in logMAR acuity of 0.33 (approximately three lines on the chart).

	Patient variable	Association between variable and visual outcome at 12 months			
		BASELINE VARIABLES		12 MONTHS VARIABLES	
		r	p	r	p
RETINA	**Macular volume**	**-**	**-**	**-0.52**	**0.045**
	RNFL	**-**	-	-0.10	0.734
OPTIC NERVE	FSE lesion length	0.03	0.910	-0.17	0.505
	Gad lesion length	0.27	0.229	-	-
	Optic nerve area	-0.08	0.740	0.03	0.898
OPTIC RADIATIONS	Lesion load	0.09	0.696	-0.05	0.853
	FA	-0.06	0.789	0.03	0.915
OCCIPITAL CORTEX	Pericalcarine surface area	-0.11	0.479	-0.10	0.703
	Pericalcarine volume	-0.02	0.834	-0.12	0.627
	Pericalcarine cortical thickness	*0.39*	*0.074*	0.02	0.941
VEP	Amplitude	*-0.41*	*0.056*	-0.13	0.575
	Latency	0.31	0.267	-0.13	0.592
fMRI	Affected V1	*-0.40*	*0.067*	0.09	0.714
	Affected LGN	-0.23	0.298	-0.06	0.826
	Affected LOC	**-0.57**	**0.007**	0.02	0.943
	Affected cuneus	0.07	0.240	0.24	0.336
	Fellow V1	0.11	0.615	0.20	0.415
	Fellow LGN	0.08	0.725	0.06	0.818
	Fellow LOC	**-0.51**	**0.020**	-0.12	0.646
	Fellow cuneus	0.07	0.756	0.23	0.357
SEVERITY OF BASELINE VISUAL LOSS	**Baseline visual acuity**	**0.52**	**0.014**	-	-
DEMOGRAPHIC	**Age**	**-0.43**	**0.040**	-	-
	Gender	-0.10	0.653	-	-
	Side of ON	-0.30	0.163	-	-

Table 5.6 Associations between structural, electrophysiological, functional and demographic variables, and visual outcome (logMAR acuity at 12 months). Partial correlation coefficients are reported, together with the associated p-value. Significant associations are highlighted in bold and borderline results in italics. FA-fractional anisotropy, FSE-fast spin echo, Gad-gadolinium-enhanced MRI scan, LGN-lateral geniculate nuclei, LOC-lateral occipital complexes, NS-non-significant, RNFL-retinal nerve fibre layer, V1-primary visual cortex.

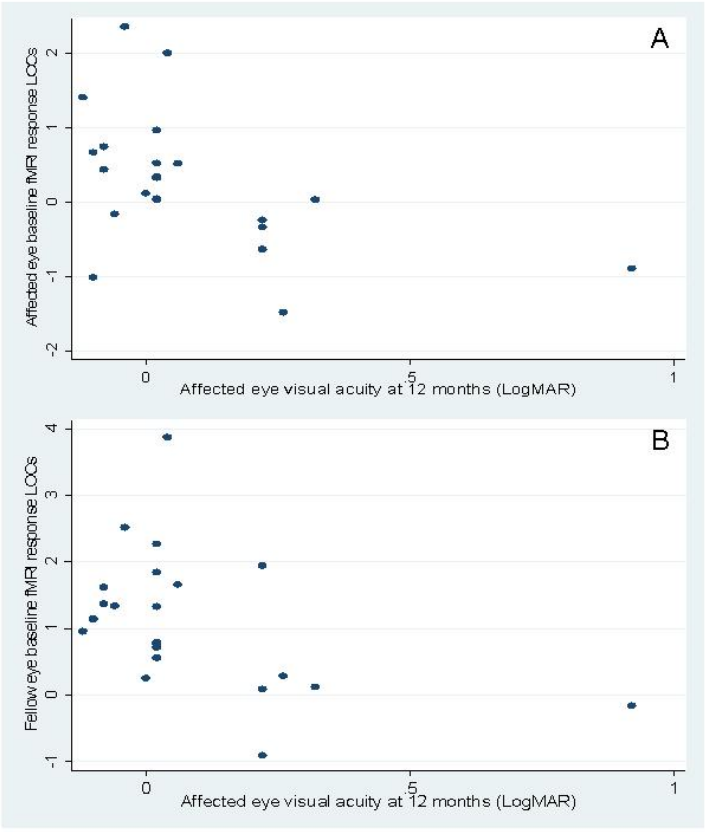

Figure 5.4 Scatter-plots of affected eye acuity at 12 months against baseline LOC fMRI response on (A) affected and (B) fellow eye stimulation. Higher logMAR scores indicate worse acuity. BOLD-blood oxygenation level dependent, LOC-lateral occipital complexes.

5.1.3.5 Relationship between baseline LOC responses and visual outcome

Figure 5.4 demonstrates increasing baseline LOC responses associated with better visual outcome. Visual recovery could be divided into a better relative outcome group (logMAR<0.2, Snellen better than 6/10), or a worse relative outcome group, on the basis of thresholding the baseline LOC activation. Baseline LOC fMRI responses were positive in the better relative outcome recovery group (mean parameter estimate 0.57 [95%CI 0.16, 0.98]), and negative in the worse relative outcome group (mean -0.59 [95%CI -1.1, -0.023], t=3.28, p=0.004). For an individual patient, a negative baseline LOC response was associated with a logMAR acuity of 0.2 or worse (Snellen >6/10), a year after ON with a sensitivity of 83% (95%CI 36%, 100%), specificity of 88% (95%CI 64%, 99%) and accuracy of 87% (95%CI 66%, 97%). Seventeen patients were in the group with relatively better outcome, whereas six were in the

other group. Visual outcome or fMRI data was unavailable for a further five patients (see section 5.1.3.2 for details).

5.1.3.6 Inter-variable structure-function relationships and visual outcome

There were complex interactions between the identified variables of interest and the other structural and functional variables, representing pathology in the acute phase (Table 5.7), and residual damage at 12 months (Table 5.8). However, the association between baseline affected eye fMRI response in the LOCs and visual outcome was independent of any demographic, structural or electrophysiological factors, from either the baseline or 12 month time-points. The relationship between baseline fellow eye fMRI response in the LOCs and visual outcome also generally maintained significance, although not as consistently as the affected eye LOC response.

Neither baseline visual acuity nor age was statistically significant in the models that adjusted for affected eye fMRI response in the LOCs, nor the models that adjusted for fellow eye responses in the LOCs. The relationship between macular volume at 12 months and visual outcome lost significance following adjustment for several of the other variables, notably baseline acuity and age.

BL INTERACTION VARIABLE	VARIABLE OF INTEREST				
		fMRI affected LOC BL regression coefficient (p value)	fMRI fellow LOC BL regression coefficient (p value)	BL acuity regression coefficient (p value)	Age regression coefficient (p value)
	OPTIC NERVE FSE lesion length	**-0.13 (0.008)** *[0.088]*	**-0.10 (0.022)** [0.198]	**0.19(0.005) [0.010]**	**-0.01 (0.046)** [0.644]
	Gad lesion length	**-0.11 (0.037)** [0.148]	**-0.09 (0.042)** [0.252]	*0.13(0.056)* [0.280]	**-0.02 (0.032)** [0.544]
	Cross-sectional area	**-0.13 (0.006)** *[0.075]*	**-0.10 (0.020)** [0.220]	**0.17(0.005) [0.010]**	*-0.01 (0.081)* [0.162]
	OPTIC RADIATIONS Lesion load	**-0.13 (0.009)** *[0.086]*	**-0.09 (0.017)** [0.204]	**0.14(0.015)** [0.233]	**-0.01 (0.046)** [0.644]
	Mean FA	**-0.12 (0.026)** [0.156]	**-0.09 (0.039)** [0.273]	**0.14(0.027)** [0.311]	*-0.01 (0.071)* [0.213]
	OCCIPITAL CORTEX Pericalcarine surf. area	**-0.13 (0.010)** *[0.080]*	**-0.08 (0.021)** [0.210]	**0.14(0.042)** [0.315]	**-0.01 (0.019)** [0.380]
	Pericalcarine volume	**-0.14 (0.006)** *[0.075]*	**-0.11 (0.013)** [0.169]	**0.14(0.042)** [0.315]	**-0.01 (0.016)** [0.336]
	Pericalcarine thickness	**-0.13 (0.002) [0.028]**	**-0.08 (0.043)** [0.215]	**0.12(0.036)** [0.324]	*-0.10 (0.059)* [0.472]
	VEP Amplitude	**-0.10 (0.046)** *[0.092]*	-0.07 (0.184) [0.184]	0.13(0.140) [0.140]	**-0.01 (0.027)** [0.704]
	Latency	**-0.06 (0.043)** [0.129]	*-0.06 (0.061)* [0.183]	*0.14(0.050)* [0.300]	**-0.01 (0.044)** [0.704]
	FMRI Affected V1	-	-	*0.12(0.098)* [0.294]	**-0.01 (0.026)** [0.494]
	Affected LGN	-	-	**0.13(0.027)** [0.311]	*-0.01 (0.056)* [0.504]
	Affected LOC	-	-	0.09(0.131) [0.262]	-0.01 (0.209) [0.209]
	Affected cuneus	-	-	**0.13(0.031)** [0.310]	*-0.01 (0.062) [0.062]*
	Fellow V1	-	-	**0.16(0.006)** [0.108]	*-0.01 (0.064)* [0.320]
	Fellow LGN	-	-	**0.14(0.015)** [0.233]	**-0.01 (0.046)** [0.644]
	Fellow LOC	-	-	*0.11(0.097)* [0.388]	*-0.01 (0.050)* [0.525]
	Fellow cuneus	-	-	**0.18(0.004)** *[0.084]*	*-0.01 (0.050)* [0.525]
	BASELINE ACUITY	*-0.09 (0.079) [0.079]*	-0.06 (0.181) [0.362]	-	*-0.01 (0.060)* [0.420]
	DEMOGRAPHIC Age	**-0.10 (0.036)** [0.180]	*-0.08 (0.052)* [0.208]	**0.12(0.019)** [0.247]	-
	Gender	**-0.12 (0.009)** *[0.086]*	**-0.12 (0.008)** [0.112]	**0.14(0.018)** [0.252]	**-0.01 (0.049)** [0.588]
	Side of ON	**-0.12 (0.021)** [0.147]	**-0.09 (0.038)** [0.304]	**0.14(0.013)** [0.221]	*-0.01 (0.068)* [0.272]

Table 5.7 (on the previous page) Structure-function interactions during the acute episode: results of multivariable regression modeling. The variables of interest associated with visual outcome (logMAR at 12 months) are listed in the columns. All baseline variables are listed in the rows. The regression coefficients are reported, together with the associated p values in parentheses, representing the significance of the association between the variable of interest with visual outcome at 12 months, *after adjusting for the interaction variable in that row.* P values uncorrected for multiple comparisons are reported in curved brackets, and following a Holm correction in square brackets. Significant results are highlighted in bold, and trends in italics. BL-baseline, FA-fractional anisotropy, Gad-gadolinium-enhanced MRI, LGN-lateral geniculate nuclei, LOC-lateral occipital complexes, V1-primary visual cortex.

12M INTERACTION VARIABLE	VARIABLE OF INTEREST					
		fMRI affected LOC BL regression cooefficient (p value)	fMRI fellow LOC BL regression coefficient (p value)	BL acuity regression coefficent (p value)	Age regression coefficent (p value)	Macular volume 12M regression coefficent (p value)
	RETINA Macular volume	**-0.14(0.039)** *[0.098]*	**-0.11(0.028)** [0.182]	0.16(0.222) [0.396]	-0.01(0.342) [0.342]	-
	RNFL thickness	**-0.16(0.016)** [0.144]	*-0.10(0.090) [0.090]*	*0.19(0.068) [1]*	-0.02(0.234) [0.468]	-
	OPTIC NERVE FSE lesion length	**-0.12(0.030)** [0.150]	**-0.13(0.007)** *[0.077]*	**0.15(0.047)** [0.799]	*-0.01(0.089)* [0.801]	**-0.85(0.001) [0.022]**
	Cross-sectional area	**-0.10(0.046) [0.046]**	**-0.10(0.026)** [0.208]	*0.12(0.087)* [1]	-0.01(0.119) [0.595]	**-0.59(0.029)** [0.551]
	OPTIC RADIATIONS Lesion load	**-0.11(0.039)** *[0.098]*	**-0.11(0.021)** [0.210]	0.11(0.105) [0.840]	*-0.01(0.079)* [0.830]	*-0.45(0.074)* [0.814]
	Mean FA	**-0.13(0.032)** [0.128]	**-0.12(0.030)** [0.150]	0.11(0.174) [0.696]	-0.02(0.114) [0.684]	*-0.46(0.086)* [0.344]
	OCCIPITAL CORTEX Pericalcarine surf. area	**-0.12(0.025)** [0.175]	**-0.10(0.031)** [0.124]	**0.13(0.045)** [0.968]	*-0.01(0.062)* [0.992]	*-0.34(0.088)* [0.675]
	Pericalcarine volume	**-0.12(0.020)** [0.160]	**-0.10(0.028)** [0.182]	**0.14(0.034)** [1]	**-0.02(0.049)** [0.882]	*-0.34(0.086)* [0.578]
	Pericalcarine thickness	**-0.10(0.028)** [0.168]	**-0.09(0.022)** [0.198]	0.10(0.102) [0.918]	*-0.02(0.077)* [0.924]	*-0.45(0.083)* [0.457]
	VEP Amplitude	**-0.16(0.007)** *[0.070]*	**-0.11(0.049)** *[0.098]*	**0.16(0.022)** [0.396]	**-0.02(0.011)** [0.209]	**-0.37(0.041)** [0.656]
	Latency	**-0.18(0.003) [0.033]**	**-0.11(0.040)** [0.120]	**0.18(0.007)** [0.133]	*-0.02(0.071)* [0.994]	**-0.38(0.031)** [0.558]
	FMRI Affected V1	-	-	0.11(0.144) [0.936]	*-0.02(0.063)* [0.945]	*-0.43(0.090)* [0.270]
	Affected LGN	-	-	0.09(0.186) [0.558]	*-0.01(0.097)* [0.776]	*-0.42(0.076)* [0.646]
	Affected LOC	-	-	0.13(0.144) [0.936]	-0.01(0.143) [0.572]	*-0.47(0.076)* [0.646]
	Affected cuneus	-	-	*0.12(0.080)* [1]	-0.01(0.111) [0.777]	*-0.44(0.083)* [0.457]
	Fellow V1	-	-	0.08(0.295) [0.295]	*-0.01(0.079)* [0.830]	**-0.56(0.046)** [0.644]
	Fellow LGN	-	-	*0.12(0.098)* [0.980]	*-0.01(0.076)* [0.988]	*-0.45(0.075)* [0.750]
	Fellow LOC	-	-	0.10(0.164) [0.820]	-0.01(0.159) [0.477]	*-0.49(0.082)* [0.574]
	Fellow cuneus	-	-	*0.13(0.070)* [1]	*-0.01(0.059)* [1]	*-0.31(0.065)* [0.780]
	BASELINE ACUITY	-	-	-	-	-0.29(0.152) [0.152]

	DEMOGRAPHIC Age	-	-	-	-	-0.29(0.109) [0.218]
	Gender	-	-	-	-	*-0.33(0.055)* [0.715]
	Side of ON	-	-	-	-	**-0.35(0.028)** [0.574]

Table 5.8 Structure-function interactions with residual damage at 12 months: results of multivariable regression modeling. The variables of interest associated with visual outcome (logMAR at 12 months) are listed in the columns. All 12 month variables are listed in the rows. The regression coefficients are reported, together with the associated p values in parentheses, representing the significance of the association between the variable of interest with visual outcome at 12 months, *after adjusting for the interaction variable in that row.* P values uncorrected for multiple comparisons are reported in curved brackets, and following a Holm correction in square brackets. Significant results are highlighted in bold, and trends in italics. BL-baseline, FA-fractional anisotropy, LGN-lateral geniculate nuclei, LOC-lateral occipital complexes, RNFL-retinal nerve fibre layer, V1-primary visual cortex, 12M-12 months.

5.1.3.7 Effect of outlier

Patient 22 had significantly worse residual visual dysfunction than the rest of the group (Table 5.1, Figure 5.4). The analyses were repeated without this subject, and all associations remained significant, except for macular volume.

5.1.4 Discussion

The most important finding from this study is the direct association between acute fMRI responses in the LOCs and visual outcome (logMAR acuity at 12 months), evident on stimulation of either eye. Visual outcome was also associated with the severity of acute visual loss, and 12 month macular volume, but not with any other markers of neuroaxonal loss in the optic nerve, demyelination, or damage to the posterior pathways. These data suggest that early adaptive neuroplasticity in the LOCs is an important determinant of visual recovery in clinically isolated ON, independent of measures of tissue damage.

5.1.4.1 Longitudinal analysis

The changes in clinical, structural and electrophysiological variables are consistent with the known pathophysiology of ON (Smith and McDonald, 1999). Acutely,

oedema, inflammation, demyelination and conduction block were evident and, as they resolved, vision improved. This is consistent with previous MRI and electrophysiological studies (Hickman et al., 2004a;Youl et al., 1991;Kupersmith et al., 2002;Hickman et al., 2004c;Frederiksen and Petrera, 1999;Jones, 1993;Brusa et al., 2001). Despite clinical recovery, there was evidence of ongoing tissue damage, such as progressive lengthening of the optic nerve lesion, which may represent secondary tract degeneration (Kapoor et al., 1998;Hickman et al., 2004c). At 12 months, VEP latencies demonstrated persistent demyelination, despite evidence for remyelination between six and 12 months, which has been seen previously, both at this time (Brusa et al., 1999) and earlier, between three and six months after the acute episode (Brusa et al., 2001). Neuroaxonal loss in the optic nerve was evident from a reduction in macular volume and RNFL thickness, in line with previous studies (Trip et al., 2005;Costello et al., 2006;Klistorner et al., 2008a), and from optic nerve atrophy, which is well recognised following ON (Hickman et al., 2001;Inglese et al., 2002;Hickman et al., 2004a).

FMRI responses in lower visual areas improved over the first three months, in parallel with vision, and consistent with an increased afferent input, as noted in previous longitudinal fMRI studies (Toosy et al., 2005;Korsholm et al., 2007). Responses in higher visual areas were more complex, with dynamic changes evident on fellow eye stimulation over time, and have not been reported previously.

5.1.4.2 Associations between visual outcome and baseline (or 12 month) variables

The strongest predictor of visual outcome was fMRI response in the LOCs, and this was evident on stimulation of either eye. The LOCs are higher order visual areas, located within the ventral processing stream, involved in identification and recognition of objects in the physical world (Eger et al., 2008). They have previously been identified as potentially important areas for neuroplasticity in ON (Toosy et al., 2005). Toosy *et al* used an indirect methodology, in a longitudinal cohort, to correlate the residual variance in clinical function with the fMRI response, in voxels throughout the whole brain, after accounting for acute optic nerve inflammation. The LOCs correlated with the residual variance in clinical function only at the baseline time-point.

A later cross-sectional study by Levin *et al* applied retinotopic mapping, and a specific LOC-localiser task, to a group of patients at differing stages of recovery, from weeks to years after acute ON. The aim was to clarify where in the visual hierarchy changes occurred. This study found that affected eye responses were smaller than fellow eye responses in lower visual areas but, in the lateral and inferior occipital gyri of the LOCs, responses were actually higher in the affected eye. All of their patients had made a good visual recovery, and no correlations with acuity were reported. They concluded that their results could be supportive of adaptive plasticity, and that higher visual areas might be robust to disruption of visual input.

A subsequent longitudinal fMRI study by Korsholm *et al* used a region-of-interest approach, similar to the one applied in this study. V1 and V2 were identified using cytoarchitectonic templates, and the LOCs were specified using spheres centred on their published landmarks. A different method was used to define the LGN. They were identified using anatomical landmarks on T1-weighted scans, and the functional data were extracted from manually drawn regions. The authors reported that in the acute stage, LOC responses in the affected eye were reduced compared with the fellow eye. Over time, this difference declined, following the pattern of V1 and V2. They reported no evidence for plasticity in the LOCs and, instead, found that in LGN the decrease in the difference between the two eyes was due not only to an increasing fMRI response from the affected eye, but also to a decreasing response from the fellow eye, which was evident between 120-180 days after the acute episode. In contrast to Levin *et al*, they concluded that fMRI activity in higher visual areas followed the same pattern as lower areas, in response to a reduced visual input. These findings are supported by the results of the present study, with regard to the LOCs, but a different pattern was evident in the cuneus, in which affected eye responses were not directly associated with vision. In addition, Korsholm *et al* hypothesised that plasticity might occur within the LGN themselves, although also considered the possibility that the changes were secondary to back-projection from cortical regions.

It appears from the present study that the LOCs play a critical role in neuroplastic responses to ON, and are not robust to disruption of afferent input. This study adds to our current knowledge, by demonstrating that reorganisation in this area appears to contribute directly towards a better visual outcome, independent of measures of tissue damage. The present study is the first to investigate neuroplasticity in the context of these complicating structure-function interactions, involving both the anterior and

posterior pathways, and the first to take into account both acute inflammation and residual tissue injury.

A reduction in macular volume (demonstrated by OCT at 12 months) is most likely to represent loss of retinal ganglion cells, secondary to axonal damage in the optic nerve (Quigley et al., 1977) (although macular volume loss is not layer-specific), and supports a role for the extent of neuroaxonal loss in determining clinical outcome. However, this study did not confirm the previously reported association between RNFL thickness and visual loss (Trip et al., 2005;Costello et al., 2006;Klistorner et al., 2008a). This may be because of differences in the study cohorts; all of the patients in the present study had clinically isolated ON, unselected for visual function. Alternatively, the lack of association could reflect type II error. There was also no association between optic nerve atrophy on MRI and visual outcome, and previous studies have reported either modest correlations between visual outcome and tissue loss in the optic nerve (Hickman et al., 2002a;Inglese et al., 2002), or none (Hickman et al., 2004a). Of the hypotheses postulated to explain this dissociation between tissue loss in the optic nerve and clinical function, there was no evidence for an impact of damage within the posterior pathways. The restricted clinical impact despite macular volume loss may represent a degree of neuroaxonal redundancy, but the relatively strong fMRI associations suggest that acute grey matter plastic changes appear to exert a greater influence.

Increasing age was also associated with a better visual outcome. This finding is somewhat surprising as, in general, increasing age is associated with a worse prognosis, for example, in studies of MS (Weinshenker et al., 1991;Confavreux and Vukusic, 2006;Debouverie et al., 2008). In MS, the worse prognosis appears to be due, in part, to a higher prevalence of secondary progression. In the ONTT, increasing age was associated with slightly worse vision, although the magnitude of the association was small and not thought to be clinically important; patients between the ages of 18 to 35 could read an average of two more letters on the 6/6 acuity line, compared with patients aged between 35 and 45 years (Beck et al., 1994). The reasons that age was associated with a better prognosis in the present study are not clear, although one could speculate that a late presentation might represent a more benign form of demyelination, which had previously remained quiescent, in this cohort sampled at a time when the disease was clinically isolated.

5.1.4.3 Relationship between baseline LOC responses and visual outcome

A negative affected eye fMRI response in the LOCs appears to be associated with a worse relative outcome, whilst a positive response is associated with a better relative outcome. This threshold effect suggests a genuine physiological role for compensatory plasticity in this cohort. A positive fMRI response may represent synaptic reorganisation or dendritic arborisation contributing to recovery. Conversely, negative responses may indicate a failure of neuroplastic mechanisms, resulting in a persistent visual deficit. In this context, fMRI deactivation might even reflect maladaptive change, and this merits further study. Acutely, a negative fMRI response in the LOCs appears to help identify individuals with a relatively worse visual prognosis, and the results reported for sensitivity, specificity and accuracy are promising from a clinical perspective, although the confidence intervals are wide, and the degree of dysfunction in the group with relatively worse visual dysfunction was variable. Further studies in larger groups of patients are required to determine whether these results are generalisable.

It is interesting that the association between visual outcome and fMRI response in the LOCs was evident on stimulation of either eye. Abnormal fellow eye responses have been reported previously, although their role in recovery was unclear. Toosy *et al* found that acute fMRI responses to fellow eye stimulation correlated with acute vision in the affected eye (Toosy et al., 2005). The findings of this study extend these results, by associating fellow eye responses with visual recovery. This might be explained through a mechanism of subclinical pathology in the fellow optic nerve. However, there was little evidence of this from the present study, as only one subject in this cohort had an asymptomatic optic nerve lesion, and there were no differences from controls in the other structural and electrophysiological measures. Therefore, these findings suggest that cortical fMRI responses are remodulated holistically, in response to pathological insult, and are detectable on visual stimulation, independent of neural conduction through the region of damage. This might indicate that stimulation of damaged axons is not necessary to trigger neuroplastic reorganisation. These observations may also be of practical use in future studies of plasticity in patients with severe visual loss, when it may be difficult to detect any fMRI response from the affected eye, due to acute conduction block.

After the acute episode, fMRI responses within the LOCs, in either the affected or fellow eye, were no longer associated with visual outcome, suggesting that the acute phase is critical in terms of brain reorganisation (Johansen-Berg, 2007).

5.1.4.4 Inter-variable structure-function relationships and visual outcome

The relationship between affected eye (and, to some degree, fellow eye) fMRI activity in the LOCs and visual outcome remained independent of measures of acute inflammation, residual demyelination and neuroaxonal loss. The severity of acute visual loss was associated with subsequent recovery, and some of the variance in visual outcome attributable to fMRI responses in the LOCs was also explained by this variable, although fMRI response remained a stronger predictor. This collinearity was not surprising, as a two-way relationship exists between visual acuity and fMRI response; on one hand a reduction in neuronal input results in a smaller fMRI response whilst, on the other hand, plastic reorganisation may influence acuity. However, the association between baseline fMRI response in the LOCs and visual recovery cannot be explained solely through a mechanism of severity of acute visual loss. This alternative mechanism should operate via the primary visual areas and when the affected eye is stimulated. However, firstly, affected eye LOC activity was a stronger predictor than the primary visual areas which were non-significant (Table 5.6). Secondly, it would be difficult to physiologically explain the significant associations between baseline *fellow* eye LOC activity and 12 month visual outcome purely on the basis of reduced visual acuity (resulting from stimulation of the affected eye only) at baseline. Thirdly, LOC fMRI activity generally maintained greater levels of significance, even after incorporating other interaction variables (for baseline and 12 months) into the model (Tables 5.7 and 5.8), whilst baseline acuity did not, implying a more critical role for LOC activity in predicting visual outcome. These results still imply, however, that higher visual areas, such as the LOCs, are not robust to disruption of visual input, a point which has been debated following contrasting results from two previous studies (Levin et al., 2006;Korsholm et al., 2007).

The relationships between visual outcome, baseline acuity, age and 12 month macular volume were more complex, and structure-function interactions were evident.

Two potential sources of error were investigated *post-hoc*. Firstly, it was determined whether the baseline fMRI responses in the LOCs were influenced by between-subject

variation in attention, potentially related to differences in baseline acuity. However, a regression analysis found no association between attention scores and baseline acuity (p=0.860). Secondly, it was considered whether it was appropriate to consider linearity for the relationship between baseline and final acuity in the multivariable regression analysis. Separate regression analyses were performed to respectively investigate three relationships between baseline and final acuity: 1) linear, 2) a combination of linear and quadratic and 3) logarithmic. The strongest association was found to be linear (p=0.031). No significant associations were found for quadratic (p=0.487) and logarithmic (p=0.142) terms. The unstandardised residuals after regression between baseline and final acuity (assuming the linear relationship) were then extracted. These residuals were, in turn, regressed with baseline LOC activation for the affected (p=0.227) and fellow (p=0.137) eye, respectively. These non-significant p values implied that there were no residual confounding factors between baseline acuity predicting final acuity that relate to LOC activation and, consequently, assuming linearity whilst controlling for baseline acuity in the multivariable regression was probably sufficient.

5.1.4.5 Methodological considerations

There are several methodological considerations for this study. Firstly is the issue of correcting for multiple comparisons. This study comprised in part hypothesis-driven aims. The key results suggesting LOC neuroplasticity are based on an *a priori* hypothesis and so, for these, multiple comparisons corrections were felt to be less essential, and the reader could place greater weight on the uncorrected p values (first two columns of Tables 5.7 and 5.8, curved brackets). Issues of multiple comparisons correction for family wise error rate (FWER) occur perennially in research. Unfortunately, there is no ideal method to adjust for them. Conventional approaches that control the FWER, such as Bonferroni, Holm and Sidak have several disadvantages (Rothman, 1990;Perneger, 1998). They are intrinsically conservative, risking an increase in type II errors, they assume that the tests are independent (which is usually not the case) and are concerned with the general null hypothesis (that all null hypotheses are true simultaneously), which is rarely of interest to researchers. In these contexts, where there is considerable biological similarity in the relationships assessed by individual tests, a biological pattern of moderately significant results (or

multiple convergent associations) is very unlikely to occur by chance, and applying a naïve FWER multiple comparisons correction may eliminate genuine associations. As an example, for the LOC analysis in Table 5.7, 28 tests were performed. Twenty three significant results (uncorrected) are tabulated, making it extremely unlikely that they have all arisen by chance. What is important in these contexts is to highlight the patterns, and to treat with great caution any moderately significant individual results which are biological isolated. Nevertheless, for the exploratory analyses in Table 5.7 and 5.8, it was important to be aware that the large number of tests performed represents a limitation of the dataset, and this potential interpretational difficulty was further addressed by applying a Holm correction. Both the uncorrected and corrected p values were reported, so that the relative statistical strength of each association was clear. It was felt that this was a sensible way to address the multiple comparisons issue.

Secondly, there were some missing data-points, which is difficult to avoid, despite making every effort, when conducting a comprehensive longitudinal study. In a minority of subjects, it was not possible to obtain all tests on the same day (Table 5.3). However, these problems were addressed during the analysis stage, by using mixed effects models, which allow for missing time-points and maximised efficient use of the available data, and by including time-to-test variables in the multivariable regression models.

Thirdly, in order to minimise scanning times, the LOCs and primary visual cortex were defined on the basis of published coordinates, rather than using a localiser task and retinotopic mapping, which better account for inter-subject variability. This approach is thus less sensitive and more prone to type II errors, but should not influence the type I error rate, so any positive results obtained may be confidently interpreted as true positives.

5.1.4.6 Conclusions

In summary, this study identified associations between fMRI activity in the LOCs during acute ON and visual outcome, which were independent of measures of optic nerve inflammation, myelination and neuroaxonal loss. These data suggest that early neuroplasticity contributes to recovery from clinically isolated ON, and helps explain the dissociation between tissue damage in the optic nerve and visual recovery,

independent of optic nerve myelination, the extent of neuroaxonal loss, or posterior pathway pathology.

SECTION 2 EXPLORING VISUAL STRUCTURE-FUNCTION RELATIONSHIPS

5.2.1 Introduction

In this section, the variables found to be associated with visual outcome, resulting from the analyses reported in section 5.1, are investigated in more detail. These were (1) affected and fellow eye fMRI responses in the LOCs at baseline, (2) visual acuity at baseline, (3) age, and (4) macular volume at 12 months. In this section, the associations between these variables and other measures of visual outcome are considered, and inter-variable relationships are investigated in greater depth. The fMRI data are also explored further, to examine changing relationships with vision in different regions of the processing hierarchy, and longitudinal changes between time-points other than baseline and 12 months. Structural and electrophysiological influences on these relationships are studied. Lastly, associations between the rates of change of the various structural, electrophysiological and fMRI variables are considered.

5.2.1.1 Associations with alternative visual outcome measures

In section 5.1, visual outcome was measured with logMAR acuity, 12 months after acute ON. The logMAR score essentially measures the function of the neural pathways arising from the macula and synapsing in primary visual cortex, in the region of the occipital poles. However, visual outcome may be measured in other ways, relating to the function of different retinal areas and specific aspects of visual processing. The relationship of each identified variable-of-interest to the following measures of visual outcome was assessed: low contrast acuity, Humphrey visual field and colour vision. The hypothesis was that there would be significant associations with each of these different aspects of visual function.

5.2.1.2 Age interactions

An association between visual outcome and age was identified in section 5.1. Therefore, the influence of age on the relationship between each of the other

variables-of-interest and visual outcome was considered. The hypothesis was that different factors might be important in determining visual recovery in patients of different ages. In particular, it was hypothesised that neuroplastic recovery mechanisms might become less efficient with increasing age.

5.2.1.3 Clinical-fMRI relationships

In section 5.1, it was seen that longitudinal changes in fMRI responses differed between lower and higher visual areas. The relationships between visual acuity and fMRI activity at different levels of the processing hierarchy were now investigated directly, by assessing cross-sectional associations at each time-point. The hypothesis was that visual acuity would be associated with the fMRI response in lower visual areas (primary visual cortex and LGN) during the acute phase. Elucidating the relationship between visual acuity and higher visual areas was of interest, in order to determine how the LOCs and cuneus responded to a disruption of visual input at different stages of recovery.

5.2.1.4 Changing longitudinal visual structure-function relationships

The changing relationships between fMRI activity and visual outcome over time were explored using a longitudinal modeling approach, incorporating lagged variables, to allow investigation of associations between visual function, fMRI activity and structural pathology, later in the recovery process. The hypothesis was that fMRI responses in different regions might be associated with visual outcome at different times, reflecting a dynamic reorganisation process, which might reflect changing responses to structural and electrophysiological factors.

5.2.1.5 Modeling associations between changes

Lastly, the relationships between the rate of change of visual acuity and the rates of change of the various structural, electrophysiological and fMRI variables were investigated. The hypothesis was that changes in measures of structural damage and fMRI activity would be associated with changes in visual function, demonstrating

interplay between pathology, its clinical consequences, and physiological responses, over time.

5.2.2 Methods

The participants and data acquisition were identical to section 5.1. The additional visual testing protocol is described here.

5.2.2.1 Visual assessment

Low contrast acuity was assessed using Sloan charts (Ferris, III et al., 1982), of 25%, 5% and 1.25% contrast, compared with the standard 100% ETDRS chart. When no letters could be correctly identified, a score of 1.7 was assigned (Optic Neuritis Study Group, 1991). The scoring system was identical to standard logMAR scoring, with higher scores indicating worse vision.

Visual fields were assessed using the 30-2 programme on the Humphrey automated field analyser (Allergan-Humphrey Inc., San Leandro, Ca., USA). The global visual field mean deviation (HMD) was calculated, which incorporates both central and peripheral visual function into an error score. More negative error scores indicate worse vision.

Colour vision was measured using the Farnsworth-Munsell 100-hue test (Farnsworth, 1943), and scored as the square root of the error score. If the visual acuity was too poor to attempt the test, an error score of 36.6 was assigned (Optic Neuritis Study Group, 1991). Higher error scores indicate worse vision.

5.2.2.2 Statistical analysis

5.2.2.2.1 Associations with alternative visual outcome measures

The variables associated with logMAR at 12 months, reported in section 5.1 (i.e. affected and fellow eye fMRI responses in the LOCs at baseline, visual function at baseline, age and macular volume at 12 months), were investigated. The association of each of these variables with the following measures of visual outcome was investigated: Sloan charts (25%, 5%, and 1.25%, to assess associations with progressively lower contrast acuity), Humphrey mean deviation score (to assess

associations with a measure incorporating peripheral vision) and Farnsworth-Munsell root error score (to assess colour vision). Separate multivariable regression models were specified, in which the score using each of these measures, at 12 months, was entered instead of logMAR as the dependent variable. Baseline LOC fMRI responses for the affected and fellow eye, baseline acuity, age and 12 month macular volume were entered, in turn, as independent variables. Visual function in the fellow eye, and the number of days to assessment, were entered as additional independent variables, to adjust for normal inter-individual variability, and the stage of evolution of pathology.

Correlations between logMAR and each of the alternative visual measures were assessed using the Pearson test, at the baseline and 12 month time-points.

5.2.2.2.2 Age interactions

The variables associated with logMAR at 12 months, and reported in section 5.1 (i.e. affected and fellow eye fMRI responses in the LOCs at baseline, visual function at baseline and macular volume at 12 months), were investigated. The relationship of each of these variables with age was investigated, by adding age, and an age interaction term, to the multivariable regression models. The interaction term was generated by multiplying age by each variable-of-interest. Models were specified separately with logMAR at 12 months always the dependent variable. Each of the following was entered, in turn, as an independent variable: affected eye fMRI response in the LOCs, fellow eye fMRI response in the LOCs, baseline acuity and macular volume. Age and the interaction term between each variable and age were added as independent variables to each model. Fellow eye acuity and the number of days to assessment were always entered as additional independent variables.

5.2.2.2.3 Clinical-fMRI relationships

The relationship between vision and each of the fMRI variables (i.e. affected and fellow eye responses in V1, LGN, LOCs and the cuneus) *at the same point in time* was investigated, for each time-point, in turn.

Separate regression models were specified. The logMAR score in the patients' clinically affected eye was the dependent variable, and fMRI activity *at the same time-point* was entered as the independent variable.

5.2.2.2.4 Changing longitudinal visual structure-function relationships

A longitudinal modeling approach was used to investigate changes in the relationship between vision and each of the fMRI variables (i.e affected and fellow eye responses in V1, LGN, LOCs and the cuneus) over time, and how this relationship was influenced by longitudinal changes in structural and electrophysiological measures.

Lagged fMRI variables were generated from the fMRI data for each region-of-interest, to facilitate investigation of associations between variables at different time-points. A lagged variable describes data derived from a given time-point, in a longitudinal dataset, which is referred to a preceding time-point, either the previous one (lag 1 model), or the one before that (lag 2 model). The advantage of this approach is that all available data is included in a single model, for each variable that is explored, permitting the assessment of associations between variables at different times. For example, using a single lag 1 model, it is possible to determine whether fMRI activity in a given region at baseline is associated with visual function at three months, whether fMRI at three months is associated with vision at six months, and whether fMRI activity at six months is associated with vision at 12 months.

It is not possible to generate a lagged variable if the preceding time-point is missing. Two patients had a missing intermediate time-point (patient 25 at three months, and patient 8 at six months). Therefore, in these two subjects, the other intermediate time-point was omitted from the analysis (i.e. six months and three months respectively), in order to be consistent with the lagged variable definition.

Each lagged variable was then entered into a separate linear mixed effects regression model, which investigate within-subject changes over time. The number of days between symptom onset and fMRI assessment was always entered as a covariate. The first model (lag 1) assessed associations between the baseline fMRI response and vision at three months. Linear combinations of the interactions between each fMRI variable and each time-point were derived from this model, which permitted assessment of associations between three month fMRI and six month acuity, and six month fMRI and 12 month acuity. The second model (lag 2) assessed for any associations between baseline fMRI and six month acuity, and a linear combination assessed for associations between the three and 12 month time-points.

For any fMRI variables resulting in significant associations with vision, additional models were specified. These were identical to the models described in the preceding paragraph, except that each model now also included each of the structural and

electrophysiological variables (i.e. optic nerve FSE lesion length, gadolinium-enhancing lesion length, optic nerve area ratio, optic radiation lesion load and FA, pericalcarine cortical surface area, volume and thickness, VEP amplitude and latency), in turn, lagged to correspond to the same time-point as the fMRI variable. This permitted investigation of the influence of concomitant structural and electrophysiological factors on the relationship between fMRI activity and visual outcome, between time-points other than baseline and 12 months.

5.2.2.2.5 Modeling associations between changes

Multivariable regression models were used to investigate associations between the *change* in vision between baseline and 12 months and the *change* in each of the structural, electrophysiological and fMRI variables (i.e. optic nerve FSE lesion length, gadolinium-enhancing lesion length, optic nerve area ratio, optic radiation lesion load and FA, pericalcarine cortical surface area, volume and thickness, VEP amplitude and latency, affected and fellow fMRI responses in primary visual cortex, LGN, LOCs and the cuneus).

Firstly, change variables were generated for each structural, electrophysiological and fMRI parameter, in each subject, by subtracting the baseline data from the 12 month data. Each of these change variables was then entered, in turn, as an independent variable in a multivariable model, in which logMAR at 12 months was always the dependent variable. Fellow eye logMAR, the number of days from symptom onset to assessment and logMAR at baseline in the affected eye were always entered as additional independent variables. The inclusion of the affected eye baseline logMAR score as an independent variable had the effect of testing associations with the change in vision over 12 months, rather than the visual outcome *per se*.

5.2.3 Results

5.2.3.1 Associations with alternative visual outcome measures

These data are summarised in Table 5.9.

		12M Sloan 25%	12M Sloan 5%	12M Sloan 1.25%	12M Humphrey MD	12M Colour vision
BL fMRI LOC affected	r	**-0.56**	**-0.55**	**-0.59**	**0.48**	*-0.41*
	p	**0.008**	**0.009**	**0.005**	**0.028**	*0.063*
BL fMRI LOC fellow	r	**-0.53**	**-0.52**	**-0.60**	0.35	-0.25
	p	**0.013**	**0.016**	**0.004**	0.118	0.284
BL visual score	r	**0.58**	**0.50**	0.17	*0.41*	**0.45**
	p	**0.005**	**0.017**	0.455	*0.055*	**0.036**
Age	r	**-0.50**	**-0.42**	**-0.50**	0.30	-0.18
	p	**0.015**	**0.048**	**0.016**	0.162	0.423
12M macular volume	r	*-0.47*	-0.41	-0.14	**0.55**	-0.43
	p	*0.076*	0.129	0.609	**0.035**	0.108

Table 5.9 Associations between variables-of-interest and measures of visual outcome other than logMAR. For each association, the partial correlation coefficient, r, is reported, together with the associated p value. Significant associations are highlighted in bold and borderline associations in italics. More positive Sloan and colour vision scores are associated with worse visual function. More negative Humphrey scores are associated with worse visual function. BL-baseline, LOC-lateral occipital complexes, MD-mean deviation.

The variables associated with logMAR acuity were generally also correlated with the low contrast acuity outcome measures. In contrast, associations were not always seen with the Humphrey score, although correlations were evident for the affected eye fMRI response in the LOCs at baseline, and macular volume at 12 months. There was a significant association between colour vision at baseline and 12 months, and borderline significance for an association between the affected eye fMRI response in the LOCs at baseline and colour vision at 12 months. The direction of the associations was the same for all significant associations: a better visual outcome was associated with greater fMRI activity, better vision at baseline, increasing age and larger macular volume.

In general, the visual measures were highly correlated with logMAR acuity. The correlation between logMAR and 1.25% Sloan low contrast acuity (at baseline), and

logMAR and colour vision (at 12 months) were less strong, and were of borderline significance. These data are summarised in Table 5.10.

Visual measure	BASELINE		12 MONTHS	
	Correlation coefficient (r)	p value	Correlation coefficient (r)	p value
Sloan 25%	**0.98**	**<0.001**	**0.96**	**<0.001**
Sloan 5%	**0.78**	**<0.001**	**0.85**	**<0.001**
Sloan 1.25%	*0.33*	*0.085*	**0.73**	**<0.001**
Humphrey MD	**-0.80**	**<0.001**	**-0.70**	**<0.001**
Colour vision	**0.93**	**<0.001**	*0.38*	*0.065*

Table 5.10 Correlations between alternative measures of visual function and logMAR. Significant results are highlighted in bold and borderline significance is indicated by italics. MD-mean deviation.

5.2.3.2 Age interactions

For the affected eye fMRI response in the LOCs, the age interaction term was significant (p=0.013), with the direction of the association indicating that the fMRI response was more strongly associated with visual outcome in younger patients. For a patient of mean age in the cohort (32 years), logMAR improved by 0.12 (6 letters) per unit increase in fMRI response (p=0.006). For a patient age 26 (lower quartile), the improvement was 0.22 (11 letters, p=0.001) for the same increase in fMRI response, whereas for a patient age 37 (upper quartile), the improvement was just 0.03 and non-significant (1-2 letters, p=0.551).

For the fellow eye fMRI response, the interaction term was not significant, indicating that there was no influence of age on the relationship between fMRI and visual outcome.

Baseline acuity was more strongly associated with outcome in younger patients (p=0.035). For a patient age 32, logMAR at 12 months improved by 0.07 (3-4 letters) for each 0.1 (5 letter) improvement in baseline acuity (p=0.014). For a patient age 26, the improvement was 0.08 at 12 months (4 letters, p=0.016) for the same improvement in baseline vision. For a patient of age 37, the improvement at 12 months was 0.06 (3 letters, p=0.012) per 5 letter improvement in baseline acuity.

Macular volume was more strongly associated with outcome in younger patients (p=0.016). For a patient age 32, logMAR improved by 0.23 (11-12 letters) per 0.1mm^3 increase in macular volume (p=0.010). For a patient age 26, the improvement was 0.27 (13-14 letters, p=0.009), whereas for a patient age 37, the improvement was 0.20 (10 letters, p=0.008).

5.2.3.3 Clinical-fMRI relationships

Associations between vision and fMRI responses *at the same time-point* were only found at baseline. These data are summarised in Table 5.11. Patients demonstrated associations in several areas between worse vision and a reduction in the fMRI response. In lower visual areas, associations were seen only on stimulating the affected eye. There was a strong correlation between vision and the fMRI response in primary visual cortex, and a weaker association within the LGN. Responses in higher visual areas appeared more complex. Strong associations between vision and fMRI activity were seen in the LOCs, and were evident on stimulation of either eye. In the cuneus, there was a borderline association, which was only evident when stimulating the fellow eye.

FMRI region-of-interest	Correlation coefficient (r)	p value
Affected eye: V1	**-0.65**	**<0.001**
Aff. LGN	*-0.33*	*0.085*
Aff. LOC	**-0.52**	**0.005**
Aff. cuneus	-0.28	0.154
Fellow eye: V1	-0.31	0.104
Fell. LGN	0.00	1.000
Fell. LOC	**-0.50**	**0.008**
Fell. cuneus	*-0.36*	*0.057*

Table 5.11 Associations between visual acuity and fMRI responses in the affected eye, in patients, at baseline. Significant associations are highlighted in bold and borderline associations in italics.

5.2.3.4 Changing longitudinal visual structure-function relationships

5.2.3.4.1 Lag 1 models

These models revealed that a greater baseline fMRI response in the LOCs was associated with better visual function at three months, on stimulation of the affected eye. There were no associations between fMRI activity in this region after baseline and visual outcome. None of the other fMRI variables were significantly associated with visual function at any of the other time-points, although there was borderline significance for an association between greater activity in the affected LGN at six months, and better visual acuity at 12 months. These data are summarised in Table 5.12.

FMRI variable	BL to 3M		3M to 6M		6M to 12M	
	coeff	p value	coeff	p value	coeff	p value
Affected V1	-0.059	NS	-0.019	NS	0.022	NS
Affected LGN	-0.161	NS	-0.198	NS	*-0.070*	*0.073*
Affected LOC	**-0.100**	**0.026**	0.027	NS	0.036	NS
Affected cuneus	-0.005	NS	0.029	NS	0.012	NS
Fellow V1	0.002	NS	0.001	NS	0.040	NS
Fellow LGN	0.061	NS	-0.025	NS	0.071	NS
Fellow LOC	-0.057	NS	-0.045	NS	0.021	NS
Fellow cuneus	-0.005	NS	0.029	NS	0.012	NS

Table 5.12 Results of the lag 1 models. The regression coefficients are reported, which summarise the association between each fMRI variable and vision in the affected eye at the subsequent time-point. Significant results are highlighted in bold and borderline results in italics, together with the associated p value. P values >0.1 are reported non-significant (NS). BL-borderline, coeff.-regression coefficient, LGN-lateral geniculate nuclei, LOC-lateral occipital complexes, M-months, V1-primary visual cortex.

5.2.3.4.2 Lag 2 models

There was an association between a greater affected eye fMRI response in the LGN at three months and worse vision at 12 months. There was borderline significance for an association between a greater baseline fMRI response in the LOCs and visual acuity at six months. These data are summarised in Table 5.13.

FMRI variable	BL to 6M		3M to 12M	
	coeff	p value	coeff	p value
Affected V1	-0.018	NS	0.019	NS
Affected LGN	0.024	NS	**0.127**	**0.026**
Affected LOC	*-0.040*	*0.094*	-0.015	NS
Affected cuneus	0.021	NS	-0.028	NS
Fellow V1	-0.012	NS	0.017	NS
Fellow LGN	-0.023	NS	0.018	NS
Fellow LOC	-0.032	NS	0.009	NS
Fellow cuneus	-0.009	NS	*-0.035*	*0.062*

Table 5.13 Results of the lag 2 models. The regression coefficients are reported, which summarise the association between each fMRI variable and vision in the affected eye two time-points later. Significant results are highlighted in bold and borderline results in italics, together with the associated p value. P values >0.1 are reported non-significant (NS). BL-borderline, coeff.-regression coefficient, LGN-lateral geniculate nuclei, LOC-lateral occipital complexes, M-months, V1-primary visual cortex.

5.2.3.4.3 Structural influences

The influence of structural variables was investigated on the significant associations between fMRI and vision in the LOCs between baseline and three months (Table 5.14), and in the LGN between three and 12 months (Table 5.15).

	Structural variable added to model	Significance of the association between BL fMRI LOCs and 3M logMAR	
		P value (fMRI)	P value (structural)
OPTIC NERVE	FSE lesion length	**0.026**	0.771
	Gad lesion length	*0.077*	0.310
	Area	**0.025**	0.754
OPTIC RADIATIONS	Lesion load	**0.028**	0.957
	Mean FA	*0.088*	0.421
OCCIPITAL CORTEX	Surface area	**0.045**	0.055
	Volume	**0.035**	0.160
	Thickness	**0.031**	0.779
VEP	Amplitude	*0.059*	0.018
	Latency	**0.004**	0.889

Table 5.14 Structure-function interactions: the influence of structural variables on the relationship between fMRI response in the LOCs at baseline and logMAR at three months. The first column of p values indicates the significance of the association between fMRI in the LOCs at baseline and visual outcome at three months, following adjustment for each structural variable, when combined in a lagged multivariable regression model. The second column of p values indicates the significance of each structural variable in that model. The models in which fMRI in the LOCs retained significance are highlighted in bold font, and those in which borderline significance was retained are highlighted in italics. BL-baseline, FA- fractional anisotropy, FSE-fast spin echo, Gad-post gadolinium-enhanced MRI, LOCs-lateral occipital complexes, M-months, VEP-visual evoked potential.

The associations between fMRI response in the LOCs and vision retained significance or borderline significance, on adding each of the structural variables to the model.

	Structural variable added to model	Significance of association between 3M fMRI LGN and 12M logMAR	
		P value (fMRI)	P value (structural)
OPTIC NERVE	FSE lesion length	*0.093*	0.525
	Gad lesion length	**0.041**	0.307
	Area	**0.024**	0.274
OPTIC RADIATIONS	Lesion load	**0.024**	0.337
	Mean FA	**0.045**	0.931
OCCIPITAL CORTEX	Surface area	**0.021**	0.288
	Volume	**0.022**	0.314
	Thickness	**0.033**	0.609
VEP	Amplitude	**0.006**	0.122
	Latency	0.359	0.173

Table 5.15 Structure-function interactions: the influence of structural variables on the relationship between fMRI response in the LGN at three months and logMAR at 12 months. The first column of p values indicates the significance of the association between fMRI in the LGN at three months and visual outcome at 12 months, following adjustment for each structural variable, when combined in a lagged multivariable regression model. The second column of p values indicates the significance of each structural variable in that model. The models in which fMRI in the LOCs retained significance are highlighted in bold font, and those in which borderline significance was retained are highlighted in italics. FA- fractional anisotropy, FSE-fast spin echo, Gad-post gadolinium-enhanced MRI, LGN-lateral geniculate nuclei, M-months, VEP-visual evoked potential.

The associations in the affected LGN retained significance, or borderline significance, except when VEP latency was added to the model.

5.2.3.5 Modeling associations between changes

A significant association was found between worse vision at 12 months, after adjusting for acuity at baseline, and a greater change in optic nerve area ratio (regression coefficient 0.47 [95%CI 0.28, 0.91], p=0.039).

There was also an association between better vision at 12 months, after adjusting for acuity at baseline, and a smaller change in fMRI activity in the LOCs, on stimulation of the affected eye (regression coefficient 0.10 [95%CI 0.02, 0.19], p=0.025).
No other significant associations were found.

5.2.4 Discussion

The results of these more detailed analyses extend the findings described in Section 1 of this chapter, and provide more insights into the complex structure-function interactions which occur at different times following recovery from ON.

5.2.4.1 Associations with alternative visual outcome measures

There were significant associations between the affected eye fMRI response in the LOCs and visual outcome, measured using low contrast acuity and Humphrey scores, and borderline significance for an association with colour vision. Although this suggested that neuroplastic mechanisms, evident on stimulation of the affected eye, were important for recovery of all aspects of vision, and not only central acuity, the interpretation was complicated by the fMRI results following fellow eye stimulation. Here, there were associations with low contrast acuity, but not with Humphrey scores, or colour vision. This was also the case for several of the other variables; generally correlations were present with low contrast acuity scores, but there were fewer associations with the other outcome measures, especially colour vision. This suggests that the influence of different factors involved in recovery differs, depending on the modality of vision. The reasons for this are not clear from this study, but clinically important dissociation in recovery of the various aspects of visual function does occur following ON (Optic Neuritis Study Group, 1991;Frederiksen et al., 1991;Cleary et al., 1997). For example, deficits of low contrast acuity or colour vision may remain, despite a good recovery of central acuity (Beck and Cleary, 1993;Optic Neuritis Study Group, 1997b;Frederiksen et al., 1997;Beck et al., 2004a;Optic Neuritis Study Group, 2008a). Previous fMRI studies in ON have generally investigated clinical-fMRI associations using measures of central acuity at standard contrast (Russ et al., 2002;Langkilde et al., 2002), measures of central and peripheral vision, such as Humphrey field mean deviation (Langkilde et al., 2002;Korsholm et al., 2008), or a

composite measure of the two (Toosy et al., 2005). One study found an association between fMRI activation and low contrast acuity, using a different measurement technique, Arden gratings (Langkilde et al., 2002). The finding of associations between fMRI activation and colour vision in ON is novel.

In general, the visual measures were highly correlated, which was not surprising, as an acute insult to the optic nerve will typically affect all modalities of vision. An exception to this was very low contrast acuity at baseline, which was not correlated with logMAR. This may be explained through a greater sensitivity of the Sloan 1.25% chart to detect subtle abnormalities in patients with relatively mild visual loss, who may have had preserved logMAR acuity. The dissociation between logMAR and colour vision at 12 months may be explained by residual deficits of colour vision, in patients who had recovered central acuity.

5.2.4.2 Age interactions

The interactions with age were interesting. In particular, the stronger association between fMRI activity in the LOCs and visual outcome in younger patients suggests that compensatory plastic processes become less important with increasing age. The associations between outcome, the severity of initial visual loss and macular volume were also stronger in younger people. It was seen in section 5.1 that, overall, older patients had a better visual outcome, and this must reflect interplay between these contrasting influences. It could be that the stronger association between initial visual loss and outcome in younger people reflects a more aggressive demyelinating process, resulting in more axonal damage (and hence a stronger correlation between visual outcome and macular volume), and therefore more dependence on neuroplastic compensatory mechanisms, which might also be more effective.

5.2.4.3 Clinical-fMRI relationships at baseline

Associations between visual acuity and the fMRI response from the affected eye, at the same time-point, were only evident at baseline. During the acute episode of ON, worse vision was associated with a reduction in the fMRI response in lower visual areas (LGN and primary visual cortex). The associations with responses in higher visual areas were more complex. In the LOCs of the ventral stream, worse vision in

the affected eye was associated with a reduction in the fMRI response from both the affected and fellow eyes. In contrast, in the cuneus there was only an association between worse vision in the affected eye and a reduction in the fMRI response from the fellow eye. Therefore, at lower levels of the processing hierarchy, there were direct relationships between afferent input and the resulting BOLD response. However, at higher levels of the visual hierarchy, processing appears to become more holistic, the input-response relationship becomes more indirect, and may be mediated through the intact fellow eye pathways.

5.2.4.4 Changing longitudinal visual structure-function relationships

The lagged variable analysis identified an association between baseline fMRI activity in the LOCs and visual outcome at three months. There was also a borderline association with vision at six months. This showed that baseline fMRI activity was also associated with early visual outcomes, and is consistent with the temporal course of clinical recovery in ON, much of which occurs in the first few months following the acute episode. The fMRI response in the LOCs after the baseline time-point was not associated with visual outcomes, suggesting that clinically relevant neuroplasticity in this region occurs during the acute phase.

An association with visual outcome at 12 months was found for fMRI activity in the LGN at three months. The direction of the association indicated that greater activity was associated with a worse outcome. This result is surprising, as fMRI activity in the LGN generally increased in parallel with improvements in vision. The possibility of a type I error should be considered. An alternative explanation is that this association may reflect decompensation in patients who fail to recover. An increase in fMRI activity in the LGN at three months in patients who are failing to recover might reflect unsuccessful attempts at a secondary reorganisation strategy, either occurring primarily in this region, or relating to backprojection from connected cortical areas.

In general, the associations between fMRI response in the LOCs and vision were relatively independent of structural influences. The association between LGN activity and vision was confounded by VEP latency, which did not itself contribute to the model. This suggested that there was some collinearity between the two variables and, therefore, the association between LGN activity at three months and vision after a year might be partly explained by changes in myelination. For example, at three

months, a more prolonged VEP latency resulting from demyelination in the optic nerve delaying conduction to the LGN might be associated with changes in the profile of the BOLD response in the LGN at three months, and also with vision at 12 months.

5.2.4.5 Visual improvement, optic atrophy and early neuroplasticity in the LOCs

The associations between the change variables were complex. The correlation between a progressive decrease in optic nerve area and relatively worse vision at 12 months, after adjusting for vision at baseline, could represent either more severe acute oedema, more marked axonal loss at 12 months, or a combination of both. A more severely swollen optic nerve has been associated with worse acute visual loss in ON, but not with visual outcome (Hickman et al., 2004a). Subsequent optic atrophy has been associated with visual function, but the correlations have been relatively modest (Hickman et al., 2002a;Inglese et al., 2002), and some investigators have found no association (Hickman et al., 2004a). The results of the present study may reflect a contribution of axonal loss to residual dysfunction, but it appears from section 5.1 that this relationship is complicated by other factors.

The association of a relatively smaller increase in affected eye fMRI response in the LOCs and a greater improvement in vision could represent either a relatively large response at baseline (probably, at least in part, through neuroplastic reorganisation activity), or a smaller response at 12 months. These associations have not been previously investigated directly in ON, but the results of section 5.1 suggest that the magnitude of the baseline response is of more importance, in terms of associations with visual improvement. In addition, no other studies have found reduced affected eye fMRI responses in the LOCs at 12 months; one found no difference between the affected and fellow eyes (Korsholm et al., 2007), and one even found a greater response on stimulation of the affected eye (Levin et al., 2006). Another study did not find any clinical-fMRI correlations in the LOCs at 12 months (Toosy et al., 2005). Therefore, the results of the present analysis appear likely to reflect complex associations between changing vision, resolving oedema, progressive axonal loss in the optic nerve and early neuroplastic reorganisation activity in the LOCs, which subsequently becomes less evident over time.

5.2.4.6 Conclusions

In summary, this study found that the affected eye fMRI responses in the LOCs at baseline remained associated with visual outcome measures, reflecting low contrast acuity, visual fields and colour vision. However, there was some dissociation for some of the other variables which had correlated with visual outcome when it was measured using logMAR.

There were complex interactions between visual outcome, age and the other variables of interest: fMRI responses in the LOCs, baseline visual function and macular volume. In particular, compensatory neuroplastic processes appeared to become less important in determining visual outcome in older people.

In lower visual areas, there were direct associations between visual loss during the acute episode and the affected eye fMRI response at that time. Associations in higher visual areas were more complex and involved the fellow eye. This suggested that responses to a reduction in afferent input differed in hierarchical visual processing areas, but that the higher areas were not robust to disrupted input.

Early neuroplastic responses relevant to visual outcome at all subsequent time-points were seen in the LOCs. At later time-points, no clinically relevant changes were found in this region. Complex interactions between vision, electrophysiological measures and fMRI activity were found in the LGN.

There were associations between changes in vision, changes in the fMRI response in the LOCs, and changes in optic nerve area, reflecting acute oedema and residual atrophy. These associations exemplify the dynamic longitudinal interactions between clinical symptoms, cortical responses and ongoing tissue damage in the optic nerve. Tissue damage following ON will be considered in more general terms in the next section.

SECTION 3 TISSUE DAMAGE IN THE VISUAL PATHWAY AND DEVELOPMENT OF MULTIPLE SCLEROSIS

5.3.1 Introduction

In the first two sections of this chapter, visual outcome following ON was considered. In this section, the focus will shift to the association between damage detected along the optic pathway and the development of MS in the year following the acute episode.

In section 5.1, it was seen that progressive tissue loss occurred in the optic nerve following ON. In addition, there was evidence of retrograde neuroaxonal degeneration, with loss of retinal ganglion cells and a reduction in the thickness of the RNFL, as measured by OCT. Lesions accumulated in the optic radiations over time, although there was no generalised decrease in the integrity of the posterior pathways. A reduction in the surface area and volume of the pericalcarine cortex was evident at the time of presentation with acute ON (Chapter 4), but no longitudinal changes in either pericalcarine or whole brain grey matter volume ensued in the following year (section 5.1). Therefore, it appeared that optic nerve inflammatory damage had resulted in secondary retrograde degeneration in the anterior pathway, but the effects on the posterior pathway were less clear. In particular, pericalcarine atrophy was evident very early, and in the absence of evidence for trans-synaptic degeneration in the optic radiations.

In this section, the reasons underlying this early pericalcarine cortical atrophy are considered in more detail. The main hypothesis, that it may represent a susceptibility of the visual system to damage from demyelinating disease, was discussed in Chapter 4. Potential mechanisms of this damage are now investigated. One hypothesis is that tract-specific visual cortical damage could occur, secondary to local pathology in other regions of the visual pathways. An alternate hypothesis is that damage is mediated through a more generalised neurodegenerative process. Similarly, tissue damage in other regions of the visual pathway could be secondary either to local or generalised disease effects.

In order to determine the contribution of local pathology to tract degeneration, associations were investigated between optic nerve atrophy and tissue damage in the visual pathways, both anterior and posterior to the site of primary insult. Finding associations between local measures of damage in different parts of the visual system

would suggest tract-specific secondary degeneration. In order to determine the role of generalised pathology, associations were investigated between measures of tissue loss in the visual system and the development of MS over the subsequent year.

5.3.2 Methods

The participants and data acquisition were identical to section 5.1.

5.3.2.1 Associations between areas of damage within the visual pathway

The influence of optic atrophy on the retina, optic radiations and pericalcarine cortex was assessed, by investigating associations between optic nerve area and retinal OCT measures at 12 months (to assess retrograde degeneration in the anterior pathway), and between optic nerve area and MRI measures of the integrity of the optic radiations and the surface area, volume and thickness of the pericalcarine cortex (to assess trans-synaptic degeneration in the posterior visual system). Multivariable regression models were specified, with optic nerve area ratio as the dependent variable. The following variables were each entered, in turn, as the independent variable: macular volume, RNFL, optic radiation FA, pericalcarine surface area, volume and thickness. For the OCT measures, the fellow eye parameter was entered to adjust for normal inter-individual variability (Alamouti and Funk, 2003).
The influence of damage in the optic radiations on the pericalcarine cortical measures was assessed, by investigating associations between optic radiation lesion load and FA with pericalcarine surface area, volume and thickness, at baseline and 12 months. Multivariable regression models were specified with each pericalcarine cortical measure, in turn, as the dependent variable. Each of the optic radiation variables was entered, in turn, as the independent variable.
All associations were adjusted for age and gender.

5.3.2.2 Development of MS

The percentage of patients who were diagnosed with MS over the year of the study was calculated, using clinical (Poser et al., 1983) and MRI criteria (McDonald et al., 2001;Polman et al., 2005). In addition, the percentage of patients with brain lesions at

each time-point was reported, and whether they fulfilled the MRI criteria for dissemination in space or time (Barkhof et al., 1997;Tintore et al., 2000), by the 12 month time-point.

5.3.2.3 Associations between tissue damage and MS

Associations between the development of MS and markers of tissue damage in the retina, optic nerve, optic radiations, pericalcarine and whole brain grey matter were investigated. A multivariable regression approach was used, with clinical MS status at the end of the study as a binary dependent variable (0-no MS, 1-clinical diagnosis of MS). Separate models were specified, entering data for each of the following as an independent variable: optic nerve lesion length, optic nerve area ratio, optic radiation lesion load and FA, pericalcarine cortical surface area, volume and thickness, and whole brain grey matter fraction. Models were specified separately for each of these variables at the baseline time-point, 12 month time-point, and for the change between baseline and 12 months. For gadolinium-enhanced lesion length, models were specified for the only available time-point at baseline. For the OCT measures (macular volume and RNFL thickness), models were specified at 12 months. Associations were adjusted for age and gender.

5.3.3 Results

5.3.3.1 Associations between areas of damage within the visual pathway

There were no associations between optic nerve atrophy and any of the retinal, optic radiation or pericalcarine cortical measures at 12 months.
There were no associations between the pericalcarine MRI measures and any of the optic radiation variables, either at baseline or 12 months.

5.3.3.2 Development of MS

Over the course of the study, 43% of patients developed MS, diagnosed on clinical criteria, and all of these patients also fulfilled the MRI criteria for MS.

An additional 32% of patients had T2 lesions suggestive of demyelination on their MRI scan by 12 months (examples shown in Figures 5.5 and 5.6), which were insufficient to fulfill the McDonald criteria in all cases. Of these nine patients, three fulfilled the criteria for dissemination in space only, four dissemination in time only, and two neither criterion. One patient had a normal brain MRI at baseline but subsequently developed lesions at 12 months (Figure 5.5). This was the only patient with a normal baseline MRI scan to subsequently develop lesions over the course of the year (classified as dissemination in time only).

The remaining 25% of patients had a normal brain MRI both at baseline and at last contact, one of whom was lost to follow-up after the baseline time-point.

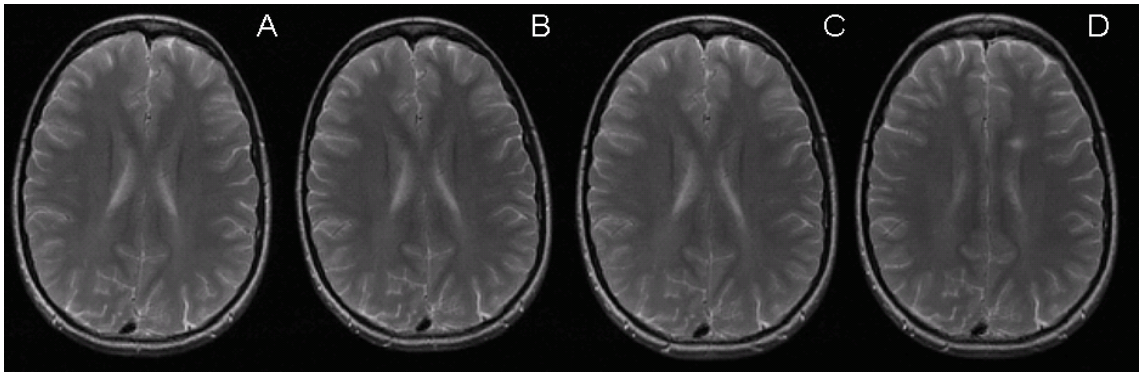

Figure 5.5 Serial MRI scans from a patient in the study, demonstrating the appearance of a first lesion suggestive of demyelination at 12 months. Axial slices are shown from the (A) baseline, (B) three month, (C) six month, and (D) 12 month time-points. The scans are normal from baseline to six months but, at 12 months, a left sided frontal periventricular lesion is seen.

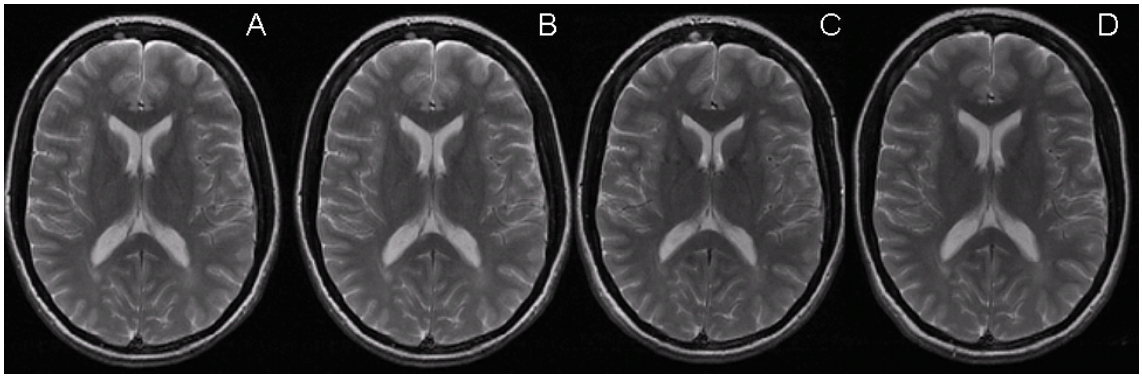

Figure 5.6 Serial MRI scans from a different patient, demonstrating lesions at baseline and new lesions developing over the course of the study. Axial slices are shown from the (A) baseline, (B) three month, (C) six month and (D) 12 month time-points. At baseline, periventricular lesions are seen on the right, adjacent to the frontal and occipital horns. In addition, there is ill-defined signal change adjacent to the occipital horn of the left lateral ventricle. A more peripheral left frontal lesion is seen. New lesions are seen at six months, with the appearance of a right frontal juxtacortical lesion. and a new discrete lesion adjacent to the occipital horn of the left lateral ventricle. At 12 months, the left frontal lesion appears less conspicuous.

5.3.3.3 Associations between tissue damage and MS

Variables which were significantly associated with the development of MS are listed in Table 5.15.

BASELINE		r	p
Optic nerve	FSE lesion length	-0.47	0.019
	Gad lesion length	-0.50	0.013
Optic radiation	Lesion load	0.51	0.010
Occipital cortex	Pericalcarine volume	-0.43	0.032
	Pericalcarine thickness	-0.40	0.049
12 MONTHS			
Optic radiation	Lesion load	0.50	0.024
Occipital cortex	Pericalcarine thickness	-0.46	0.038
CHANGE			
Optic radiation	Lesion load	0.48	0.032

Table 5.16 Variables associated with the development of MS at 12 months. The correlation coefficient (r) is reported, together with the associated p value. FSE-fast spin echo, Gad-gadolinium-enhanced scan.

At baseline, the following factors were associated with the development of MS by the end of the study: a shorter optic nerve lesion, on both fast spin echo and gadolinium-enhanced MRI, a greater lesion load in the optic radiations, a smaller pericalcarine volume and a thinner pericalcarine cortex.

At 12 months, associations remained between MS and the following factors: a greater optic radiation lesion load and a thinner pericalcarine cortex.

With regard to the change variables, an increase in optic radiation lesion load was the only parameter associated with the development of MS.

All associations survived correction for age and gender, except pericalcarine cortical thickness, which retained borderline significance (p=0.065 and 0.057 at baseline and 12 months, respectively). The association of pericalcarine cortical volume with MS remained after correction for whole brain grey matter volume (p=0.038).

There were no associations for any of the other tested variables, either at baseline, 12 months, or for change over time.

5.3.4 Discussion

The most important finding of this study was the association between pericalcarine cortical atrophy, evident at baseline, and the subsequent development of MS. These

results suggest that early pericalcarine cortical atrophy in clinically isolated ON relates to damage from generalised disease, rather than tract-specific pathology, and may indicate that the visual system is especially susceptible to damage in demyelinating disease. In the following sections, damage within the visual system, the development of generalised disease, and associations between tissue damage and MS will each be discussed, in turn.

5.3.4.1 Lack of associations between areas of damage within the visual pathway

No associations were found between measures of tissue loss in the optic nerve and damage in either the anterior or posterior visual pathways. In the retina, this could be because the measurement of optic nerve area may be confounded by changes in tissues other than axons, for example, glial cells. In addition, the relationship between axonal loss in the optic nerve and secondary neuroaxonal degeneration in the retina might not be one-to-one. The extent of secondary effects could be under the influence of other factors, for example, remyelination. Alternatively, the MRI and OCT measures might not be sufficiently sensitive to detect an existing association.

In the posterior visual system, it was not possible to confirm the findings of previous studies, which have found evidence for trans-synaptic degeneration affecting the optic radiations and occipital cortex, following ON (Ciccarelli et al., 2005;Audoin et al., 2006;Calabrese et al., 2007). This may be due to methodological differences in the studies, or related to the different size and composition of the cohorts. For example, the majority of the subgroup of patients in which associations were found by Calabrese *et al* fulfilled the MRI criteria for dissemination in space. Therefore, these patients represented a more advanced disease stage than the present cohort. It may be that tract-specific trans-synaptic changes become increasingly evident later in the course of demyelinating disease, or that they are not an invariable consequence of optic nerve damage and are also under the influence of other factors.

5.3.4.2 Development of MS

The proportion of patients who developed MS in this study was slightly higher than the ONTT cohort from the USA, and an Italian study, but similar to a previous UK study of a mixed cohort with various clinically isolated syndromes.

In the ONTT, the overall risk of MS at five years was 30%, increasing to 51% in those with an abnormal baseline MRI (Optic Neuritis Study Group, 1997a). The number of patients with an abnormal MRI scan at baseline was also higher in the present study than the 49% reported in the ONTT (Optic Neuritis Study Group, 1991). An Italian study of patients with ON reported that 37% developed clinically definite MS at a mean of two years following their first clinical episode (Ghezzi et al., 1999). In contrast, a study from the UK reported an MS conversion rate of 48% at one year, using the McDonald criteria, although the proportion with clinically definite MS at this time was smaller (20%) (Dalton et al., 2002). These disparities may be related to differences in risk profiles between the American, Italian and British populations that were studied, or to random sampling differences. In general, there has been some variability in reported conversion rates from different regions, even after considering differing durations of follow-up.

5.3.4.3 Associations between volume loss in the visual cortex and MS

A shorter acute lesion in the optic nerve was associated with the development of MS. This is consistent with previous clinical studies, which have reported that severe optic nerve inflammation is relatively unusual in ON related to MS, although it does occur. Severe symptomatology is recognised as a "red flag" in ON, to consider alternative aetiologies, such as the steroid-responsive optic neuritides (Hickman et al., 2002b). None of the patients in this study were diagnosed with any conditions other than MS over the course of the study, although it is possible that alternative diagnoses may emerge in the future. These results are consistent with clinical observations that ON, in the context of MS, is typically of mild to moderate severity.

The strong associations between lesions in the optic radiations and the development of MS are not surprising. It is well recognised that asymptomatic brain MRI lesions are associated with a much higher risk of subsequent MS (Optic Neuritis Study Group, 1997a;Brex et al., 2002;Beck et al., 2003;Optic Neuritis Study Group, 2008b), and the optic radiations are a common site for incidental lesions (Hornabrook et al., 1992). Higher numbers of lesions have been linked to a higher risk of MS (Optic Neuritis Study Group, 1997a).

The most interesting associations were between the pericalcarine cortical measures and the development of MS over the ensuing 12 months. Pericalcarine volume loss

was evident at baseline, compared to controls (Chapter 4). The finding from this study of an association with MS suggests that this region-specific atrophy may be related to generalised damage from subclinical MS, rather than the effects of local pathology, such as damage in the optic nerve or optic radiations. This was further supported by associations between a reduced pericalcarine cortical thickness and MS, which were evident at baseline, as well as 12 months. It is worth noting that the association between pericalcarine cortical volume and MS lost significance at 12 months. This may reflect a loss of statistical power, as fewer patients were able to perform MRI at this time (see section 5.1.3.2).

It has been reported previously that progressive generalised cerebral cortical atrophy occurs following a clinically isolated syndrome in patients who develop MS (Dalton et al., 2004;Fisher et al., 2008;Fisniku et al., 2008), but not in those whose disease remains isolated (Fisher et al., 2008), even after 20 years (Fisniku et al., 2008). In the present study, pericalcarine cortical atrophy was evident in the absence of detectable generalised grey matter volume loss. The patients were recruited early following their first clinical attack. Therefore, these data appear to support the hypothesis that the visual system is especially susceptible to damage early in MS. It is known that the white matter of the visual system is commonly affected early, and it appears that the grey matter of the pericalcarine cortex is similarly vulnerable. The reasons for this are not clear from this study. Possible explanations could include anatomical factors, related to vascular supply or adjacency to CSF spaces, or antigenic factors, specific to the neurons of the visual system. The observation is of interest, as studying damage in the visual system may offer insights into the factors which are important at an early stage of MS.

5.3.4.4 Conclusions

In summary, this study found an association between measures of pericalcarine cortical atrophy, in patients presenting with acute ON, and the development of MS over the following year. No associations were found between measures of tissue damage at different sites in the visual system. Together, these results suggest that pericalcarine cortical atrophy, evident at baseline, is more likely to reflect an early manifestation of generalised grey matter volume loss in people with early subclinical MS, rather than secondary tract-specific degeneration. The grey matter of the visual

system may be particularly susceptible to damage in demyelinating disease, in a similar manner to the white matter.

CHAPTER 6

INVESTIGATING RECOVERY OF VISUAL FIELD DEFECTS AND THE ROLE OF THE FELLOW EYE IN OPTIC NEURITIS, USING QUADRANT-SPECIFIC FMRI

In this chapter, the mechanisms of damage and repair of the optic nerve that underlie visual field defects in ON are considered. A wide variety of visual field defects are seen in ON, reflecting the patchy nature of the underlying inflammatory pathology. Differential involvement of fibres within the optic nerve leads to different patterns of visual loss in the individual patient. Whilst any field defect can occur, some are more common than others, and it is not known whether some fibres are more susceptible to injury. The pattern of visual loss seen on field testing reflects the retinotopic nature of visual organisation, and is a direct representation of regions of disruption of the afferent input to occipital cortex. However, this inter-individual variability in clinical deficit makes recovery from visual field defects particularly difficult to study at group level, as the clinical features are so heterogeneous. Selective stimulation of individual quadrants of the visual field was performed during the fMRI experiment and the neurophysiological assessment, in order to constrain anatomically the region of the afferent pathway investigated with each stimulus condition. The aim was to reduce heterogeneity in patterns of visual field defect at group level in this manner, improving sensitivity to detect region-specific plastic reorganisation responses. In addition, this approach allowed investigation of cortical activation, in regions which usually process input from identical areas of retina in each eye, as a result of homologous retinotopic organisation. This provided an opportunity to directly contrast processing in response to normal and abnormal afferent input and, in particular, to study fellow eye responses in more depth.

6.1 Introduction

6.1.1 Pathophysiology of visual field defects

Any type of visual field defect may occur in acute ON, and abnormality is detectable in 97% of patients, which may be diffuse or localised. However, some patterns are

more common than others. For example, three years after the acute episode, residual defects are more common in the central field than peripherally (Keltner et al., 1999). A diffuse pattern is commonest, and altitudinal and centro-caecal patterns are also found relatively frequently (Keltner et al., 1993b) Generally, recovery is good and does not differ between diffuse and localised deficits (Fang et al., 1999), but some people are left with residual areas of visual loss.

The mechanisms of damage underlying ON have been discussed in previous chapters, and involve inflammation and conduction block in the optic nerve. The nature of the resulting visual field defect reflects the affected fibres involved, and the retinotopic regions of retina that they serve. Recovery may follow resolution of inflammation and restoration of conduction, but residual demyelination and axonal loss can occur. Intuitively, it might be anticipated that any regions of persistent defect might reflect areas of retina supplied by fibres that have sustained more axonal damage, but this is difficult to demonstrate experimentally *in vivo*. It is not known if there is differential sensitivity of axons to damage, or differential predisposition to repair, within the optic nerve in demyelinating diseases. In established progressive MS, OCT studies have reported greater loss of axons in the temporal quadrant (Henderson et al., 2008).

Therefore, the factors contributing to a permanent visual field defect in ON remain unclear, and it is possible that the relative importance of each factor varies, depending on the location of the defect. For example, there might be differential sensitivity to demyelination, axonal loss or gliosis, or the margin of axonal redundancy could vary in different parts of the optic nerve. Finally, it is possible that the location and importance of cortical reorganisation might differ, depending on the anatomical location of the defect.

The heterogeneity in clinical pattern of visual field defects, both with regard to location of scotomas and rate of improvement, leads to problems when studying mechanisms of recovery with fMRI. It is challenging to capture and characterise differences in visual function within individuals which affect fMRI responses at the subject level, whilst remaining sensitive to group-level fMRI effects, which may represent repair mechanisms that can be generalised to the whole patient population. Previous studies have applied whole field stimulation and addressed this problem at the analysis stage. Different data modeling approaches have been used, including a fixed-effects analysis strategy, the exclusion of patients with little clinical change in their field defects over time, and higher level design matrices (Korsholm et al., 2008).

Inter-session differences in lower visual areas were demonstrated but, using this approach, it was more difficult to generalise inferences to the whole population of patients with ON. The idea in the present study was that region-specific stimulation would address the issue of clinical heterogeneity at the stage of data acquisition, by refining anatomical localisation of activation, and increase sensitivity to region-specific effects, allowing generalisable inferences at the analysis stage.

6.1.2 Homologous retinotopic representation and the fellow eye

The results reported in Chapter 5 indicated that fellow eye responses are abnormal in higher visual areas, during the first few weeks following acute ON. Acute fellow eye responses in the LOCs directly correlated with visual outcome in the affected eye. Previous studies have reported abnormal responses in lower visual areas following ON. In one study, fellow eye fMRI response in primary visual cortex during the acute episode correlated with affected eye acuity (Toosy et al., 2005). In another, sustained supra-normal responses were found in the LGN for four months following ON, reducing subsequently to the same level as the affected eye by six months (Korsholm et al., 2007). Therefore, it was of interest to determine if fellow eye responses were abnormal in retinotopic regions of primary visual cortex, perhaps indicating compensatory plasticity at this level of the visual hierarchy.

The homologous retinotopic organisation of the visual system facilitates investigation of the role of the fellow eye in recovery from ON. Previous studies reporting abnormalities of fellow eye responses have all applied visual stimulation to the whole visual field, including central areas. This type of stimulus results in diffuse cortical activation, which differs slightly between the two eyes, as some peripheral regions have only monocular representation. However, region-specific peripheral checkerboard stimulation, using the quadrant method described in detail in Chapter 3, presented, in turn, to the affected and fellow eyes should normally result in activation of an identical, well localised, region of visual cortex, due to homologous retinotopic organisation. Studying responses in this region then provides an opportunity to directly compare cortical responses from a diseased region of optic nerve, representing a discrete visual field defect, with the corresponding healthy region of visual field, optic nerve, and cortex representing the fellow eye.

6.1.3 Aims

The underlying objectives of this chapter were to elucidate the mechanisms of damage and recovery underlying visual field defects in ON, and the role of the fellow eye in recovery. The specific aims were derived from three separate hypotheses:

(1) Firstly, mechanisms of damage were considered, in terms of the susceptibility of different fibres to damage, and the reasons for the differing patterns of acute field defect, both acutely and during recovery. The hypothesis was that the fibres of the temporal disc quadrant, representing the central field, might be particularly susceptible to axonal damage. This was investigated by examining region-specific clinical data, complemented by region-specific VEP amplitudes and latencies, to assess axonal function and myelination, respectively.

(2) Secondly, mechanisms of recovery were considered, with a focus on cortical plasticity. The hypothesis was that different patterns of visual field defect might result in different anatomical, and perhaps temporal, patterns of extra-striate cortical reorganisation during recovery, consistently within individuals.

(3) Lastly, the role of fellow eye responses in visual recovery was considered. The hypothesis was that supra-normal activation in the fellow eye might be seen acutely, compared with subsequent time-points, indicating a compensatory regional increase in brain activity, which might indicate plasticity. This might also be evident as greater activity on stimulation of patients' fellow eyes, compared with control eyes.

In the course of addressing these hypotheses, the feasibility of using region-specific stimuli to investigate patients with visual field defects was tested. In particular, the use of quadrant-specific VEP and fMRI stimuli, and their combination with quadrant-specific clinical data, was a novel approach. Correlations between clinical, electrophysiological and fMRI parameters were investigated during the acute episode, as it was hypothesised that between-subject variance would be maximal at this time.

6.2 Methods

Aspects of the methodology which been described in preceding chapters will not be replicated. In particular, the region-specific fMRI visual stimulation paradigm is described in detail in Chapter 3. New elements, specific to this part of the study, will be fully reported in this section.

6.2.1 Participants

The same cohort of subjects was studied that participated in the experiments reported in Chapter 5, at the same time-points (baseline, three months, six months and 12 months).

6.2.2 Region-specific clinical assessment

Visual fields were examined using the 30-2 programme on the Humphrey automated field analyser (Allergan-Humphrey Inc., San Leandro, Ca., USA). Patients were assessed longitudinally, and each control was assessed once. The field was split into four peripheral quadrants and a central circle. The central circle comprised the central 6^{o} of the field, and the rest of the test-points in each field were allocated to four quadrants, divided according to the vertical and horizontal meridians, and extending up to 15^{o} from the fixation point, covering a similar proportion of field (30^{o}x30^{o}) as the visual fMRI display. There were four test-points in the central circle, and either seven or eight in each quadrant, depending on the presence or absence of the blind-spot. Data summarising the total deviation from the mean at each point of the field were averaged for each region, as a measure of the regional field defect. The quadrants were referred to as upper left, upper right, lower left, lower right and central circle for each eye (Figure 6.1). Therefore, for each quadrant category, cortical representation was the same, regardless of which eye was affected.

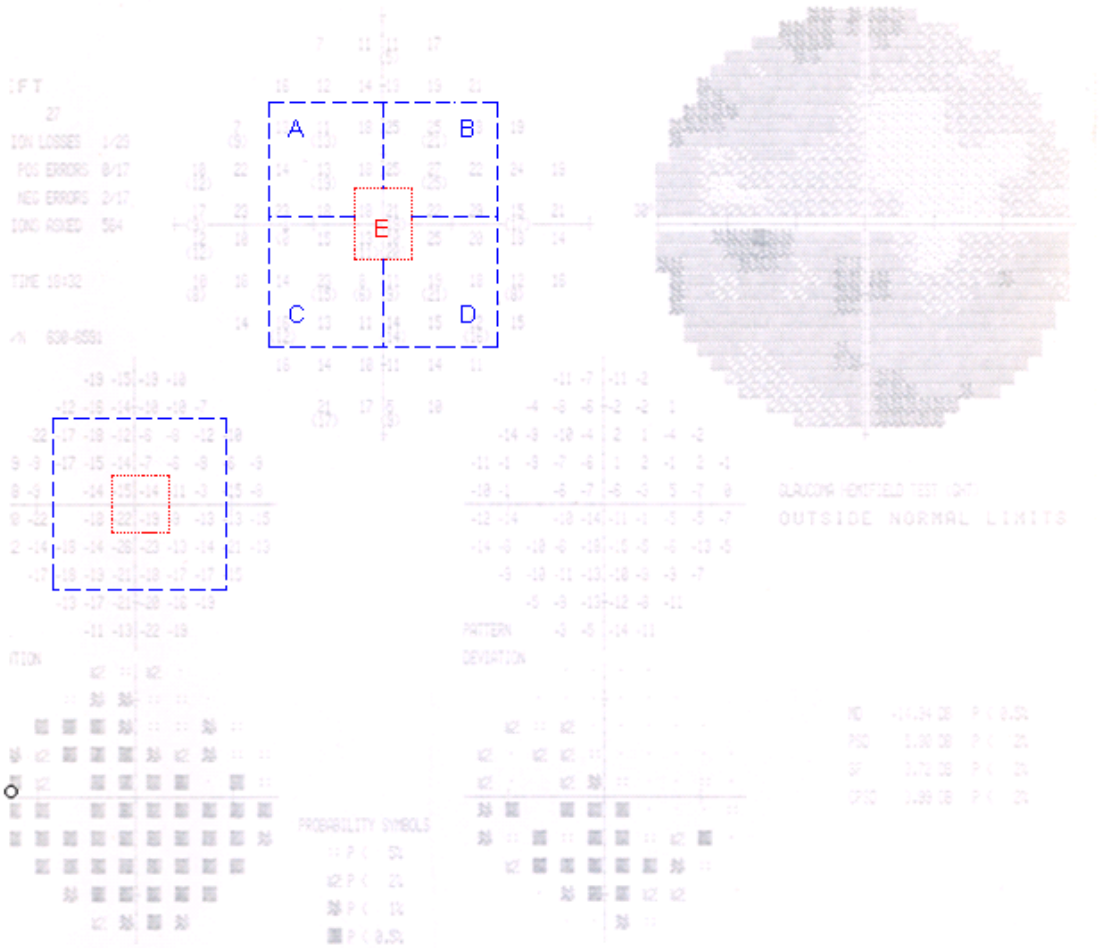

Figure 6.1 Method of extraction of region-specific Humphrey data. An example of a Humphrey visual field printout from a patient's left eye is shown. The qualititative grey map corresponds to each quantitative numbered map. Each number indicates the allocated score for that point in the field. The upper numbered map, adjacent to the grey map, show how the field was divided to extract the raw scores. The numbers represent the minimal luminance stimulus that the subject could detect at that point in the visual field. The divisions used in this study are outlined on this map, in blue for the quadrants: (A) left upper, (B) right upper, (C) left lower and (D) right lower, and (E) in red for the central field. The lower numbered fields contain the corresponding data, adjusted for age with respect to the reference population and was the dataset actually used in this study.

6.2.3 Region-specific electrophysiology

Quadrant-specific VEP data was collected longitudinally for the patients, and once for the controls. The screen subtended 28^{o} of visual angle horizontally and 22^{o} vertically, and the central circle extended from 0 to 4^{o}. Each quadrant extended 14^{o} from the horizontal meridian and 11^{o} from the vertical meridian, excluding the region occupied by the central circle. Check size was 40'. An occipital electrode 5cm above the inion

was used to reference Fz. The amplitude of the response and the latency of the P100 waveform were calculated.

6.2.4 Region-specific functional MRI

Quadrant-specific fMRI stimuli were presented, as described in Chapter 3. The presentation screen subtended 30^o horizontally and 28^o vertically, and the central circle extended from 0 to 5^o. Thus, there were minimal differences in the dimensions of the display media for the clinical, electrophysiological and fMRI stimuli. The central circle varied between 4-6^o, the horizontal extent of the quadrants between 28-30^o, and the vertical extent between 22-30^o. This variability was the minimum that could be achieved, given practical constraints in the apparatus used. It is of note that activation following VEP stimuli is mostly dependent on the central 10^o of stimulation (Rinalduzzi et al., 2001).

6.2.5 Statistical analysis

6.2.5.1 Clinical data

The raw grey maps were copied and displayed, in order to illustrate to the reader qualititative changes in visual field defects over time. In order to quantify field defects in each quadrant and the central circle, the region-specific total deviation data were extracted, for each region, for each eye, for each subject, at each time-point. Means and standard deviations were calculated for each region, at each time-point. A one-way analysis of variance model was estimated, in Stata-9.2, to assess differences in clinical scores between regions, at each time-point. Mixed effects linear regression models were used to analyse changes over time. The type of model was identical to those described in Chapter 5. Paired t-tests were used to assess residual differences between affected and fellow eyes at 12 months.

The Humphrey analyser had a minor calibration error, identified at the start of the study, which resulted in an overestimation of error scores. Therefore, data from the control group, who were age and sex-matched to the patient group, were used to recalibrate the patient data. The mean total error score was calculated in the control group and averaged for right and left eyes. The resulting value (-5.066) was taken to

represent a true error score of zero and, therefore, this value was subtracted from the patient data, at each point in the visual field.

6.2.5.2 Electrophysiology

Mixed effects linear regression models were used to assess changes in region-specific VEP amplitude and latency over time.

6.2.5.3 Voxel-based and region-of-interest approaches to fMRI data

Two different analysis approaches were used: a voxel-based whole brain analysis and a region-of-interest approach, and the results of both are reported.

The location of any brain reorganisation contributing to region-specific recovery of field defects in ON is not known. In this situation, as there is no anatomical *a priori* hypothesis, a whole brain voxel-wise analysis is the preferred approach, as it is unbiased and may identify hitherto unsuspected important areas. However, the large number of multiple comparisons inherent in this method requires relatively stringent statistical correction and this, combined with normal inter-subject variability, can lead to a lack of sensitivity to detect subtle effects at group level.

In contrast, to investigate the role of the fellow eye, it was possible to identify regions-of-interest, based on areas of maximal group activation, corresponding to the relevant areas of retinotopic visual cortex. Although this approach constrains the anatomical hypothesis, it has the advantage of a greater sensitivity to subtle effects, as statistical correction for every voxel in the brain is not required.

Therefore, both methods were used. The voxel-based approach was used to assess any cortical reorganisation across the whole brain, by testing the following: (1) Cross-sectional fMRI response to affected and fellow eye stimulation at each time-point; (2) Longitudinal changes in fMRI response in affected and fellow eyes over time; (3) Differences between affected and fellow eye responses at each time-point; (4) Differences between patients and controls at each time-point. Each of these tests was repeated individually for each condition of region-specific stimulation.

The region-of-interest approach was used to investigate the role of the fellow eye, by testing the following: (1) Longitudinal differences in affected and fellow eyes over time; (2) Cross-sectional differences in affected and fellow eye responses at each time-point; (3) Cross-sectional differences between patients and controls at each time-

point. Each of these tests was again repeated, in turn, for each condition of region-specific stimulation.

In addition, in order to assess the feasibility of the quadrant-specific approach, both methods were used to assess correlations between clinical, electrophysiological and fMRI data during the acute episode, and the results compared.

Therefore, each of the following sections is split into two parts, first describing the voxel-based approach and then the region-of-interest approach.

All voxel-based analysis was performed in SPM5, and all region-of-interest analysis in Stata-9.2. Results were considered significant at $p<0.05$, unless otherwise stated.

6.2.5.4 FMRI activation in patients and controls

6.2.5.4.1 Voxel-based

One-sample t-tests were specified in order to identify the main effect of stimulation and any areas of extra-striate activation, for each quadrant, at each time-point, in patients and controls. Covariates indicating whether ON affected the left or right side were entered into the model. For controls, a randomly selected eye was designated "affected", so that the methodology was identical to the patients.

This analysis was performed twice. Firstly all available data were entered at each time-point. The analysis was then repeated including only those subjects who had fMRI data available at every time-point. This was to allow a meaningful visual comparison of the activation patterns at each time-point within an identical group. The cohort with fMRI data available at all time-points comprised 16 patients, and 8 controls. Of the remainder, reasons for missing time-points are described in Results section 6.3.1. Images were thresholded at cluster-level $p<0.05$ (corrected).

The spatial extent of activation was assessed in each patient, at each time-point, by extracting the total number of activated voxels from each map, thresholded at cluster-level $p<0.05$ (corrected). Linear mixed effects models were used to assess the significance of any changes over time.

Flexible factorial models were specified, in order to quantitatively assess differences between patients' affected and fellow eyes, longitudinal changes over time, and differences between patients and controls. The flexible factorial model in SPM5 allows for missing data-points, so all available data were used for this analysis.

Three factors were specified: (1) Subject, (2) Group (affected/fellow or patient/control) and (3) Time-point. The distribution of errors and error variances were specified as follows: (1) within-subject level- independent and equal; (2) group level for affected/fellow comparisons- non-independent and equal; group level for patient/control comparisons- independent and unequal; (3) time-point level- non-independent and equal. The interaction between group and time was specified, and side affected was entered as a covariate. This resulted in the following model (Figure 6.2), which allowed two-sample t-tests to compare groups at each time-point. For example, to test patients at baseline versus controls at baseline, the contrast (1 0 0 0 -1 0 0 0 0) was entered.

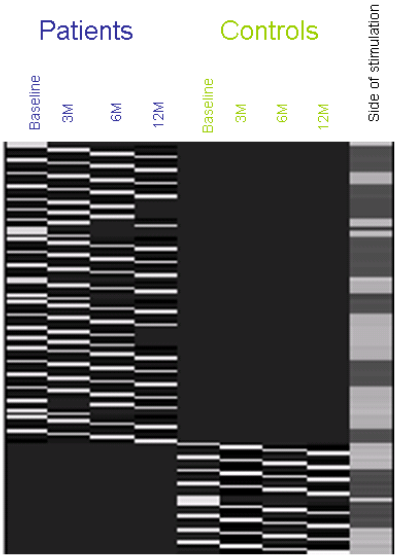

Figure 6.2 SPM5 flexible factorial design matrix for two-group comparisons.

To assess longitudinal effects, linear and second order changes were investigated. In addition, an exponential model was specified, which aimed to capture any changes in fMRI signal which paralleled the temporal pattern of clinical improvement in ON (Figure 6.3).

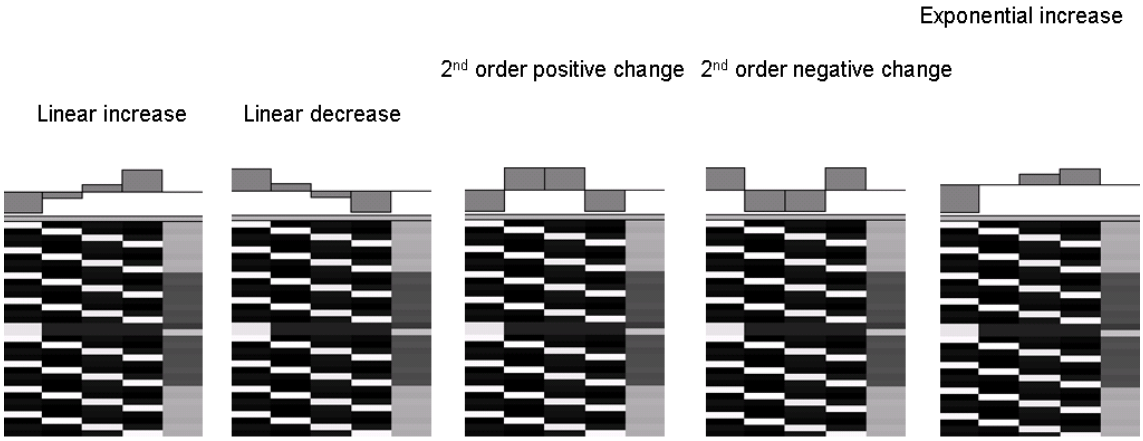

Figure 6.3 An illustration of contrasts used to assess different patterns of change over time.

The contrasts illustrated above were specified as follows:
Linear increase (-1.5 -0.5 0.5 1.5)
Linear decrease (1.5 0.5 -0.5 -1.5)
Second order positive change (-1 1 1 -1)
Second order negative change (1 -1 -1 1)
Exponential increase (-5 0 2 3)

Interpretation of longitudinal changes using a voxel-based approach over the whole brain can be difficult, because fMRI is sensitive to changes over time due to scanner drift, attention and adaptation/habituation effects. These may cause artefacts, which can be difficult to separate from genuine disease effects. For these reasons, and because of concerns that the region-specific approach might result in lower signal-to-noise than whole field stimulation, a preliminary analysis was performed in the control group to identify an appropriate threshold to apply to the maps, in which artefact was minimised. A cluster-level threshold of $p<0.001$ (corrected) was selected, which was subsequently applied to the patient group. A further discussion of problems inherent to longitudinal fMRI studies is included in Appendix III for the interested reader.

6.2.5.4.2 Regions-of-interest

The cortical regions-of-interest involved in processing afferent input from each corresponding region of stimulated visual field were specified using the group fMRI data from the study cohort. In this manner, retinotopic areas of early visual cortex

were identified, in which it was possible to directly compare affected and fellow eye activation. This methodology involved extracting data from SPM5 and analysing it, together with the corresponding VEP and clinical data, in Stata-9.2. This was a useful benefit of the approach as, in SPM5, fMRI response is constrained as the dependent variable whereas, in the investigation of disease, clinical outcomes may be of interest.

The steps involved in specifying the regions-of-interest were as follows: firstly, fMRI scans were combined, for all patients and all controls, at all time-points, for affected and fellow eyes, for each of the four quadrants and the central circle conditions, in turn, using one-sample t-tests in SPM5. All time-points were combined, rather than averaging at each individual time-point, to increase signal-to-noise, in order to optimise the estimates for this group. This was felt to be more important for region-specific stimuli than the potential disadvantage of introducing a bias to the estimates from subject dropout, as previously discussed in Chapter 4.

Regions-of-interest were then created, using the MarsBar SPM toolbox (Brett et al., 2002), above and below the calcarine fissure, on the right and left sides, corresponding to stimuli in the lower and upper quadrants, on the left and right sides, respectively. Bilateral clusters at the occipital poles were used for the central circle. The size of the regions was standardised by specifying spheres of radius 1cm, contained within the clusters, centred on the group global maxima (Figure 6.4).

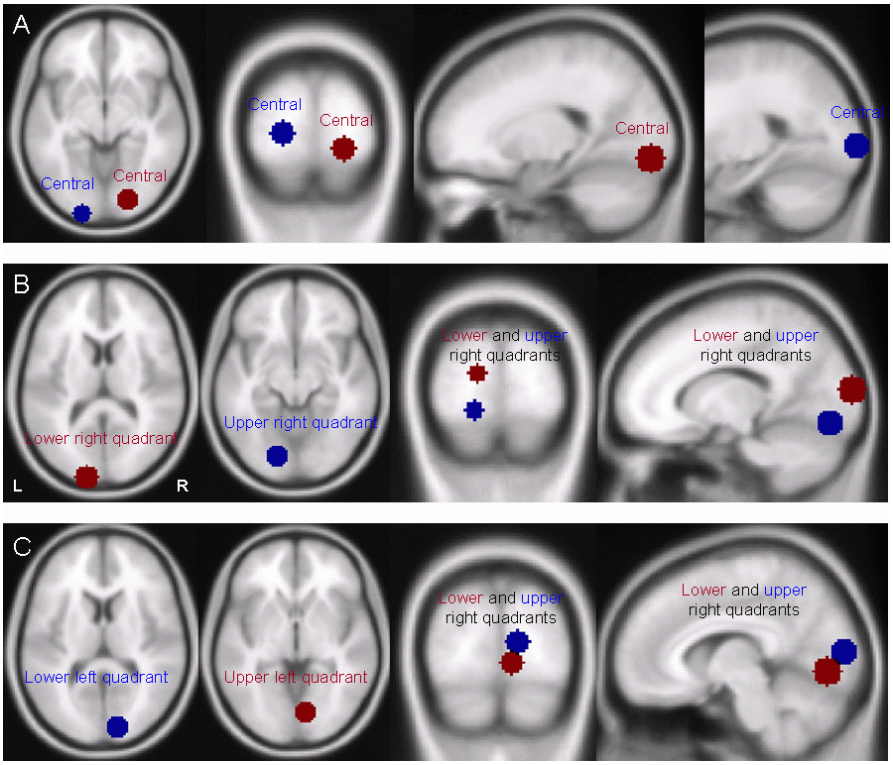

Figure 6.4 The regions-of-interest from which fMRI data were extracted are shown, overlaid on to a normalised brain in MNI space. In (A), the bilateral regions responding to central stimulation are shown in axial, coronal, left sagittal and right sagittal section. In (B), the regions of response to lower right quadrant stimulation are shown in red, and to upper right quadrant stimulation in blue. In (C), regions of response to lower left quadrant stimulation are shown in blue, and upper left stimulation in red. L-left, R-right.

The mean parameter estimates were extracted, representing the mean BOLD response in each region over the course of the experiment, for each subject, at each time-point. For the central circle, data from the two spheres were averaged.

Longitudinal changes were assessed using mixed effects linear regression models, for the patients' affected eye, fellow eye, and a randomly selected control eye. The magnitude of any differences at a given time-point was calculated from the difference in predicted means at that time, calculated from the regression slopes, in order to use all available data. Differences were calculated by dividing the affected eye parameter estimate by the fellow eye, and multiplying by 100%. The results were then expressed as the percentage difference in BOLD signal change in the affected eye, with respect to the fellow. For example, BOLD parameter estimates of 0.8 for the affected eye and 1.0 for the fellow would be expressed as -20%. The same methodology was used for patients' eyes, with respect to controls.

Cross-sectional differences between affected and fellow eyes, and patients and controls, were assessed using paired and unpaired t-tests, respectively.

6.2.5.5 Correlation analyses in the acute phase

6.2.5.5.1 Clinical-electrophysiological correlations

Multivariable regression models were specified in Stata-9.2 to assess correlations between clinical data and each affected eye VEP parameter (amplitude and latency), in turn, at the baseline time-point.

6.2.5.5.2 FMRI correlations with clinical and electrophysiological data: voxel-based

Both voxel-based and region-of-interest approaches were used to assess correlations between region-specific fMRI responses and clinical and VEP data, at the baseline time-point.

Voxel-based analyses were performed using group-level multivariable regression models in SPM5. Separate models were specified for each condition, entering the first-level fMRI contrast images for each patient, together with the corresponding clinical or electrophysiological variable: either Humphrey data, VEP amplitude or VEP latency from the affected eye. Side of stimulation and the relevant fellow eye variable (either clinical or electrophysiological) were added as covariates, in order to account for normal inter-individual variability in visual acuity and VEP parameters. The clinical or electrophysiological regressor relating to the affected eye was interrogated, to identify any positive (1 0 0) or negative (-1 0 0) associations with the fMRI data.

The location of any significant clusters was identified using the SPM5 Anatomy toolbox (Eickhoff et al., 2005).

6.2.5.5.3 FMRI correlations with clinical and electrophysiological data: regions-of-interest

Separate multivariable regression models were specified to investigate associations between the extracted fMRI data, from each region, and each of the corresponding clinical and electrophysiological variables, in turn. The relevant, corresponding fellow eye data (either clinical or electrophysiological) was again entered into the model, to correct for any normal inter-individual variability.

6.3 Results

6.3.1 Participants

Clinical data was available for all 99 patient attendances and 9/10 controls. In one control, it was not possible to acquire Humphrey data for logistical reasons.
Quadrant-specific VEP data was available for 96/99 patient attendances, and 10/10 control time-points. Data was missing for three time-points due to unavailability of technical staff. Quadrant-specific fMRI data was available for 123/133 subject attendances, and was unavailable for one patient at three months, three patients at six months, and six patients at the 12 month time-point. The reasons for missing data were as follows: patient pregnancy in five cases, scanner hardware or software problems in four cases, and claustrophobia in the scanner in the remaining case.
Sixteen patients and eight controls had fMRI data available at all time-points, and were entered into the additional cross-sectional analysis of fMRI activation patterns, as described in section 6.2.5.4.1. The reasons that data was unavailable for at least one time-point in the remainder were as follows: four patients and two controls decided they did not want to continue in the study, five patients missed at least one visit due to pregnancy, one due to claustrophobia, and two due to scanner hardware/software failure.

6.3.2 Region-specific clinical data

There were no significant differences between regions in the severity of visual loss in the affected eye at any time-point (baseline $F=0.33$, $p=0.854$; three months $F=0.31$, $p=0.868$; six months $F=0.89$, $p=0.473$; 12 months $F=1.05$, $p=0.387$). In terms of mean visual scores, the lowest during the acute episode was in the central field and, following recovery at 12 months, was in the right upper quadrant (Table 6.1).

Region-of-interest	Controls	Patients affected	Patients fellow	Patients differences
Central circle: BL	0.20 (1.23)	-16.55 (11.30)	0.49 (1.20)	-17.04
3M		-3.14 (4.11)	0.56 (1.59)	-3.70
6M		-2.96 (3.13)	0.50 (1.19)	-3.46
12M		-1.65 (2.45)	0.65 (1.37)	-2.30
Right upper quadrant: BL	-0.51 (2.18)	-13.78 (10.54)	-0.58 (1.68)	-13.2
3M		-3.50 (4.72)	-0.10 (1.89)	-3.40
6M		-3.63 (4.14)	-0.14 (2.03)	-3.49
12M		-2.76 (3.74)	-0.07 (1.67)	-2.69
Right lower quadrant: BL	0.12 (1.70)	-14.70 (10.73)	-0.13 (1.62)	-14.57
3M		-2.42 (3.23)	0.51 (1.83)	-2.93
6M		-2.05 (2.93)	0.46 (1.17)	-2.51
12M		-1.81 (2.66)	0.19 (1.38)	-2.00
Left lower quadrant: BL	0.38 (1.44)	-14.20 (10.66)	-0.49 (1.46)	-13.71
3M		-2.84 (4.27)	0.34 (1.87)	-3.18
6M		-2.29 (2.99)	0.36 (1.64)	-2.65
12M		-1.44 (2.24)	0.25 (1.29)	-1.69
Left upper quadrant: BL	-0.18 (2.03)	-13.73 (9.91)	-1.23 (1.64)	-12.5
3M		-3.61 (4.83)	0.02 (1.92)	-3.63
6M		-2.58 (2.30)	0.09 (1.60)	-2.67
12M		-2.61 (2.85)	-0.23 (1.72)	-2.38

Table 6.1 Mean region-specific Humphrey scores for patients' affected eyes, patients' fellow eyes, controls' eyes and inter-ocular differences in patients (calculated by subtracting the fellow eye score from the affected eye score). Standard deviations are given in brackets.

Changes in the patients' visual fields in the affected eye over time are illustrated in Figure 6.5. The visual score at each point in the field was used to create a grey-scale map, with darker regions indicating progressively denser field defects, in which progressively higher luminance stimuli were required to elicit a response.

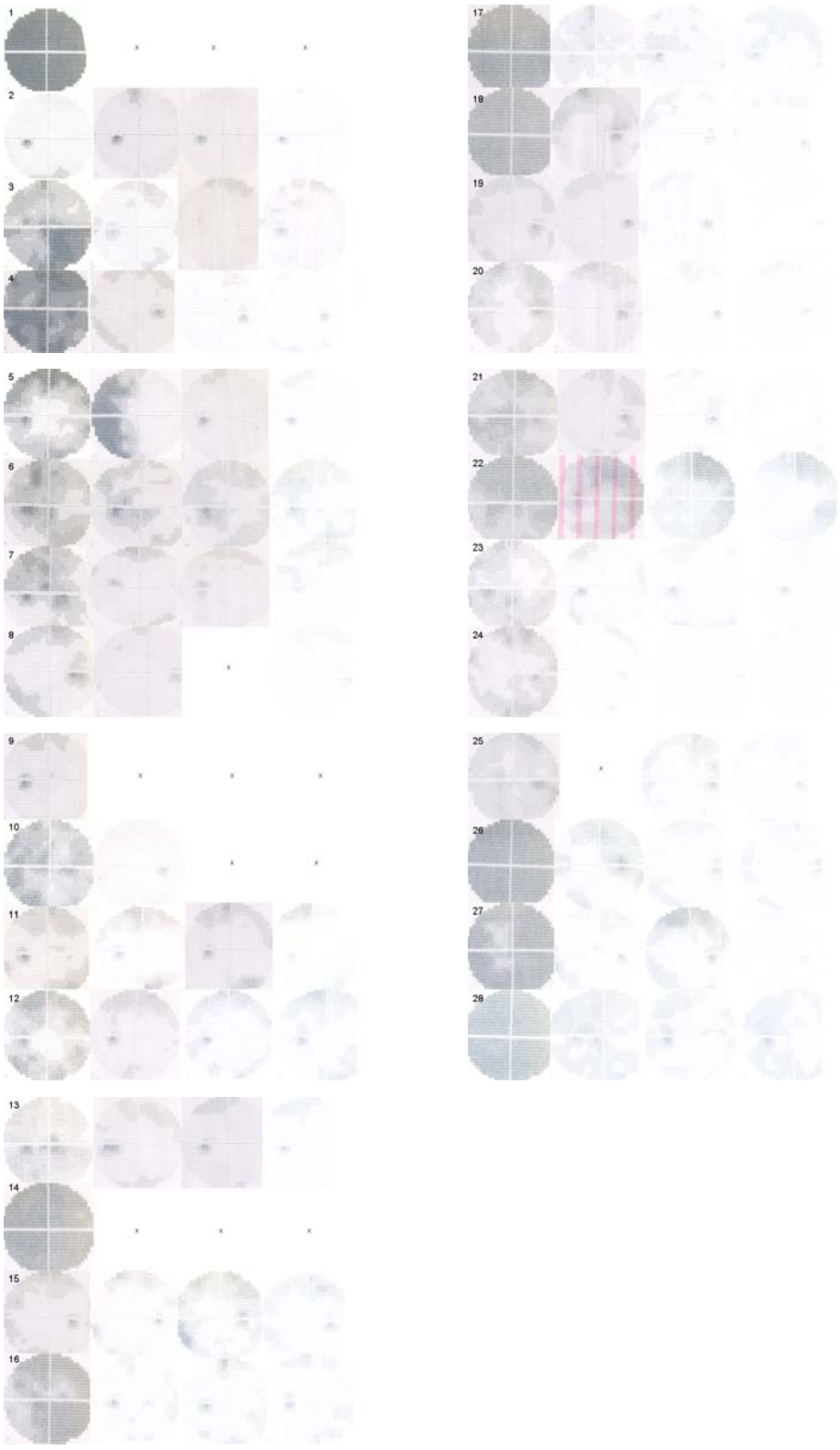

Figure 6.5 Visual field data is shown for the 28 patients involved in the study. The four fields in each row correspond to the four time-points, in chronological order. A missing time-point is denoted by x.

In Figure 6.6, quantitative longitudinal changes in visual field scores are plotted. Most of the improvement in the affected eye occurred in the first three months for all regions (Table 6.2). There were still significant differences between the affected and fellow eye, at 12 months.

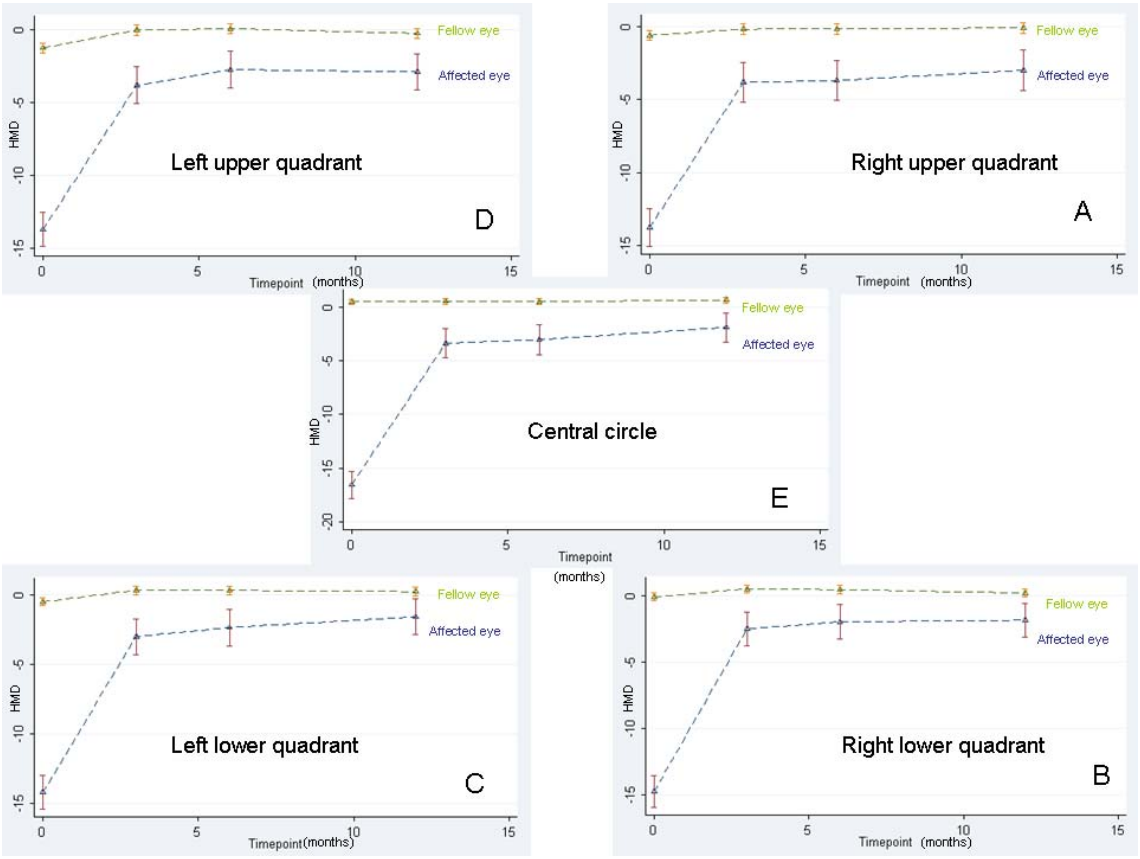

Figure 6.6 Graphs illustrating changes in region-specific Humphrey deviation scores over time, for each of the four quadrants and the central circle. The bars show standard errors.

Region	Baseline to 3 months Rate of change (HMD /month)			Baseline to 12 months Rate of change (HMD /month)			Difference at 12 months (Aff-fell)	
	Rate	95% CI	p value	Rate	95% CI	p value	HMD	p value
Aff central	**+4.39**	**3.40, 5.39**	**<0.001**	**+1.22**	**0.97, 1.47**	**<0.001**	**-2.30**	**<0.001**
Fell central	+0.02	-0.16,0.20	NS	+0.01	-0.03,0.06	NS		
Aff right upper	**+3.32**	**2.45, 4.20**	**<0.001**	**+0.90**	**0.68, 1.12**	**<0.001**	**-2.69**	**0.002**
Fell right upper	+0.14	-0.08,0.37	NS	+0.04	-0.01,0.10	NS		
Aff right lower	**+4.06**	**3.10, 5.02**	**<0.001**	**+1.07**	**0.83, 1.31**	**<0.001**	**-2.00**	**0.001**
Fell right lower	+0.20	-0.01,0.10	NS	+0.03	-0.03,0.08	NS		
Aff left lower	**+3.74**	**2.71, 4.76**	**<0.001**	**+1.05**	**0.80, 1.31**	**<0.001**	**-1.69**	**<0.001**
Fell left lower	**+0.28**	**0.06, 0.50**	**0.013**	**+0.06**	**0.01, 1.40**	**0.029**		
Aff left upper	**+3.31**	**2.44, 4.18**	**<0.001**	**+0.90**	**0.69,1.12**	**<0.001**	**-2.38**	**<0.001**
Fell left upper	**+0.41**	**0.15, 0.67**	**0.002**	**+0.08**	**0.02, 0.15**	**0.013**		

Table 6.2 Rates of change in clinical scores, between baseline and three months, and baseline and 12 months, derived from the linear regression models. The p-value refers to the significance of the slope. The residual difference between affected and fellow eyes at twelve months is reported. The p-values are derived from a two-sample t-test. Aff-affected, CI-confidence intervals, Fell-fellow, HMD-Humphrey mean deviation, NS-non-significant.

There were also some changes in fellow eye scores, which were small in magnitude but statistically significant.

6.3.3 Region-specific electrophysiology

Changes in region-specific VEP amplitude over time are illustrated in Figure 6.7, and the significance of the regression slopes is reported in Table 6.3.

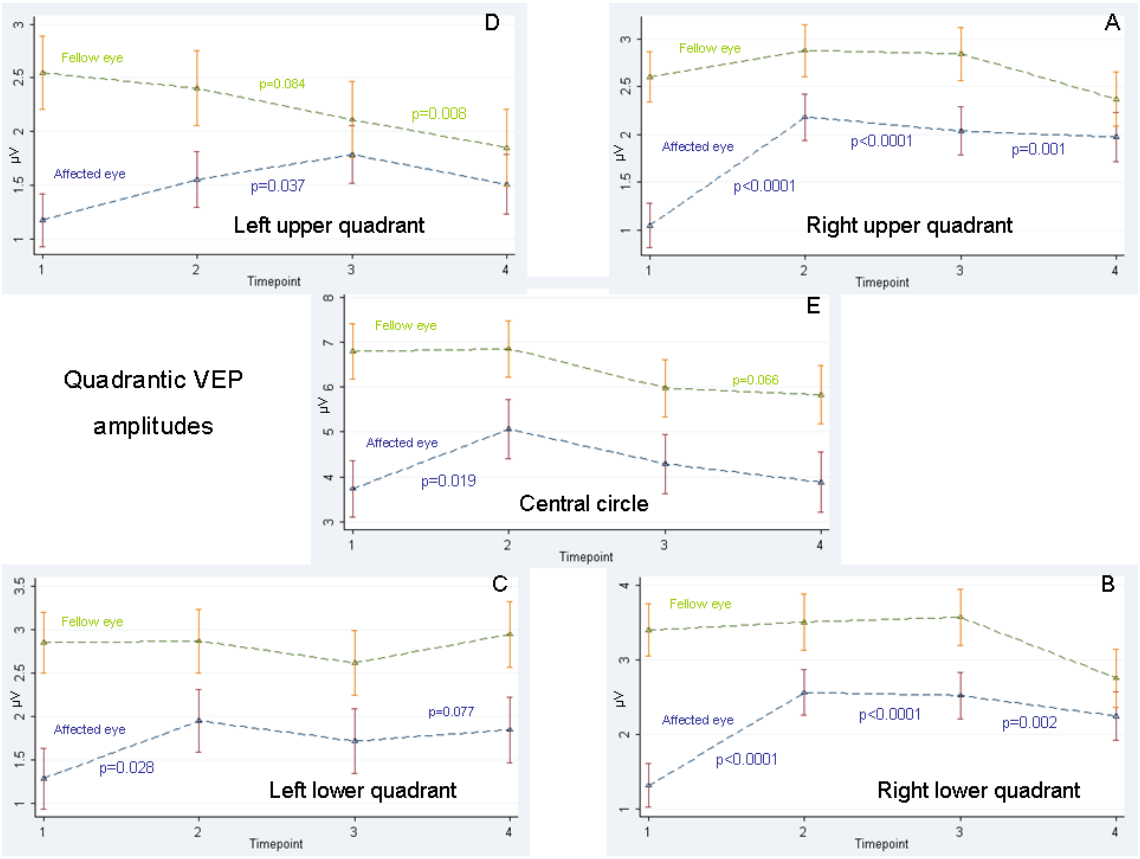

Figure 6.7 Graphs illustrating changes in VEP amplitude over time, for each of the four quadrants and the central circle. The graphs show standard errors. All significant ($p<0.05$) and borderline ($p<0.1$) p values are reported. For clarity, p values >0.1 are not shown.

Region	Baseline to 3 months Rate of change (μV /month)			Baseline to 12 months Rate of change (μV /month)			Difference at 12 months (Aff-fellow)	
	Rate	95% CI	p value	Rate	95% CI	p value	VEP amp	p value
Aff central	**0.44**	**0.07,0.81**	**0.019**	0.01	-0.08,0.11	NS	**-1.93**	**0.001**
Fell central	0.02	-0.31,0.35	NS	-0.08	-0.17,0.01	NS		
Aff right upper	**0.38**	**0.20,0.55**	**<0.001**	**0.08**	**0.03, 0.12**	**0.001**	-0.41	NS
Fell right upper	0.09	-0.07,0.26	NS	-0.02	-0.06,0.02	NS		
Aff right lower	**0.42**	**0.23,0.60**	**<0.001**	**0.08**	**0.03, 0.13**	**0.002**	-0.38	NS
Fell right lower	0.04	-0.21,0.28	NS	-0.05	-0.12,0.01	NS		
Aff left lower	**0.22**	**0.02,0.42**	**0.028**	0.05	-0.01,0.10	NS	**-0.87**	**0.010**
Fell left lower	0.01	-0.20,0.21	NS	0.01	-0.05,0.06	NS		
Aff left upper	0.13	-0.06,0.31	NS	0.03	0.02, 0.08	NS	-0.23	NS
Fell left upper	-0.05	-0.21,0.11	NS	**-0.06**	**-0.10,-0.02**	**0.008**		

Table 6.3 Rates of change in VEP amplitudes, between baseline and three months, and baseline and 12 months, derived from the linear regression models. The p-value refers to the significance of the slope. The residual difference between affected and fellow eyes at twelve months is reported. The p-values are derived from a two-sample t-test. Aff-affected, amp-amplitude, CI-confidence intervals, Fell-fellow, NS-non-significant, VEP-visual evoked potential.

Affected eye amplitudes increased in all quadrants in the first three months, except for the left upper quadrant, which did not improve significantly until six months. After six months, affected eye amplitudes generally reached a plateau. Fellow eye VEPs either remained stable, or decreased in amplitude over time.

Changes in region-specific VEP latency are illustrated in Figure 6.8.

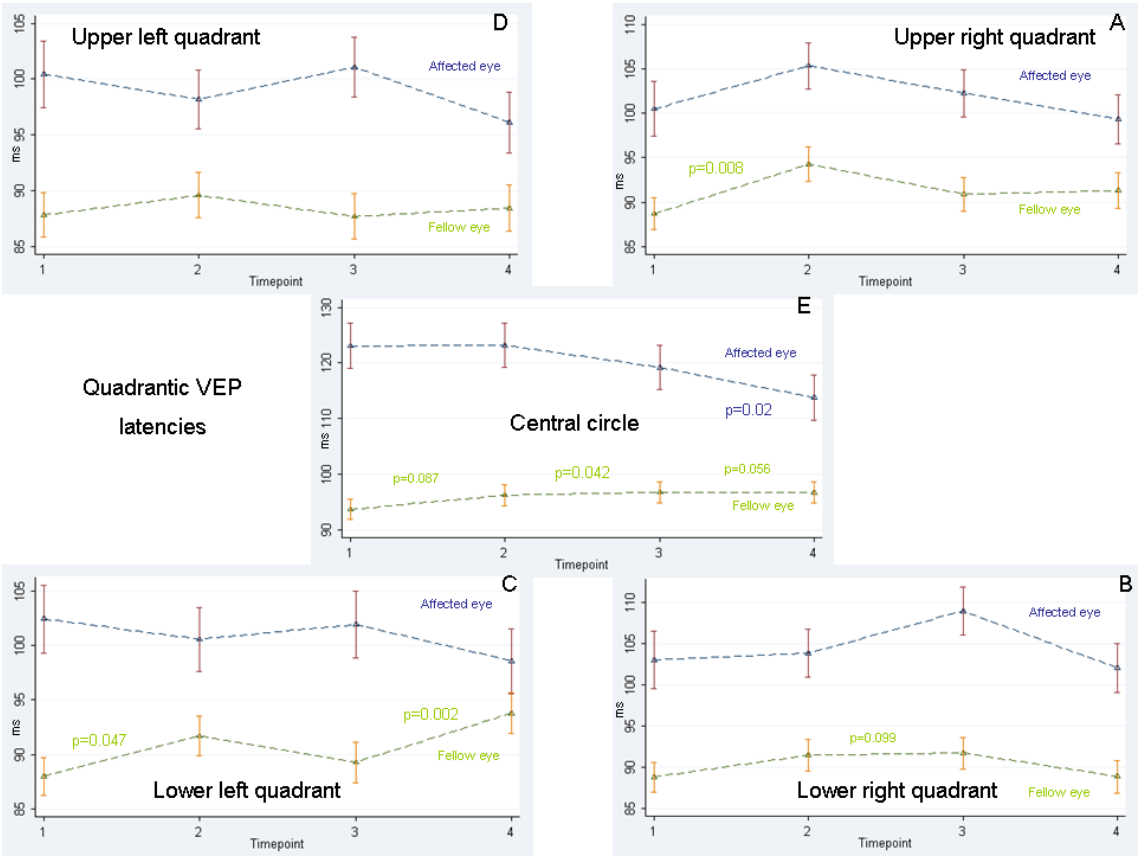

Figure 6.8 Graphs illustrating changes in VEP latency over time, for each of the four quadrants and the central circle. The graphs show standard errors. All significant ($p<0.05$) and borderline ($p<0.1$) p values are shown. For clarity, p values >0.1 are not shown.

There was a decrease in VEP latency, on stimulating the central circle, between baseline and 12 months (-0.78ms/month [-0.12, -1.43], p=0.020), but no changes in any of the other quadrants. In the fellow eye, VEP latency remained stable or marginally increased over time.

6.3.4 Region-specific functional MRI

6.3.4.1 Controls

6.3.4.1.1 Voxel-based: cross-sectional fMRI responses

Firstly, in order to demonstrate normal responses to region-specific fMRI stimulation, control group activation maps are shown for each of the four quadrants and the central circle, at each time-point (Figures 6.9-6.13).

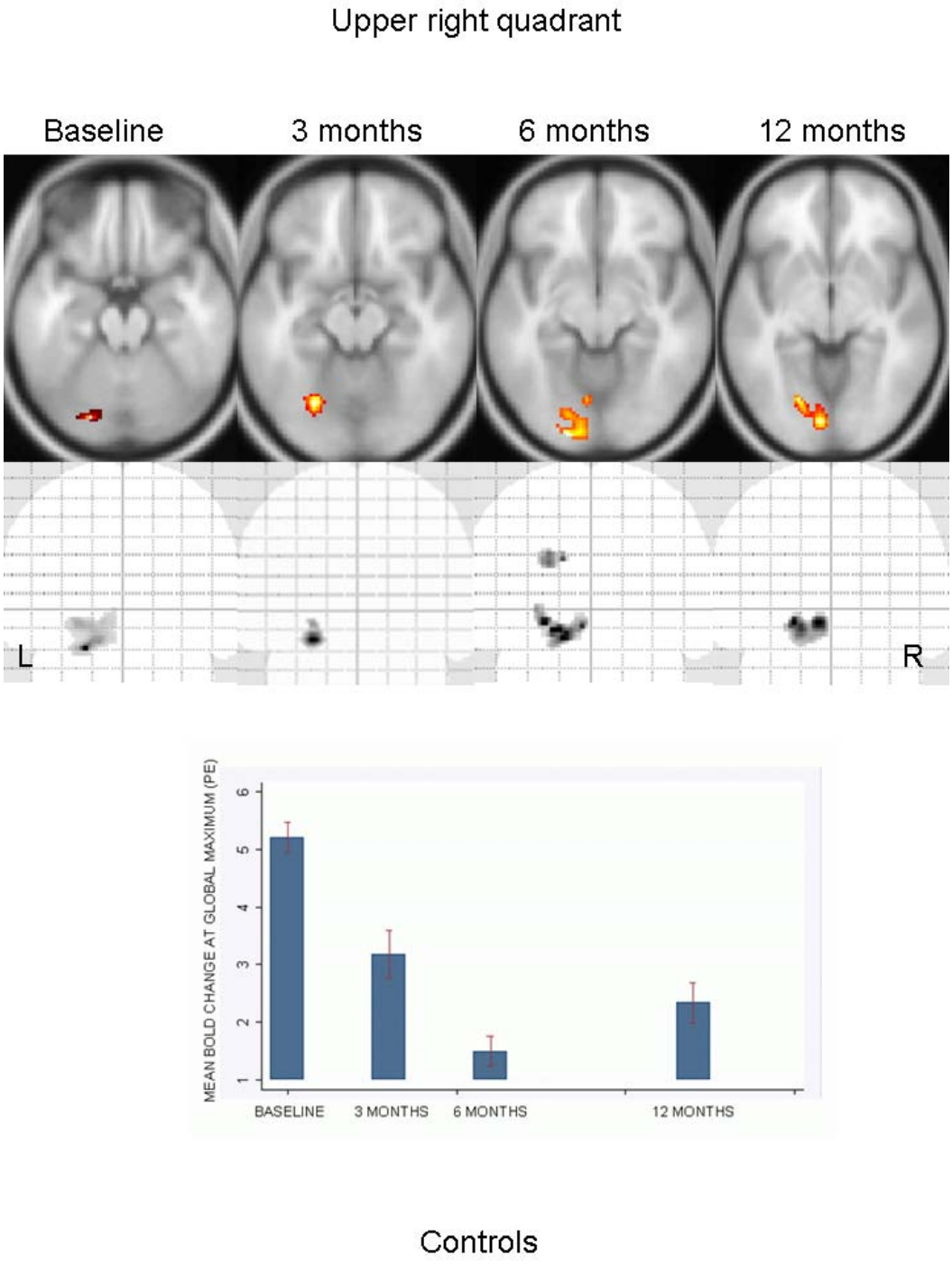

Figure 6.9 Statistical parametric maps showing fMRI activation in controls, over time, in response to upper right quadrant stimulation, overlaid on to an axial section of the SPM5 canonical MNI-152 brain template, and a coronal section of the SPM5 glass brain. The graph plots the global maximal parameter estimate (PE) at each of the four time-points, and the error bars represent 95% confidence intervals.

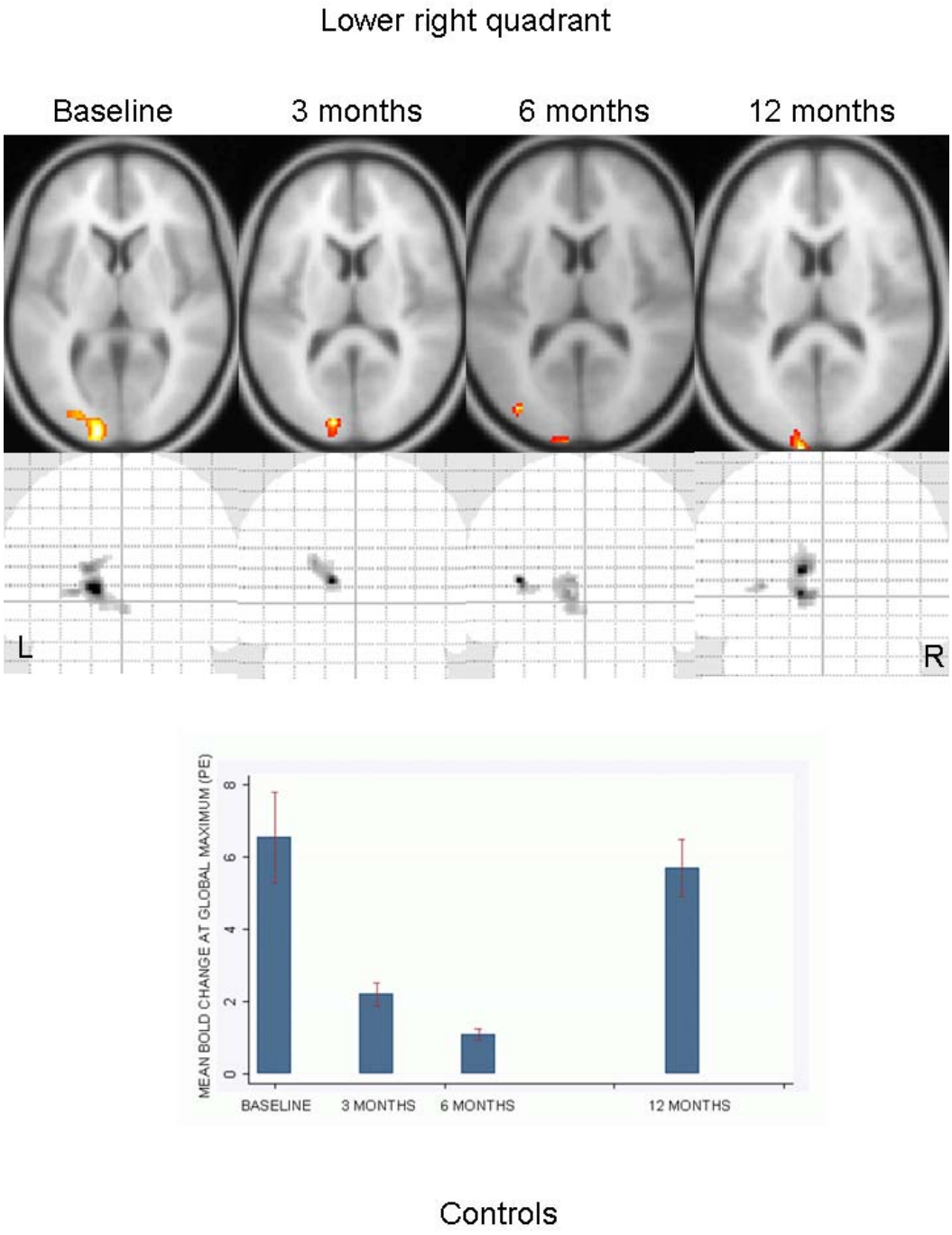

Figure 6.10 Statistical parametric maps showing fMRI activation in controls, over time, in response to lower right quadrant stimulation, overlaid on to an axial section of the SPM5 canonical MNI-152 brain template, and a coronal section of the SPM5 glass brain. The graph plots the global maximal parameter estimate (PE) at each of the four time-points, and the error bars represent 95% confidence intervals.

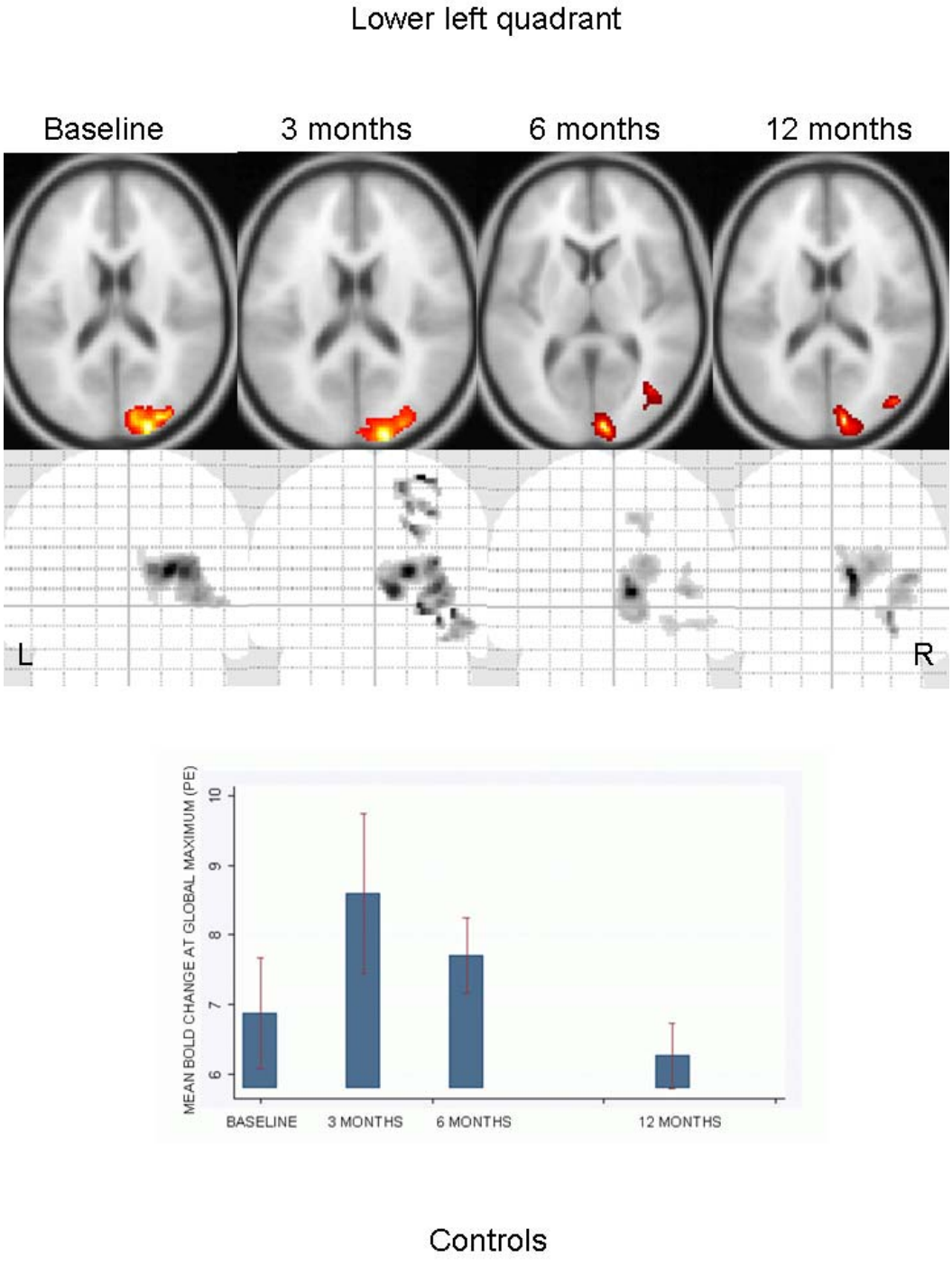

Figure 6.11 Statistical parametric maps showing fMRI activation in controls, over time, in response to lower left quadrant stimulation, overlaid on to an axial section of the SPM5 canonical MNI-152 brain template, and a coronal section of the SPM5 glass brain. The graph plots the global maximal parameter estimate (PE) at each of the four time-points, and the error bars represent 95% confidence intervals.

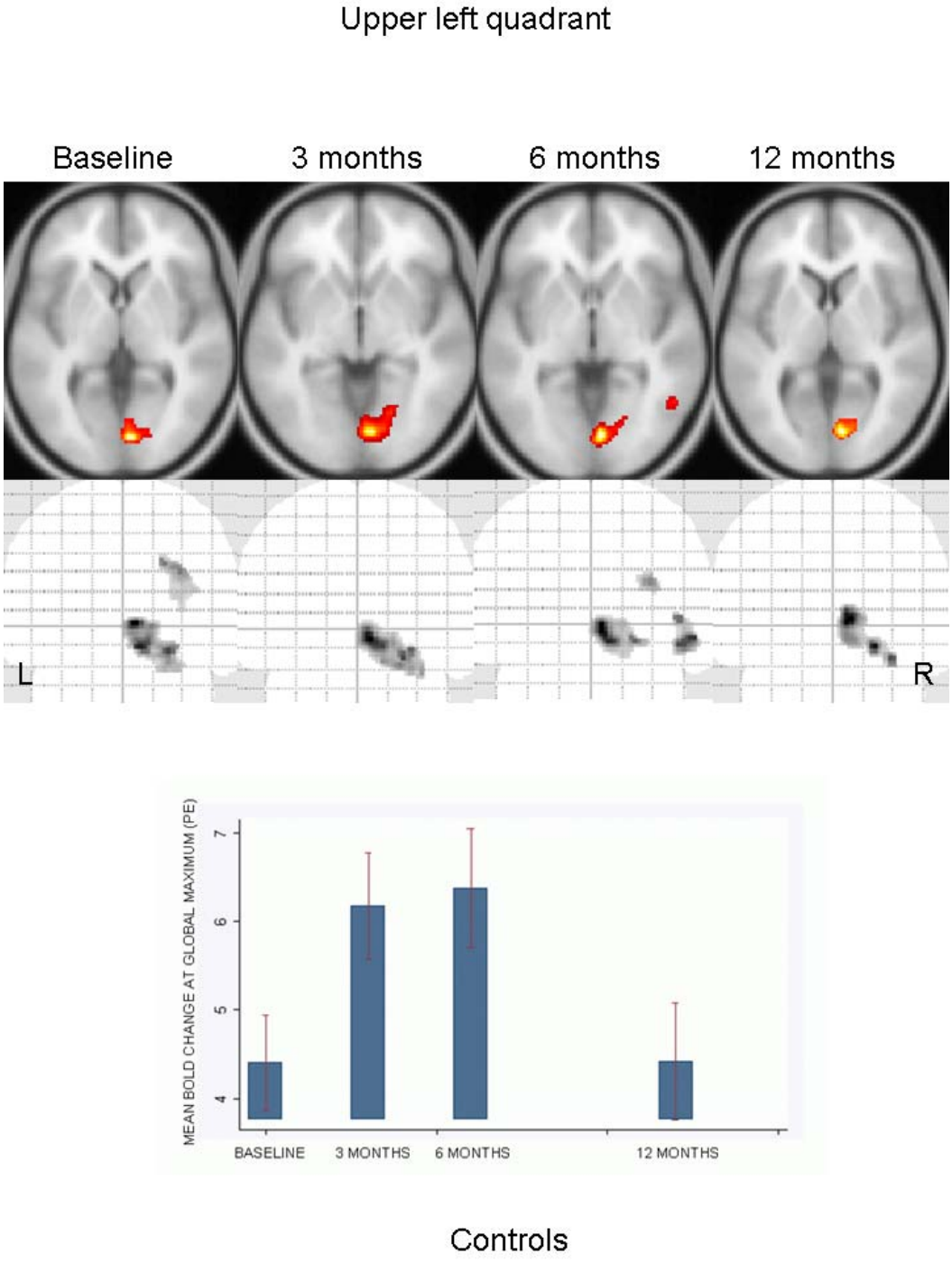

Figure 6.12 Statistical parametric maps showing fMRI activation in controls, over time, in response to upper left quadrant stimulation, overlaid on to an axial section of the SPM5 canonical MNI-152 brain template, and a coronal section of the SPM5 glass brain. The graph plots the global maximal parameter estimate (PE) at each of the four time-points, and the error bars represent 95% confidence intervals.

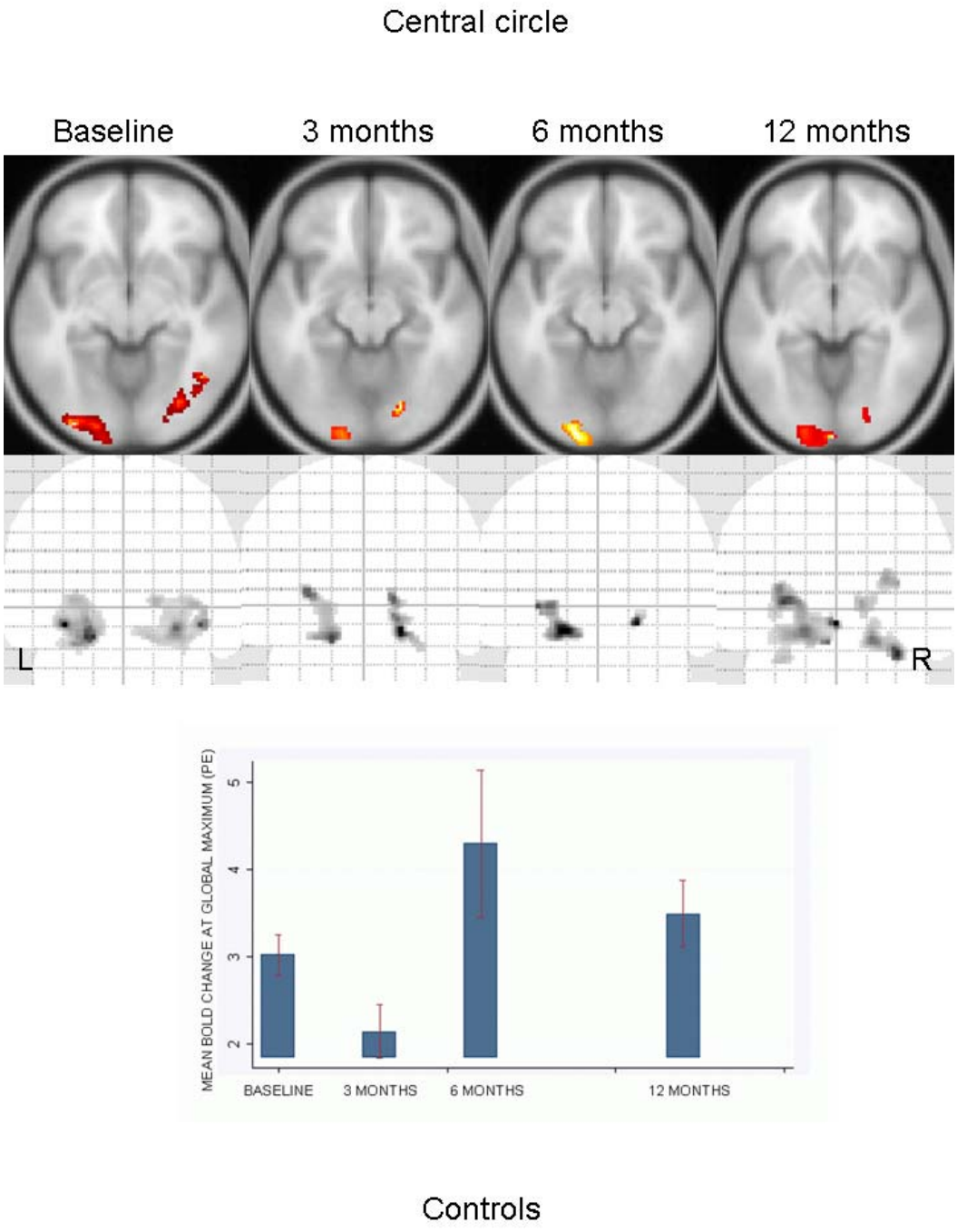

Figure 6.13 Statistical parametric maps showing fMRI activation in controls, over time, in response to stimulation of the central circle, overlaid on to an axial section of the SPM5 canonical MNI-152 brain template, and a coronal section of the SPM5 glass brain. The graph plots the global maximal parameter estimate (PE) at each of the four time-points, and the error bars represent 95% confidence intervals.

Accurate lateralisation was demonstrated and reasonable localisation above, or below, the calcarine fissure. The voxel-based longitudinal models, including all available data, showed no significant changes over time. Examining the graphs, no clear pattern of change in the global maximal signal change was evident.

6.3.4.1.2 Voxel-based: longitudinal changes

Longitudinal models, including all available data, showed no significant changes over time in the control group.

6.3.4.1.3 Voxel-based: differences between eyes

There were no differences between the two control eyes.

6.3.4.1.4 Regions-of-interest: longitudinal changes

There were no longitudinal changes over time in the control group.

6.3.4.1.5 Regions-of-interest: differences between eyes

There were no differences between the two control eyes.

6.3.4.2 Patients: affected and fellow eyes

6.3.4.2.1 Voxel-based: cross-sectional fMRI responses

Figures 6.14-6.18 illustrate group activation in patients, for each of the four quadrants and the central circle, at each time-point, for both the affected and fellow eye.

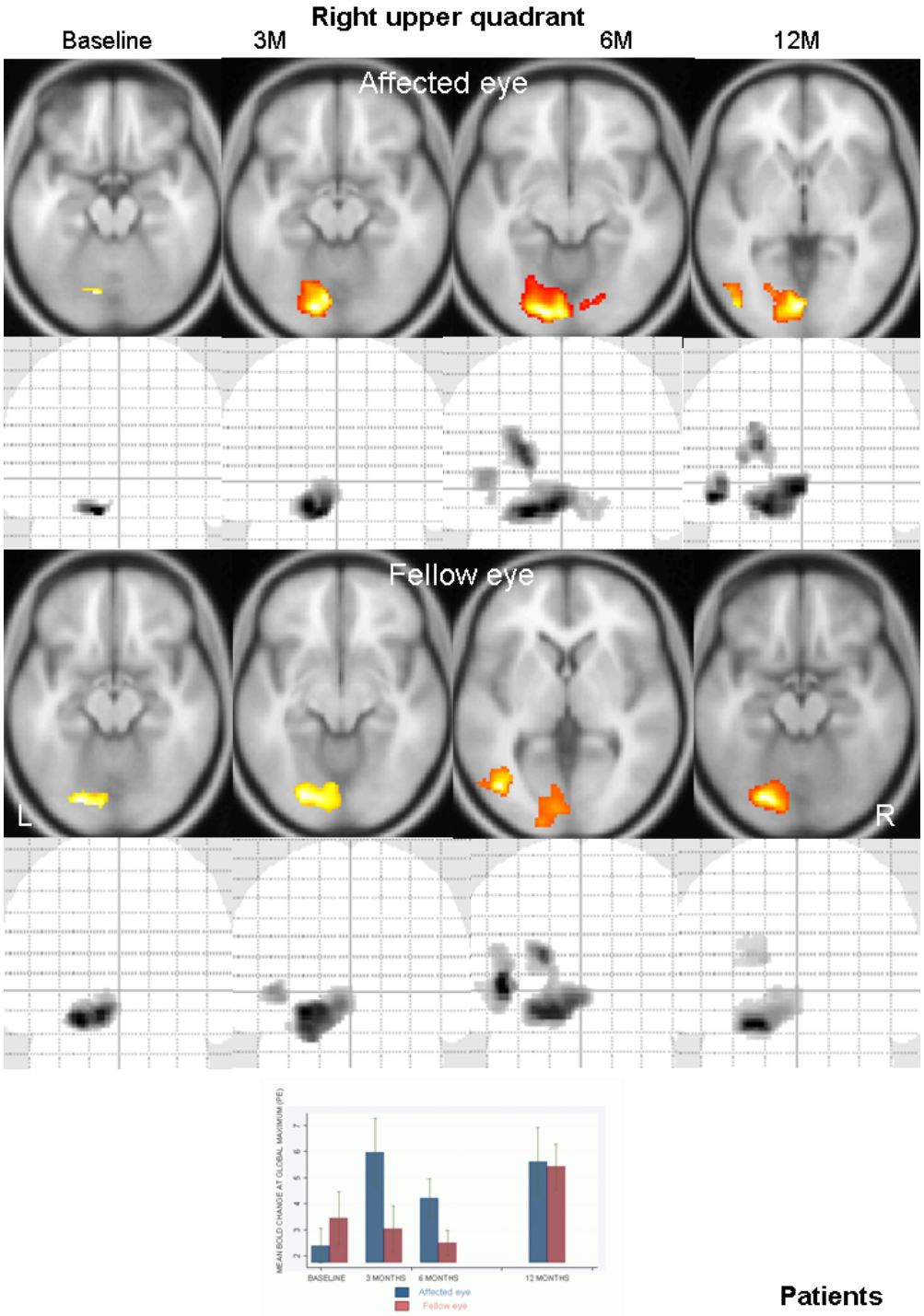

Figure 6.14 Statistical parametric maps showing fMRI activation in patients, in the affected and fellow eyes, over time, in response to stimulation of the right upper quadrant, overlaid on to an axial section of the SPM5 canonical MNI-152 brain template, and a coronal section of the SPM5 glass brain. The graphs plot the group mean global maximal parameter estimate at each of the four time-points, for the affected eye (in blue) and the fellow eye (in pink). The error bars represent 95% confidence intervals.

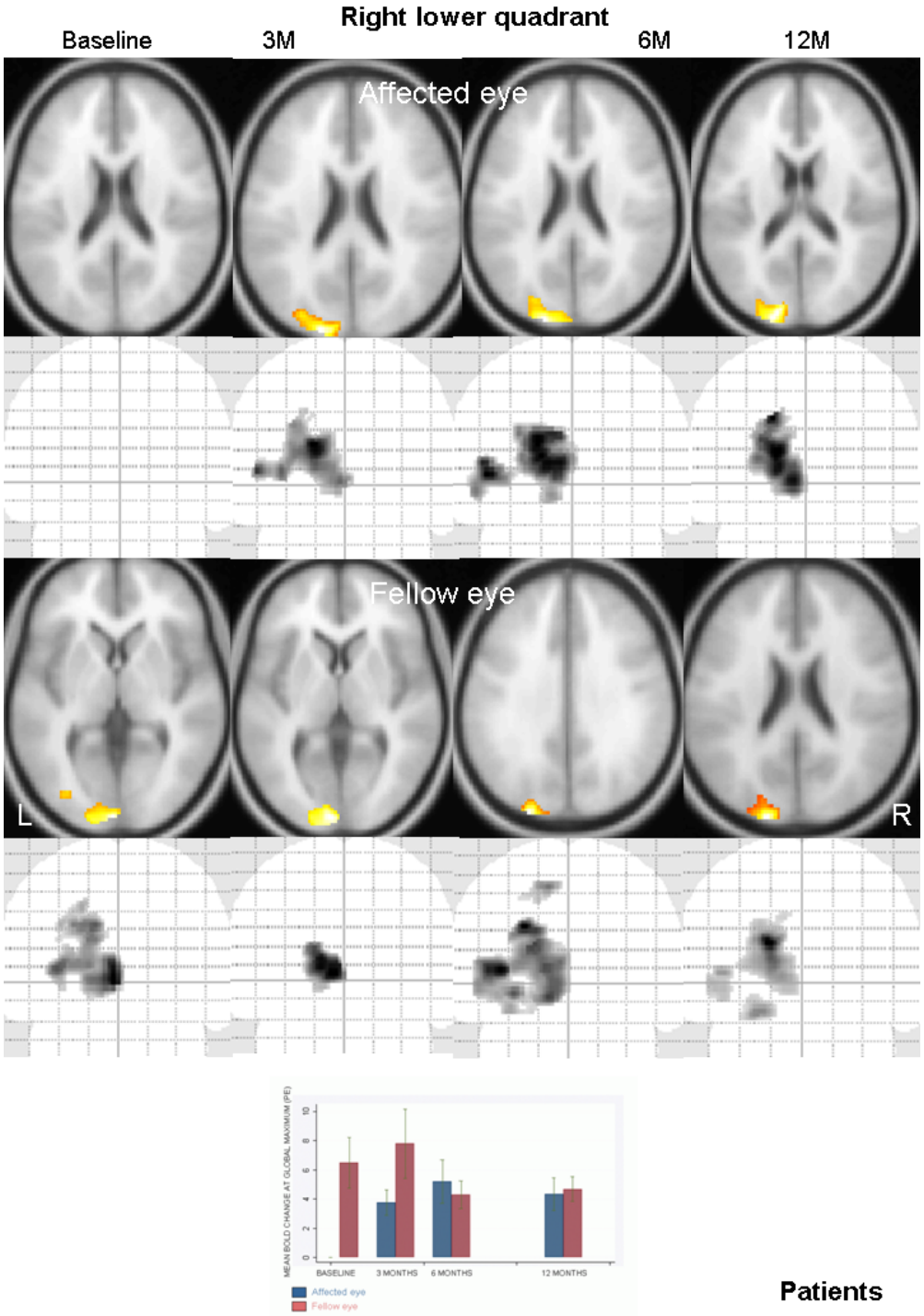

Figure 6.15 Statistical parametric maps showing fMRI activation in patients, in the affected and fellow eyes, over time, in response to stimulation of the right lower quadrant, overlaid on to an axial section of the SPM5 canonical MNI-152 brain template, and a coronal section of the SPM5 glass brain. The graphs plot the group mean global maximal parameter estimate at each of the four time-points, for the affected eye (in blue) and the fellow eye (in pink). The error bars represent 95% confidence intervals.

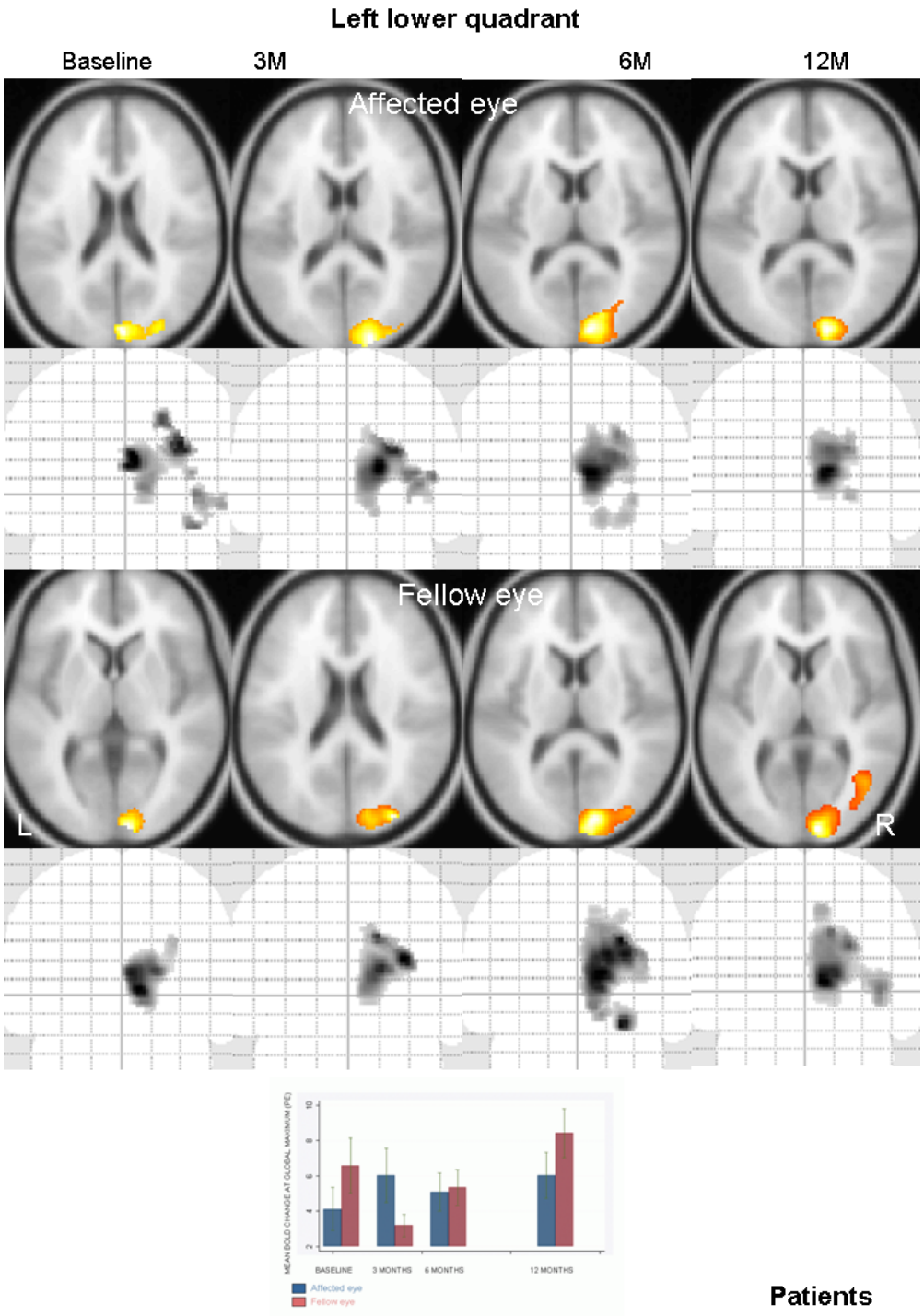

Figure 6.16 Statistical parametric maps showing fMRI activation in patients, in the affected and fellow eyes, over time, in response to stimulation of the left lower quadrant, overlaid on to an axial section of the SPM5 canonical MNI-152 brain template, and a coronal section of the SPM5 glass brain. The graphs plot the group mean global maximal parameter estimate at each of the four time-points, for the affected eye (in blue) and the fellow eye (in pink). The error bars represent 95% confidence intervals.

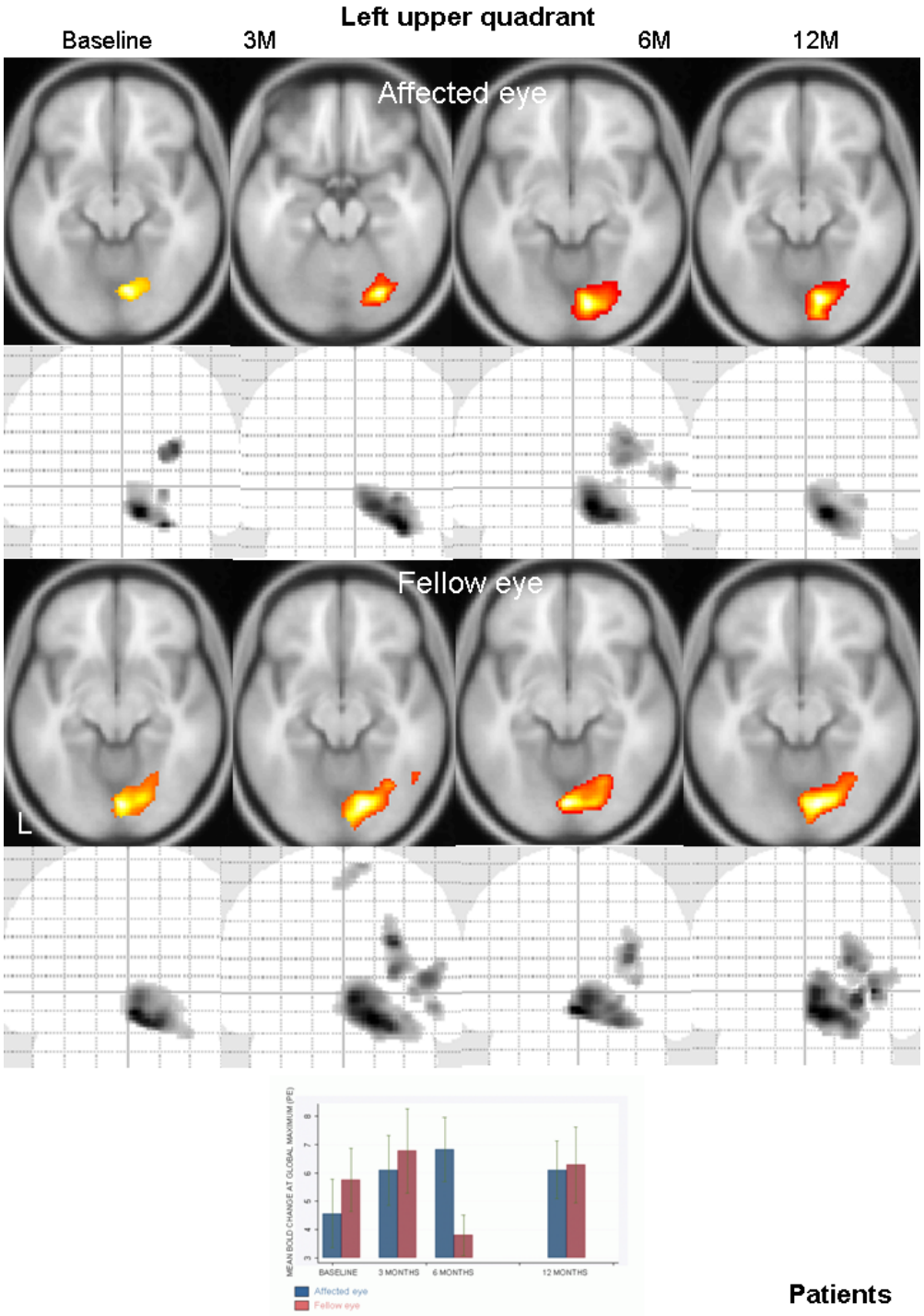

Figure 6.17 Statistical parametric maps showing MRI activation in patients, in the affected and fellow eyes, over time, in response to stimulation of the left upper quadrant, overlaid on to an axial section of the SPM5 canonical MNI-152 brain template, and a coronal section of the SPM5 glass brain. The graphs plot the group mean global maximal parameter estimate at each of the four time-points, for the affected eye (in blue) and the fellow eye (in pink). The error bars represent 95% confidence intervals.

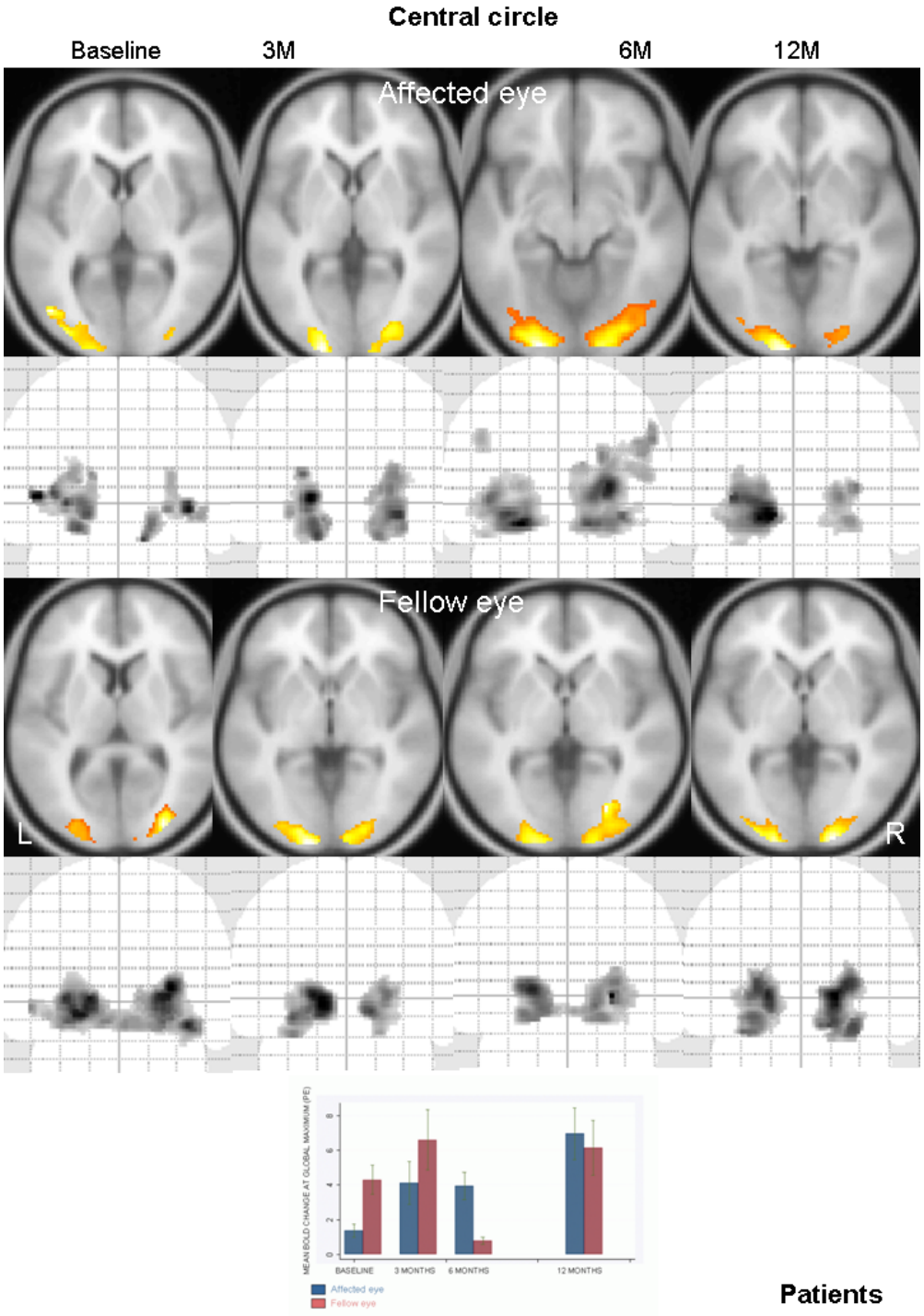

Figure 6.18 Statistical parametric maps showing MRI activation in patients, in the affected and fellow eyes, over time, in response to stimulation of the central circle, overlaid on to an axial section of the SPM5 canonical MNI-152 brain template, and a coronal section of the SPM5 glass brain. The graphs plot the group mean global maximal parameter estimate at each of the four time-points, for the affected eye (in blue) and the fellow eye (in pink). The error bars represent 95% confidence intervals.

There were no significant longitudinal changes in the spatial extent of activation and no clear evidence of extra-striate activation. The mean global maximal response in the affected eye was lower than fellow at baseline, but increased over time, and no differences were evident at 12 months.

6.3.4.2.2 Voxel-based: longitudinal changes

No significant longitudinal changes were seen in the patient group over time, either in the affected eye or the fellow eye.

6.3.4.2.3 Voxel-based: affected versus fellow

No significant differences between patients' affected and fellow eye responses were seen at any time-point.

6.3.4.2.4 Regions-of-interest: longitudinal changes in affected and fellow eyes

Longitudinal changes in the fMRI response in the regions-of-interest in the patient group, on stimulation of the affected and fellow eyes, are summarised in Figure 6.19.

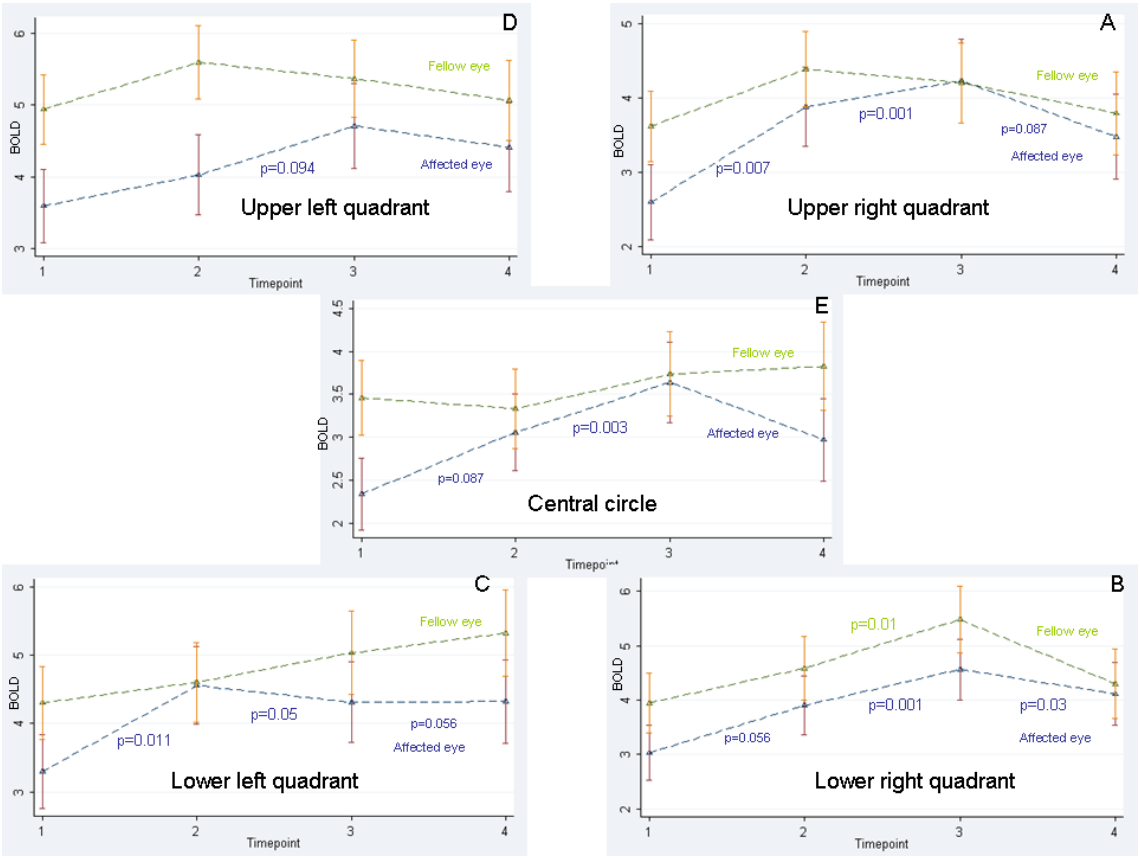

Figure 6.19 Graphs illustrate changes in fMRI response over time, for each of the four quadrants and the central circle. The bars show standard errors. All significant ($p<0.05$) and borderline ($p<0.1$) p values are shown. For clarity, p values >0.1 are not shown. The scale on the y axis refers to the group mean extracted parameter estimates, a measure of BOLD response. BOLD-blood oxygenation level dependent.

Region	Baseline to 3 months Rate of change (BOLD parameter estimate /month)			Baseline to 12 months Rate of change (BOLD parameter estimate /month)			Difference at 12 months (Aff-fellow)	
	Rate	95% CI	p value	Rate	95% CI	p value	BOLD	p
Aff central	0.24	-0.03,0.51	NS	0.05	-0.02,0.13	NS	-0.73	NS
Fell central	0.04	-0.35,0.27	NS	0.03	-0.05,0.12	NS		
Aff right upper	**0.43**	**0.12,0.74**	**0.007**	0.07	-0.01,0.15	NS	-0.15	NS
Fell right upper	0.26	-0.08,0.59	NS	0.01	-0.08,0.11	NS		
Aff right lower	0.29	-0.01,0.59	NS	**0.09**	**0.01,0.17**	**0.03**	0.00	NS
Fell right lower	0.21	-0.15,0.58	NS	0.03	-0.07,0.13	NS		
Aff left lower	**0.42**	**0.10,0.74**	**0.011**	0.09	0.00,0.17	NS	-0.66	NS
Fell left lower	0.10	-0.30,0.49	NS	0.08	-0.02,0.19	NS		
Aff left upper	0.14	-0.27,0.56	NS	0.07	-0.04,0.18	NS	-0.60	NS
Fell left upper	0.22	-0.09,0.53	NS	0.01	-0.07,0.10	NS		

Table 6.4 Rates of change in fMRI activity between baseline and three months, and baseline and 12 months, derived from the linear regression models. The p-value refers to the significance of the slope. The residual difference between affected and fellow eyes at twelve months is reported. The p-values are derived from a two-sample t-test. Aff-affected, BOLD- blood oxygenation level-dependent, CI-confidence intervals, Fell-fellow, NS-non-significant.

There was at least a trend for an increase in the fMRI response in all regions between baseline and three months, except in the left upper quadrant, in which the improvement was not significant at three months, and was borderline at six months. After six months, increases reached a plateau. The only significant changes in the fellow eye were for the lower right quadrant, with an increase between baseline and six months. There were no significant decreases in fellow eye fMRI response.

6.3.4.2.5 Regions-of-interest: affected versus fellow eyes

The magnitude and significance of differences in BOLD response between affected and fellow eyes, in each region-of-interest, are summarised in Table 6.5.

Region	Baseline % diff (p value)	3 months % diff (p value)	6 months % diff (p value)	12months % diff (p value)
Central circle	**-32% (0.017)**	-8% (0.551)	-3% (0.898)	-22% (0.231)
Right upper quadrant	**-28% (0.025)**	-12% (0.212)	+1% (0.856)	-8% (0.794)
Right lower quadrant	**-23% (0.006)**	-15% (0.107)	-17% (0.061)	-4% (1.000)
Left lower quadrant	-23% (0.061)	-1% (0.656)	-14% (0.269)	-19% (0.124)
Left upper quadrant	**-27% (0.040)**	**-28% (<0.001)**	-12% (0.456)	-13% (0.188)

Table 6.5 Differences in BOLD fMRI response between affected and fellow eyes, from the region-of-interest analysis. The percentage mean difference in BOLD change is reported, with respect to the affected eye (for example, a difference of -32% indicates that the BOLD signal change was 32% less in the affected eye than the fellow). The associated p values are reported in parentheses, which were derived from two-sample paired t-tests. Significant results are highlighted in bold.

Fellow eye responses were greater than affected eye responses at baseline. At three months, there were no significant differences between the two eyes, except for the left upper quadrant, in which recovery of fMRI response appeared to lag behind. This is the same quadrant in which recovery of VEP amplitude was slower (Figure 6.7). It also had the lowest mean visual score at three months (Table 6.1). There were no significant differences between eyes for the other regions at three months, and for any regions at six or 12 months.

6.3.4.3 Patients versus controls

6.3.4.3.1 Voxel-based

No significant differences were found between controls and patients, for either the affected or fellow eye, using the voxel-based analysis approach.

6.3.4.3.2 Regions-of-interest

Differences in BOLD responses for corresponding regions in patients and controls are summarised in Table 6.6.

Region	Affected/fellow eye	Baseline % diff (p value)	3 months % diff (p value)	6 months % diff (p value)	12months % diff (p value)
Central circle	Affected vs controls	-31% (0.186)	-3% (0.858)	+56% (0.193)	-2% (0.983)
	Fellow vs controls	-6% (0.783)	+20% (0.514)	+1% (0.960)	+13% (0.639)
Right upper quadrant	Affected vs controls	-41% (0.119)	+14% (0.491)	-5% (0.915)	-18% (0.895)
	Fellow vs controls	-18% (0.396)	+9% (0.590)	+13% (0.465)	-12% (0.957)
Right lower quadrant	**Affected vs controls**	**-51% (0.011)**	-7% (0.664)	+20% (0.460)	+6% (0.605)
	Fellow vs controls	-15% (0.575)	-5% (0.874)	+35% (0.247)	-11% (0.831)
Left lower quadrant	Affected vs controls	-39% (0.052)	-10% (0.568)	-15% (0.568)	-18% (0.481)
	Fellow vs controls	-3% (0.898)	+1% (0.892)	-7% (0.724)	-1% (0.990)
Left upper quadrant	**Affected vs controls**	**-40% (0.021)**	-24% (0.217)	+11% (0.666)	0% (0.852)
	Fellow vs controls	+8% (0.680)	+14% (0.230)	+28% (0.301)	+28% (0.320)

Table 6.6 Differences in BOLD fMRI response between patients and controls, from the region-of-interest analysis. The percentage mean difference in BOLD response is reported, with respect to patients (for example, a difference of -31% indicates that the BOLD signal change was 31% less in the patients' eyes than the controls). The associated p value is reported in parentheses, derived from a two-sample unpaired t-test. Significant results are highlighted in bold font.

Differences were identified between patients' affected eyes and controls at the baseline time-point only. At this time, patients' affected eye responses were smaller than controls, although this did not reach statistical significance in all regions.
There were no significant differences between fellow eye and control responses at any time-point.

6.3.5 Correlation analysis

6.3.5.1 Clinical-electrophysiological correlations

There were strong correlations between region-specific Humphrey visual field scores and region-specific VEP amplitude for all of the quadrants and the central circle at the baseline time-point (Table 6.7). The direction of the association indicated that greater VEP amplitude was associated with better vision.

Region	Partial correlation coefficient (r)	P value
Central circle	**0.83**	**<0.001**
Right upper quadrant	**0.57**	**0.002**
Right lower quadrant	**0.78**	**<0.001**
Left lower quadrant	**0.56**	**0.003**
Left upper quadrant	**0.53**	**0.006**

Table 6.7 Correlations between region-specific VEP amplitude and region-specific Humphrey scores, for each of the four quadrants and the central circle of the affected eye, at baseline. CI-confidence interval.

There was borderline significance for an association between baseline VEP latency and visual function for the central circle (r=-0.41, p=0.091), with people with shorter latencies tending to have better vision. No significant associations were found for the quadrants (RUQ p=0.722; RLQ p=0.310, LLQ p=0.783, LUQ p=0.783).

6.3.5.2 FMRI correlations with clinical data

6.3.5.2.1 Voxel-based

Using a voxel-based whole brain approach, regions of correlation were found at baseline between affected eye region-specific Humphrey scores and affected eye region-specific fMRI activation, on stimulating the central circle (Figure 6.20A), left

lower quadrant (Figure 6.20D), and left upper quadrant (Figure 6.20E). A greater fMRI response was associated with better vision. No significant regions were found for the right upper or lower quadrants.

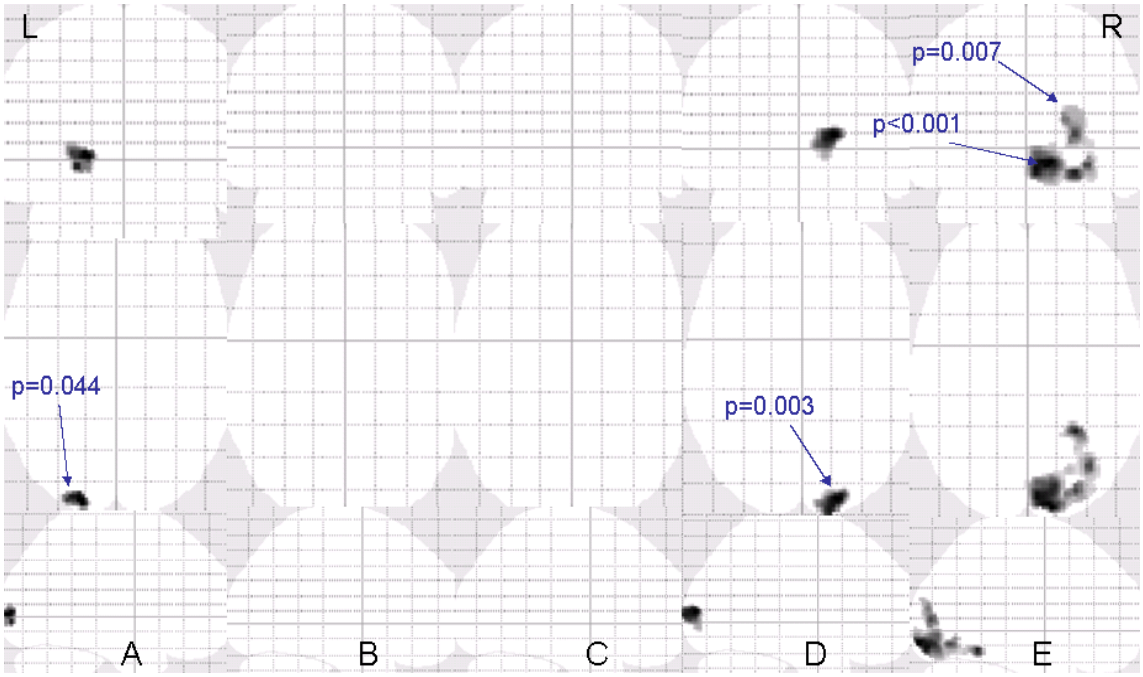

Region of stimulation	Figure	MNI coordinates	Region
Central circle	6.20A	-18 -94 2	Left visual cortex
Left lower quadrant	6.20D	20 -90 8	Right visual cortex
Left upper quadrant	6.20E (upper cluster)	14 -92 -6	Right visual cortex Right fusiform gyrus Right inferior occipital gyrus
Left upper quadrant	6.20E (lower cluster)	28 -82 8	Right superior occipital gyrus Right middle occipital gyrus

Figure 6.20 Regression of region-specific Humphrey scores against region-specific fMRI activations, for (A) the central circle, (B) upper right, (C) lower right, (D) lower left and (E) upper left quadrants of the affected eye, at baseline, overlaid on to the SPM5 glass brain, in coronal, axial and sagittal planes. The maps are thresholded at $p<0.05$ (corrected). The table indicates the location of the clusters. The Montreal Neurological Institute (MNI) coordinates refer to the centre of the global maximal cluster.

6.3.5.2.2. Regions-of-interest

There were associations between affected eye vision and affected eye fMRI response in all regions at baseline, but not for any regions on fellow eye stimulation (Table 6.8). A greater fMRI response was associated with better vision.

Stimulation	Partial correlation coefficient (r)	p value
Affected central circle	**0.52**	**0.005**
Affected right upper quadrant	**0.26**	**0.016**
Affected right lower quadrant	**0.45**	**0.018**
Affected left lower quadrant	**0.45**	**0.004**
Affected left upper quadrant	**0.54**	**<0.001**
Fellow central circle	0.08	0.694
Fellow right upper quadrant	-0.14	0.898
Fellow right lower quadrant	0.26	0.234
Fellow left lower quadrant	-0.09	0.912
Fellow left upper quadrant	-0.24	0.530

Table 6.8 Correlations between region-specific fMRI response and region-specific Humphrey scores, for each of the quadrants and the central circle, at baseline. Significant associations are highlighted in bold type.

6.3.5.3 FMRI correlations with electrophysiological data

6.3.5.3.1 Voxel-based

Associations were found at baseline between region-specific affected eye VEP amplitude and region-specific affected eye fMRI response for the central circle (Figure 6.21A) and left upper quadrant (Figure 6.21E). A greater fMRI response was associated with greater amplitude VEPs.

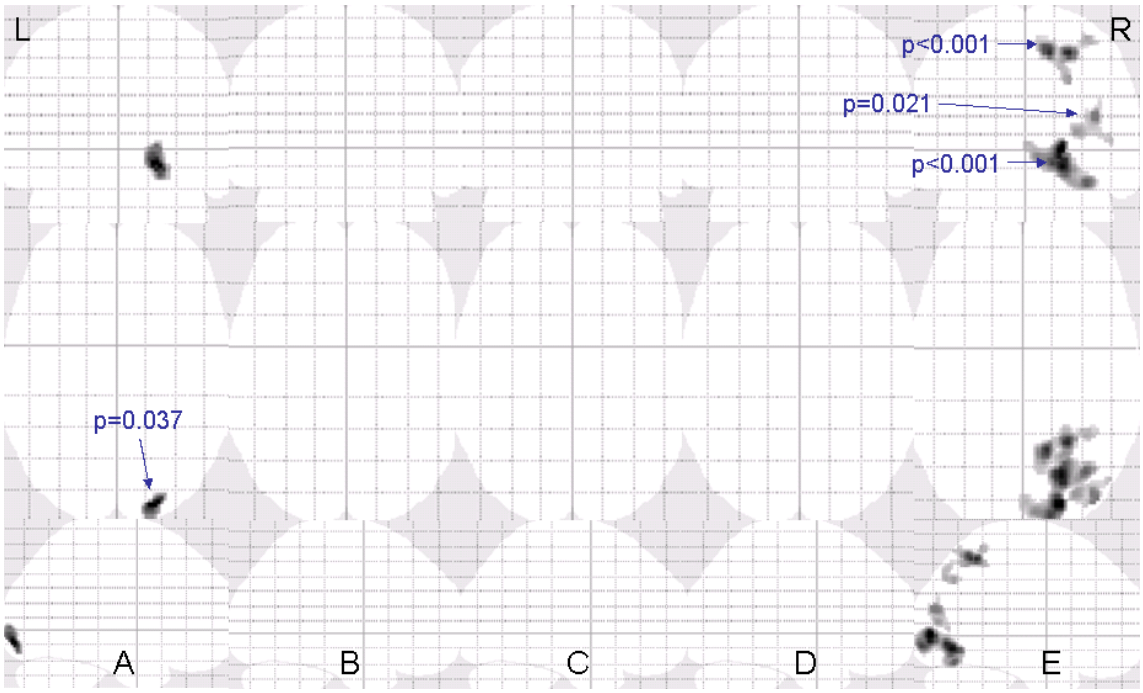

Region of stimulation	Figure	MNI coordinates	Region
Central circle	6.21A	22 -90 -6	Right visual cortex
Left upper quadrant	6.21E (upper cluster)	26 -50 54	Right post-central gyrus Right precuneus Right superior parietal lobule Right superior occipital gyrus
Left upper quadrant	6.21E (middle cluster)	42 -80 18	Right middle occipital gyrus Right middle temporal gyrus
Left upper quadrant	6.21E (lower cluster)	22 -84 2	Right visual cortex

Figure 6.21 Regression of region-specific VEP amplitude against region-specific fMRI activations, for (A) the central circle, (B) upper right, (C) lower right, (D) lower left and (E) upper right quadrants of the affected eye, at baseline, overlaid on to the SPM5 glass brain, in coronal, axial and sagittal planes. The maps are thresholded at $p<0.05$ (corrected).

The left upper quadrant correlations were right-sided, which is consistent with the retinotopic organisation. They were localised above the calcarine sulcus, extending into higher processing areas of the parietal lobe. Bilateral occipital activation was seen on stimulation of the central circle at lower thresholds, but the left sided occipital cluster did not reach statistical significance.

No significant associations were found between affected eye VEP latency and occipital fMRI responses at baseline.

6.3.5.3.2 Regions-of-interest

Associations were found between affected eye region-specific VEP amplitude and region-specific fMRI response, at baseline, on stimulation of the central circle, right lower and left upper quadrants (Table 6.9). For all associations, a greater fMRI response was associated with greater VEP amplitude. There were no associations between fellow eye fMRI responses and affected eye VEP amplitude.

Stimulation	Partial correlation coefficient (r)	p value
Affected central circle	**0.46**	**0.003**
Affected right upper quadrant	0.33	0.147
Affected right lower quadrant	**0.33**	**0.029**
Affected left lower quadrant	0.13	0.675
Affected left upper quadrant	**0.47**	**0.010**
Fellow central circle	0.03	0.766
Fellow right upper quadrant	-0.02	0.901
Fellow right lower quadrant	0.20	0.146
Fellow left lower quadrant	-0.30	0.135
Fellow left upper quadrant	-0.15	0.885

Table 6.9 Correlations between region-specific fMRI response and region-specific VEP amplitude, for each of the four quadrants and the central circle, at baseline. Significant associations are highlighted in bold type.

No correlations were found with VEP latency in either eye.

6.4 Discussion

In this study, the feasibility of combining region-specific clinical data, electrophysiology, and fMRI data was investigated, and used to study recovery from visual field defects in ON, including the role of the fellow eye. With regard to the

primary hypotheses, these data did not demonstrate any convincing evidence of regional susceptibility to damage, extra-striate fMRI activation contributing to visual recovery, or supra-normal fMRI activity on stimulating the fellow eye.

The conclusions that may be drawn from this data are now discussed. In general terms, there are two main possibilities for each of the hypotheses investigated; either the effect under investigation does not exist, or the methodology used has failed to detect it.

6.4.1 No regional susceptibility to damage

There were no differences between the different regions in severity of visual loss, either acutely or during follow-up. The central region had the lowest mean visual score during the acute stage at baseline, and the upper quadrants the lowest at 12 months, but there were no statistically significant differences between groups. This is in line with previous studies that have shown a wide variety of different defects (Keltner et al., 1993b), and suggests that fibres in the optic nerve are affected randomly by the patchy inflammatory process, and there is no clear evidence that any optic nerve axons are more susceptible to damage or repair than others.

With regard to clinical testing, the small improvements seen over time in fellow eye Humphrey scores are likely to reflect a practice effect.

6.4.2 No evidence for extra-striate responses to region-specific activation

The results of the fMRI experiments are more complex, and could be explained in three ways; either region-specific extra-striate plasticity does not contribute to recovery from visual field defects, or it occurs but varies in location (and perhaps timing) in individual patients, explaining the lack of group effects, or the methodology applied has failed to detect it.

There is a growing body of evidence for the importance of adaptive plasticity in recovery from ON (Werring et al., 2000;Toosy et al., 2002;Toosy et al., 2005;Levin et al., 2006;Korsholm et al., 2007), and abundant evidence in other neurological conditions (Frackowiak, 1997;Comi et al., 2004;Desmurget et al., 2007;Johansen-Berg, 2007;Di Filippo et al., 2008). Results previously reported from this cohort of patients, in Chapters 4 and 5 of this thesis, suggested the occurrence of compensatory

neuroplasticity, with areas of commonality detectable at group level, interacting with visual function at baseline, and contributing to visual outcome. However, these results were obtained using an fMRI visual paradigm comprising whole field stimulation, and logMAR acuity as a visual outcome measure. LogMAR acuity is sensitive to abnormalities of central vision, which is of primary clinical importance to the patient, but is not sensitive to peripheral field pathology. In addition, whole field fMRI stimulation results in responses dominated by central field effects. This was the reason for including a quadrant-specific paradigm, as it was hypothesised that plastic mechanisms might also be important in peripheral recovery. However, the present study failed to demonstrate any convincing evidence of extra-striate fMRI activation in response to region-specific stimulation. None was seen on investigating the main effect of stimulation in patients, there were no differences between affected and fellow eyes, and no differences between patients and controls.

One possible interpretation of these contrasting results is that neuroplasticity is genuinely less important in recovery from peripheral defects than for central vision. Previous large studies from the ONTT cohort reported that peripheral defects in sensitivity were more frequent than central defects at six months (Fang et al., 1999), but after three years the relationship had reversed and residual problems with central vision were more common (Keltner et al., 1999), which may suggest a differential response to recovery processes in different regions of the visual field, at different times. It is possible that reorganisation responses are triggered and modulated in a hierarchical manner, depending on functional importance. When plasticity is evident, it appears to occur during the acute phase of ON, and if it genuinely does not contribute to recovery of the peripheral field, this could explain why recovery was less good in the ONTT cohort peripherally at six months. However, this does not explain why extra-striate responses were not evident on central field stimulation. In addition, a different recovery process would have to be postulated to explain the later reversal in frequency of residual defects. It also seems unlikely that mechanisms of repair should differ so much, in the absence of any clear evidence of a differential susceptibility to damage, either during the acute phase, or following recovery.

The second possibility is that neuroplasticity in response to peripheral field defects is a more heterogeneous process than for central field defects and occurs in different anatomical locations, and perhaps at different times, following symptom onset in different individuals. The heterogeneity of patterns of visual field defects which is

seen clinically could be consistent with this interpretation. For example, if neuroplasticity was occurring through a mechanism of map expansion, then the anatomical location of fMRI activity might differ greatly depending on the retinotopic cortical location of reduced afferent input. Similarly, if cross-modal reassignment was occurring, it is possible that the regions of extra-striate cortex recruited might be anatomically more adjacent to the region of reduced afferent input. For example, ventral stream higher processing areas might be recruited in response to reduced neuronal input in infra-calcarine regions (representing upper field defects), and dorsal stream areas in response to reduced input in supra-calcarine regions (representing lower field defects). Whilst this is a possibility, it remains speculative, and would be difficult to confirm or refute experimentally.

Lastly, there is the possibility that the experimental approach used was insufficiently sensitive to detect any effects of interest which may, or may not, have been present. This is the first study to apply a quadrant-specific fMRI stimulation paradigm; all previous studies have used either whole field (Rombouts et al., 1998;Gareau et al., 1999;Werring et al., 2000;Russ et al., 2002;Toosy et al., 2002;Langkilde et al., 2002;Toosy et al., 2005;Levin et al., 2006;Korsholm et al., 2007) or hemi-field (Langkilde et al., 2002) stimuli. The idea was that this would address the problem of heterogeneity of defects at the stage of data acquisition, rather than the analysis stage. However, region-specific stimulation activated a relatively smaller proportion of the visual field than either the hemi-field or whole field methods. In particular, selective stimulation of the peripheral quadrants tended to result in smaller changes in fMRI signal, perhaps because of the lower density of retinal photoreceptors in these regions, compared with the macula. However, stimulation with the central circle also resulted in relatively less fMRI activity than anticipated. This could also be methodological. A fixation cross was presented together with the central circle, as described in Chapter 3, and some control subjects in the pilot study reported that it intermittently disappeared. This was likely to be due to a phenomenon called background "filling in" (Ramachandran and Gregory, 1991;Weil et al., 2007), which may occur in the context of two competing stimuli, and it is possible that this affected the fMRI signal. Another difficulty that arose using the region-specific approach was the influence of inter-individual variability, both in severity of visual loss and, more importantly, in visual cortical anatomy. This variability is a problem common to all studies in which group effects are of interest. However, inter-individual variability in the cortical

representation of visual areas may be especially large, which is becoming apparent with the increased application of retinotopic mapping techniques. Therefore, together these factors may have resulted in a reduction of sensitivity to detect effects of disease and responses to them.

This hypothesis is supported by the results of the correlation analyses. The issue of multiple comparison testing, previously discussed in section 5.1.4.5, is also relevant here. Associations between visual function and fMRI activation were modest using both the voxel-based and region-of-interest approaches, and were only evident for 2/5 conditions using the former method and 3/5 for the latter. These modest region-specific correlations are in contrast to the results of whole field visual stimulation, reported in Appendix III, in which more robust activation and correlations with clinical scores were seen. For example, using whole field stimulation, physiologically anticipated associations were demonstrated between fMRI signal and vision in primary visual areas during the acute phase. This was not apparent for some of the quadrants using more localised region-specific stimuli, probably for the reasons discussed; relatively low signal-to-noise, high inter-individual anatomical variability in cortical representation in those areas, and also possibly the slight inequalities in the proportion of the visual field sampled during fMRI, VEP and clinical data acquisition. Together, these factors could explain why no evidence for plasticity was demonstrated, as this effect might reasonably be expected to be more subtle than clinical-fMRI or VEP amplitude-fMRI associations.

Some of these difficulties were compounded by the mass univariate voxel-based analysis approach. In general, the region-of-interest approach appeared more sensitive to detecting effects-of-interest, for example, strong correlations were demonstrated between extracted fMRI parameters and both VEP amplitude and Humphrey scores in all regions. This illustrates some generic difficulties in studying plasticity in a condition such as ON. There are only two studies which have detected evidence of plasticity using a whole brain voxel-based analysis approach (Werring et al., 2000;Toosy et al., 2005), and more recent studies have generally focused on regions-of-interest identified from previous work. It is likely that difficulties in demonstrating plasticity using a voxel-based approach are related partly to the subtlety of the effect in ON. FMRI detects small increases in local blood flow representing averaged neural events occurring at sub-cellular level (Logothetis et al., 2001). In ON, these changes

are in response to localised pathology in a remote white matter tract, namely the optic nerve. The magnitude of detected cortical responses is smaller in ON than in conditions of direct brain injury, such as ischaemic stroke and brain tumours. In addition, the disease process in ON results in a direct reduction of afferent input to the cortical regions under investigation, resulting in reduced fMRI signal, and complicating detection of effects-of-interest. These two-way interactions between fMRI response, structural damage and clinical effects have been explored in previous chapters of this thesis. These difficulties may be compounded by the multiple comparisons corrections necessary using a whole brain voxel-based approach.

This leads to the issue of thresholding statistical parametric maps. There is no universal agreement on what constitutes a "robust" threshold, and the level selected has varied considerably in the literature. The decision depends on many factors, including sample size, signal characteristics of the effect under investigation (Friston et al., 1994), and effect size. The correction for multiple comparisons in SPM is implemented using random field theory (Chapter 2). This may be addressed at either voxel or cluster level. Cluster-level inference relies on the signal of interest being more spatially extended than the noise coherence, and tends to be a more sensitive and powerful method (Friston et al., 1996a), as it takes into account information in neighbouring voxels. However, at lower thresholds, it is more prone to false positives than the more conservative voxel-level inference strategy (Smith and Nichols, 2009). Therefore, interpretation of fMRI data can be complex, and requires caution, especially for longitudinal analyses. The approach used in this study was to select a threshold based on the results of a preliminary analysis of the control data, in order to identify a level at which physiologically anticipated fMRI activity was seen and noise successfully removed, and then apply it to the patient group. In this longitudinal dataset, this empirical solution resulted in the application of a relatively high cluster-level threshold of $p<0.001$ (corrected) which may have also contributed to missing genuine effects-of-interest in the patient group.

Therefore, it appears most likely that the results reported in this chapter represent a lack of sensitivity of the region-specific stimulation approach, and it remains unclear if region-specific responses to visual field defects occur or not. In the future, ongoing development and optimisation of fMRI hardware and analysis techniques may help address these problems, for example, multi-variate analysis, which has been applied to

detect subtle effects in the study of consciousness (Haynes and Rees, 2006). Future directions will be discussed in Chapter 7.

6.4.3 No evidence for supra-normal responses in fellow eye

Similarly, with regard to the role of the fellow eye, there are several possible interpretations of these results. It could be that fellow eye responses to region-specific stimulation are genuinely not important to recovery from localised visual field defects, or that they do occur but not in the regions investigated, or occur but have not been detected, through a type II error.

There is evidence from several previous studies (Toosy et al., 2005;Korsholm et al., 2007), and the previous chapters of this thesis, that fellow eye responses are abnormal in ON. However, the precise role of fellow eye responses remains unclear. The motivation for this part of the study was to clarify whether a dynamic increase in fMRI activity occurred in regions of early retinotopic cortex. However, there was no evidence for the occurrence of supra-normal responses in patients' fellow eyes, either in comparison to controls, or during the acute phase relative to later time-points.

This is less likely to be due to type II error than for the voxel-based analysis, as the region-of-interest approach used had greater sensitivity, for example, in detecting fMRI correlations with clinical and electrophysiological parameters. However, it illustrates the converse problem inherent in the approach. By definition, the extent of the brain which is assessed is limited and this could explain the failure to detect any differences in the fellow eye. Primary visual areas were selected, as it was possible to identify the relevant areas corresponding to the regions of stimulation, but it is possible that supra-normal changes were occurring in other brain regions, such as the LGN or higher visual areas, that were not studied.

Therefore, whilst it is possible to conclude with a greater degree of certainty that abnormal fellow eye responses genuinely did not occur in the visual cortical areas studied, it remains unclear whether undetected effects occurred elsewhere. It is interesting to note that for the left upper quadrant, the mean response was actually greater than in the control group, but this was not statistically significant and, therefore, must be interpreted as a chance effect, and would need to be confirmed by future studies in different patient cohorts. Nonetheless, it is mentioned as there were anomalies in other tests with regard to this quadrant, which will be discussed further.

6.4.4 Slow recovery in the left upper quadrant

During follow-up, recovery of VEP amplitudes in the left upper quadrant lagged behind the other regions. This correlated with a lag in improvement in fMRI responses, and the lowest mean visual score at three months. In contrast, fellow eye VEP amplitude decreased over time, which might be explained by subtle subclinical axonal loss, but was not evident on whole field testing, and is more likely to be technical, or related to habituation.

The lagged recovery in affected eye electrophysiology and fMRI in the left upper quadrant could be explained through a chance differential effect of damage mechanisms; possibly oedema, inflammation and the resulting conduction block took slightly longer to resolve in this region, and this also influenced the resulting fMRI response. It seems less likely that demyelination was more severe in the fibres of the optic nerve related to this region, given that the region-specific VEP latency was not prolonged. More severe axonal loss is a possibility that merits consideration. Previous studies have found that peripheral areas recover progressively less completely, perhaps secondary to reduced axonal redundancy (Fang et al., 1999). However, this does not explain why the recovery rate was different from the other quadrants, and there were no residual defects.

Alternatively, the slower recovery observed in this region could be secondary to a differential effect of repair mechanisms, either by chance or perhaps for reasons of vascular supply, or provision of neurotrophic factors. The upper left quadrant of the visual field in each eye is represented by the lower right quadrant of each retina. Fibres from this region originating in the left eye decussate in the optic chiasm, whilst those from the right eye remain uncrossed. They then run together in the optic tract, and synapse in the LGN, with neurons whose axonal processes proceed in the optic radiations to the right occipital cortex, inferior to the calcarine fissure. There is no clear anatomical explanation why recovery should be slower in fibres which are part of this pathway, compared with the other peripheral regions. Therefore, the observation is noted, together with the higher mean fellow eye fMRI response than controls in this region, but is most likely due to chance.

6.4.5 Remyelination only evident on stimulation of central field

VEP latency decreased over 12 months in the central circle, but not in any of the quadrants, suggesting remyelination. Although this could indicate that there is prioritisation of repair for the most functionally eloquent fibres, it is more likely to represent a technical issue; macular stimulation results in greater amplitude responses than peripheral stimulation, which facilitates measurement of the P100 segment.

6.4.6 Conclusions and future challenges

Overall, many aspects of the mechanisms of damage and recovery of visual field defects in ON remain unclear. This was the first study to investigate this using quadrant-specific fMRI, and combining it with quadrant-specific electrophysiology and clinical measures. It was anticipated that this method would reduce clinical heterogeneity, and refine anatomical localisation, increasing sensitivity to region-specific effects. However, the approach was somewhat undermined in its ability to detect group effects by its sensitivity to inter-individual variability in cortical representation and relatively low signal-to-noise, compared with whole field stimulation. However, the feasibility of correlating region-specific clinical, VEP and fMRI measures was demonstrated, using a region-of-interest approach. Region-specific longitudinal changes were demonstrated in clinical, VEP and fMRI data, and slower recovery was noted in the left upper quadrant in this cohort. In addition, although inconclusive with regard to region-specific plasticity, this study found that all regions of the visual field are equally susceptible to damage in ON, and recover equally well. There was no evidence for supra-normal fMRI activity in regions of retinotopic visual cortex, on stimulation of the fellow eye.

It is possible that the approach used in this study may be optimised further. In particular, signal-to-noise may be improved with the development of higher field strength MRI, and formal retinotopic mapping may help address issues of inter-individual variability. Therefore, in the future, technological developments may facilitate the investigation of recovery of visual field defects. In the next chapter, future directions in the development of MRI technology, and the investigation of neuroplasticity, are discussed. Conclusions are drawn regarding the contribution to the field of the work described in this thesis.

CHAPTER 7

CONCLUSIONS AND FUTURE DIRECTIONS

In this chapter, the main results and conclusions of this thesis are summarised, and novel aspects of methodology are highlighted. The contribution of these investigations to the study of mechanisms of damage and recovery in ON is considered. Future research directions are identified, from both technological and clinical perspectives.

7.1 Mechanisms of damage

The results of this thesis confirm and extend those of previous studies, with regard to mechanisms of damage and visual loss in ON. In the acute stage, inflammation was prominent in the optic nerve, with gadolinium enhancement evident in 92% of cases. Acute demyelination and conduction block occurred. In most cases, vision improved over the following three months, and was paralleled by an increase in VEP amplitude. Despite visual recovery, there was evidence of residual demyelination and axonal loss in the optic nerve at 12 months, with persistent prolongation of VEP latency, loss of macular volume, thinning of the RNFL, optic atrophy and a reduction in VEP amplitude. There was a progressive increase in the length of the optic nerve lesion, consistent with secondary tract degeneration, of either retrograde or Wallerian type. Optic radiation lesion load increased over the course of the year, and localised pericalcarine cortical atrophy was evident at presentation, before there was any detectable generalised loss of grey matter, and in the absence of associations with tract-specific damage. Both the increasing lesion load and pericalcarine cortical atrophy were associated with the development of MS. This suggests that this regional atrophy might represent an early manifestation of generalised grey matter damage, and the visual system may be particularly susceptible to damage in demyelinating disease. There was evidence of significant tissue damage in the optic nerve and throughout the visual system, even in patients who made a good visual recovery.

During the acute episode of ON, the inflammatory lesion length in the optic nerve and VEP amplitude, reflecting the degree of conduction block, were associated with acute visual loss. However, the only structural marker of damage associated with visual

outcome at 12 months was macular volume, a marker of secondary retinal neuronal loss.

7.2 Mechanisms of recovery

The key findings of this thesis relate to mechanisms of visual recovery, and in particular the role of cortical neuroplasticity. During the acute episode, an association was identified between acute fMRI activity in the cuneus, part of the dorsal stream of visual processing, and visual function at the same time, which was independent of the identified structural predictors. It is argued that this suggests a role for the cuneus in modulating the degree of acute visual loss, through a mechanism of neuroplastic cortical reorganisation. The subsequent longitudinal study identified dynamic changes in this region over time.

The key results from the longitudinal study were an association between a greater early fMRI response in the lateral occipital complexes (LOCs) and a better visual outcome. This suggests a role for neuroplastic changes in the ventral visual processing stream, contributing to recovery. These changes were evident on stimulation of either eye, and were independent of markers of acute inflammation, persistent demyelination and residual neuroaxonal loss in the optic nerve. A negative fMRI response in the LOCs during the acute phase was associated with a poor outcome, with sufficient sensitivity and specificity to suggest that it might be useful in a clinical setting, although this requires confirmation in larger cohorts.

The central argument of this thesis is that neuroplastic responses in the grey matter may be more important in determining visual outcome following ON than previously recognised, and may contribute to clinical recovery despite marked tissue damage. This could have implications for future therapeutic strategies in demyelinating disease.

It is interesting that different higher visual processing areas appear to play different roles at different times. During the acute phase, the cuneus of the dorsal stream seems to modulate the severity of acute visual dysfunction, whilst activity in the lateral occipital complexes of the ventral stream appears to be critical for long-term visual outcome. The reasons for this are not clear from this study, and further work is required to clarify the apparently complex interactions between neuroplasticity, structural damage and clinical function.

7.3 Novel aspects of methodology

It was necessary to develop several technical innovations during the course of this thesis. The visual fMRI paradigm presentation identified and addressed issues of attention, adaptation and loss-of-fixation biases that had not been resolved in previous studies. The methodology used for tractography was innovative, combining diffusion and functional MRI data to define seed-points in the visual system, in order to improve reproducibility. The exploration of structure-function interactions required an extensive structural protocol and this, combined with visual fMRI, comprised the most comprehensive MRI assessment of the visual pathways in ON in the literature. This was also the first time that associations have been investigated between OCT and fMRI in this condition, and this was a valuable method of elucidating the relative influences of neuroaxonal degeneration and plasticity. The acquisition of quadrant-specific visual, electrophysiological and fMRI data was a novel method of investigating visual field defects and the role of the fellow eye in ON. However, this approach was undermined by inter-individual variability in the size of V1 (Dougherty et al.,2003), which is correlated with the size of other visual areas, such as LGN (Andrews et al., 1997). Future studies could apply retinotopic mapping to allow for this variability and improve sensitivity in the investigation of visual field defects.

7.4 Future technological directions

One of the difficulties of investigating ON *in vivo* is that MRI of the optic nerve remains challenging, and future technical advances are required in order to broaden the applications of some of the more recently developed, quantitative techniques. Optic nerve DTI is now feasible (Chabert et al., 2005;Wheeler-Kingshott et al., 2006;Trip et al., 2006b), and provides a valuable measure of tissue integrity, which may prove to be a more sensitive index of damage than either T2-weighted or enhancing lesion length. However, at present, acquisition times remain lengthy, in the region of 40-45 minutes, and problems remain in achieving adequate signal-to-noise, and sampling the whole nerve. A recently developed zonal coronal-oblique single-shot sequence is an important advance in terms of improving signal-to-noise in a tolerable timeframe for patients (Dowell et al., 2009). In the future, this may facilitate the integration of optic nerve DTI sequences, and perhaps optic tract DTI, into multi-

modal MRI protocols. Recent optic nerve DTI studies have also suggested that pathological specificity may be improved by using alternative DTI-derived parameters, such as the axial and radial diffusivities (Naismith et al, 2009), and this may help distinguish demyelination from axonal damage (Wu et al., 2007;Sun et al., 2008). Future developments will aim to improve resolution, in order to reduce partial volume effects, and to increase signal-to-noise ratio (SNR) and nerve coverage. SNR may be improved by the use of higher gradient strengths, multichannel receiver coils, parallel imaging techniques and higher field strength scanners, though all require detailed evaluation.

This study was the first to combine OCT with fMRI, but OCT data was only available at the 12 month time-point. OCT appears a promising technique, in terms of its sensitivity to axonal loss, and is probably superior to optic nerve MRI in this regard. Combining longitudinal OCT and fMRI, in the first few weeks after acute ON, could be used to clarify the temporal relationship between the appearance of retinal neuroaxonal loss and cortical plastic responses at that time.

In addition to advances in imaging hardware, more sophisticated analysis techniques have been developed recently. A multivariate, rather than mass univariate, approach has been applied in recent fMRI studies (Haxby et al., 2001;Cox and Savoy, 2003;Haynes and Rees, 2005c;Kriegeskorte et al., 2006;Haynes and Rees, 2006;Hassabis et al., 2009). Multivariate analysis takes into account patterns of information present across multiple voxels, and appears to improve sensitivity to detect subtle effects. It would be interesting to apply this technique to the visual stimulation data from this study. In particular, this might improve the sensitivity to detect neuroplastic responses to region-specific visual deficits.

7.5 Future clinical directions

In demyelinating disease, recent therapeutic strategies have started to focus on brain repair, for example, stem cells for remyelination (Pluchino and Martino, 2005;Kolappan et al., 2008a). Therapeutic manipulation of mechanisms of brain repair appears to be an area of promise. An important question is whether it might be possible to manipulate plastic reorganisation for therapeutic gain. Previous studies

have demonstrated benefits of visual restitution therapy in patients with visual field defects of heterogeneous aetiology (Kasten et al., 1998). Following daily visual stimulation using a computer programme, in which stimuli were presented at the border of the normal and abnormal visual fields, improvements of around five degrees of visual angle were demonstrated. In order to develop pharmacological treatments, a better understanding of the processes that occur within the LOCs during the acute episode is necessary. In particular, the pathophysiological correlates of adaptive plasticity require clarification and, perhaps more importantly, the correlates of maladaptive change in patients who fail to recover need to be identified. It is conceivable that cellular factors inhibit important reorganisation responses in a subset of patients, and this could provide a therapeutic target. Future *in vivo* studies could focus on the LOCs, in order to define the metabolic substrates of reorganisation, using magnetic resonance spectroscopy. This is another quantitative *in vivo* technique, which has contributed to elucidating the pathophysiology of demyelinating disease of the brain, by enabling assessment of the composition of living tissues at a molecular level. Indices are derived which reflect processes such as axonal damage and gliosis, and local levels of neurotransmitters. From this study, it appears that the spectroscopy of the LOCs should be targetted during the acute phase of ON, in patients with a longitudinal follow-up, to determine clinical recovery. The clinical outcome could then be correlated with the acute metabolic findings. Combining spectroscopy data with techniques such as DTI, to measure structural integrity, and fMRI, to assess plasticity, is an exciting prospect, which could elucidate metabolic correlates of structural damage and functional reorganisation at a cellular level.

An alternative, complementary approach to the investigation of the substrates of neuroplasticity at cellular level would be to use animal models, with a focus on the key factors triggering successful and unsuccessful reorganisation. This might be achieved in a combined fMRI-histopathological correlation study. This approach has been previously applied successfully to identify the substrates of conventional MRI-visible lesions in EAE (Hart et al., 1998;Karlik et al.,1999), gadolinium-enhancing lesions (Karlik et al., 1999), MTR, T2 relaxation abnormalities (Gareau et al., 1999) and spectroscopic changes (Richards et al., 1995) in the brain, and, more recently, to identify DTI parameters specific to axonal injury in the spinal cord (Feng et al., 2009;Budde et al., 2009).

The timing and location of neuroplastic reorganisation identified in this study may have other implications for future work. Early reorganisation, during the acute episode, appeared to be crucial. The finding of a potential fMRI predictor of visual outcome, evident during the acute phase, merits further investigation in larger groups of patients. If confirmed, this could prove to be a valuable clinical tool. In particular, patient counselling at the time of diagnosis would be facilitated, and the fMRI response might be used to help select candidates for clinical trials of emerging experimental therapies, such as stem cells. The timing of reorganisation activity may have other implications for future potential therapies. Previous authors have speculated that a delay between symptom onset and delivery of steroids may explain the lack of benefit seen in clinical trials (Compston and Coles, 2002). It may be that the visual prognosis is determined early, whether through a mechanism of plasticity or severity of damage, and for future therapies to be effective, they will need to be delivered during the first few days to weeks. This provides a challenge for health service provision, as early assessment and availability of investigations would be required, in addition to early provision of treatment.

The location of the neuroplastic responses in higher visual areas is interesting. The results of this thesis suggested that both the ventral and dorsal streams appear to be involved, influencing visual function in different ways, at different times. It is unclear how this relates to their usual functions in health. It would be interesting to investigate whether there are detectable clinical abnormalities specific to a particular region in patients with ON, i.e. whether object recognition is especially affected (a ventral stream function) or, alternatively, whether there are difficulties with spatial localisation of objects in the physical world (a dorsal stream function). This has not previously been investigated, and it is conceivable that some of the residual symptoms seen following ON might be related to dysfunction of one or other of these regions. Patients with recovered ON could have residual, unreported difficulties with object recognition. In addition, frequently reported residual symptoms following recovery, such as Pulfrich's phenomenon, in which patients find it difficult to track the trajectory of a moving object, could be related to dorsal stream dysfunction, in addition to delayed afferent conduction. These hypotheses could be investigated using an fMRI approach.

The varying influence of different regions on vision at different times during the recovery process requires further clarification. It will be important to determine

whether there is a dynamic changing role of area in neuroplasticity during recovery, and whether the dynamics of recovery vary between individuals, or are common across different populations of patients.

It is interesting to consider whether the factors associated with recovery from clinically isolated ON remain important in established MS. In particular, the effects of progressively accumulating demyelination and axonal loss may influence the contribution of neuroplastic reorganisation to recovery. A "threshold effect" has been reported, in terms of optic nerve axonal damage, below which vision is well preserved, and above which dysfunction is clinically eloquent, in previous animal (Frisen and Quigley, 1984) and *in vivo* studies (Costello et al., 2006). In established MS, it is possible that recurrent insults, in the context of a more aggressive and chronic disease process, begin to overwhelm compensatory responses, such as plasticity. This is an area that merits further study, by applying an *in vivo* methodology, similar to the one used in this thesis, to a cohort of patients with acute ON, in the context of established MS.

7.6 Summary

In summary, this thesis has elucidated aspects of damage and recovery from clinically isolated ON. In particular, the identification of a direct association between acute fMRI activity in the LOCs and subsequent visual outcome provides a foundation for further investigation. Elucidating the importance of adaptive neuroplasticity, independent of structural damage, and the timing and location of compensatory responses provides a focus for future investigation of the metabolic correlates of plasticity at a cellular level, and a potential target for novel therapeutic approaches.

APPENDIX I

VISUAL SCORING CONVERSION TABLE

LogMAR	Snellen (UK)	Snellen (USA)
1.7	6/300	20/1000
1.6	6/230	20/800
1.5	6/190	20/630
1.4	6/150	20/500
1.3	6/120	20/400
1.2	6/90	20/300
1.1	6/75	20/250
1.0	6/60	20/200
0.9	6/48	20/160
0.8	6/37.5	20/125
0.7	6/30	20/100
0.6	6/24	20/80
0.5	6/18	20/63
0.4	6/15	20/50
0.3	6/12	20/40
0.2	6/10	20/32
0.1	6/7.5	20/25
0	6/6	20/20
-0.1	6/5	20/16
-0.2	6/4	20/13
-0.3	6/3	20/10

Table S1 Conversion from logMAR to Snellen UK and USA visual scoring systems.

APPENDIX II

KURTZKE EXPANDED DISABILITY SCALE (EDSS)

Score	Neurological status
0	Normal neurological examination (all functional systems (FS) grade 0)
1.0	No disability, minimal signs in one FS (i.e. grade 1)
1.5	No disability, minimal signs in more than one FS (more than one grade 1)
2.0	Minimal disability in one FS (one FS grade 2, others 0 or 1)
2.5	Minimal disability in two FS (two FS grade 2, others 0 or 1)
3.0	Moderate disability in one FS (one FS grade 3, others 0 or 1), or mild disability in three or four FS (three/four FS grade 2, others 0 or 1), though fully ambulatory
3.5	Fully ambulatory but with moderate disability in one FS (one FS grade 3) and one or two FS grade 2
4.0	Ambulatory without aid or rest for >500m; up and about some 12 hours a day despite relatively severe disability consisting of one FS grade 4 (others 0 or 1), or combinations of lower grades exceeding limits of previous steps
4.5	Ambulatory without aid or rest for >300m; up and about much of the day; characterised by relatively severe disability usually consisting of one FS grade 4 or combinations of lesser grades exceeding limits of previous steps
5.0	Ambulatory without aid or rest for >200m (usual FS equivalents are one grade 5 alone, others 0 or 1; or combinations of lesser grades usually exceeding specifications for step 4.5)
5.5	Ambulatory without aid or rest >100m
6.0	Unilateral assistance (cane or crutch) required to walk at least 100m with or without resting
6.5	Constant bilateral assistance (canes or crutches) required to walk at least 20m without resting
7.0	Unable to walk 5m even with aid, essentially restricted to wheelchair; wheels self and transfers alone; up and about in wheelchair some 12 hours a day
7.5	Unable to take more than a few steps; restricted to wheelchair; may need some help in transfer and in wheeling self
8.0	Essentially restricted to bed or chair or perambulated in wheelchair, but out of bed most of day; retains many self-care functions; generally has effective use of arms
8.5	Essentially restricted to bed much of the day; has some effective use of arm(s); retains some self-care functions
9.0	Helpless bed patient; can communicate and eat
9.5	Totally helpless bed patient; unable to communicate effectively or eat/swallow
10.0	Death due to MS

Table S2 Kurtzke Expanded Disability Status Score (EDSS) scale. The functional systems assessed are visual, brainstem, pyramidal, cerebellar, sensory, bowel/bladder and cerebral. Mood alteration does not affect the EDSS score.

APPENDIX III

VOXEL-BASED LONGITUDINAL FMRI ANALYSIS

Interpretation of longitudinal fMRI data may be complicated by several factors, such as varying attention and adaptation/habituation effects. In order to investigate the magnitude of these effects in controls, a longitudinal voxel-based analysis approach was used, and the results are reported in this appendix. The same approach was applied to the patient data, and the resulting difficulties in interpretation are discussed.

The fMRI data for each control and patient were pre-processed in SPM5, as described in chapters 3 to 6, and the resulting contrast images, representing whole field stimulation through the chromatic goggles, were entered into a second-level analysis. Flexible factorial models were specified, as described in Chapter 6. Several different second-level models were specified, to investigate different temporal profiles of change. In addition to linear changes and second order models, an exponential model was estimated, to test for voxels which followed the temporal course of clinical recovery in ON.

The contrasts were specified as follows: linear increases (-1.5 -0.5 0.5 1.5), linear decreases (1.5 0.5 -0.5 -1.5), second order increases (-1 1 1 -1), second order decreases (1 -1 -1 1), exponential increases (-1 0.33 0.33 0.33) and exponential decreases (1 -0.33 -0.33 -0.33). The statistical parametric maps were thresholded at $p<0.05$ (corrected).

Occipital regions were identified, in which the fMRI signal decreased over time in a linear fashion in the control group (Figure S1), and increased exponentially in the patient group (Figure S2).

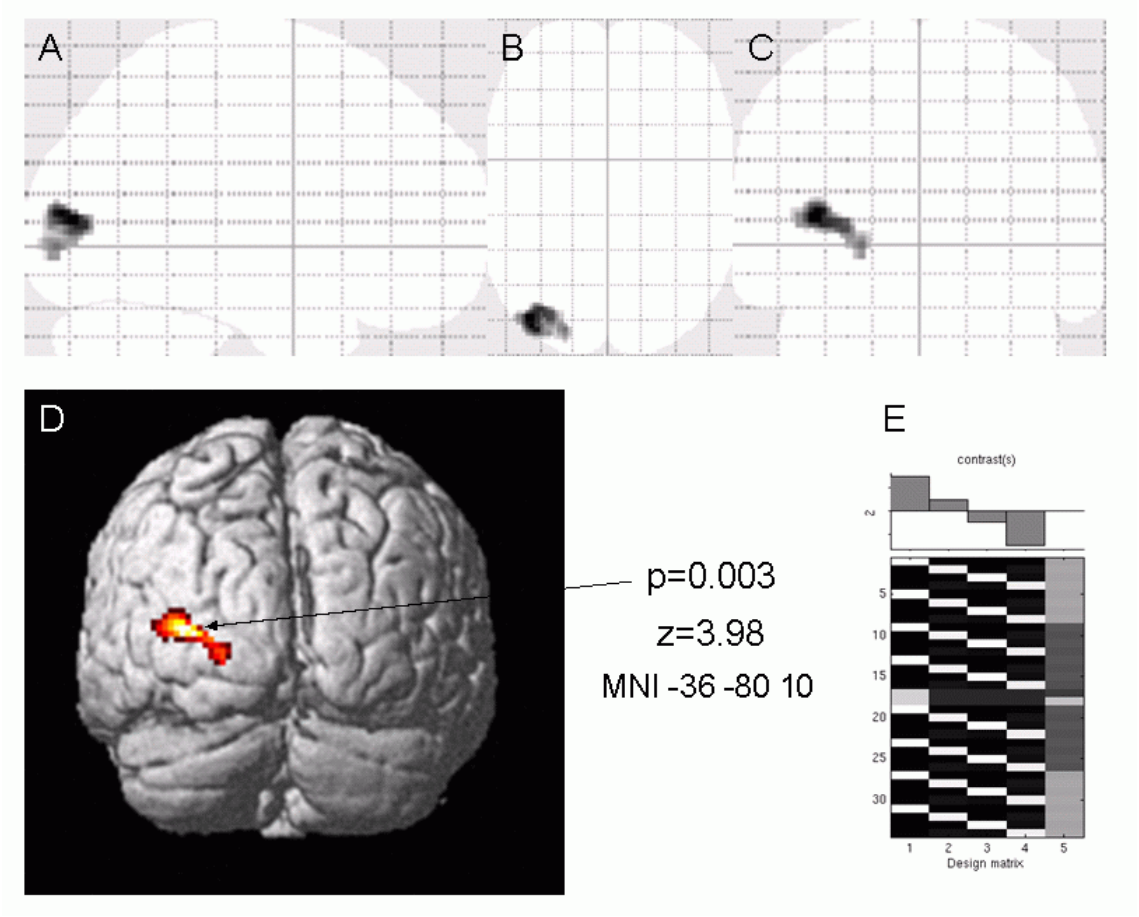

Figure S1 A statistical parametric map showing voxels in which there was a linear decrease in signal over time in controls. The results are overlaid on to the SPM5 glass brain in (A) sagittal, (B) axial and (C) coronal section, and (D) rendered on to the canonical SPM5 template. The Montreal Neurological Institute (MNI) coordinates of the global maximum, z score and cluster-level p value are reported. (E) The design matrix is shown.

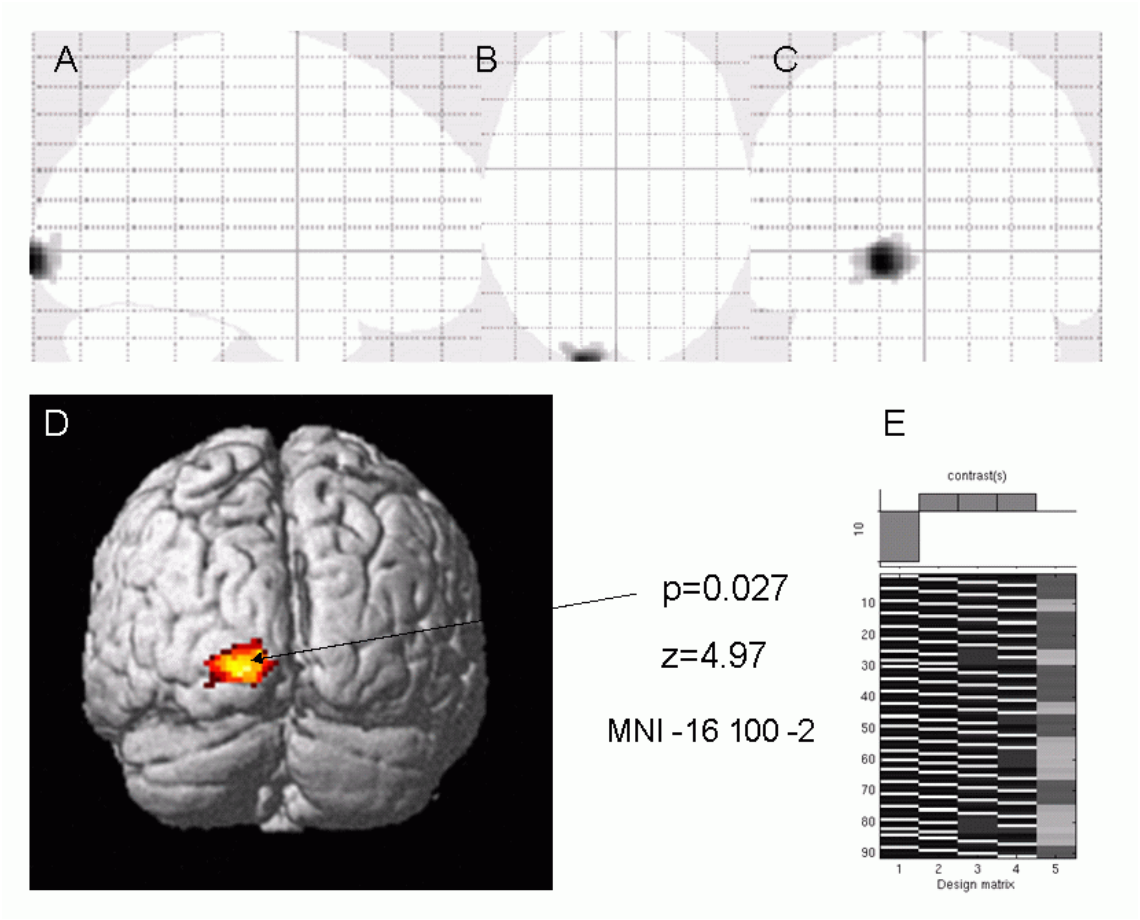

Figure S2 A statistical parametric map showing voxels in which there was an exponential increase in signal over time in patients. The results are overlaid on to the SPM5 glass brain in (A) sagittal, (B) axial and (C) coronal section, and (D) rendered on to the canonical SPM5 template. The Montreal Neurological Institute (MNI) coordinates of the global maximum, z score and cluster-level p value are reported. (E) The design matrix is shown.

These results illustrate some of the problems interpreting longitudinal fMRI data. The changes in patients are consistent with an increasing neuronal input between baseline and three months, as vision improved. However, there were also changes in primary visual cortex in the control group, with a linear decrease evident over time. These changes probably relate to adaptation/habituation and reduced attention with repeated stimuli. The magnitude of these changes can be quite large, but fortunately are in the opposite direction to changes relating to improving vision.

REFERENCES

ABN (2007) Association of British Neurologists' guidelines for treatment of multiple sclerosis with beta-interferon and glatiramer acetate. London.

Aickin M, Gensler H (1996) Adjusting for multiple testing when reporting research results: the Bonferroni vs Holm methods. Am J Public Health 86:726-728.

Alamouti B, Funk J (2003) Retinal thickness decreases with age: an OCT study. Br J Ophthalmol 87:899-901.

Anderson JC, Martin KA (2005) Connection from cortical area V2 to V3 A in macaque monkey. J Comp Neurol 488:320-330.

Anderson VM, Fernando KT, Davies GR, Rashid W, Frost C, Fox NC, Miller DH (2007) Cerebral atrophy measurement in clinically isolated syndromes and relapsing remitting multiple sclerosis: a comparison of registration-based methods. J Neuroimaging 17:61-68.

Andersson JL, Hutton C, Ashburner J, Turner R, Friston K (2001) Modeling geometric deformations in EPI time series. Neuroimage 13:903-919.

Andrews TJ, Halpern SD, Purves D (1997) Correlated size variations in human visual cortex, lateral geniculate nucleus, and optic tract. J Neurosci 17:2859-2868.

Arden GB, Gucukoglu AG (1978) Grating test of contrast sensitivity in patients with retrobulbar neuritis. Arch Ophthalmol 96:1626-1629.

Arnett HA, Fancy SP, Alberta JA, Zhao C, Plant SR, Kaing S, Raine CS, Rowitch DH, Franklin RJ, Stiles CD (2004) bHLH transcription factor Olig1 is required to repair demyelinated lesions in the CNS. Science 306:2111-2115.

Ascherio A, Munger KL (2007a) Environmental risk factors for multiple sclerosis. Part I: the role of infection. Ann Neurol 61:288-299.

Ascherio A, Munger KL (2007b) Environmental risk factors for multiple sclerosis. Part II: Noninfectious factors. Ann Neurol 61:504-513.

Ashburner J, Friston KJ (1999) Nonlinear spatial normalization using basis functions. Hum Brain Mapp 7:254-266.

Audoin B, Fernando KT, Swanton JK, Thompson AJ, Plant GT, Miller DH (2006) Selective magnetization transfer ratio decrease in the visual cortex following optic neuritis. Brain 129:1031-1039.

Baier ML, Cutter GR, Rudick RA, Miller D, Cohen JA, Weinstock-Guttman B, Mass M, Balcer LJ (2005) Low-contrast letter acuity testing captures visual dysfunction in patients with multiple sclerosis. Neurology 64:992-995.

Baker CI, Peli E, Knouf N, Kanwisher NG (2005) Reorganization of visual processing in macular degeneration. J Neurosci 25:614-618.

Balcer LJ, Baier ML, Pelak VS, Fox RJ, Shuwairi S, Galetta SL, Cutter GR, Maguire MG (2000) New low-contrast vision charts: reliability and test characteristics in patients with multiple sclerosis. Mult Scler 6:163-171.

Balcer LJ, Baier ML, Cohen JA, Kooijmans MF, Sandrock AW, Nano-Schiavi ML, Pfohl DC, Mills M, Bowen J, Ford C, Heidenreich FR, Jacobs DA, Markowitz CE, Stuart WH, Ying GS, Galetta SL, Maguire MG, Cutter GR (2003) Contrast letter acuity as a visual component for the Multiple Sclerosis Functional Composite. Neurology 61:1367-1373.

Balcer LJ (2006) Clinical practice. Optic neuritis. N Engl J Med 354:1273-1280.

Balcer LJ, Galetta SL, Calabresi PA, Confavreux C, Giovannoni G, Havrdova E, Hutchinson M, Kappos L, Lublin FD, Miller DH, O'Connor PW, Phillips JT, Polman CH, Radue EW, Rudick RA, Stuart WH, Wajgt A, Weinstock-Guttman B, Wynn DR, Lynn F, Panzara MA (2007) Natalizumab reduces visual loss in patients with relapsing multiple sclerosis. Neurology 68:1299-1304.

Bandettini PA, Wong EC, Hinks RS, Tikofsky RS, Hyde JS (1992) Time course EPI of human brain function during task activation. Magn Reson Med 25:390-397.

Bandettini PA, Kwong KK, Davis TL, Tootell RB, Wong EC, Fox PT, Belliveau JW, Weisskoff RM, Rosen BR (1997) Characterization of cerebral blood oxygenation and flow changes during prolonged brain activation. Hum Brain Mapp 5:93-109.

Bandettini PA, Ungerleider LG (2001) From neuron to BOLD: new connections. Nat Neurosci 4:864-866.

Barkhof F, Filippi M, Miller DH, Scheltens P, Campi A, Polman CH, Comi G, Ader HJ, Losseff N, Valk J (1997) Comparison of MRI criteria at first presentation to predict conversion to clinically definite multiple sclerosis. Brain 120:2059-2069.

Barkhof F, VanWalderveen M (1999) Characterization of tissue damage in multiple sclerosis by nuclear magnetic resonance. Philos Trans R Soc Lond B Biol Sci 354:1675-1686.

Barnes GR, Hess RF, Dumoulin SO, Achtman RL, Pike GB (2001) The cortical deficit in humans with strabismic amblyopia. J Physiol 533:281-297.

Basser PJ, Mattiello J, LeBihan D (1994) Estimation of the effective self-diffusion tensor from the NMR spin echo. J Magn Reson B 103:247-254.

Basser PJ, Pierpaoli C (1996) Microstructural and physiological features of tissues elucidated by quantitative-diffusion-tensor MRI. J Magn Reson B 111:209-219.

Beck RW, Cleary PA, Anderson MM, Jr., Keltner JL, Shults WT, Kaufman DI, Buckley EG, Corbett JJ, Kupersmith MJ, Miller NR. (1992) A randomized, controlled trial of corticosteroids in the treatment of acute optic neuritis. The Optic Neuritis Study Group. N Engl J Med 326:581-588.

Beck RW, Kupersmith MJ, Cleary PA, Katz B (1993a) Fellow eye abnormalities in acute unilateral optic neuritis. Experience of the optic neuritis treatment trial. Ophthalmology 100:691-697.

Beck RW, Arrington J, Murtagh FR, Cleary PA, Kaufman DI (1993b) Brain magnetic resonance imaging in acute optic neuritis. Experience of the Optic Neuritis Study Group. Arch Neurol 50:841-846.

Beck RW, Cleary PA (1993c) Optic neuritis treatment trial. One-year follow-up results. Arch Ophthalmol 111:773-775.

Beck RW, Cleary PA, Backlund JC (1994) The course of visual recovery after optic neuritis. Experience of the Optic Neuritis Treatment Trial. Ophthalmology 101:1771-1778.

Beck RW, Chandler DL, Cole SR, Simon JH, Jacobs LD, Kinkel RP, Selhorst JB, Rose JW, Cooper JA, Rice G, Murray TJ, Sandrock AW (2002) Interferon beta-1a for early multiple sclerosis: CHAMPS trial subgroup analyses. Ann Neurol 51:481-490.

Beck RW, Trobe JD, Moke PS, Gal RL, Xing D, Bhatti MT, Broadsky MC, Buckley EG, Chrousos GA, Corbett J, Eggenberger E, Goodwin JA, Katz B, Kaufman DI, Keltner JL, Kupersmith MJ, Miller NR, Nazarian S, Orengo-Nania S, Savino PJ, Shults WT, Smith CH, Wall M; Optic Neuritis Study Group (2003) High- and low-risk profiles for the development of multiple sclerosis within 10 years after optic neuritis: experience of the optic neuritis treatment trial. Arch Ophthalmol 121:944-949.

Beck RW, Gal RL, Bhatti MT, Brodsky MC, Buckley EG, Chrousos GA, Corbett J, Eggenberger E, Goodwin JA, Katz B, Kaufman DI, Keltner JL, Kupersmith MJ, Niller NR, Moke PS, Nazarian S, Orengo-Nania S, Savino PJ, Shults WT, Smith CH, Trobe JD, Wall M, Xing D; Optic Neuritis Study Group (2004a) Visual function more than 10 years after optic neuritis: experience of the optic neuritis treatment trial. Am J Ophthalmol 137:77-83.

Beck RW, Smith CH, Gal RL, Xing D, Bhatti MT, Brodsky MC, Buckley EG, Chrousos GA, Corbett J, Eggenberger E, Goodwin JA, Katz B, Kaufman DI, Keltner JL, Kupersmith MJ, Miller NR, Moke PS, Nazarian S, Orengo-Nania S, Savino PJ, Shults WT, Trobe JD, Wall M; Optic Neuritis Study Group (2004b) Neurologic impairment 10 years after optic neuritis. Arch Neurol 61:1386-1389.

Behrens TE, Johansen-Berg H, Woolrich MW, Smith SM, Wheeler-Kingshott CA, Boulby PA, Barker GJ, Sillery EL, Sheehan K, Ciccarelli O, Thompson AJ, Brady JM, Matthews PM (2003a) Non-invasive mapping of connections between human thalamus and cortex using diffusion imaging. Nat Neurosci 6:750-757.

Behrens TE, Woolrich MW, Jenkinson M, Johansen-Berg H, Nunes RG, Clare S, Matthews PM, Brady JM, Smith SM (2003b) Characterization and propagation of uncertainty in diffusion-weighted MR imaging. Magn Reson Med 50:1077-1088.

Behrens TE, Berg HJ, Jbabdi S, Rushworth MF, Woolrich MW (2007) Probabilistic diffusion tractography with multiple fibre orientations: What can we gain? Neuroimage 34:144-155.

Berry C, Harman P (1956) Neuroanatomical distribution of action potentials evoked by photic stimulation in cat fore- and mid brain. J Comp Neurol 105:395-416.

Bloch F, Hansen WW, Packard M (1946) The nuclear induction experiment. Phys Rev 70:474-485.

Bo L, Dawson TM, Wesselingh S, Mork S, Choi S, Kong PA, Hanley D, Trapp BD (1994) Induction of nitric oxide synthase in demyelinating regions of multiple sclerosis brains. Ann Neurol 36:778-786.

Bolanos JP, Almeida A, Stewart V, Peuchen S, Land JM, Clark JB, Heales SJ (1997) Nitric oxide-mediated mitochondrial damage in the brain: mechanisms and implications for neurodegenerative diseases. J Neurochem 68:2227-2240.

Boorstein JM, Moonis G, Boorstein SM, Patel YP, Culler AS (1997) Optic neuritis: imaging with magnetization transfer. AJR Am J Roentgenol 169:1709-1712.

Bostock H, Sears TA (1976) Continuous conduction in demyelinated mammalian nerve fibers. Nature 263:786-787.

Boxerman JL, Bandettini PA, Kwong KK, Baker JR, Davis TL, Rosen BR, Weisskoff RM (1995) The intravascular contribution to fMRI signal change: Monte Carlo modeling and diffusion-weighted studies *in vivo*. Magn Reson Med 34:4-10.

Braddick OJ, O'Brien JM, Wattam-Bell J, Atkinson J, Hartley T, Turner R (2001) Brain areas sensitive to coherent visual motion. Perception 30:61-72.

Brett M, Anton J-L, Valabregue R, Poline J-B (2002) Region-of-interest analysis using an SPM toolbox (Abstract). Presented at the 8th International conference on functional mapping of the human brain, June 2-6th 2002, Sendai, Japan.

Brex PA, Ciccarelli O, O'Riordan JI, Sailer M, Thompson AJ, Miller DH (2002) A longitudinal study of abnormalities on MRI and disability from multiple sclerosis. N Engl J Med 346:158-164.

Brown R (1828) A brief account of the microscopical observations made in the months of June, July and August, 1827, on the particles contained in the pollen of plants; and on the general existence of active molecules in organic and inorganic bodies. Phil Mag 4:161-173.

Bruder H, Fischer H, Reinfelder HE, Schmitt F (1992) Image reconstruction for echo planar imaging with nonequidistant k-space sampling. Magn Reson Med 23:311-323.

Brusa A, Jones SJ, Kapoor R, Miller DH, Plant GT (1999) Long-term recovery and fellow eye deterioration after optic neuritis, determined by serial visual evoked potentials. J Neurol 246:776-782.

Brusa A, Jones SJ, Plant GT (2001) Long-term remyelination after optic neuritis: A 2-year visual evoked potential and psychophysical serial study. Brain 124:468-479.

Brusaferri F, Candelise L (2000) Steroids for multiple sclerosis and optic neuritis: a meta-analysis of randomized controlled clinical trials. J Neurol 247:435-442.

Budde MD, Xie M, Cross AH, Song SK (2009) Axial diffusivity is the primary correlate of axonal injury in the experimental autoimmune encephalomyelitis spinal cord: a quantitative pixelwise analysis. J Neurosci 29:2805-2813.

Buxton RB, Wong EC, Frank LR (1998) Dynamics of blood flow and oxygenation changes during brain activation: the balloon model. Magn Reson Med 39:855-864.

Calabrese M, Atzori M, Bernardi V, Morra A, Romualdi C, Rinaldi L, McAuliffe MJ, Barachino L, Perini P, Fischl B, Battistin L, Gallo P (2007) Cortical atrophy is relevant in multiple sclerosis at clinical onset. J Neurol 254:1212-1220.

Caruana PA, Davies MB, Weatherby SJM, Williams R, Haq N, Foster DH, Hawkins CP (2000) Correlation of MRI lesions with visual psychophysical deficit in secondary progressive multiple sclerosis. Brain 123:1471-1480.

Centonze D, Rossi S, Boffa L, Versace V, Palmieri MG, Caramia MD, Bernardi G (2005) CSF from MS patients can induce acute conduction block in the isolated optic nerve. Eur J Neurol 12:45-48.

Cercignani M, Horsfield MA (2001) The physical basis of diffusion-weighted MRI. J Neurol Sci 186 Suppl 1:S11-S14.

Chabert S, Molko N, Cointepas Y, Le RP, Le BD (2005) Diffusion tensor imaging of the human optic nerve using a non-CPMG fast spin echo sequence. J Magn Reson Imaging 22:307-310.

Chan H, Odom JV, Coldren J, Dove C, Chao GM (1986) Acuity estimated by visually evoked potentials is affected by scaling. Doc Ophthalmol 62:107-117.

Chao CC, Hu S, Peterson PK (1995) Glia, cytokines, and neurotoxicity. Crit Rev Neurobiol 9:189-205.

Chard DT, Parker GJ, Griffin CM, Thompson AJ, Miller DH (2002) The reproducibility and sensitivity of brain tissue volume measurements derived from an SPM-based segmentation methodology. J Magn Reson Imaging 15:259-267.

Chauhan DS, Marshall J (1999) The interpretation of optical coherence tomography images of the retina. Invest Ophthalmol Vis Sci 40:2332-2342.

Chawla D, Rees G, Friston KJ (1999) The physiological basis of attentional modulation in extrastriate visual areas. Nat Neurosci 2:671-676.

Ciccarelli O, Toosy AT, Hickman SJ, Parker GJ, Wheeler-Kingshott CA, Miller DH, Thompson AJ (2005) Optic radiation changes after optic neuritis detected by tractography-based group mapping. Hum Brain Mapp 25:308-316.

Ciccarelli O, Behrens TE, Altmann DR, Orrell RW, Howard RS, Johansen-Berg H, Miller DH, Matthews PM, Thompson AJ (2006) Probabilistic diffusion tractography: a potential tool to assess the rate of disease progression in amyotrophic lateral sclerosis. Brain 129:1859-1871.

Ciccarelli O, Wheeler-Kingshott CA, McLean MA, Cercignani M, Wimpey K, Miller DH, Thompson AJ (2007) Spinal cord spectroscopy and diffusion-based tractography to assess acute disability in multiple sclerosis. Brain 130:2220-2231.

Ciccarelli O, Catani M, Johansen-Berg H, Clark C, Thompson A (2008) Diffusion-based tractography in neurological disorders: concepts, applications, and future developments. Lancet Neurol 7:715-727.

Cleary PA, Beck RW, Bourque LB, Backlund JC, Miskala PH (1997) Visual symptoms after optic neuritis. Results from the Optic Neuritis Treatment Trial. J Neuroophthalmol 17:18-23.

Cole SR, Beck RW, Moke PS, Kaufman DI, Tourtellotte WW (1998) The predictive value of CSF oligoclonal banding for MS 5 years after optic neuritis. Optic Neuritis Study Group. Neurology 51:885-887.

Comi G, Filippi M, Barkhof F, Durelli L, Edan G, Fernandez O, Hartung H, Seeldrayers P, Sorensen PS, Rovaris M, Martinelli V, Hommes OR (2001) Effect of early interferon treatment on conversion to definite multiple sclerosis: a randomised study. Lancet 357:1576-1582.

Comi G, Rocca MA, Filippi M (2004) Brain plasticity in multiple sclerosis. Eur Neurol 51:189-190.

Comi G, Martinelli V, Rodegher M, Moiola L, Bajenaru O, Carra A, Elovaara I, Fazekas F, Hartung HP, Hillert J, King J, Komoly S, Lubetzki C, Montalban X, Myhr KM, Ravnborg M, Rieckmann P, Wynn D, Young C, Filippi M; PreCISe study group (2009). Effect of glatiramer acetate on conversion to clinically definite multiple sclerosis in patients with clinically isolated syndrome (PreCISe study): a randomised, double-blind, placebo-controlled trial. Lancet 374:1503-1511.

Compston A, Coles A (2002) Multiple sclerosis. Lancet 359:1221-1231.

Compston A, Coles A (2008) Multiple sclerosis. Lancet 372:1502-1517.

Confavreux C, Vukusic S (2006) Natural history of multiple sclerosis: a unifying concept. Brain 129:606-616.

Conturo TE, Lori NF, Cull TS, Akbudak E, Snyder AZ, Shimony JS, McKinstry RC, Burton H, Raichle ME (1999) Tracking neuronal fiber pathways in the living human brain. Proc Natl Acad Sci USA 96:10422-10427.

Cook PA, Symms M, Boulby PA, Alexander DC (2007) Optimal acquisition orders of diffusion-weighted MRI measurements. J Magn Reson Imaging 25:1051-1058.

Costello F, Coupland S, Hodge W, Lorello GR, Koroluk J, Pan YI, Freedman MS, Zackon DH, Kardon RH (2006) Quantifying axonal loss after optic neuritis with optical coherence tomography. Ann Neurol 59:963-969.

Cox DD, Savoy RL (2003) Functional magnetic resonance imaging (fMRI) "brain reading": detecting and classifying distributed patterns of fMRI activity in human visual cortex. Neuroimage 19: 261-270.

Cox TA, Thompson HS, Corbett JJ (1981) Relative afferent pupillary defects in optic neuritis. Am J Ophthalmol 92:685-690.

Craner MJ, Lo AC, Black JA, Waxman SG (2003) Abnormal sodium channel distribution in optic nerve axons in a model of inflammatory demyelination. Brain 126:1552-1561.

Craner MJ, Newcombe J, Black JA, Hartle C, Cuzner ML, Waxman SG (2004) Molecular changes in neurons in multiple sclerosis: altered axonal expression of Nav1.2 and Nav1.6 sodium channels and Na+/Ca2+ exchanger. Proc Natl Acad Sci USA 101:8168-8173.

Dale AM, Fischl B, Sereno MI (1999) Cortical surface-based analysis. I. Segmentation and surface reconstruction. Neuroimage 9:179-194.

Dalton CM, Brex PA, Miszkiel KA, Hickman SJ, MacManus DG, Plant GT, Thompson AJ, Miller DH (2002) Application of the new McDonald criteria to patients with clinically isolated syndromes suggestive of multiple sclerosis. Ann Neurol 52:47-53.

Dalton CM, Chard DT, Davies GR, Miszkiel KA, Altmann DR, Fernando K, Plant GT, Thompson AJ, Miller DH (2004) Early development of multiple sclerosis is

associated with progressive grey matter atrophy in patients presenting with clinically isolated syndromes. Brain 127:1101-1107.

Darian-Smith C, Gilbert CD (1994) Axonal sprouting accompanies functional reorganization in adult cat striate cortex. Nature 368:737-740.

Darian-Smith C, Gilbert CD (1995) Topographic reorganization in the striate cortex of the adult cat and monkey is cortically mediated. J Neurosci 15:1631-1647.

Davies MB, Williams R, Haq N, Pelosi L, Hawkins CP (1998). MRI of optic nerve and postchiasmal visual pathways and visual evoked potentials in secondary progressive multiple sclerosis. Neuroradiology 40: 765-770.

Debouverie M, Pittion-Vouyovitch S, Louis S, Guillemin F (2008) Natural history of multiple sclerosis in a population-based cohort. Eur J Neurol 15:916-921.

Desikan RS, Segonne F, Fischl B, Quinn BT, Dickerson BC, Blacker D, Buckner RL, Dale AM, Maguire RP, Hyman BT, Albert MS, Killiany RJ (2006) An automated labeling system for subdividing the human cerebral cortex on MRI scans into gyral based regions of interest. Neuroimage 31:968-980.

Desmurget M, Bonnetblanc F, Duffau H (2007) Contrasting acute and slow-growing lesions: a new door to brain plasticity. Brain 130:898-914.

Di Filippo M, Tozzi A, Costa C, Belcastro V, Tantucci M, Picconi B, Calabresi P (2008) Plasticity and repair in the post-ischaemic brain. Neuropharmacology 55:353-262.

Dougherty RF, Koch VM, Brewer AA, Fischer B, Modersitzki J, Wandell BA (2003) Visual field representations and locations of visual areas V1/2/3 in human visual cortex. J Vis 3:586-598.

Dowell NG, Jenkins TM, Ciccarelli O, Miller DH, Wheeler-Kingshott CAM (2009) Contiguous-slice diffusion tensor imaging (CO-ZOOM): examples of in vivo spinal cord and optic nerve applications. J Magn Reson Imaging 29:454-450.

Dunker S, Wiegand W (1996) Prognostic value of magnetic resonance imaging in monosymptomatic optic neuritis. Ophthalmology 103:1768-1773.

Dutta R, McDonough J, Yin X, Peterson J, Chang A, Torres T, Gudz T, Macklin WB, Lewis DA, Fox RJ, Rudick R, Mirnics K, Trapp BD (2006) Mitochondrial dysfunction as a cause of axonal degeneration in multiple sclerosis patients. Ann Neurol 59:478-489.

Eger E, Ashburner J, Haynes JD, Dolan RJ, Rees G (2008) FMRI activity patterns in human LOC carry information about object exemplars within category. J Cogn Neurosci 20:356-370.

Eickhoff SB, Stephan KE, Mohlberg H, Grefkes C, Fink GR, Amunts K, Zilles K (2005) A new SPM toolbox for combining probabilistic cytoarchitectonic maps and functional imaging data. Neuroimage 25:1325-1335.

ETDRS investigators (1991) Early Treatment Diabetic Retinopathy Study design and baseline patient characteristics. ETDRS report number 7. Ophthalmology 98:741-756.

Evangelou N, Konz D, Esiri MM, Smith S, Palace J, Matthews PM (2001) Size-selective neuronal changes in the anterior optic pathways suggest a differential susceptibility to injury in multiple sclerosis. Brain 124:1813-1820.

Evans AC, Collins DL, Mills SR, Brown ED, Kelly RL, Peters TM (1993) 3D statistical neuroanatomical models from 305 MRI volumes. Proc IEEE Nucl Sci Symp Med Imaging Conf 1813-1817.

Fang JP, Lin RH, Donahue SP (1999) Recovery of visual field function in the optic neuritis treatment trial. Am J Ophthalmol 128:566-572.

Farnsworth D (1943) The Farnsworth-Munsell 100-hue and dichotomous tests for color vision. J Opt Soc Am 33:568-578.

Fazzone HE, Lefton DR, Kupersmith MJ (2003) Optic neuritis: correlation of pain and magnetic resonance imaging. Ophthalmology 110:1646-1649.

Felts PA, Baker TA, Smith KJ (1997) Conduction in segmentally demyelinated mammalian central axons. J Neurosci 17:7267-7277.

Felts PA, Kapoor R, Smith KJ (1995) A mechanism for ectopic firing in central demyelinated axons. Brain 118 (Pt 5):1225-1231.

Feng S, Hong Y, Zhou Z, Jinsong Z, Xiaofeng D, Zaizhong W, Yali G, Ying L, Yingjuan C, Yi H (2009) Monitoring of acute axonal injury in the swine spinal cord in EAE by diffusion tensor imaging. J Magn Reson Imaging 30: 277-285.

Fercher AF, Hitzenberger CK, Drexler W, Kamp G, Sattmann H (1993) *In vivo* optical coherence tomography. Am J Ophthalmol 116:113-114.

Ferris FL, III, Kassoff A, Bresnick GH, Bailey I (1982) New visual acuity charts for clinical research. Am J Ophthalmol 94:91-96.

Fischl B, Sereno MI, Dale AM (1999) Cortical surface-based analysis. II: Inflation, flattening, and a surface-based coordinate system. Neuroimage 9:195-207.

Fischl B, Dale AM (2000) Measuring the thickness of the human cerebral cortex from magnetic resonance images. Proc Natl Acad Sci USA 97:11050-11055.

Fischl B, van der KA, Destrieux C, Halgren E, Segonne F, Salat DH, Busa E, Seidman LJ, Goldstein J, Kennedy D, Caviness V, Makris N, Rosen B, Dale AM (2004) Automatically parcellating the human cerebral cortex. Cereb Cortex 14:11-22.

Fisher E, Lee JC, Nakamura K, Rudick RA (2008) Gray matter atrophy in multiple sclerosis: a longitudinal study. Ann Neurol 64:255-265.

Fisher JB, Jacobs DA, Markowitz CE, Galetta SL, Volpe NJ, Nano-Schiavi ML, Baier ML, Frohman EM, Winslow H, Frohman TC, Calabresi PA, Maguire MG, Cutter GR, Balcer LJ (2006) Relation of visual function to retinal nerve fiber layer thickness in multiple sclerosis. Ophthalmology 113:324-332.

Fisniku LK, Chard DT, Jackson JS, Anderson VM, Altmann DR, Miszkiel KA, Thompson AJ, Miller DH (2008) Gray matter atrophy is related to long-term disability in multiple sclerosis. Ann Neurol 64:247-254.

Fleishman JA, Beck RW, Linares OA, Klein JW (1987) Deficits in visual function after resolution of optic neuritis. Ophthalmology 94:1029-1035.

Fox PT, Raichle ME (1986) Focal physiological uncoupling of cerebral blood flow and oxidative metabolism during somatosensory stimulation in human subjects. Proc Natl Acad Sci USA 83:1140-1144.

Frackowiak RS (1997) The cerebral basis of functional recovery. In: Human Brain Function (Frackowiak RS, Friston KJ, Frith CD, Dolan RJ, Mazziotta JC, eds), pp 275-299. San Diego, USA.

Frank LR (2002) Characterization of anisotropy in high angular resolution diffusion-weighted MRI. Magn Reson Med 47:1083-1099.

Frederiksen JL, Larsson HB, Ottovay E, Stigsby B, Olesen J (1991) Acute optic neuritis with normal visual acuity. Comparison of symptoms and signs with psychophysiological, electrophysiological and magnetic resonance imaging data. Acta Ophthalmol (Copenh) 69:357-366.

Frederiksen JL, Sorensen TL, Sellebjerg FT (1997) Residual symptoms and signs after untreated acute optic neuritis. A one-year follow-up. Acta Ophthalmol Scand 75:544-547.

Frederiksen JL, Petrera J (1999) Serial visual evoked potentials in 90 untreated patients with acute optic neuritis. Surv Ophthalmol 44 Suppl 1:S54-S62.

Frisen L, Quigley HA (1984) Visual acuity in optic atrophy: a quantitative clinicopathological analysis. Graefes Arch Clin Exp Ophthalmol 222:71-74.

Friston KJ, Worsley KJ, Frackowiak RSJ, Mazziotta JC, Evans AC (1994) Assessing the significance of focal activations using their spatial extent. Human Brain Mapping 1:210-220.

Friston KJ, Ashburner J, Frith CD, Poline JB, Heather JD, Frackowiak RSJ (1995a) Spatial registration and normalization of images. Hum Brain Mapp165-189.

Friston KJ, Holmes AP, Worsley KJ, Poline JB, Frith CD, Frackowiak RSJ (1995b) Statistical parametric maps in functional imaging: A general linear approach. Hum Brain Mapp 2:189-210.

Friston KJ, Holmes A, Poline JB, Price CJ, Frith CD (1996a) Detecting activations in PET and fMRI: levels of inference and power. Neuroimage 4:223-235.

Friston KJ, Williams S, Howard R, Frackowiak RS, Turner R (1996b) Movement-related effects in fMRI time-series. Magn Reson Med 35:346-355.

Friston KJ, Zarahn E, Josephs O, Henson RN, Dale AM (1999) Stochastic designs in event-related fMRI. Neuroimage 10:607-619.

Friston KJ (2003) Introduction: experimental design and statistical parametric mapping. In: Human Brain Function, 2nd edition (Friston KJ, Frith CD, Dolan RJ, Price CJ, eds), pp 1-67. London: Academic Press.

Gareau PJ, Gati JS, Menon RS, Lee D, Rice G, Mitchell JR, Mandelfino P, Karlik SJ (1999) Reduced visual evoked responses in multiple sclerosis patients with optic neuritis: comparison of functional magnetic resonance imaging and visual evoked potentials. Mult Scler 5:161-164.

Gareau PJ, Rutt BK, Karlik SJ, Mitchell JR (2000). Magnetization transfer and multicomponent T2 relaxation measurements with histopathological correlation in an experimental model of MS. J Magn Reson Imaging 11:586-595.

Gartner S (1953) Optic neuropathy in multiple sclerosis; optic neuritis. AMA Arch Ophthalmol 50:718-726.

Gass A, Moseley IF, Barker GJ, Jones S, MacManus D, McDonald WI, Miller DH (1996) Lesion discrimination in optic neuritis using high-resolution fat-suppressed fast spin-echo MRI. Neuroradiology 38:317-321.

Geller AM, Hudnell HK, Vaughn BV, Messenheimer JA, Boyes WK (2005) Epilepsy and medication effects on the pattern visual evoked potential. Doc Ophthalmol 110:121-131.

Geurts JJ, Barkhof F (2008) Grey matter pathology in multiple sclerosis. Lancet Neurol 7:841-851.

Ghezzi A, Martinelli V, Torri V, Zaffaroni M, Rodegher M, Comi G, Zibetti A, Canal N (1999) Long-term follow-up of isolated optic neuritis: the risk of developing multiple sclerosis, its outcome, and the prognostic role of paraclinical tests. J Neurol 246:770-775.

Gold R, Linington C, Lassmann H (2006) Understanding pathogenesis and therapy of multiple sclerosis via animal models: 70 years of merits and culprits in experimental autoimmune encephalomyelitis research. Brain 129:1953-1971.

Goldby F (1957) A note on transneuronal atrophy in the human lateral geniculate body. J Neurol Neurosurg Psychiatry 20:202-207.

Golde S, Chandran S, Brown GC, Compston A (2002) Different pathways for iNOS-mediated toxicity in vitro dependent on neuronal maturation and NMDA receptor expression. J Neurochem 82:269-282.

Goodale MA, Milner AD (1992) Separate visual pathways for perception and action. Trends Neurosci 15:20-25.

Gordon-Lipkin E, Chodkowski B, Reich DS, Smith SA, Pulicken M, Balcer LJ, Frohman EM, Cutter G, Calabresi PA (2007) Retinal nerve fiber layer is associated with brain atrophy in multiple sclerosis. Neurology 69:1603-1609.

Gray H (1918) Anatomy of the human body. Philadelphia: Lea and Febiger.

Gregori B, Pro S, Bombelli F, La RM, Accornero N (2006) VEP latency: sex and head size. Clin Neurophysiol 117:1154-1157.

Grootoonk S, Hutton C, Ashburner J, Howseman AM, Josephs O, Rees G, Friston KJ, Turner R (2000) Characterization and correction of interpolation effects in the realignment of fMRI time series. Neuroimage 11:49-57.

Grossman RI, Gonzalez-Scarano F, Atlas SW, Galetta S, Silberberg DH (1986) Multiple sclerosis: gadolinium enhancement in MR imaging. Radiology 161:721-725.

Guy J, Fitzsimmons J, Ellis EA, Beck B, Mancuso A (1992a) Intraorbital optic nerve and experimental optic neuritis. Correlation of fat suppression magnetic resonance imaging and electron microscopy. Ophthalmology 99:720-725.

Guy J, Mao J, Bidgood WD, Jr., Mancuso A, Quisling RG (1992b) Enhancement and demyelination of the intraorbital optic nerve. Fat suppression magnetic resonance imaging. Ophthalmology 99:713-719.

Guye M, Parker GJ, Symms M, Boulby P, Wheeler-Kingshott CA, Salek-Haddadi A, Barker GJ, Duncan JS (2003) Combined functional MRI and tractography to demonstrate the connectivity of the human primary motor cortex *in vivo*. Neuroimage 19:1349-1360.

Halliday AM, McDonald WI, Mushin J (1972) Delayed visual evoked response in optic neuritis. Lancet 1:982-985.

Halliday AM, McDonald WI, Mushin J (1973) Visual evoked response in diagnosis of multiple sclerosis. Br Med J 4:661-664.

Halliday AM, McDonald WI (1977) Pathophysiology of demyelinating disease. Br Med Bull 33:21-27.

Han X, Jovicich J, Salat D, van der KA, Quinn B, Czanner S, Busa E, Pacheco J, Albert M, Killiany R, Maguire P, Rosas D, Makris N, Dale A, Dickerson B, Fischl B (2006) Reliability of MRI-derived measurements of human cerebral cortical thickness: the effects of field strength, scanner upgrade and manufacturer. Neuroimage 32:180-194.

Harrison BJ, Pujol J, Lopez-Sola M, Hernandez-Ribas R, Deus J, Ortiz H, Soriano-Mas C, Yucel M, Pantelis C, Cardoner N (2008) Consistency and functional specialization in the default mode brain network. Proc Natl Acad Sci USA 105:9781-9786.

Hart BA, Bauer J, Muller HJ, Melchers B, Nicolay K, Brok H, Bontrop RE, Lassmann H, Massacesi L (1998) Histopathological characterization of magnetic resonance imaging-detectable brain white matter lesions in a primate model of multiple sclerosis: a correlative study in the experimental autoimmune encephalomyelitis model in common marmosets (Callithrix jacchus). Am J Pathol 153:649-663.

Hassabis D, Chu C, Rees G, Weiskopf N, Molyneux PD, Maguire EA (2009) Decoding neuronal ensembles in the human hippocampus. Curr Biol 19:546-554.

Hauser SL, Oksenberg JR, Lincoln R, Garovoy J, Beck RW, Cole SR, Moke PS, Kip KE, Gal RL, Long DT (2000) Interaction between HLA-DR2 and abnormal brain

MRI in optic neuritis and early MS. Optic Neuritis Study Group. Neurology 54:1859-1861.

Hawkins CP, Munro PM, MacKenzie F, Kesselring J, Tofts PS, du Boulay EP, Landon DN, McDonald WI (1990). Duration and selectivity of blood-brain barrier breakdown in chronic relapsing experimental allergic encephalomyelitis studied by gadolinium-DTPA and protein markers. Brain 113:365-368.

Haxby JV, Gobbini MI, Furey ML, Ishai A, Schoulten JL, Pietrini P (2001) Distributed and overlapping representations of faces and objects in ventral temporal cortex. Science 293:2425-2430.

Hayashi T, Morimoto C, Burks JS, Kerr C, Hauser SL (1988) Dual-label immunocytochemistry of the active multiple sclerosis lesion: major histocompatibility complex and activation antigens. Ann Neurol 24:523-531.

Haynes JD, Tregellas J, Rees G (2005a) Attentional integration between anatomically distinct stimulus representations in early visual cortex. Proc Natl Acad USA 102:14925-14930.

Haynes JD, Deichmann R, Rees G (2005b) Eye-specific effects of binocular rivalry in the human lateral geniculate nucleus. Nature 438: 496-499.

Haynes JD, Rees G (2005c) Predicting the orientation of invisible stimuli from activity in human primary visual cortex. Nature Neurosci 8:686-691.

Haynes JD, Rees G (2006) Decoding mental states from brain activity in humans. Nature Neurosci 7:523-534.

Hayreh SS, Massanari RM, Yamada T, Hayreh SM (1981) Experimental allergic encephalomyelitis. I. Optic nerve and central nervous system manifestations. Invest Ophthalmol Vis Sci 21:256-269.

Henderson AP, Trip SA, Schlottmann PG, Altmann DR, Garway-Heath DF, Plant GT, Miller DH (2008) An investigation of the retinal nerve fibre layer in progressive multiple sclerosis using optical coherence tomography. Brain 131:277-287.

Hickman SJ, Brex PA, Brierley CM, Silver NC, Barker GJ, Scolding NJ, Compston DA, Moseley IF, Plant GT, Miller DH (2001) Detection of optic nerve atrophy following a single episode of unilateral optic neuritis by MRI using a fat-saturated short-echo fast FLAIR sequence. Neuroradiology 43:123-128.

Hickman SJ, Brierley CM, Brex PA, MacManus DG, Scolding NJ, Compston DA, Miller DH (2002a) Continuing optic nerve atrophy following optic neuritis: a serial MRI study. Mult Scler 8:339-342.

Hickman SJ, Dalton CM, Miller DH, Plant GT (2002b) Management of acute optic neuritis. Lancet 360:1953-1962.

Hickman SJ, Toosy AT, Jones SJ, Altmann DR, Miszkiel KA, MacManus DG, Barker GJ, Plant GT, Thompson AJ, Miller DH (2004a) A serial MRI study following optic nerve mean area in acute optic neuritis. Brain 127:2498-2505.

Hickman SJ, Toosy AT, Jones SJ, Altmann DR, Miszkiel KA, MacManus DG, Barker GJ, Plant GT, Thompson AJ, Miller DH (2004b) Serial magnetization transfer imaging in acute optic neuritis. Brain 127:692-700.

Hickman SJ, Toosy AT, Miszkiel KA, Jones SJ, Altmann DR, MacManus DG, Plant GT, Thompson AJ, Miller DH (2004c) Visual recovery following acute optic neuritis-a clinical, electrophysiological and magnetic resonance imaging study. J Neurol 251:996-1005.

Hickman SJ, Wheeler-Kingshott CA, Jones SJ, Miszkiel KA, Barker GJ, Plant GT, Miller DH (2005) Optic nerve diffusion measurement from diffusion-weighted imaging in optic neuritis. AJNR Am J Neuroradiol 26:951-956.

Hinds OP, Rajendran N, Polimeni JR, Augustinack JC, Wiggins G, Wald LL, Diana RH, Potthast A, Schwartz EL, Fischl B (2008) Accurate prediction of V1 location from cortical folds in a surface coordinate system. Neuroimage 39:1585-1599.

Hoftberger R, boul-Enein F, Brueck W, Lucchinetti C, Rodriguez M, Schmidbauer M, Jellinger K, Lassmann H (2004) Expression of major histocompatibility complex class I molecules on the different cell types in multiple sclerosis lesions. Brain Pathol 14:43-50.

Hohlfeld R, Wekerle H (2004) Autoimmune concepts of multiple sclerosis as a basis for selective immunotherapy: from pipe dreams to (therapeutic) pipelines. Proc Natl Acad Sci USA 101:14599-14606.

Holm S (1979) A simple sequentially rejective multiple test procedure. Scand J Statistics 6:65-70.

Holodny AI, Ollenschleger MD, Liu WC, Schulder M, Kalnin AJ (2001) Identification of the corticospinal tracts achieved using blood-oxygen-level-dependent and diffusion functional MR imaging in patients with brain tumors. AJNR Am J Neuroradiol 22:83-88.

Honmou O, Felts PA, Waxman SG, Kocsis JD (1996) Restoration of normal conduction properties in demyelinated spinal cord axons in the adult rat by transplantation of exogenous Schwann cells. J Neurosci 16:3199-3208.

Hornabrook RS, Miller DH, Newton MR, MacManus DG, du Boulay GH, Halliday AM, McDonald WI (1992) Frequent involvement of the optic radiation in patients with acute isolated optic neuritis. Neurology 42:77-79.

Horton JC, Landau K, Maeder P, Hoyt WF (1990) Magnetic resonance imaging of the human lateral geniculate body. Arch Neurol 47:1201-1206.

Horton JC, Hoyt WF (1991) Quadrantic visual field defects. A hallmark of lesions in extrastriate (V2/V3) cortex. Brain 114: 1703-1718.

Howell OW, Palser A, Polito A, Melrose S, Zonta B, Scheiermann C, Vora AJ, Brophy PJ, Reynolds R (2006) Disruption of neurofascin localization reveals early changes preceding demyelination and remyelination in multiple sclerosis. Brain 129:3173-3185.

Huang D, Swanson EA, Lin CP, Schuman JS, Stinson WG, Chang W, Hee MR, Flotte T, Gregory K, Puliafito CA (1991) Optical coherence tomography. Science 254:1178-1181.

IFNB Multiple Sclerosis study group (1993) Interferon beta-1b is effective in relapsing remitting multiple sclerosis. I. Clinical results of a multi-center, randomized,

double-blind, placebo-controlled trial. The IFNB Multiple Sclerosis study group. Neurology 43:555-561.

Imaizumi T, Lankford KL, Kocsis JD (2000) Transplantation of olfactory ensheathing cells or Schwann cells restores rapid and secure conduction across the transected spinal cord. Brain Res 854:70-78.

Inglese M, Ghezzi A, Bianchi S, Gerevini S, Sormani MP, Martinelli V, Comi G, Filippi M (2002) Irreversible disability and tissue loss in multiple sclerosis: a conventional and magnetization transfer magnetic resonance imaging study of the optic nerves. Arch Neurol 59:250-255.

Ishihara S (1917) Tests for colour blindness. Tokyo, Hongo Harukicho: Handaya.

Iwasawa T, Matoba H, Ogi A, Kurihara H, Saito K, Yoshida T, Matsubara S, Nozaki A (1997) Diffusion-weighted imaging of the human optic nerve: a new approach to evaluate optic neuritis in multiple sclerosis. Magn Reson Med 38:484-491.

Jackson A, Sheppard S, Laitt RD, Kassner A, Moriarty D (1998) Optic neuritis: MR imaging with combined fat- and water-suppression techniques. Radiology 206:57-63.

Jacobs KM, Donoghue JP (1991) Reshaping the cortical motor map by unmasking latent intracortical connections. Science 251:944-947.

Jacobs LD, Beck RW, Simon JH, Kinkel RP, Brownscheidle CM, Murray TJ, Simonian NA, Slasor PJ, Sandrock AW (2000) Intramuscular interferon beta-1a therapy initiated during a first demyelinating event in multiple sclerosis. CHAMPS Study Group. N Engl J Med 343:898-904.

Jeffery ND, Blakemore WF (1997) Locomotor deficits induced by experimental spinal cord demyelination are abolished by spontaneous remyelination. Brain 120:27-37.

Jenkins TM, Mancini L, Ciccarelli O, Toosy AT, Altmann D, Chappell K, Plant GT, Miller DH, Thompson AJ (2008) Using structural and functional magnetic resonance imaging to explain visual loss at the onset of acute optic neuritis (Abstract). Multiple sclerosis 14:S1:276.

Jenkinson M, Smith S (2001) A global optimisation method for robust affine registration of brain images. Med Image Anal 5:143-156.

Jin YP, de Pedro-Cuesta J, Soderstrom M, Stawiarz L, Link H (1998) Incidence of optic neuritis in Stockholm, Sweden 1990-1995: I. Age, sex, birth and ethnic-group related patterns. J Neurol Sci 159:107-114.

Jin YP, de Pedro-Cuesta J, Soderstrom M, Link H (1999) Incidence of optic neuritis in Stockholm, Sweden, 1990-1995: II. Time and space patterns. Arch Neurol 56:975-980.

Johansen-Berg H, Behrens TE (2006) Just pretty pictures? What diffusion tractography can add in clinical neuroscience. Curr Opin Neurol 19:379-385.

Johansen-Berg H (2007) Structural plasticity: rewiring the brain. Curr Biol 17:R141-R144.

Johnson KP, Brooks BR, Cohen JA, Ford CC, Goldstein J, Lisak RP, Myers LW, Panitch HS, Rose JW, Schiffer RB (1995) Copolymer 1 reduces relapse rate and improves disability in relapsing-remitting multiple sclerosis: results of a phase III multicenter, double-blind placebo-controlled trial. The Copolymer 1 Multiple Sclerosis Study Group. Neurology 45:1268-1276.

Jones SJ (1993) Visual evoked potentials after optic neuritis. Effect of time interval, age and disease dissemination. J Neurol 240:489-494.

Jones SJ, Brusa A (2003) Neurophysiological evidence for long-term repair of MS lesions: implications for axon protection. J Neurol Sci 206:193-198.

Jones TA, Schallert T (1992) Overgrowth and pruning of dendrites in adult rats recovering from neocortical damage. Brain Res 581:156-160.

Kahle W, Frotscher M (2003) Color atlas and textbook of human anatomy. Stuttgart: Thieme.

Kapoor R, Smith KJ, Felts PA, Davies M (1993) Internodal potassium currents can generate ectopic impulses in mammalian myelinated axons. Brain Res 611:165-169.

Kapoor R, Li YG, Smith KJ (1997) Slow sodium-dependent potential oscillations contribute to ectopic firing in mammalian demyelinated axons. Brain 120:647-652.

Kapoor R, Miller DH, Jones SJ, Plant GT, Brusa A, Gass A, Hawkins CP, Page R, Wood NW, Compston DA, Moseley IF, McDonald WI (1998) Effects of intravenous methylprednisolone on outcome in MRI-based prognostic subgroups in acute optic neuritis. Neurology 50:230-237.

Kappos L, Polman CH, Freedman MS, Edan G, Hartung HP, Miller DH, Montalban X, Barkhof F, Bauer L, Jakobs P, Pohl C, Sandbrink R (2006) Treatment with interferon beta-1b delays conversion to clinically definite and McDonald MS in patients with clinically isolated syndromes. Neurology 67:1242-1249.

Kappos L, Freedman MS, Polman CH, Edan G, Hartung HP, Miller DH, Montalban X, Barkhof F, Radu EW, Bauer L, Dahms S, Lanius V, Pohl C, Sandbrink R (2007) Effect of early versus delayed interferon beta-1b treatment on disability after a first clinical event suggestive of multiple sclerosis: a 3-year follow-up analysis of the BENEFIT study. Lancet 370:389-397.

Karlik SJ, Munoz D, St Louis J, Strejan G (1999). Correlation between MRI and clinico-pathological manifestations in Lewis rats protected from experimental allergic encephalomyelitis by acylated synthetic peptide of myelin basic protein. Magn Reson Imaging 17:731-737.

Karmarkar UR, Dan Y (2006) Experience-dependent plasticity in adult visual cortex. Neuron 52:577-585.

Kasten E, Wust S, Behrens-Baumann W, Sabel BA (1998) Computer-based training for the treatment of partial blindness. Nat Med 4:1083-1087.

Katz D, Taubenberger JK, Cannella B, McFarlin DE, Raine CS, McFarland HF (1993) Correlation between magnetic resonance imaging findings and lesion development in chronic, active multiple sclerosis. Ann Neurol 34:661-669.

Keltner JL, Johnson CA, Beck RW, Cleary PA, Spurr JO (1993a) Quality control functions of the Visual Field Reading Center (VFRC) for the Optic Neuritis Treatment Trial (ONTT). Control Clin Trials 14:143-159.

Keltner JL, Johnson CA, Spurr JO, Beck RW (1993b) Baseline visual field profile of optic neuritis. The experience of the optic neuritis treatment trial. Optic Neuritis Study Group. Arch Ophthalmol 111:231-234.

Keltner JL, Johnson CA, Spurr JO, Beck RW (1999) Comparison of central and peripheral visual field properties in the optic neuritis treatment trial. Am J Ophthalmol 128:543-553.

Klistorner A, Arvind H, Nguyen T, Garrick R, Paine M, Graham S, O'Day J, Grigg J, Billson F, Yiannikas C (2008a) Axonal loss and myelin in early ON loss in postacute optic neuritis. Ann Neurol 64:325-331.

Klistorner A, Fraser C, Garrick R, Graham S, Arvind H (2008b) Correlation between full-field and multifocal VEPs in optic neuritis. Doc Ophthalmol 116:19-27.

Kolappan M, Connick P, Compston A, Thompson AJ, Chandran S, Miller D (2008a) Optic neuritis as a sentinel lesion to study neuroprotection and repair in a trial of autologous mesenchymal stem cells in multiple sclerosis (Abstract) Multiple sclerosis 14:S1:284.

Kolappan M, Henderson A, Jenkins T, Wheeler-Kingshott C, Plant G, Thompson A, Miller D (2008b) Assessing structure and function of the afferent visual pathway in multiple sclerosis and associated optic neuritis. J Neurol 256:305-319.

Kolbe S, Chapman C, Nguyen T, Bajraszewski C, Johnston L, Kean M, Mitchell P, Paine M, Butzkueven H, Kilpatrick T, Egan G (2009) Optic nerve diffusion changes and atrophy jointly predict visual dysfunction after optic neuritis. Neuroimage 45:679-686.

Koles ZJ, Rasminsky M (1972) A computer simulation of conduction in demyelinated nerve fibres. J Physiol 227:351-364.

Korsholm K, Madsen KH, Frederiksen JL, Skimminge A, Lund TE (2007) Recovery from optic neuritis: an ROI-based analysis of LGN and visual cortical areas. Brain 130:1244-1253.

Korsholm K, Madsen KH, Frederiksen JL, Rowe JB, Lund TE (2008) Cortical neuroplasticity in patients recovering from acute optic neuritis. Neuroimage 42:836-844.

Kotter MR, Li WW, Zhao C, Franklin RJ (2006) Myelin impairs CNS remyelination by inhibiting oligodendrocyte precursor cell differentiation. J Neurosci 26:328-332.

Kriegeskorte N, Goebel R, Bandettini P (2006) Information-based functional brain mapping. Proc Natl Acad USA 103: 3863-3868.

Krings T, Reinges MH, Thiex R, Gilsbach JM, Thron A (2001) Functional and diffusion-weighted magnetic resonance images of space-occupying lesions affecting the motor system: imaging the motor cortex and pyramidal tracts. J Neurosurg 95:816-824.

Kupersmith MJ, Alban T, Zeiffer B, Lefton D (2002) Contrast-enhanced MRI in acute optic neuritis: relationship to visual performance. Brain 125:812-822.

Kupersmith MJ, Gal RL, Beck RW, Xing D, Miller N (2007) Visual function at baseline and 1 month in acute optic neuritis: predictors of visual outcome. Neurology 69:508-514.

Kwong KK, Belliveau JW, Chesler DA, Goldberg IE, Weisskoff RM, Poncelet BP, Kennedy DN, Hoppel BE, Cohen MS, Turner R, . (1992) Dynamic magnetic resonance imaging of human brain activity during primary sensory stimulation. Proc Natl Acad Sci USA 89:5675-5679.

Langkilde AR, Frederiksen JL, Rostrup E, Larsson HB (2002) Functional MRI of the visual cortex and visual testing in patients with previous optic neuritis. Eur J Neurol 9:277-286.

Lappe-Siefke C, Goebbels S, Gravel M, Nicksch E, Lee J, Braun PE, Griffiths IR, Nave KA (2003) Disruption of Cnp1 uncouples oligodendroglial functions in axonal support and myelination. Nat Genet 33:366-374.

Lassmann H, Bruck W, Lucchinetti CF (2007) The immunopathology of multiple sclerosis: an overview. Brain Pathol 17:210-218.

Lauterbur PC (1973) Image formation by induced local interactions. Examples of employing nuclear magnetic resonance. Nature 242:190-191.

Le Bihan D, Breton E, Lallemand D, Grenier P, Cabanis E, Laval-Jeantet M (1986) MR imaging of intravoxel incoherent motions: application to diffusion and perfusion in neurologic disorders. Radiology 161:401-407.

LePage E, Leray E, Taurin G, Coustans M, Chaperon J, Edan G (2006) Mitoxantrone as induction therapy in aggressive relapsing remitting multiple sclerosis: a descriptive analysis of 100 consecutive patients. Rev Neurol (Paris) 162:185-194.

LePage E, Leray E, Taurin G, Coustans M, Chaperon J, Morrissey SP, Edan G (2008) Mitoxantrone as induction treatment in aggressive relapsing remitting multiple sclerosis: treatment response factors in a 5 year follow-up observational study of 100 consecutive patients. J Neurol Neurosurg Psychiatry 79:52-56.

Levin N, Orlov T, Dotan S, Zohary E (2006) Normal and abnormal fMRI activation patterns in the visual cortex after recovery from optic neuritis. Neuroimage 33:1161-1168.

Li Z, Chapleau MW, Bates JN, Bielefeldt K, Lee HC, Abboud FM (1998) Nitric oxide as an autocrine regulator of sodium currents in baroreceptor neurons. Neuron 20:1039-1049.

Lightman S, McDonald WI, Bird AC, Francis DA, Hoskins A, Batchelor JR, Halliday AM (1987) Retinal venous sheathing in optic neuritis. Its significance for the pathogenesis of multiple sclerosis. Brain 110:405-414.

Logothetis NK, Pauls J, Augath M, Trinath T, Oeltermann A (2001) Neurophysiological investigation of the basis of the fMRI signal. Nature 412:150-157.

Lucchinetti C, Bruck W, Parisi J, Scheithauer B, Rodriguez M, Lassmann H (2000) Heterogeneity of multiple sclerosis lesions: implications for the pathogenesis of demyelination. Ann Neurol 47:707-717.

Lumer ED, Friston KJ, Rees G (1998) Neural correlates of perceptual rivalry in the human brain. Science 280:1930-1934.

Madigan MC, Rao NS, Tenhula WN, Sadun AA (1996) Preliminary morphometric study of tumor necrosis factor-alpha (TNF alpha)-induced rabbit optic neuropathy. Neurol Res 18:233-236.

Mancini L, Ciccarelli O, Manfredonia F, Thornton JS, Agosta F, Barkhof F, Beckmann C, De Stefano N, Enzinger C, Fazekas F, Filippi M, Gass A, Hirsch JG, Johansen-Berg H, Kappos L, Korteweg T, Manson SC, Marino S, Matthews PM, Montalban X, Palace J, Polman C, Rocca M, Ropele S, Rovira A, Wegner C, Friston K, Thompson A, Yousry T (2009) Short-term adaptation to a simple motor task is a physiological process preserved in multiple sclerosis. Neuroimage 45:500-511.

Martins A, Balachandran C, Klistorner AI, Graham SL, Billson FA (2003) Effect of pupil size on multifocal pattern visual evoked potentials. Clin Experiment Ophthalmol 31:354-356.

McDonald BK, Cockerell OC, Sander JW, Shorvon SD (2000) The incidence and lifetime prevalence of neurological disorders in a prospective community-based study in the UK. Brain 123:665-676.

McDonald WI, Sears TA (1970) The effects of experimental demyelination on conduction in the central nervous system. Brain 93:583-598.

McDonald WI, Sears TA (1969) Effect of demyelination on conduction in the central nervous system. Nature 221:182-183.

McDonald WI, Barnes D. (1992) The ocular manifestations of multiple sclerosis. 1. Abnormalities of the afferent visual system. J. Neurol Neurosurg Psychiatry 55: 747-752.

McDonald WI, Compston A, Edan G, Goodkin D, Hartung HP, Lublin FD, McFarland HF, Paty DW, Polman CH, Reingold SC, Sandberg-Wollheim M, Sibley W, Thompson A, van den NS, Weinshenker BY, Wolinsky JS (2001) Recommended diagnostic criteria for multiple sclerosis: guidelines from the International Panel on the diagnosis of multiple sclerosis. Ann Neurol 50:121-127.

Melzi L, Rocca MA, Marzoli SB, Falini A, Vezzulli P, Ghezzi A, Brancato R, Comi G, Scotti G, Filippi M (2007) A longitudinal conventional and magnetization transfer magnetic resonance imaging study of optic neuritis. Mult Scler 13:265-268.

Merzenich MM, Nelson RJ, Stryker MP, Cynader MS, Schoppmann A, Zook JM (1984) Somatosensory cortical map changes following digit amputation in adult monkeys. J Comp Neurol 224:591-605.

Miller DH, Newton MR, van der Poel JC, du Boulay EP, Halliday AM, Kendall BE, Johnson G, MacManus DG, Moseley IF, McDonald WI (1988a) Magnetic resonance imaging of the optic nerve in optic neuritis. Neurology 38:175-179.

Miller DH, Rudge P, Johnson G, Kendall BE, MacManus DG, Moseley IF, Barnes D, McDonald WI (1988b) Serial gadolinium enhanced magnetic resonance imaging in multiple sclerosis. Brain 111:927-939.

Miller DH, Barkhof F, Frank JA, Parker GJ, Thompson AJ (2002) Measurement of atrophy in multiple sclerosis: pathological basis, methodological aspects and clinical relevance. Brain 125:1676-1695.

Mitchell KW, Howe JW, Spencer SR (1987) Visual evoked potentials in the older population: age and gender effects. Clin Phys Physiol Meas 8:317-324.

Moreau T, Coles A, Wing M, Isaacs J, Hale G, Waldmann H, Compston A (1996) Transient increase in symptoms associated with cytokine release in patients with multiple sclerosis. Brain 119:225-237.

Mori S, Crain BJ, Chacko VP, van Zijl PC (1999) Three-dimensional tracking of axonal projections in the brain by magnetic resonance imaging. Ann Neurol 45:265-269.

Mori S, van Zijl PC (2002) Fiber tracking: principles and strategies - a technical review. NMR Biomed 15:468-480.

Mullen KT, Plant GT (1986) Colour and luminance vision in human optic neuritis. Brain 109:1-13.

Naismith RT, Xu J, Tutlam NT, Snyder A, Benzinger T, Shimony J, Shepherd J, Trinkaus K, Cross AH, Song SK (2009) Disability in optic neuritis correlates with diffusion tensor-derived directional diffusivities. Neurology 72:589-594.

NICE (2002) National Institute for Clinical Excellence. Beta interferon and glatiramer acetate for the treatment of multiple sclerosis. NICE technology appraisal guidance no.32. London, UK.

NICE (2003) National Collaborating Centre for Chronic Conditions. Multiple sclerosis: management of multiple sclerosis in primary and secondary care. NICE clinical guideline 8. London, UK.

Nilsson P, Larsson EM, Maly-Sundgren P, Perfekt R, Sandberg-Wollheim M (2005) Predicting the outcome of optic neuritis: evaluation of risk factors after 30 years of follow-up. J Neurol 252:396-402.

Noble J, Forooghian F, Sproule M, Westall C, O'Connor P (2006) Utility of the National Eye Institute VFQ-25 questionnaire in a heterogeneous group of multiple sclerosis patients. Am J Ophthalmol 142:464-468.

Noseworthy JH, O'Brien PC, Petterson TM, Weis J, Stevens L, Peterson WK, Sneve D, Cross SA, Leavitt JA, Auger RG, Weinshenker BG, Dodick DW, Wingerchuk DM, Rodriguez M (2001) A randomized trial of intravenous immunoglobulin in inflammatory demyelinating optic neuritis. Neurology 56:1514-1522.

Odom JV, Bach M, Barber C, Brigell M, Marmor MF, Tormene AP, Holder GE, Vaegan (2004) Visual evoked potentials standard (2004). Doc Ophthalmol 108:115-123.

Ogawa S, Lee TM, Kay AR, Tank DW (1990) Brain magnetic resonance imaging with contrast dependent on blood oxygenation. Proc Natl Acad Sci USA 87:9868-9872.

Ogawa S, Tank DW, Menon R, Ellermann JM, Kim SG, Merkle H, Ugurbil K (1992) Intrinsic signal changes accompanying sensory stimulation: functional brain mapping with magnetic resonance imaging. Proc Natl Acad Sci USA 89:5951-5955.

Optic Neuritis Study Group (1991) The clinical profile of optic neuritis. Experience of the Optic Neuritis Treatment Trial. Optic Neuritis Study Group. Arch Ophthalmol 109:1673-1678.

Optic Neuritis Study Group (1997a) The 5-year risk of MS after optic neuritis. Experience of the optic neuritis treatment trial. Optic Neuritis Study Group. Neurology 49:1404-1413.

Optic Neuritis Study Group (1997b) Visual function 5 years after optic neuritis: experience of the Optic Neuritis Treatment Trial. The Optic Neuritis Study Group. Arch Ophthalmol 115:1545-1552.

Optic Neuritis Study Group (2008a) Visual Function 15 Years after Optic Neuritis A Final Follow-up Report from the Optic Neuritis Treatment Trial. Ophthalmology 115:1079-1082.

Optic Neuritis Study Group (2008b) Multiple sclerosis risk after optic neuritis: final optic neuritis treatment trial follow-up. Arch Neurol 65:727-732.

Parisi V, Manni G, Spadaro M, Colacino G, Restuccia R, Marchi S, Bucci MG, Pierelli F (1999) Correlation between morphological and functional retinal impairment in multiple sclerosis patients. Invest Ophthalmol Vis Sci 40:2520-2527.

Parker GJ, Haroon HA, Wheeler-Kingshott CA (2003) A framework for a streamline-based probabilistic index of connectivity (PICo) using a structural interpretation of MRI diffusion measurements. J Magn Reson Imaging 18:242-254.

Patrikios P, Stadelmann C, Kutzelnigg A, Rauschka H, Schmidbauer M, Laursen H, Sorensen PS, Bruck W, Lucchinetti C, Lassmann H (2006) Remyelination is extensive in a subset of multiple sclerosis patients. Brain 129:3165-3172.

Pauling L, Coryell CD (1936) The Magnetic Properties and Structure of Hemoglobin, Oxyhemoglobin and Carbonmonoxyhemoglobin. Proc Natl Acad Sci USA 22:210-216.

Pelli DG, Robson J.G., Wilkins AJ (1988) The design of a new letter chart for measuring contrast sensitivity. Clin Vision Sci 2:187-199.

Perneger TV (1998) What's wrong with Bonferroni adjustments. BMJ 316:1236-1238.

Phillips ML, Foster DH, Honan WP, Edgar GK, Heron JR (1994) Optic neuritis. Differential losses of luminance and chromatic function near a scotoma. Brain 117:767-773.

Pirko I, Blauwet LK, Lesnick TG, Weinshenker BG (2004) The natural history of recurrent optic neuritis. Arch Neurol 61:1401-1405.

Pitt D, Werner P, Raine CS (2000) Glutamate excitotoxicity in a model of multiple sclerosis. Nat Med 6:67-70.

Plant GT, Hess RF (1987) Regional threshold contrast sensitivity within the central visual field in optic neuritis. Brain 110:489-515.

Plant GT, Kermode AG, Turano G, Moseley IF, Miller DH, MacManus DG, Halliday AM, McDonald WI (1992) Symptomatic retrochiasmal lesions in multiple sclerosis: clinical features, visual evoked potentials, and magnetic resonance imaging. Neurology 42:68-76.

Pluchino S, Martino G (2005) The therapeutic use of stem cells for myelin repair in autoimmune demyelinating disorders. J Neurol Sci 233:117-119.

Plummer DL (1992) DispImage: A display and analysis tool for medical images. Rivista di Neuroradiologia 5:489-495.

Polman CH, Reingold SC, Edan G, Filippi M, Hartung HP, Kappos L, Lublin FD, Metz LM, McFarland HF, O'Connor PW, Sandberg-Wollheim M, Thompson AJ, Weinshenker BG, Wolinsky JS (2005) Diagnostic criteria for multiple sclerosis: 2005 revisions to the "McDonald Criteria". Ann Neurol 58:840-846.

Polman CH, O'Connor PW, Havrdova E, Hutchinson M, Kappos L, Miller DH, Phillips JT, Lublin FD, Giovannoni G, Wajgt A, Toal M, Lynn F, Panzara MA, Sandrock AW (2006) A randomized, placebo-controlled trial of natalizumab for relapsing multiple sclerosis. N Engl J Med 354:899-910.

Pons TP, Garraghty PE, Ommaya AK, Kaas JH, Taub E, Mishkin M (1991) Massive cortical reorganization after sensory deafferentation in adult macaques. Science 252:1857-1860.

Porciatti V, Sartucci F (1996) Retinal and cortical evoked responses to chromatic contrast stimuli. Specific losses in both eyes of patients with multiple sclerosis and unilateral optic neuritis. Brain 119:723-740.

Poser CM, Paty DW, Scheinberg L, McDonald WI, Davis FA, Ebers GC, Johnson KP, Sibley WA, Silberberg DH, Tourtellotte WW (1983) New diagnostic criteria for multiple sclerosis: guidelines for research protocols. Ann Neurol 13:227-231.

Posner MI, Petersen SE (1990) The attention system of the human brain. Annu Rev Neurosci 13:25-42.

Powell HW, Parker GJ, Alexander DC, Symms MR, Boulby PA, Wheeler-Kingshott CA, Barker GJ, Koepp MJ, Duncan JS (2007) Abnormalities of language networks in temporal lobe epilepsy. Neuroimage 36:209-221.

PRISMS study group (1998) Randomised double-blind placebo-controlled study of interferon-beta-1a in relapsing/remitting multiple sclerosis. PRISMS (Prevention of relapses and disability by inerferon beta-1a subcutaneously in multiple sclerosis) Study Group. Lancet 352:1498-1504.

Quigley HA, Davis EB, Anderson DR (1977) Descending optic nerve degeneration in primates. Invest Ophthalmol Vis Sci 16:841-849.

Ramachandran VS, Gregory RL (1991) Perceptual filling in of artificially induced scotomas in human vision. Nature 350:699-702.

Rao NA, Tso MO, Zimmerman EL (1977) Experimental allergic optic neuritis in guinea pigs: preliminary report. Invest Ophthalmol Vis Sci 16:338-342.

Rasminsky M, Sears TA (1972) Internodal conduction in undissected demyelinated nerve fibres. J Physiol 227:323-350.

Redford EJ, Kapoor R, Smith KJ (1997) Nitric oxide donors reversibly block axonal conduction: demyelinated axons are especially susceptible. Brain 120:2149-2157.

Rees G, Lavie N (2001) What can functional imaging reveal about the role of attention in visual awareness? Neuropsychologia 39:1343-1353.

Regan D, Kothe AC, Sharpe JA (1991) Recognition of motion-defined shapes in patients with multiple sclerosis and optic neuritis. Brain 114:1129-1155.

Richards TL, Alvord EC Jr., Peterson J, Cosgrove S, Petersen R, Petersen K, Heide AC, Cluff J, Rose LM (1995) Experimental allergic encephalomyelitis in non-human primates: MRI and MRS may predict the type of brain damage. NMR Biomed 8:49-58.

Rinalduzzi S, Brusa A, Jones SJ (2001) Variation of visual evoked potential delay to stimulation of central, nasal, and temporal regions of the macula in optic neuritis. J Neurol Neurosurg Psychiatry 70:28-35.

Ritchie JM, Rogart RB (1977) Density of sodium channels in mammalian myelinated nerve fibers and nature of the axonal membrane under the myelin sheath. Proc Natl Acad Sci USA 74:211-215.

Rivers TM, Spunt DH, Berry GP (1933) Observations on attempts to produce acute disseminated encephalomyelitis in monkeys. J Exp Med 58:39-53.

Rizzo JFI (1998) Anatomy and physiology of the retina. In: Walsh and Hoyt's clinical neuro-ophthalmology (Miller NR, Newman NJ, eds), pp 25-56. Baltimore: Williams and Wilkins.

Rocca MA, Colombo B, Falini A, Ghezzi A, Martinelli V, Scotti G, Comi G, Filippi M (2005) Cortical adaptation in patients with MS: a cross-sectional functional MRI study of disease phenotypes. Lancet Neurol 4:618-626.

Rodriguez M, Siva A, Cross SA, O'Brien PC, Kurland LT (1995) Optic neuritis: a population-based study in Olmsted County, Minnesota. Neurology 45:244-250.

Roed HG, Langkilde A, Sellebjerg F, Lauritzen M, Bang P, Morup A, Frederiksen JL (2005) A double-blind, randomized trial of IV immunoglobulin treatment in acute optic neuritis. Neurology 64:804-810.

Rombouts SA, Lazeron RH, Scheltens P, Uitdehaag BM, Sprenger M, Valk J, Barkhof F (1998) Visual activation patterns in patients with optic neuritis: an fMRI pilot study. Neurology 50:1896-1899.

Rorden C, Brett M (2000) Stereotaxic display of brain lesions. Behav Neurol 12:191-200.

Rosas HD, Liu AK, Hersch S, Glessner M, Ferrante RJ, Salat DH, van der KA, Jenkins BG, Dale AM, Fischl B (2002) Regional and progressive thinning of the cortical ribbon in Huntington's disease. Neurology 58:695-701.

Rothman KJ (1990) No adjustments are needed for multiple comparisons. Epidemiology 1:43-46.

Rudick RA, Stuart WH, Calabresi PA, Confavreux C, Galetta SL, Radue EW, Lublin FD, Weinstock-Guttman B, Wynn DR, Lynn F, Panzara MA, Sandrock AW (2006) Natalizumab plus interferon beta-1a for relapsing multiple sclerosis. N Engl J Med 354:911-923.

Russ MO, Cleff U, Lanfermann H, Schalnus R, Enzensberger W, Kleinschmidt A (2002) Functional magnetic resonance imaging in acute unilateral optic neuritis. J Neuroimaging 12:339-350.

Russell MH, Murray IJ, Metcalfe RA, Kulikowski JJ (1991) The visual defect in multiple sclerosis and optic neuritis. A combined psychophysical and electrophysiological investigation. Brain 114:2419-2435.

Sabel BA (1999) Restoration of vision I: neurobiological mechanisms of restoration and plasticity after brain damage - a review. Restor Neurol Neurosci 15:177-200.

Sannita WG, Fatone M, Garbarino S, Giglioli D, Massimilla S, Riela S (1995) Effects of physiological changes of serum glucose on the pattern-VEP of healthy volunteers. Physiol Behav 58:1021-1026.

Schild HH (1990) Magnetic resonance imaging made easy. Berlin: Schering.

Schmierer K, Wheeler-Kingshott CA, Boulby PA, Scaravilli F, Altmann DR, Barker GJ, Tofts PS, Miller DH (2007) Diffusion tensor imaging of post mortem multiple sclerosis brain. Neuroimage 35:467-477.

Schneck ME, Haegerstrom-Portnoy G (1997) Color vision defect type and spatial vision in the optic neuritis treatment trial. Invest Ophthalmol Vis Sci 38:2278-2289.

Selhorst JB, Saul RF (1995) Uhthoff and his symptom. J Neuroophthalmol 15:63-69.

Sereno MI, Dale AM, Reppas JB, Kwong KK, Belliveau JW, Brady TJ, Rosen BR, Tootell RB (1995) Borders of multiple visual areas in humans revealed by functional magnetic resonance imaging. Science 268:889-893.

Skaf M, Bernardes AB, Cardillo JA, Costa RA, Melo LA, Jr., Castro JC, Varma R (2006) Retinal nerve fibre layer thickness profile in normal eyes using third-generation optical coherence tomography. Eye 20:431-439.

Slagsvold JE (1978) Pulfrich pendulum phenomenon in patients with a history of acute optic neuritis. Acta Ophthalmol (Copenh) 56:817-826.

Slamovitis TL, Rosen CE, Cheng KP, Striph GG (1991) Visual recovery in patients with optic neuritis and visual loss to no light perception. Am J Ophthalmol 111:209-214.

Slotnick SD, Klein SA, Carney T, Sutter EE (2001) Electrophysiological estimate of human cortical magnification. Clin Neurophysiol 112:1349-1356.

Smith EJ, Blakemore WF, McDonald WI (1979) Central remyelination restores secure conduction. Nature 280:395-396.

Smith KJ, McDonald WI (1980) Spontaneous and mechanically evoked activity due to central demyelinating lesion. Nature 286:154-155.

Smith KJ, McDonald WI (1982) Spontaneous and evoked electrical discharges from a central demyelinating lesion. J Neurol Sci 55:39-47.

Smith KJ (1994) Conduction properties of central demyelinated and remyelinated axons, and their relation to symptom production in demyelinating disorders. Eye 8:224-237.

Smith KJ, McDonald WI (1999) The pathophysiology of multiple sclerosis: the mechanisms underlying the production of symptoms and the natural history of the disease. Philos Trans R Soc Lond B Biol Sci 354:1649-1673.

Smith KJ, Kapoor R, Hall SM, Davies M (2001) Electrically active axons degenerate when exposed to nitric oxide. Ann Neurol 49:470-476.

Smith KJ, Lassmann H (2002) The role of nitric oxide in multiple sclerosis. Lancet Neurol 1:232-241.

Smith KJ (2007) Sodium channels and multiple sclerosis: roles in symptom production, damage and therapy. Brain Pathol 17:230-242.

Smith SM, Nichols TE (2009) Threshold-free cluster enhancement: addressing problems of smoothing, threshold dependence and localisation in cluster inference. Neuroimage 44:83-98.

Sorensen TL, Frederiksen JL, Bronnum-Hansen H, Petersen HC (1999) Optic neuritis as onset manifestation of multiple sclerosis: a nationwide, long-term survey. Neurology 53:473-478.

Stejskal EO, Tanner JE (1965) Spin diffusion measurements: spin echos in the presence of a time-dependent field gradient. J Chem Phys 42:288-292.

Stewart WA, Alvord EC, Hruby S, Hall LD, Paty DW (1985) Early detection of experimental allergic encephalomyelitis by magnetic resonance imaging. Lancet 2:898.

Stewart WA, Hall LD, Berry K, Paty DW (1984) Correlation between NMR scan and brain slice data in multiple sclerosis. Lancet 2:412.

Straatsma BR, Foos RY, Heckenlively JR, Taylor GN (1981) Myelinated retinal nerve fibers. Am J Ophthalmol 91:25-38.

Stys PK (1998) Anoxic and ischemic injury of myelinated axons in CNS white matter: from mechanistic concepts to therapeutics. J Cereb Blood Flow Metab 18:2-25.

Sun SW, Liang HF, Cross AH, Song SK (2008) Evolving Wallerian degeneration after transient retinal ischemia in mice characterized by diffusion tensor imaging. Neuroimage 40:1-10.

Talairach J, Tournoux P (1988) Co-planar stereotaxic atlas of the human brain. New York.

Thorpe JW, Barker GJ, Jones SJ, Moseley I, Losseff N, MacManus DG, Webb S, Mortimer C, Plummer DL, Tofts PS (1995) Magnetisation transfer ratios and transverse magnetisation decay curves in optic neuritis: correlation with clinical findings and electrophysiology. J Neurol Neurosurg Psychiatry 59:487-492.

Thottakara P, Lazar M, Johnson SC, Alexander AL (2006) Application of Brodmann's area templates for ROI selection in white matter tractography studies. Neuroimage 29:868-878.

Thulborn KR, Waterton JC, Matthews PM, Radda GK (1982) Oxygenation dependence of the transverse relaxation time of water protons in whole blood at high field. Biochim Biophys Acta 714:265-270.

Tien RD, Hesselink JR, Szumowski J (1991) MR fat suppression combined with Gd-DTPA enhancement in optic neuritis and perineuritis. J Comput Assist Tomogr 15:223-227.

Tien RD (1992) Fat-suppression MR imaging in neuroradiology: techniques and clinical application. AJR Am J Roentgenol 158:369-379.

Tintore M, Rovira A, Martinez MJ, Rio J, az-Villoslada P, Brieva L, Borras C, Grive E, Capellades J, Montalban X (2000) Isolated demyelinating syndromes: comparison of different MR imaging criteria to predict conversion to clinically definite multiple sclerosis. AJNR Am J Neuroradiol 21:702-706.

Tong F, Meng M, Blake R (2006) Neural bases of binocular rivalry. Trends Cogn Sci 10:502-511.

Toosy AT, Werring DJ, Bullmore ET, Plant GT, Barker GJ, Miller DH, Thompson AJ (2002) Functional magnetic resonance imaging of the cortical response to photic stimulation in humans following optic neuritis recovery. Neurosci Lett 330:255-259.

Toosy AT, Ciccarelli O, Parker GJ, Wheeler-Kingshott CA, Miller DH, Thompson AJ (2004) Characterizing function-structure relationships in the human visual system with functional MRI and diffusion tensor imaging. Neuroimage 21:1452-1463.

Toosy AT, Hickman SJ, Miszkiel KA, Jones SJ, Plant GT, Altmann DR, Barker GJ, Miller DH, Thompson AJ (2005) Adaptive cortical plasticity in higher visual areas after acute optic neuritis. Ann Neurol 57:622-633.

Toth CA, Narayan DG, Boppart SA, Hee MR, Fujimoto JG, Birngruber R, Cain CP, DiCarlo CD, Roach WP (1997) A comparison of retinal morphology viewed by optical coherence tomography and by light microscopy. Arch Ophthalmol 115:1425-1428.

Toussaint D, Perier O, Verstappen A, Bervoets S (1983) Clinicopathological study of the visual pathways, eyes, and cerebral hemispheres in 32 cases of disseminated sclerosis. J Clin Neuroophthalmol 3:211-220.

Trapp BD, Peterson J, Ransohoff RM, Rudick R, Mork S, Bo L (1998) Axonal transection in the lesions of multiple sclerosis. N Engl J Med 338:278-285.

Trauzettel-Klosinski S, Diener HC, Dietz K, Zrenner E (1995) The effect of oral prednisolone on visual evoked potential latencies in acute optic neuritis monitored in a prospective, randomized, controlled study. Doc Opthalmol 91:165-179.

Trip SA, Schlottmann PG, Jones SJ, Altmann DR, Garway-Heath DF, Thompson AJ, Plant GT, Miller DH (2005) Retinal nerve fiber layer axonal loss and visual dysfunction in optic neuritis. Ann Neurol 58:383-391.

Trip SA, Schlottmann PG, Jones SJ, Li WY, Garway-Heath DF, Thompson AJ, Plant GT, Miller DH (2006a) Optic nerve atrophy and retinal nerve fibre layer thinning

following optic neuritis: evidence that axonal loss is a substrate of MRI-detected atrophy. Neuroimage 31:286-293.

Trip SA, Wheeler-Kingshott C, Jones SJ, Li WY, Barker GJ, Thompson AJ, Plant GT, Miller DH (2006b) Optic nerve diffusion tensor imaging in optic neuritis. Neuroimage 30:498-505.

Trip SA, Schlottmann PG, Jones SJ, Li WY, Garway-Heath DF, Thompson AJ, Plant GT, Miller DH (2007) Optic nerve magnetization transfer imaging and measures of axonal loss and demyelination in optic neuritis. Mult Scler 13:875-879.

Trobe JD, Beck RW, Moke PS, Cleary PA (1996) Contrast sensitivity and other vision tests in the optic neuritis treatment trial. Am J Ophthalmol 121:547-553.

Turner R, Le BD, Moonen CT, Despres D, Frank J (1991) Echo-planar time course MRI of cat brain oxygenation changes. Magn Reson Med 22:159-166.

Vanzetta I, Grinvald A (1999) Increased cortical oxidative metabolism due to sensory stimulation: implications for functional brain imaging. Science 286:1555-1558.

Wakakura M, Mashimo K, Oono S, Matsui Y, Tabuchi A, Kani K, Shikishima K, Kawai K, Nakao Y, Tazawa Y, Kiyosawa M, Abe H, Ohba N, Yago K, Maeda S, Sugita M, Ishikawa S (1999a) Multicenter clinical trial for evaluating methylprednisolone pulse treatment of idiopathic optic neuritis in Japan. Optic Neuritis Treatment Trial Multicenter Cooperative Research Group (ONMRG). Jpn J Ophthalmol 43:133-138.

Wakakura M, Minei-Higa R, Oono S, Matsui Y, Tabuchi A, Kani K, Shikishima K, Kawai K, Nakao Y, Tazawa Y, Kiyosawa M, Abe H, Ohba N, Yago K, Maeda S, Sugita M, Ishikawa S (1999b) Baseline features of idiopathic optic neuritis as determined by a multicenter treatment trial in Japan. Optic Neuritis Treatment Trial Multicenter Cooperative Research Group (ONMRG). Jpn J Ophthalmol 43:127-132.

Wall M (1990) Loss of P retinal ganglion cell fuction in resolved optic neuritis. Neurology 40: 649-653.

Waller A (1850) Experiments on the section of the glossopharyngeal and hypoglossal nerves of the frog and observations of the alterations produced thereby in the structure of their primitive fibres. Philos Trans R Soc Lond 1850:423-429.

Watanabe T, Sasaki Y, Miyauchi S, Putz B, Fujimaki N, Nielsen M, Takino R, Miyakawa S (1998) Attention-regulated activity in human primary visual cortex. J Neurophysiol 79:2218-2221.

Waxman SG (1977) Conduction in myelinated, unmyelinated, and demyelinated fibers. Arch Neurol 34:585-589.

Waxman SG (1995) Sodium channel blockade by antibodies: a new mechanism of neurological disease? Ann Neurol 37:421-423.

Weil RS, Kilner JM, Haynes JD, Rees G (2007) Neural correlates of perceptual filling-in of an artifical scotoma in humans. Proc Natl Acad USA 104:5211-5216.

Weinshenker BG, Rice GP, Noseworthy JH, Carriere W, Baskerville J, Ebers GC (1991) The natural history of multiple sclerosis: a geographically based study. 3. Multivariate analysis of predictive factors and models of outcome. Brain 114:1045-1056.

Werring DJ, Bullmore ET, Toosy AT, Miller DH, Barker GJ, MacManus DG, Brammer MJ, Giampietro VP, Brusa A, Brex PA, Moseley IF, Plant GT, McDonald WI, Thompson AJ (2000) Recovery from optic neuritis is associated with a change in the distribution of cerebral response to visual stimulation: a functional magnetic resonance imaging study. J Neurol Neurosurg Psychiatry 68:441-449.

Wheeler-Kingshott CA, Parker GJ, Symms MR, Hickman SJ, Tofts PS, Miller DH, Barker GJ (2002) ADC mapping of the human optic nerve: increased resolution, coverage, and reliability with CSF-suppressed ZOOM-EPI. Magn Reson Med 47:24-31.

Wheeler-Kingshott CA, Trip SA, Symms MR, Parker GJ, Barker GJ, Miller DH (2006) *In vivo* diffusion tensor imaging of the human optic nerve: pilot study in normal controls. Magn Reson Med 56:446-451.

Wilkins A, Chandran S, Compston A (2001) A role for oligodendrocyte-derived IGF-1 in trophic support of cortical neurons. Glia 36:48-57.

Wilkins A, Majed H, Layfield R, Compston A, Chandran S (2003) Oligodendrocytes promote neuronal survival and axonal length by distinct intracellular mechanisms: a novel role for oligodendrocyte-derived glial cell line-derived neurotrophic factor. J Neurosci 23:4967-4974.

Wilkins A, Compston A (2005) Trophic factors attenuate nitric oxide mediated neuronal and axonal injury in vitro: roles and interactions of mitogen-activated protein kinase signalling pathways. J Neurochem 92:1487-1496.

Williams A, Piaton G, Aigrot MS, Belhadi A, Theaudin M, Petermann F, Thomas JL, Zalc B, Lubetzki C (2007) Semaphorin 3A and 3F: key players in myelin repair in multiple sclerosis? Brain 130:2554-2565.

Wingerchuk DM, Lennon VA, Pittock SJ, Lucchinetti CF, Weinshenker BG (2006) Revised diagnostic criteria for neuromyelitis optica. Neurology 66:1485-1489.

Wolff SD, Balaban RS (1989) Magnetization transfer contrast (MTC) and tissue water proton relaxation in vivo. Magn Reson Med 10:135-144.

Woodruff RH, Franklin RJ (1999) Demyelination and remyelination of the caudal cerebellar peduncle of adult rats following stereotaxic injections of lysolecithin, ethidium bromide, and complement/anti-galactocerebroside: a comparative study. Glia 25:216-228.

Woodruff RH, Fruttiger M, Richardson WD, Franklin RJ (2004) Platelet-derived growth factor regulates oligodendrocyte progenitor numbers in adult CNS and their response following CNS demyelination. Mol Cell Neurosci 25:252-262.

Worsley KJ, Friston KJ (1995) Analysis of fMRI time-series revisited--again. Neuroimage 2:173-181.

Worsley KJ, Marrett S, Neelin P, Vandal AC, Friston KJ, Evans AC (1996) A unified statistical approach for determining significant signals in images of cerebral activation. Hum Brain Mapp 4:58-73.

Wu Q, Butzkueven H, Gresle M, Kirchhoff F, Friedhuber A, Yang Q, Wang H, Fang K, Lei H, Egan GF, Kilpatrick TJ (2007) MR diffusion changes correlate with ultra-structurally defined axonal degeneration in murine optic nerve. Neuroimage 37:1138-1147.

Youl BD, Turano G, Miller DH, Towell AD, MacManus DG, Moore SG, Jones SJ, Barrett G, Kendall BE, Moseley IF (1991) The pathophysiology of acute optic neuritis. An association of gadolinium leakage with clinical and electrophysiological deficits. Brain 114:2437-2450.

Zhang Y, Brady M, Smith S (2001) Segmentation of brain MR images through a hidden Markov random field model and the expectation-maximization algorithm. IEEE Trans Med Imaging 20:45-57.

Zhu B, Moore GR, Zwimpfer TJ, Kastrukoff LF, Dyer JK, Steeves JD, Paty DW, Cynader MS (1999) Axonal cytoskeleton changes in experimental optic neuritis. Brain Res 824:204-217.